Restoration of blood vessel function, using nanotechnology

C ASTLEY

PhD 2020

Restoration of blood vessel function, using nanotechnology

CAI ASTLEY

A thesis submitted in partial fulfilment of the requirements of the Manchester Metropolitan University for the degree of Doctor of Philosophy

Department of Life Sciences

Faculty of Science and Engineering

2020

Acknowledgements

Firstly, I would like to express my sincere gratitude to my director of studies, Dr. May Azzawi for the continuous support of my PhD study and related research, for her patience, motivation, and immense knowledge. Her guidance has helped me throughout my research and in the writing of this thesis.

Besides my advisor, I would like to thank the rest of my co-supervisors: Prof. Yvonne Alexander, Dr. Fiona Wilkinson, and Dr. Debra Whitehead, for their insightful comments and support, but also for encouraging me to widen my research perspective. Many thanks to Dr. Alex Langford-Smith for his friendship, guidance and technical assistance throughout our many hours in the laboratory together.

I would like to acknowledge Dr. Chahinez Houacine and Prof. Kamalinder Singh at the University of Central Lancashire (UCLAN) as well as Dr. Lynda Harris and Dr. Lewis Renshall at the University of Manchester (UoM), for providing the organic nanoparticles utilised throughout this thesis.

It has been a pleasure collaborating and hope to continue our work in future. I would also like to acknowledge Dave Maskew for his assistance in the maintenance of equipment and preparation of reagents, and all the staff at the University of Manchester's Animal Unit, particularly Michael Jackson, Raymond Hodgkiss and Graham Morrissey who have been exceptional at organising the management and collection of animal tissue.

I thank my fellow students for all the stimulating discussions and fun we have shared over the last three years. I wish them all the best and hope to work together again in the coming years.

I would like to dedicate this thesis to my parents, Rhys and Myfanwy, whose encouragement and support have been invaluable. And finally, I acknowledge my partner, Emily, whose unending patience and understanding has carried me throughout.

LIST OF FIGURES

LIST OF TABLES

LIST OF ABBREVIATIONS

$^{\bullet}OH$	Hydroxyl radical
± SEM	± Standard error of the mean
5-HT	Serotonin
AA	Arachidonic acid
AC	Adenylate cyclase
ACh	Acetylcholine
AMP	Adenosine monophosphate
AMPK	AMP-activated protein kinase
APTES	(3-Aminopropyl)triethoxysilane
BH_4	Tetrahydrobiopterin
BKCa	Large conductance calcium-activated potassium channels
$CaCl_2.2H_2O$	Calcium chloride dihydrate
CAT	Catalase
CeNPs	Cerium oxide nanoparticles
CeO_2	Cerium oxide; ceria
COX	Cyclooxygenase
CVD	Cardiovascular disease
CYP450	Cytochrome P450
DCFH-DA	Dichlorofluorescein diacetate
DHE	Dihydroethidium
DLS	Dynamic light scattering
DMSO	Dimethyl sulfoxide
ED	Endothelial dysfunction

EDH	Endothelial derived hyperpolarisation
EDHF	Endothelial derived hyperpolarising factor
EDRF	Endothelial derived relaxing factor
EET	Epoxyeicosatrienoic acids
EtOH	Ethanol
FBS	Foetal bovine serum
FITC	Fluorescein isothiocyanate
FTIR	Fourier transform infrared spectroscopy
H_2O_2	Hydrogen peroxide
HCAEC	Human coronary artery endothelial cell
HETE	Hydroxyeicosatetraenoic acid
HRP	Horseradish peroxidase
IKCa	Intermediate conductance calcium-activated potassium channels
IMS	Industrially methylated spirit
IP	Prostacyclin receptor
$K_2EDTA.2H_2O$	Ethylenediaminetetraacetic acid dipotassium salt dihydrate
KH_2PO_4	Potassium dihydrogen orthophosphate
KPSS	High potassium salt solution
LDME	Laser doppler micro-electrophoresis
L-NNA	Nω-nitro-l-arginine
MCA	Middle cerebral artery
MeOH	Methanol

$MgSO_4.7H_2O$	Magnesium sulfate heptahydrate
MPTES	(3-Mercaptopropyl)trimethoxysilane
MSN	Mesoporous silica nanoparticle
NaCl	Sodium chloride
$NaHCO_3$	Sodium bicarbonate
NaOH	Sodium hydroxide
NH_4OH	Ammonium hydroxide
NLC	Nanolipid carrier
NO	Nitric oxide
NOS	Nitric oxide synthase
NP	Nanoparticle
$O_2^{\bullet-}$	Superoxide radical
OH	Hydroxyl
$ONOO^-$	Peroxynitrite
PAPA	Papaverine
PBS	Phosphate buffered saline
PEG	Polyethylene glycol
PFA	Paraformaldehyde
PGH_2	Prostaglandin H_2
PGI_2	Prostacyclin
PKA	Protein kinase A
PKG	Protein kinase G
PLA_2	Phospholipase A_2
PSS	Physiological salt solution

ROS	Reactive oxygen species
RV	Resveratrol
RV-NLC	Resveratrol-loaded nanolipid carrier
SEM	Scanning electron microscopy
SiNP	Silica nanoparticle
SiO_2	Silicon dioxide
SIRT-1	Silent Mating Type Information Regulation 2 Homolog-1
SKCa	Small conductance calcium-activated potassium channels
SNP	Sodium nitroprusside
SOD	Superoxide dismutase
TEM	Transmission electron microscopy
TEOS	Tetraethyl orthosilicate
TGA	Thermogravimetric analysis
TMS	2,3',4,5'-tetramethoxystilbene
TX-100	Triton X-100
TXA_2	Thromboxane A_2
UV-VIS	Ultraviolet–visible spectroscopy
VSMC	Vascular smooth muscle cell

List of Publications

Original Research

- **Astley, C.**, Houacine, C., Zaabalawi, A., Wilkinson, F., Lightfoot, A. P., Alexander, Y., Whitehead, D., Singh, K. K., Azzawi, M. 'Trimyrstin nanostructured lipid carriers deliver resveratrol, restoring attenuated dilation in small coronary arteries, via the AMPK pathway.' – Submitted
- Zaabalawi, A., **Astley, C.**, Renshall, L., Beards, F., Lightfoot, A. P., Degens, H., Whitehead, D., Alexander, Y., Harris, L. K. and Azzawi, M. (2019) 'Tetramethoxystilbene-Loaded Liposomes Restore Reactive-Oxygen-Species-Mediated Attenuation of Dilator Responses in Rat Aortic Vessels Ex vivo.' Molecules (Basel, Switzerland), 24(23).
- Farooq, A., Shukur, A., **Astley, C.**, Tosheva, L., Kelly, P., Whitehead, D. and Azzawi, M. (2018) 'Titania coating of mesoporous silica nanoparticles for improved biocompatibility and drug release within blood vessels.' Acta biomaterialia. England, 76, August, pp. 208–216.

Published Conference Abstracts

- **Astley, C.**, Houacine, C., Wilkinson, F. L., Lightfoot, A., Singh, K., Whitehead, D., Alexander, Y. and Azzawi, M. (2019) 'Resveratrol-Loaded Nanostructured Lipid Carriers Restore Dilator Function Following Acute Pressure Elevation, Ex Vivo.' JOURNAL OF VASCULAR RESEARCH. ALLSCHWILERSTRASSE 10, CH-4009 BASEL, SWITZERLAND: KARGER, 56(1) p. 7.

List of Scientific Meetings Attended

2020

1. British Microcirculation Society Meeting, Southampton. Oral presentation.

2019

1. British Society for NanoMedicine, Glasgow. Oral presentation. Awarded second place oral presentation prize.
2. Manchester Metropolitan University Science and Engineering Symposium. Poster presentation. Awarded first place poster presentation prize.
3. European Vascular Biology Organisation, Maastricht, Netherlands. Poster presentation.

2018

1. Northern Vascular Biology Forum, Bradford. Poster presentation.
2. British Society for Cardiovascular Research, Manchester. Poster presentation.
3. British Society for NanoMedicine, London. Poster presentation.

2017

1. Manchester Metropolitan University Science and Engineering Symposium. Poster presentation.
2. European Nanomedicine Meeting, London. Poster presentation.
3. British Society for Cardiovascular Research, Manchester. Poster presentation.
4. International Symposium on Resistance Arteries, Manchester. Poster presentation.

2016

1. Northern Vascular Biology Forum, Hull. Poster presentation.

Thesis Structure

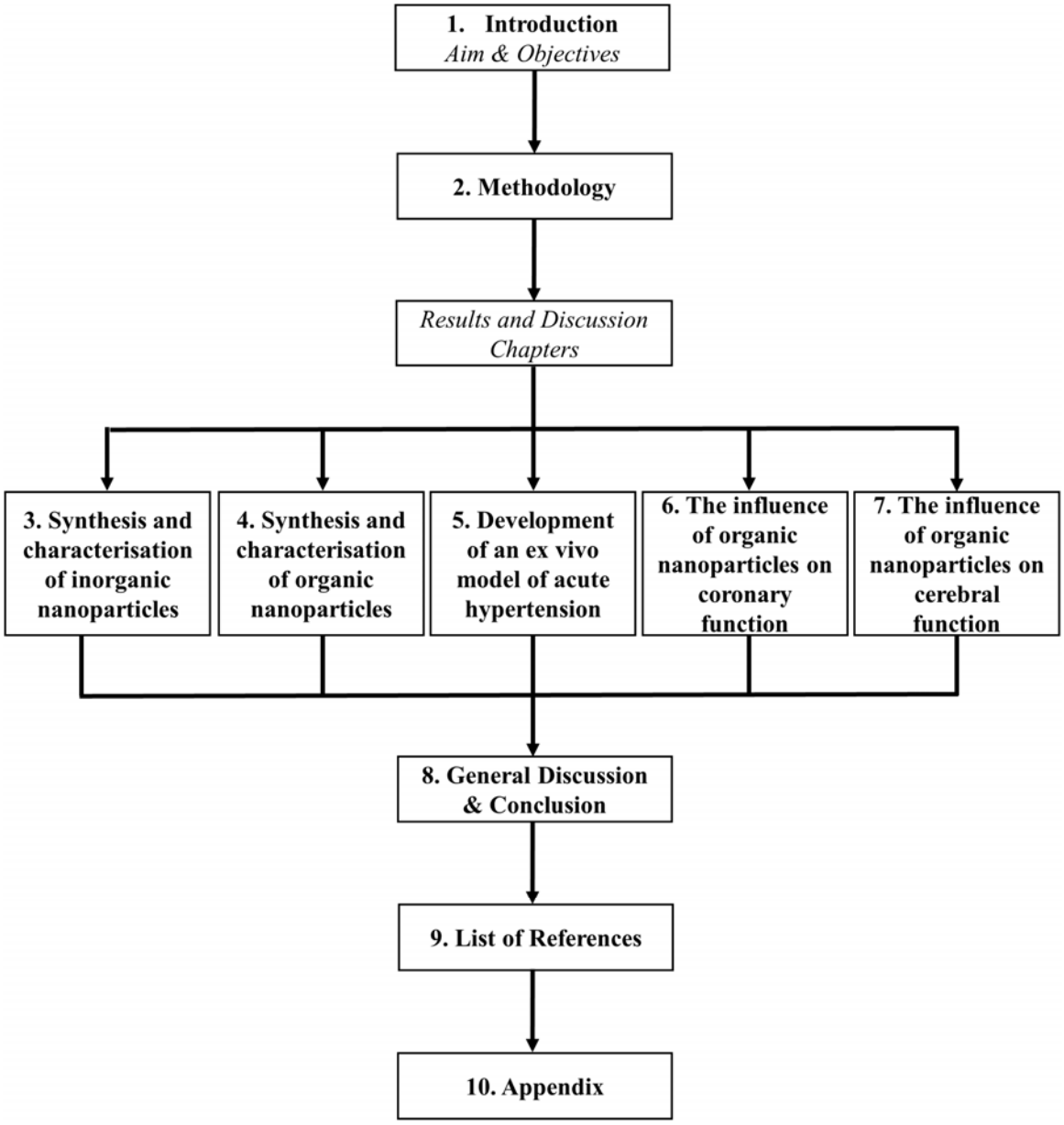

Abstract

Nanoparticles are emerging drug delivery platforms for improved stability and bioavailability of drugs and vasoprotective nutraceutical compounds, such as resveratrol (RV) for the treatment of cardiovascular disease (CVD). Hypertension is a significant contributor to CVD, and while its pathophysiology is unclear, oxidative stress is thought to be a key contributor. It is evident that there is a growing need for treatment strategies to prevent future cardiovascular events. This project aimed to develop a potential therapeutic tool for the treatment of CVDs associated with oxidative stress.

Nanoparticles (inorganic and organic) were synthesised and characterised using a range of chemi-analytical techniques and their potential for the delivery of nutraceutical compounds assessed. The effects of the drug-loaded nanoparticles were assessed using human coronary artery endothelial cells (HCAECs) *in vitro* and using a developed model of acute hypertension in isolated coronary and cerebral vessels to replicate an oxidative environment. Silica nanoparticles (SiNPs) functionalised with cerium oxide (CeO_2) reduced SiNP surface reactivity and demonstrated antioxidant capacity, improving biocompatibility *in vitro*. Uptake of novel RV-loaded NLCs (RV-NLCs) by HCAECs maintained their viability and reduced both mitochondrial and cytosolic superoxide levels; vessel incubation in RV-NLCs restored the magnitude of dilation via NO following acute pressure elevation, mediated via AMPK in the coronary artery. In contrast, organic nanoparticles (RV-NLCs and TMS-liposomes) were incapable of restoring elevated pressure induced attenuated dilation in cerebral arteries, suggesting alternate mechanisms of impairment.

Findings from the present study support the use of nanoparticles for the treatment of CVD, whereby they offer improved biocompatibility, potency and sustained drug release into the vasculature; whilst also highlighting the tissue-specific variability in treatment responses, hence a need for in-depth, comparative studies in the development of novel clinical solutions.

Chapter 1: Introduction

1.1 Nanomedicine

The field of nanomedicine has advanced exponentially since its establishment in the 1990s and is focused on the development and application of nanotechnology for the diagnosis, prevention and treatment of disease. Interest has been heightened due to current constraints and limitations conferred by conventional treatments, including; the unspecific targeting of drugs, toxicity, and inadequate bioavailability. Nanoparticles have become widely adopted in the nanomedical field in recent years due to their ease of synthesis, adaptability and potential use within a variety of biomedical disciplines. Whilst the precise definition of a nanoparticle is disputed amongst scientific and international regulatory corporations, it is generally defined as a nano-object with all three external dimensions in the nanoscale; ranging in size from approximately 1-100 nm (Royaume, 2011). At the nanoscale, nanoparticles exhibit novel physicochemical properties, distinct from those of their conventional bulk chemical equivalents, typically attributed to an increased surface area to volume ratio and heightened reactivity. These unique properties, as well as the versatility of nanoparticles, owing to the extensive range of material composites and surface chemistry available, have resulted in the application of nanoparticles for diagnosis and therapeutic intervention. Whilst oncology was the first field to harness the properties of nanoparticles for drug delivery, with several formulations receiving clinical approval to date; interest in the development of cardiovascular nanomedicines is now growing and is supported by a significant increase in promising laboratory and clinical research (Flores et al., 2019). This thesis will focus on the use of nanoparticles to target the vasculature with the long-term goal of vascular disease treatment.

1.2 The use of nanoparticles as a drug delivery modality in the treatment of cardiovascular disease

Nanoparticles are exceedingly adjustable in terms of size, shape and surface functionalisation, allowing specific alterations to suit distinct requirements, such as; targeted and optimised drug release, enhanced circulation and/or clearance time (Figure 1.1). Furthermore, the underlying material composition of nanoparticles can significantly alter their properties, with various materials hosting diverse intrinsic effects (Tong et al., 2009; Wahajuddin and Arora, 2012). Nanoparticles may be sub-categorised according to their material composition as organic, (including liposomes and nanolipid carriers) or inorganic, (including silica and cerium oxide nanoparticles). Both physical and surface characteristics are significant in determining how nanoparticles interact with their environment; where size, shape, and surface charge can directly influence the efficiency, mode of uptake and circulation time (Huang et al., 2010; Gramatke, 2014; Suk et al., 2016).

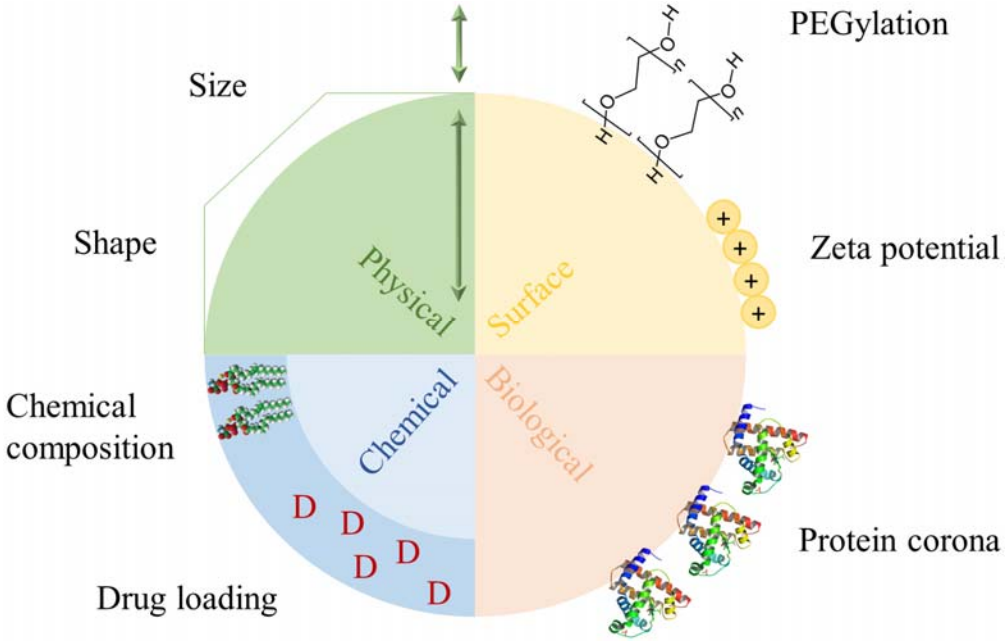

Figure 1.1. A schematic illustration of the variable physicochemical characteristics of nanoparticles. *Nanoparticle synthesis is highly versatile, with a variety of adjustments available. These modifiable components include physical characteristics such as size and shape; surface modification via the alteration of surface charge (zeta potential) or addition of glycol groups (PEGylation); interactions with biological components resulting in corona formation; and changes in chemical composition and potential drug loading. Adapted from* (Borgos et al., 2017).

Common pharmacological treatment strategies are principally concerned with maximising therapeutic delivery and/or exposure time; hence, it is evident that the large surface area conferred by vascular endothelial cells is vitally important as it constitutes the first site of exposure to any systemically delivered drug/compound. However, very little is known about the potential vascular effects of introducing nanoparticles into the systemic circulation. The variable size and function of vessels, as well as the increased reactivity and exposure of nanoscale compounds to cellular proteins and endothelial beds, make it imperative that the underlying effects are appropriately assessed prior to clinical use. This project will assess the potential use of these nanoparticles (inorganic & organic) in the restoration of endothelial

dysfunction using an *ex vivo* model of hypertension and hence, evidence implicating these nanoparticles in the treatment of CVD will be discussed in further detail below.

1.2.1 Inorganic Nanoparticles

1.2.1.1 Silica Nanoparticles

Silicon dioxide (SiO_2) nanoparticles, otherwise known as silica nanoparticles (SiNPs), are non-metal oxides extensively utilised in the biomedical sector, with applications in bio-sensing, drug-delivery and imaging-diagnostics (Wunderbaldinger et al., 2002; Li et al., 2010; Masood, 2016). The rapid adoption of SiNPs can be attributed to several factors including, low cost; ease of fabrication; and of particular interest, their well characterised and tunable surface chemistry. The fabrication of SiNPs results in a high density of silanol groups (Si-OH) on the particle surface, increasing their solubility, making them highly effective within *in vivo* applications. Combined with their large surface area to volume ratio, allowing efficient interaction with biological material, SiNPs provide an excellent therapeutic delivery platform and biomedical research imaging tool.

The addition of different dyes and a range of modifications to surface groups allows the creation of multimodal nanoparticles for theranostic applications, e.g. the incorporation of an imaging component along with a therapeutic payload. These properties have resulted in the successful use of mesoporous silica nanoparticles (MSNs) as a potential delivery platform for the release of vasodilator drugs into tissues *ex vivo* and in *in vivo* cardiovascular disease (CVD) models (Farooq et al., 2016, 2018; Hou et al., 2018). Whilst the health effects of SiNPs have been widely investigated and are considered largely biocompatible both *in vitro* and *in vivo* (Lai et al., 2003; Lu et al., 2007, 2010); biocompatibility is highly dependent

on size, dosage, cell type and production method (Asefa and Tao, 2012; Gramatke, 2014). Furthermore, several studies have implicated surface group reactivity as a critical modulator of biocompatibility, implicating SiNP mediated oxidative stress in the generation of reactive oxygen species (ROS) and as an inducer of cytotoxicity both *in vitro* and *in vivo* (Corbalan et al., 2012; Ahamed, 2013; Duan et al., 2013a).

In order to assess the biocompatibility of SiNPs in the cardiovascular system, studies from the Azzawi group focus on the use of isolated vessels; demonstrating that the influence of SiNPs on dilator responses is dependent on size, surface charge, dye-encapsulation, as well as vessel diameter. For example, isolated conduit arteries were incubated *in vitro* with SiNPs of variable size (100 nm or 200 nm) and charge (positive and neutral). In response to cumulative doses of acetylcholine (ACh; 0.01 μM - 1.0 mM) and sodium nitroprusside (SNP; 0.01 -10 μM), endothelial-dependent and -independent responses were assessed prior to and following 30-minutes incubation with SiNPs (1 x 10^{11} NPs/ml), respectively. SiNPs had no significant impact on dilator responses, however, positively charged SiNPs resulted in greater attenuation compared to non-modified, suggesting the effects of surface modification may be more pronounced in comparison to size (Akbar et al., 2011). Subsequent studies built upon these findings, demonstrating that attenuation was more specifically related to surface area rather than size, as well as dye-encapsulation (Farooq et al., 2014a). A study on the influence of SiNP dosage (1.01 x 10^{11} and 5.32 × 10^{11} NPs/ml) on small mesenteric arterial function, both *ex vivo* and *in vivo* demonstrated that exposure to 5.32 × 10^{11} NPs/ml *ex vivo,* under static conditions, attenuated endothelial-dependent ACh dilator responses (ACh, 10^{-13}-10^{-3} M); whereas lower SiNP dosages (1.01 × 10^{11} NPs/ml) had no effect (Shukur et al., 2016). The endothelial-independent (SNP) vasodilator responses were unaffected by incubation in SiNPs, suggesting impairment was localised to the endothelial cells and not vascular smooth muscle cells (VSMC). In contrast, when

administered *in vivo*, SiNPs only had a detrimental effect on endothelial-dependent (ACh) dilator responses at lower concentrations. Furthermore, inhibition studies demonstrated the attenuated dilator responses observed following SiNPs exposure to be related to alterations in the production and/or release of endothelial-derived relaxing factors. This study will investigate the potential to reduce SiNP-mediated oxidative stress using the antioxidant mimetic, cerium oxide.

1.2.1.2 Cerium oxide

Cerium oxide (CeO_2) is a rare-earth element belonging to the lanthanide series of the periodic table. One of CeO_2's most notable qualities is its ability to exist in both trivalent (Ce^{3+}) or tetravalent (Ce^{4+}) oxidation states, in comparison to that of its lanthanide counterparts which exist primarily in a trivalent state. Progressive advancements within material science have stimulated research into their potential use as therapeutic agents, owing to their antioxidant-mimetic activity. CeO_2 nanoparticles (CeNPs) have demonstrated their capacity to actively scavenge a range of ROS both *in vitro* and *in vivo*, owing to the active redox cycling between Ce^{3+} and Ce^{4+} ions on the nanoparticle surface (Hirst et al., 2013; Fiorani et al., 2015; Kwon et al., 2016; El Shaer et al., 2017). The ratio of Ce^{3+} / Ce^{4+} sites on the nanoparticle surface is strongly associated with antioxidant activity; with initial studies having identified the ability to catalyse the dismutation of superoxide ($O_2^{\bullet-}$) into hydrogen peroxide (H_2O_2)(Korsvik et al., 2007). Subsequent studies investigated these mechanisms, demonstrating that CeNPs synthesised with a higher ratio of Ce^{3+} displayed heightened SOD-mimetic efficiency (Heckert et al., 2008); whilst counterparts fabricated with higher Ce^{4+} displayed catalase (CAT)-mimetic activity in the presence of H_2O_2 (Rzigalinski et al., 2006). Collectively, both studies demonstrate the importance of the nanoparticle surface on the regulation of catalytic activity, whether as a predominant SOD- or CAT-mimetic. These

properties are highly dependent on the mode of synthesis, purity of reagents and method of surface functionalisation.

Several groups have examined the effects of CeNPs on cell viability and vascular reactivity. Gojova *et al.* discovered that CeO_2 was largely non-toxic in human aortic endothelial cells following 4-hours exposure, resulting in significantly less inflammation in comparison to materials such as zinc oxide or yttrium oxide, even at the highest dosages (Gojova et al., 2009). They have also been shown to improve vascular dysfunction in hypertensive rats via the reduction of ROS (Minarchick et al., 2015), apoptosis (Chen et al., 2014), and promotion of angiogenesis through the modulation of oxygen within intracellular environments (Das et al., 2012). Vascular function studies within the Azzawi group have demonstrated that the use of CeNP conjugated SiNPs resulted in partially restored vasodilatory function in murine aortic vessels *ex vivo* (Farooq, 2014), suggesting CeO_2 has a capacity to be used as a therapeutic tool for the treatment of ROS associated diseases. These studies highlight the need for improved biocompatibility of SiNPs and potential of CeO_2 as a means of attenuating ROS-mediated toxicity; however, further assessment into their safety is essential prior to clinical application. This study will investigate whether CeO_2 modification of SiNPs can improve their biocompatibility using isolated human coronary artery endothelial cells (HCAECs), offering a potential mechanism for antioxidant delivery.

1.2.2 Organic Nanoparticles

1.2.2.1 Liposomes

Lipidic delivery systems have gained popularity due to their improved biocompatibility when compared with inorganic nanoparticles such as silica; furthermore, they possess the ability to cross challenging physiological barriers (e.g. the blood-brain barrier). They can be categorised according to their mode of synthesis and physicochemical characteristics; one of the most heavily investigated of these is liposomes. Liposomes are spherical vesicles composed of a phospholipid bilayer made of cholesterol, other natural lipids and an aqueous core (Pattni et al., 2015). To date, several liposome formulations have received clinical approval and are used for pain management (e.g. DepoDur®), cancer treatment (e.g. Doxil®), and vaccine delivery (e.g. Inflexal®)(Li et al., 2019); however, none are currently available for the treatment of CVD. Whilst useful, liposomes are limited in their potential applications because of short shelf-life, poor stability and low encapsulation efficiency; stimulating research into the generation of more reliable, robust delivery modalities.

1.2.2.2 Nanolipid carriers

Nanostructured lipid carriers (NLCs) are an emerging drug delivery platform developed to overcome the limitations affiliated with previous-generation counterparts (such as liposomes). In contrast to liposomal delivery systems, NLCs can be administered intravenously or orally, increasing patient stratification and improving outcome. However, the most notable improvement associated with NLCs is their improved drug loading capacity, primarily attributed to their mode of fabrication. NLCs have been shown to increase the bioavailability of poorly soluble antihypertensive drugs (Cirri et al., 2018; Khan

et al., 2018) and vasoprotective nutraceutical products (Magyar et al., 2012; Theodotou et al., 2017), protecting contents from rapid metabolism, whilst also allowing fine manipulation of release kinetics (Burns et al., 2002; Teskac and Kristl, 2010; Neves et al., 2013). The development of site-specific delivery systems that have the potential to preserve drug stability whilst enhancing bioavailability is an attractive option (Shah et al., 2016).

NLC fabrication involves the use of a mixture of liquid and solid lipid, resulting in the formation of partially crystallised lipid matrix dispersed within an aqueous phase containing emulsifiers, enhancing drug loading (within matrix imperfections) and reduced leaching of the drug during storage (Khosa et al., 2018). It is well documented that the specific type, concentrations and ratios of lipids, oils and emulsifiers used during fabrication are essential in determining the degradation and release behaviour of NLCs (Khosa et al., 2018). The release profile of NLCs is typically biphasic, characterised by an initial burst release due to the rapid diffusion of contents within the liquid phase of the NLC, and the comparatively slower release of contents from the solid lipid core. The unique chemical structure of individual lipids, such as that of the triglyceride triolein, have demonstrated the potential to disrupt the packing of trimyristin crystals, altering the release kinetics of NLCs (Yang et al., 2014). For the first time, this project will assess the use of novel trimyristin (solid lipid) based NLCs stabilised with the triglyceride, triolein (liquid lipid) for improved stability, encapsulation efficiency and sustained delivery of antioxidant compounds for the treatment of CVD.

1.3 Hypertension – A clinical perspective and unmet need for innovative treatment strategies

Hypertension is a significant contributor to CVD, characterised by a persistent elevation of arterial blood pressure, and is the most prevalent risk factor associated with cardiovascular morbidity and mortality. Due to global acculturation to the western lifestyle, the incidence of hypertension has increased exponentially since 1990, accounting for 14% of total deaths (Forouzanfar et al., 2017). Despite extensive study, the multifactorial nature of hypertension makes its pathophysiology unclear; however, much attention has been focused on the vascular endothelium, which has been shown to be aberrantly regulated in hypertension in the presence of oxidative stress (Massaro et al., 2019). The vascular endothelium is integral in the maintenance of vascular health, regulating a multitude of processes, including vascular tone. Although it is unknown if dysfunction of the vascular endothelium is the cause or consequence of hypertension, it is evident that there is a growing need for treatment strategies that target the direct cause of the disease or help manage its associated symptoms. Antioxidants are an attractive therapeutic strategy; however, many suffer from low bioavailability and poor stability. This thesis will investigate the use of nanoparticles for the improved delivery and release of drugs for the treatment of hypertension associated endothelial dysfunction. Hypertension associated endothelial dysfunction will be discussed in further detail in this chapter; hence, an overview of the mechanisms regulating vessel diameter will first be provided below.

1.3.1 Regulation of vessel diameter

The vascular endothelium is a highly differentiated monolayer of simple squamous epithelium which plays an integral role in regulating a multitude of critical processes including vascular permeability, immune responses, coagulation/anticoagulation cascades and vascular tone (Krüger-Genge et al., 2019). The regulatory function of the endothelium is heavily reliant on its ability to detect ions, agonists and physical forces, as well as its interactions with the surrounding VSMC layer; which is critical in providing structural integrity to the blood vessel wall and maintaining vascular tone, through dynamic modulation of constriction and dilation, in response to mechanical and vasoactive stimuli (external or endothelial-derived). Arteries release a range of dilators via three major pathways, including; nitric oxide (NO); prostaglandin (PGI); and endothelial-derived hyperpolarising factor (EDHF) -dependent pathways, the distribution of which are vascular bed and size-specific. These are briefly described below.

1.3.1.1 Nitric oxide

Nitric oxide (NO) was the first gaseous molecule discovered that was produced by the endothelium and led to the relaxation of VSMCs (Furchgott and Zawadzki, 1980). The production and release of NO from the endothelium are mediated by NO synthases (NOS), including endothelial NOS (eNOS), promoting the conversion of L-arginine into stoichiometric L-citrulline (Tejero et al., 2019). NO diffuses out of the endothelial cells into surrounding VSMCs, stimulating the activation of Protein Kinase G (PKG); promoting ion channel activation (e.g. large-conductance Ca^{2+} activated K^{+} channels (BKCa)), Ca^{2+}

reduction (e.g. sarcoplasmic reticulum mediated sequestration, plasma membrane extrusion) and activation of the myosin light-chain phosphatase apparatus.

1.3.1.2 Prostacyclin

Prostacyclin (PGI_2) is a cyclooxygenase (COX) derived metabolite, produced within endothelial cells in response to mechanical, endogenous and pharmacological agonist stimulation. The production of PGI_2 is heavily reliant on the release of arachidonic acid (AA) from phospholipids by the enzyme phospholipase A_2 (PLA_2); the activity of which is determined by intracellular calcium concentrations. Following its release, AA is converted into a range of prostanoid mediators (such as PGI_2) by COX-1 and COX-2 enzymes. PGI_2 is a lipid-soluble compound capable of traversing cellular membranes, readily diffusing out of endothelial cells and binding to prostacyclin receptors (IP) on the VSMC surface. The activation of IP receptors results in vasorelaxation by activating adenylate cyclase (AC), which leads to the production of cyclic adenosine monophosphate (cAMP). Elevated cAMP leads to the activation of protein kinase A (PKA), which subsequently phosphorylates myosin light chain kinase; reducing constriction and promoting dilation (Mitchell and Kirkby, 2019).

1.3.1.3 Endothelial hyperpolarisation

Endothelial hyperpolarisation is a consequence of potassium (K^+) efflux, with several mechanisms known to exist that can induce endothelial and VSMC hyperpolarisation. The process involves the activation of endothelial K^+ channels; the small (SK_{Ca}) and intermediate (IK_{Ca}) conductance Ca^{2+}-sensitive K^+ channels. The electrical coupling of cells within the

endothelial and VSMC layer promotes the propagation and subsequent hyperpolarisation and closing of voltage-gated K^+ channels in VSMCs. Alternatively, K^+ efflux may result in the activation of sodium/potassium channels (Na^+/K^+). Endothelium-derived hyperpolarizing factor (EDHF) is the third class of endothelial-derived vasodilator identified since the initial observations of researchers in the 1980s, demonstrating that an endothelial-derived substance was capable of inducing VSMC hyperpolarisation in NOS and COX-independent experimental models, elegantly reviewed elsewhere (Goto and Kitazono, 2019). Several substances have been found to induce VSMC hyperpolarisation directly and are hence called EDHFs, including; epoxyeicosatrienoic acids (EETs), potassium ions (K^+) and H_2O_2 (Ellinsworth et al., 2016). Epoxyeicosatrienoic acids (EETs) are metabolically derived products of cytochrome P450 epoxygenases (CYP450) and arachidonic acid (AA) (Imig, 2016). Following their synthesis, EETs traverse the extracellular compartment, leading to VSMC hyperpolarisation and relaxation via the activation of large-conductance BK_{Ca}^+ channels (Yang et al., 2015). H_2O_2 is a metabolic by-product of cellular metabolism in aerobic organisms, primarily produced through the dismutation of $O_2^{\bullet-}$ by the enzyme superoxide dismutase (SOD). Despite the reputation of H_2O_2 as a cell-damaging oxidative agent, recent studies have suggested H_2O_2 plays an integral role in cell signalling and K^+ release. Whereas ROS such as $O_2^{\bullet-}$ have previously demonstrated an ability to attenuate endothelium-dependent relaxation, H_2O_2 has been found to promote endothelium-dependent as well as independent responses, mediating hyperpolarisation via the activation of endothelial K^+ channels; however, there is considerable species-specific variation in the type of K^+ channels activated (Shimokawa, 2010) (Figure 1.2).

It is clear that the types of mediators elaborated during endothelium-dependent relaxation vary according to the particular vascular bed as well as vessel size. Experimental studies suggest that the role of endothelial-derived hyperpolarisation (EDH) increases as the vessel

size decreases, whereby EDHF activity predominates in resistance vessels, often compensating for any reduced NO availability. The respective contribution of these pathways in mediating endothelial-dependent dilator responses in an *ex vivo* model of hypertension will be assessed, using pressure myography.

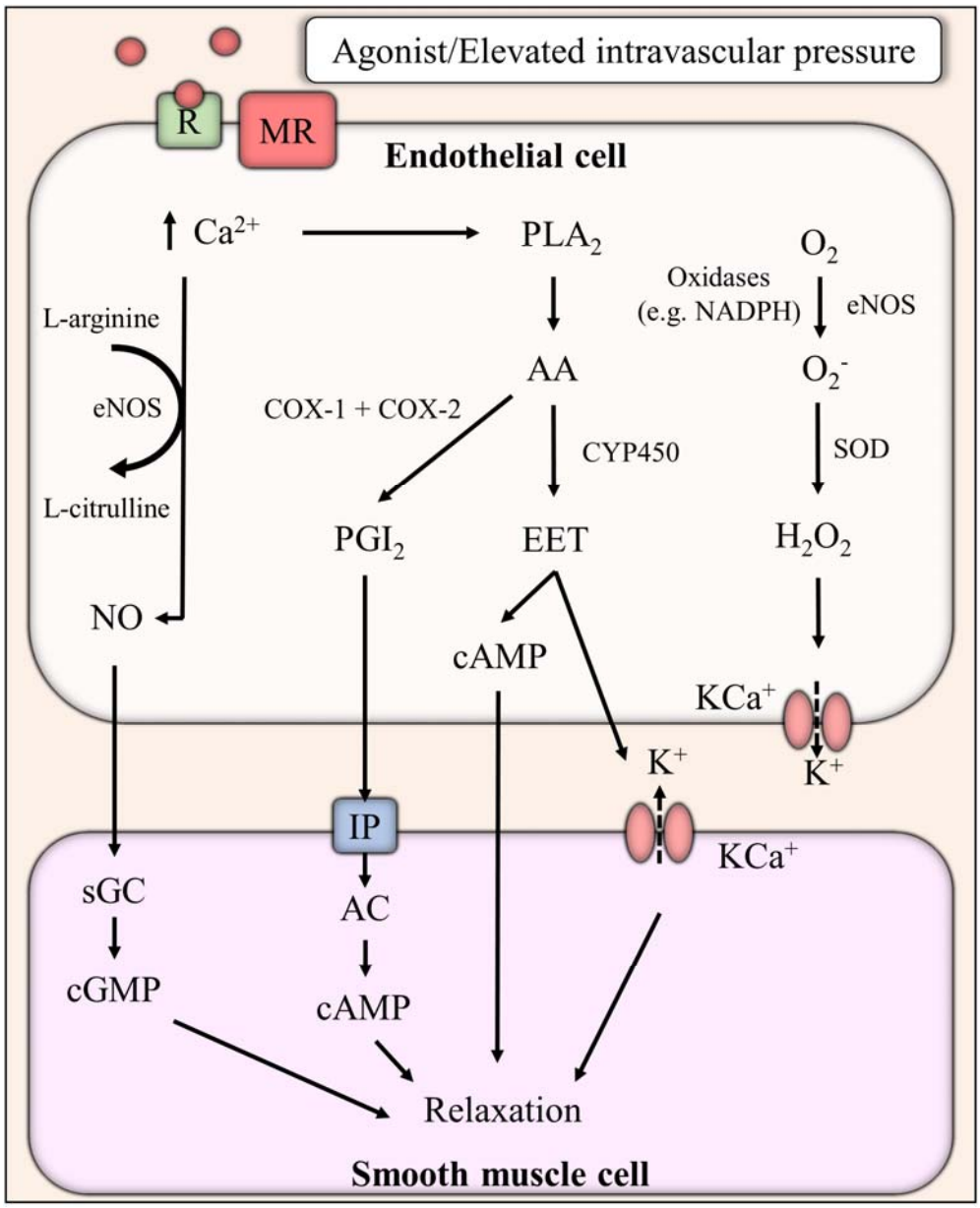

Figure 1.2. Mechanisms for endothelial cell mediated relaxation. *Activation of agonist-sensitive (ACh) or mechanosensitive (shear stress) receptors leads to elevated intracellular Ca^{2+}, resulting in the activation of NO-, PGI- and EDHF-dilator pathways. Endothelial nitric oxide synthase (eNOS); nitric oxide (NO); prostacyclin I2 (PGI_2); arachidonic acid (AA); cytochrome P450 (CYP450); epoxyeicosatrienoic acid (EET); oxygen (O_2);*

superoxide ($O_2^{\bullet-}$); hydrogen peroxide (H_2O_2); soluble guanylate cyclase (sGC); cyclic guanosine monophosphate (cGMP); prostacyclin receptor (IP); adenylate cyclase (AC); cyclic adenosine monophosphate (cAMP); calcium (Ca^{2+}); calcium activated potassium channel (KCa^{+}); phospholipase A2 (PLA_2); cyclooxygenase 1 & 2 (COX-1 & COX-2); receptor (R); mechanoreceptor (MR). Adapted from (Ozkor and Quyyumi, 2011).

1.3.2 Mechanism of impaired dilation in hypertension

1.3.2.1 Endothelial dysfunction

Endothelial dysfunction is a pathological condition of the vascular endothelium, associated with elevated oxidative stress and modulation of pathways important for the control of systemic vascular resistance, including NO (Hamilton et al., 2001; Hendre et al., 2013). Decreased bioavailability of NO has been observed in several experimental models of hypertension, resulting in elevated vascular resistance and blunting of vasodilator responses to endothelium-dependent vasodilator agonists (Watt and Thurston, 1989; Linder et al., 1990; Deng et al., 1995; Adler and Huang, 2002; Paulis et al., 2008). Studies have also shown that endothelial-independent dilator responses caused by dilators such as nitro-glycerine remained unchanged, suggesting the aberrant function was related to the endothelium and not the VSMCs. Studies have recapitulated these findings, demonstrating the importance of NO in the resistance vasculature, with inhibitors of eNOS or NO attenuating dilation and promoting constriction (Hsieh et al., 2004); restorable following NO donor administration (Torok and Kristek, 2002). The reduced bioavailability of NO in endothelial dysfunction is concurrently associated with elevated ROS production; chemically reactive compounds with oxidative capacity, damaging proteins, carbohydrates, lipids and DNA. ROS are known to scavenge NO, reducing its bioavailability within endothelial cells. Furthermore, studies have demonstrated the ability of ROS by-products (e.g. peroxynitrite) to inhibit PGI_2 synthase via tyrosine nitration (Zou, 2007), as well as inactivate EDH receptors (Brzezinska et al., 2000;

Yanping et al., 2002). The resulting imbalance of these critical mediators leads to an impairment of endothelium-dependent vasodilatory responses (Craige, 2015).

1.3.2.2 Reactive oxygen species

Multiple endogenous examples of ROS exist in mammalian biology, including, $O_2^{\bullet-}$ and hydroxyl radical ($^{\bullet}OH$). Although not strictly considered free radicals, H_2O_2 and peroxynitrite ($ONOO^-$) obtain a similar classification due to their wide-spanning oxidative effects. Several sources of ROS production have been identified, though three have been studied extensively within the cardiovascular system; xanthine oxidase; NADH/NAD(P)H oxidase; and NO synthase. Studies have suggested that NADH/NADPH oxidases are the key enzyme complex and predominant source of $O_2^{\bullet-}$ (Lennicke et al., 2015; Panday et al., 2015). eNOS is a CYP450 enzyme responsible for the catalysation of flavin mediated electron transport from NADH donor molecules. In order to promote the active production of NO, eNOS requires the binding cofactor tetrahydrobiopterin (BH_4), or sapropterin as it is otherwise known, and is thought to interact with L-arginine, synthesising NO (Bendall et al., 2013). The oxidative depletion of this essential cofactor has been shown to shift eNOS from a dimeric to a monomeric form, becoming uncoupled; this process referred to as eNOS uncoupling and is associated with the formation of $O_2^{\bullet-}$, H_2O_2 and secondary by-products such as $ONOO^-$; propagating a self-perpetuating cycle of free radical formation. The significance of BH_4 and its contribution to eNOS uncoupling has been demonstrated on several occasions, whereby BH_4 supplementation lowered systemic blood pressure and restored attenuated endothelial-dependent dilator responses in models of hypertension (Khoo et al., 2005; Porkert et al., 2008; Francis et al., 2018).

In addition to impaired dilator bioavailability, the production of ROS can facilitate and exacerbate the appearance of conditions associated with cardiovascular complications (e.g. atherosclerosis); including the generation of oxidised low-density lipoprotein and the activation of immunoregulatory transcription factors (Rhoads and Major, 2018). Several endogenous defence mechanisms have evolved to afford protection and mitigate oxidative damage in tissues, the most notable being SOD and CAT. SOD is a biological enzyme found within the cytoplasmic compartment and mitochondria and is one of the body's primary defence mechanisms, eliminating $O_2^{\bullet-}$ through a two-step dismutation reaction, producing H_2O_2 and O_2 (Fukai and Fukai, 2011). Through comparable mechanisms, CAT converts H_2O_2 into chemically inert H_2O and O_2. In addition to endogenous sources of ROS, several exogenous sources of ROS are implicated in the generation of oxidative stress; including, smoke, pollutants, radiation and drugs (Prasad et al., 2017). In the vasculature, oxidative stress has demonstrated its ability to interfere with endothelial derived relaxing factor (EDRF) signalling in a range of models and vascular beds, resulting in attenuated dilator responses (Salheen et al., 2015; Zaabalawi et al., 2019). Small size arteries, such as those found within the coronary and cerebral vasculature, play a vital role in the regulation of peripheral resistance; however, due to their elevated metabolic demand, they are highly susceptible to oxidative injury. As such, these vascular beds will be the primary focus for the duration of this investigation.

1.3.2.3 Coronary artery dilation

The coronary arteries play a pivotal role in providing a continuous supply of oxygen and nutrients to the metabolically active myocardium of the heart. The maintenance of normal vascular function is integral to health since a disruption may precede the development of conditions such as atherosclerosis or present as clinical manifestations such as myocardial ischemia (Biswas and Khan, 2019). Multiple studies have attempted to clarify the

mechanistic regulation of dilation in the coronary arteries in order to combat disease; however, limited studies have focused on characterising the underlying dilator component since the turn of the century. In the healthy coronary endothelium, NO is believed to be the dominant vasodilator; with inhibition increasing basal coronary vascular resistance and blunting vasodilator responses to endothelium-dependent vasodilator agonists (Beverelli et al., 1997).

Furthermore, incubation with COX inhibitors have demonstrated an ability to significantly impair endothelial-dependent dilation, indicating that a portion of dilator component is mediated by endogenous prostanoids (Hiroto and Gutterman, 1998); however, the effects of endogenous prostanoids have been found to decrease with age both in pigs and humans, which may reflect an age-dependent role in coronary arterial control of tone (Willis and Leffler, 1999; Beyer et al., 2017). In addition to NO- and PGI-mediated responses, the coronary endothelium is known to produce factors resulting in EDH, with inhibition resulting in attenuated dilation (Hiroto et al., 1999; Toyotaka et al., 2003). However, as discussed previously, EDRF release is known to be not only species-dependent but also tissue bed and vessel size-dependent also. In the dog coronary artery, responsiveness to different relaxing factors was found to differ between proximal and distal parts of the vessel; suggesting that ACh-induced dilation in large coronary arterioles is predominantly mediated by NO, whereas both NO and EDHF mediate dilation in small arterioles (Nagao et al., 1992; Nishikawa et al., 1999). There is evidence to suggest that under physiological conditions, the production of EDHF is dampened by NO via feedback inhibition. Impaired NO synthesis may thus, at least in part, maintain endothelial vasodilator function (Bauersachs et al., 1996). However, whilst studies state the vessel (e.g. coronary), a significant quantity fail to specify the precise size or location from which the vessel was taken, producing difficulty in applying findings in the appropriate experimental context. Thus, there are complex anatomical,

biochemical, and functional interrelationships between NO and EDHF that are still incompletely defined.

1.3.2.4 Cerebral artery dilation

The cerebral arteries are responsible for regulating the perfusion of blood into the cerebrum of the brain; stimulating significant interest in assessing normal function and how this may be implicated in disease (e.g. hypertension, vascular dementia). Whilst the distribution of EDRFs within the cerebral vasculature share similarities with that of the coronary artery, i.e. the significance of NO and EDHF, with the size of vessels having a direct effect on dilator component; the cerebrovascular circulation also has distinct variations (Davis et al., 2011). For example, in porcine coronary arteries, abolishment of EDHF–mediated responses require the simultaneous inhibition of both SK_{Ca} and IK_{Ca} (Burnham et al., 2002; Bychkov et al., 2002); whereas inhibition of endothelial cell IK_{Ca} channels alone is sufficient to block EDHF-mediated relaxation and hyperpolarisation in rat middle cerebral arteries (MCAs) in the absence of NO (Alister et al., 2006). There is evidence to suggest that NO is capable of dampening EDHF-mediated responses; however, this is not the case in the MCAs, suggesting that it is also important in the uninjured state in the presence of NO (Schildmeyer and Bryan, 2002). Whilst the differential receptivity to EDRF signalling between vascular beds has briefly been discussed, metabolic and anatomical variations are likely to contribute to vascular regulation and treatment efficacy; it was, therefore, of interest to establish whether an *ex vivo* model of hypertension, discussed below, could be used to assess dilator function in cerebral vessels too.

1.4 Models of acute hypertension

In several forms of hypertension, elevated arterial $O_2^{\bullet-}$ generation is considered a key contributor to the pathogenesis of endothelial dysfunction, leading to decreased bioavailability of NO and the promotion and activation of pathways regulating vascular smooth muscle contraction, contributing to maintenance elevated vascular resistance (Koller and Huang, 1994; Cardillo et al., 1998; Beswick et al., 2001). However, the underlying mechanisms of $O_2^{\bullet-}$ generation in hypertension are not entirely understood. Despite diverse and multifactorial underpinnings, oxidative stress appears to be present in all forms of hypertension, including genetic-, renovascular-, and angiotensin II-induced hypertension, to name a few (Higashi et al., 2002; Mollnau et al., 2002). Some of the first convincing evidence implicating ROS in the pathogenesis of hypertension was conducted by Wei and colleagues in 1985, using a pharmacologically induced model of hypertension. Following the intravenous administration of norepinephrine to feline cerebral arteries, a significant increase in $O_2^{\bullet-}$ generation was observed in the extravascular cranial space, which was maintained for at least an hour after hypertension subsided. The concurrent impairment of ACh induced endothelial-dependent relaxation was restored following the administration of SOD and CAT, implicating $O_2^{\bullet-}$ and H_2O_2 in the attenuation of dilator responses (Wei et al., 1985). Subsequently, De Bruyn and colleagues investigated the relationship between perfusion pressure and ROS generation in the canine coronary artery. Incremental increases in perfusion pressure promoted serotonin (5-HT) mediated constriction, which was restored following incubation with SOD, CAT, and deferoxamine (inhibitor of $^{\bullet}OH$ generation); further implicating the role of $O_2^{\bullet-}$, H_2O_2 and their downstream metabolic by-products in endothelial dysregulation (De Bruyn et al., 1994).

Because of the multifactorial nature and variable pathologies of hypertension, the use of *in vivo* studies, although more physiologically relevant, make experimental cause and effect difficult to ascertain. To clarify the fundamental mechanisms underpinning elevated O_2^- production, researchers investigated whether high pressure itself could lead to the production of oxidative stress *in vitro* in the absence of neurohumoral factors. Functional studies on femoral arteries of Wistar rats subjected to elevated pressure over 30-minutes showed impaired flow-mediated dilation, which was restored following incubation with SOD (Ungvari et al., 2003). These findings are consistent with previous studies, showing short bursts of increased pressure can impair endothelial function (Wei et al., 1985; De Bruyn et al., 1994; Huang et al., 1998; Vecchione et al., 2009). Incubation with apocynin, diphenyleneiodonium (an NADP(H) oxidase inhibitors) and staurosporine/chelerythrine (protein kinase C inhibitors) could prevent $O_2^{\bullet-}$ generation, suggesting elevated pressure leads to the production of $O_2^{\bullet-}$ by inducing PKC-dependent phosphorylation and activation of the NAD(P)H oxidase. Similar findings were found in a chronic hypertension model *in vivo* and *in vitro*, with the presence of humoral factors leading to enhanced PKC-dependent phosphorylation (Ungvari et al., 2004) (Figure 1.3). A summary of studies implicating ROS in the pathogenesis of hypertension can be found in Table 1.

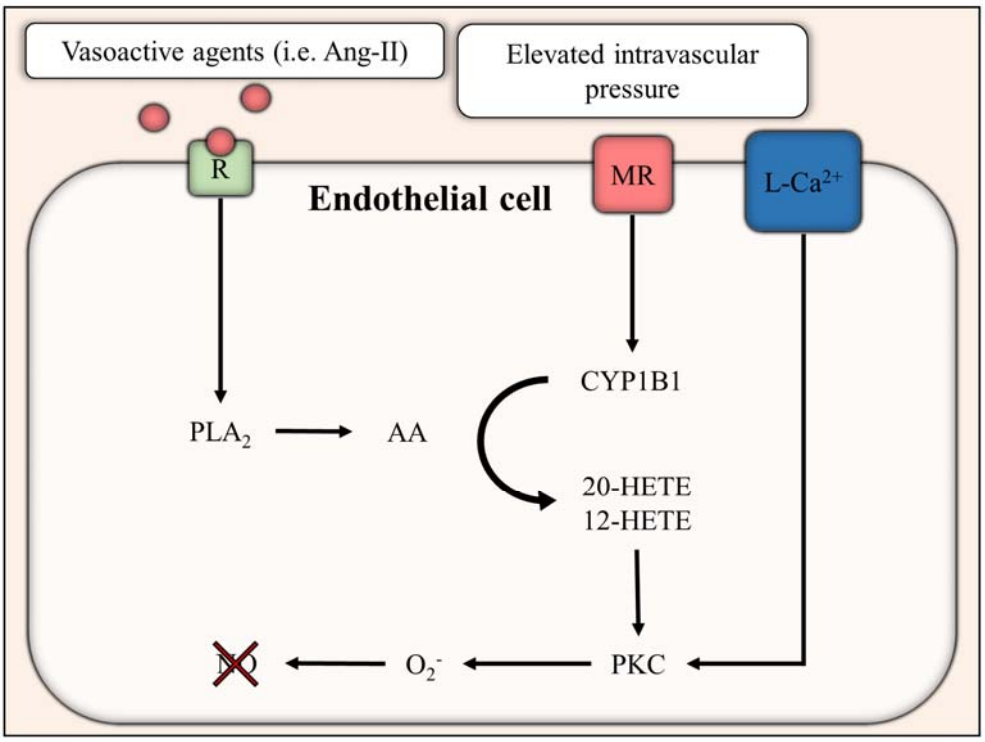

Figure 1.3. Mechanisms of hypertension-induced oxidative stress. *Under normal conditions, vasoactive agents such as Ang-II lead to the activation and release of AA from phospholipids. In the presence of elevated intravascular pressure, mechanoreceptor activation results in the activation of CYP1B1; converting AA into 20- and 12-HETE. HETEs induce the activation of PKC, producing O_2^- as a by-product which leads to the quenching of NO, impairing dilation and promoting constriction. Angiotensin-II (Ang-II); receptor (R); mechanoreceptor (MR); L-type calcium channel (L-Ca^{2+}); phospholipase A_2 (PLA_2); arachidonic acid (AA); cytochrome P450 1B1 (CYP1B1); 20-,12- hydroxyeicosatetraenoic acid (20-, 12-HETE); protein kinase C (PKC); superoxide ($O_2^{\bullet-}$); nitric oxide (NO). Author generated.*

Table 1. Summary of studies utilising acute pressure elevation models.

Author and Date	***In vivo/ex vivo***	**Vascular Bed**	**Aim of the Study**	**The technique of Pressure Elevation/Protocol**	**Results**	**Physiological Response**
Wei *et al*., 1985	Anaesthetised cats *in vivo*	Feline cerebral arteries	Assess superoxide generation in the extracellular cerebral space after acute hypertension.	Intravenous administration of norepinephrine (3-6 μg/min) for 15-minutes.	Elevated superoxide.	▪ Elevated pressure significantly impaired ACh-induced endothelium-dependent vasodilation ($P < 0.05$). ▪ Protected by SOD and CAT.
De Bruyn *et al*., 1994	Anaesthetised dogs *in vivo*	Canine coronary arteries	Examine the role of perfusion pressure and ROS in response to acute hypertension.	Increased perfusion pressure from 80 to 100, 120,150 or 200 mmHg for 15-minutes. Intravenous infusion of Ang II (50-75 μg/min) for 5-minutes.	Elevated ROS, particularly hydroxyl radicals.	▪ Increased perfusion pressure and Ang-II infusion significantly augmented constriction to 5-HT ($P < 0.05$). ▪ Protected by SOD, CAT and deferoxamine (hydroxyl radical scavenger).
Huang *et al.*, 1998	WKY rats *ex vivo*	Gracilis muscle arterioles	Examine the effects of high intravascular pressure on flow- and agonist-induced dilator responses.	Elevated perfusion pressure from 80 to 140 mmHg for 30-minutes, using pressure myography.	Elevated superoxide.	▪ Elevated intravascular pressure significantly impaired endothelium-dependent vasodilation ($P < 0.05$). ▪ Prevented by SOD and CAT, but not CAT alone.
Ungvari *et al.*, 2003	Wistar rats *ex vivo*	Femoral artery	Assess the influence of NADPH oxidase and PKC-dependent signalling pathways in acute hypertension.	Elevated intraluminal pressure from 80 to 160 mmHg for 30-minutes, using pressure myography.	Elevated superoxide.	▪ Elevated pressure significantly impaired endothelium-dependent dilation ($P < 0.05$). ▪ Protected by SOD, apocynin, diphenyleneiodonium, staurosporine and chelerythrine.
Beyer *et al.*, 2014	Human omentum *ex vivo*	Omental arterioles	To elucidate the mechanism of FMD following a transient increase in intraluminal pressure.	Pressure myography. Elevated intraluminal pressure from 60 to 150 mmHg for 30-minutes, using pressure myography.	Elevated superoxide.	▪ Transient pressure elevation induced FMD mediator change from NO to mitochondria derived H_2O_2, which acts as the principal dilator component. ▪ Significantly impaired NO-mediated dilation ($P < 0.05$).

1.5 Antioxidants for the treatment of cardiovascular disease

It is well established that treatment of CVD significantly reduces the risk of morbidity and mortality. Currently, guidelines recommend that the initial treatment of CVD should start with lifestyle intervention (i.e. weight loss, smoking cessation, regular exercise, diet); however, in many cases, pharmacological therapy is necessary (Stewart et al., 2017). Whilst these treatment strategies have demonstrated their effectiveness in mitigating the effects of several CVDs (e.g. hypertension, atherosclerosis, diabetes), they do not appear to target the underlying cause. Given the implications of oxidative stress in the pathophysiology of various cardiovascular disorders, as such, an external supply of antioxidants may circumvent its associated damage, offering an attractive treatment strategy (Jain et al., 2015).

A variety of antioxidants, biologically or chemically derived, are available for the therapeutic management of CVD (Goszcz et al., 2015). In patients with coronary artery disease or hyperglycaemia-induced impairment of vasodilation, NO-mediated vasodilation is restored with either oral (6 g over 2 days) or intra-arterial infusion (24 mg/min for 10 min) of vitamin C (Levine et al., 1996; Beckman et al., 2001). Similarly, antioxidant studies investigating coronary artery risk development in young adults have found that high-plasma carotenoid concentrations are associated with reduced inflammation, oxidative stress, and endothelial dysfunction (Hozawa et al., 2007). Whilst promising, the deliverability of antioxidants is often limited by their poor physicochemical and pharmacokinetic properties, resulting in inadequate systemic bioavailability. Antioxidants obtained from dietary sources play an essential role in regulating oxidative stress via endogenous action or by their synergistic effects on host antioxidants, with several emerging as potential treatment candidates due to their prevalence and noted benefits in treating CVD *in vitro* and *in vivo*;

such as resveratrol and its synthetically methylated analogue trans-3,4,5,4′-tetramethoxystilbene, which will be discussed in further detail, in this section.

Previous work within our laboratory has investigated the effects of resveratrol (RV) *ex vivo* using aged mice as a model of endothelial dysfunction. Following intervention, it was found that RV (45 μM) enhanced ACh induced dilator responses in the femoral arteries of both young and aged mice after one hour, with inhibition studies attributing the enhanced dilator response to elevated NO production. This dilator response was maintained in an eNOS -/- mouse yet was completely abolished in the presence of potassium channel blockers; implicating RV in the stimulation of both NO and EDHF dilator pathways. Furthermore, using high performance liquid chromatography it was demonstrated that RV was rapidly degraded over the one-hour test period, observing an average loss of 27.3 ± 4.6 % (Diaz et al., 2019). Building upon this work, Diaz *et al.* went onto conduct a clinical trial investigating the effects of oral RV administration (300 mg, 3x day) on the dilator responses of older coronary artery disease patients over a three-day period. RV supplementation was found to significantly improve flow-mediated dilation in patients who had undergone coronary artery bypass surgery, highlighting the cardioprotective effects and clinical benefit (Diaz et al., 2020).

Enhancement strategies, such as the encapsulation of antioxidants within nanoparticles for enhanced targeted delivery, may overcome these limitations and will be investigated over the course of this study.

1.5.1 Resveratrol

Resveratrol (trans-3,5,4′-trihydroxystilbene; RV) is a polyphenolic phytoalexin compound derived from a variety of plant species. RV is found in two geometric isomers, *trans* and *cis*. Although both exist concurrently, *trans*-RV is more biologically active and is primarily used in research applications. RV has been shown to enhance blood pressure reduction when combined with traditional anti-hypertensive therapy. This is attributed to its antioxidant and anti-inflammatory properties (Burns et al., 2002), including scavenging a range of ROS moieties (Leonard et al., 2003); upregulating the expression of several antioxidant enzymes (Sayin et al., 2012); and increasing NO production (Thomas et al., 2002), via activation of SIRT-1 (silent mating type information regulation 2 homolog 1 or sirtuin 1) (Arunachalam et al., 2010; Ma et al., 2017) (Figure 1.4). Sirtuins have been extensively studied and identified as playing an integral role in multiple pathways including; metabolism, cell survival, stress resistance, cell senescence, inflammation, and endothelial function. Whether RV is a direct agonist of SIRT-1 or is a consequence of other signalling mechanisms, is unclear.

The involvement of AMPK (adenosine monophosphate-activated protein kinase) as an alternate target has also been proposed, possibly via the inhibition of mitochondrial ATP synthesis (Lan et al., 2008). AMPK mediated signalling promotes an increase in the production of nicotinamide adenine dinucleotide (NAD^+), which has the capacity to indirectly activate SIRT-1. Supporting evidence for this can been observed in AMPK deficient mice, which are resistant to the beneficial metabolic effects conferred by RV. Conversely, other studies have demonstrated the SIRT-1 mediated activation of AMPK via liver kinase B1 (LKB1) (Lan et al., 2008). It is evident that the interactions between SIRT-1 and AMPK play an important role in potentiating the beneficial effects of RV.

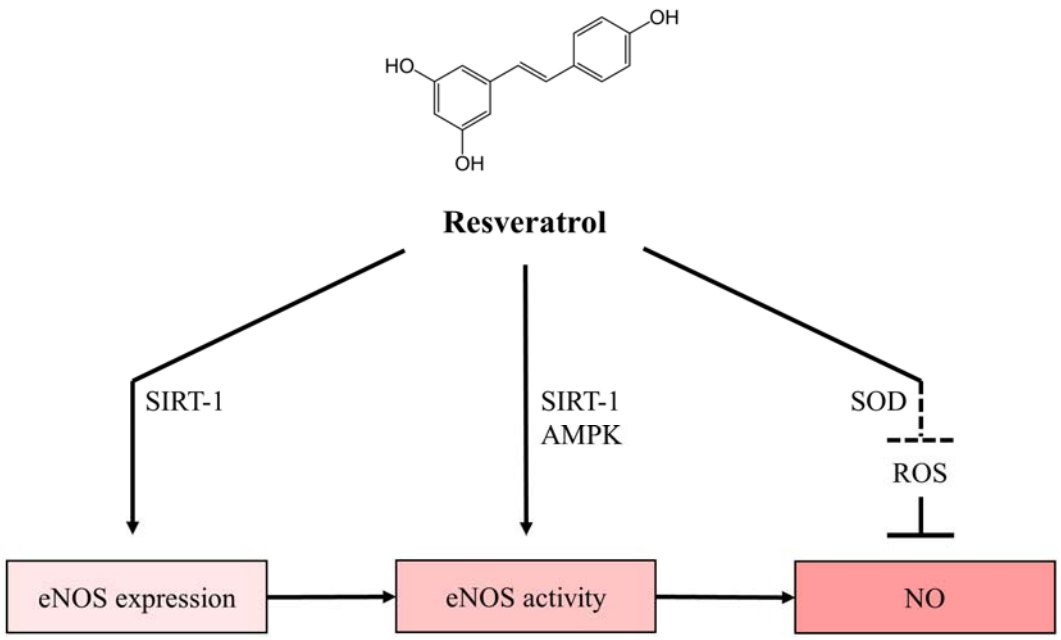

Figure 1.4. Mechanisms influencing nitric oxide generation by resveratrol. *Prolonged exposure to RV has been associated with the upregulation of eNOS and subsequent production of NO, as well as the upregulation of antioxidant enzymes such as SOD. Acute exposure likely results in phosphorylation and acetylation of eNOS by SIRT-1 and AMPK, leading to enhanced activity. Endothelial nitric oxide synthase (eNOS); nitric oxide (NO); superoxide dismutase (SOD); silent mating type information regulation 2 homolog) 1 (SIRT-1); adenosine monophosphate-activated protein kinase (AMPK). Author generated.*

Our laboratory has recently demonstrated that RV can potentiate endothelial-dependent dilator responses in aortic vessels and femoral arteries from young and aged mice (Diaz et al., 2019). In human studies, data from the Azzawi lab has shown that RV improves flow-mediated dilation (FMD) in CVD patients after coronary artery bypass graft surgery (Diaz et al., 2020); improves ventricular systolic and diastolic function, and decreases cholesterol levels after myocardial infarction. However, other studies have reported inconclusive or contradictory findings, which may be due to insufficient RV bioavailability *in vivo*, particularly following oral administration, with <1 % available globally (Cottart et al., 2010; Chachay et al., 2014; van der Made et al., 2015; Zortea et al., 2016). Despite RV's good absorption profile (75% uptake), the resulting low plasma concentration leads to inadequate

systemic distribution and limited exposure to specific activation sites, resulting in insufficient pharmacological effects. This lack of bioavailability is widely considered to be a result of RV's metabolic instability, resulting from multiple rapid glucordination and sulfation reactions during phase I and II metabolism (de Santi et al., 2000). Because of its low bioavailability and poor stability, it is evident that different modes of RV administration are required. In this study, the effectiveness of nanoparticle encapsulated RV will be investigated, and the underlying mechanism of action within vascular tissue characterised. In addition, the effectiveness of the synthetically modified analogue, trans-3,4,5,4′-tetramethoxystilbene will be investigated.

1.5.2 Trans-3,4,5,4′-tetramethoxystilbene (3,4,5,4′-TMS)

Due to the limitations conferred by RV, many studies have focused on the development and synthesis of novel RV derivatives with enhanced bioavailability and pharmacological activity (Nawaz et al., 2017). Trans-3,4,5,4′-tetramethoxystilbene (3,4,5,4′-TMS), a methylated analogue of RV has demonstrated promising metabolic stability and bioavailability (Figure 1.5). Whilst RV undergoes metabolisation into to sulphate or glucuronate conjugates, TMS undergoes demethylation; leaving bioactive phenolic groups intact, providing a compelling rationale for investigating its use as a therapeutic treatment strategy in conditions whereby RV might be useful. Similar to RV, TMS has demonstrated cardioprotective properties. In hypertension, TMS has demonstrated increased potency compared to RV (1000-fold) and has been shown to reduce oxidative stress via direct inhibition of the CYP450 pathway, improving endothelial function and vascular reactivity (Jennings et al., 2014). Furthermore, TMS has been shown to reduce vascular reactivity to

vasoconstrictor agents such as phenylephrine and endothelin-1, as well by DOCA-salt and angiotensin-II infusion via modulation of CYP1B1 activity (Jennings et al., 2010, 2014; Sahan-Firat et al., 2010). Whilst intravenous administration of TMS in murine models has demonstrated improved bioavailability in comparison to RV, its total availability remains low (Sale et al., 2004; Lin et al., 2010, 2011). The Azzawi lab has previously demonstrated that TMS-loaded liposomes can restore attenuated endothelial-dependent dilator responses induced by an oxidative stress by reducing NADPH-oxidase-derived ROS and potentiating the release of the vasodilator NO (Zaabalawi et al., 2019); as such, this study will assess the potential of encapsulated TMS-liposomes in restoring dilator function in the cerebral vasculature after acute pressure elevation.

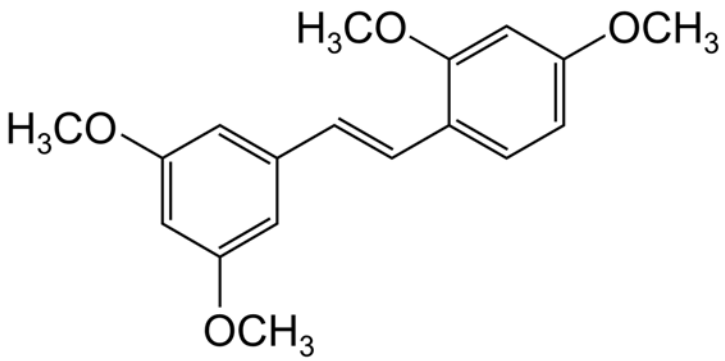

Figure 1.5. Molecular structure of trans-3,4,5,4'-tetramethoxystilbene (TMS). *TMS is a synthetic analogue of RV, with hydroxyl groups (OH) substituted for synthetically conjugated methyl groups (H3CO).*

1.6 Aims & Objectives

Hypothesis: The hypothesis of the present investigation is that nanoparticles will improve the delivery and release of RV and analogues (compared to their unencapsulated form) for the alleviation of ROS mediated endothelial dysfunction in hypertension.

Overall aim: To develop a potential therapeutic tool for the treatment of CVDs associated with elevated ROS, including hypertension. This will be achieved in the following specific objectives:

1. Synthesise and characterise nanoparticles for use in drug delivery.

- **1.1.** Synthesise and characterise inorganic (silica) nanoparticles and determine their effect on endothelial cell viability, *in vitro* (Chapter 3).
- **1.2.** Characterise organic lipid nanoparticles and define their antioxidant capacity and effect on endothelial cell viability *in vitro* (Chapter 4).

2. Establish alterations in vascular function in coronary and cerebral arteries following acute pressure elevation using an *ex vivo* model of acute hypertension, via pressure myography (Chapter 5).

3. Determine the influence of RV (and analogues)-loaded nanoparticles on the restoration of dilator function, using the *ex vivo* model of acute hypertension.

- **3.1.** Determine whether RV-NLCs have the capacity to restore attenuated dilation following acute pressure elevation in the coronary artery (Chapter 6).
- **3.2.** Determine whether RV-NLCs and TMS-liposomes have the capacity to restore attenuated dilation following acute pressure elevation in the cerebral artery (Chapter 7).

Chapter 2: Methodology

2.1 Nanoparticle synthesis

2.1.1 Silica nanoparticle synthesis

Dye-encapsulated SiNPs were synthesised using the Stöber sol-gel method, as previously described (Stöber et al., 1968). Briefly, ethanol (EtOH; 103.9 ml; 17.1 M), methanol (MeOH; 103.9 ml; 24.8 M), ammonium hydroxide (NH_4OH; 22 ml; 1 M) and water (H_2O; 10.7 ml) were placed in a round-bottomed flask, heated to 55 ºC and stirred for 1-hour. In order to initiate the hydrolysis and polycondensation reactions that would ultimately form the SiO_2 colloid, tetraethyl orthosilicate (TEOS; 9.5 ml; 4.7 M) was added dropwise over a 15-minute period. Next, entrapment of the fluorescein isothiocyanate (FITC; F2502, Sigma) dye was performed by adding 1 ml of the dye mixture [FITC powder (16.5 mg), anhydrous EtOH (6 ml; 17.1 M) and 3-aminopropyltrimethoxysilane (APTES; 36 µl; 5.46 M) stirred overnight under a nitrogen atmosphere] into the solution. The solution was stirred for a further hour and sub-divided into batches prior to further modification. Of the 250 ml stock produced, 50 ml was set aside and retained as blanks; another 50 ml was functionalised with an amine phosphonate (5 ml) solution [APTES (25 µl; 4.47 M), 3-(trihydroxysilyl) propyl methyl-phosphonate (25 µl; 2.09 M), anhydrous EtOH (10 ml; 17.1 M)]. The remaining 150 ml was functionalised with a 3-mercaptopropyltriethoxysilane (MPTES; 1 ml) linker solution [MPTES (50 µl; 4.83 M), MeOH (100 ml; 3.70 M)]. The solutions were subsequently placed on a magnetic hot plate and attached to a condenser to minimise solvent evaporation. The solutions were heated to 80 ºC, stirred for 1-hour and cooled to room temperature (22 ºC).

The resulting mercapto-functionalised solution was divided into two batches. One batch (75 ml) was functionalised with a 40 µM poly(ethylene glycol) methyl ether (mPEG; 1 ml)

solution [mPEG (10 mg), H_2O (50 ml)]. The remaining 75 ml was functionalized with mPEG (1 ml) and a CeNP suspension (5 ml; see 2.1.2). The reaction solutions were centrifuged at 4,500 g for 10-minutes (x 3) in order to remove contaminants. SiNPs were re-dispersed in absolute EtOH (17.1 M), vortexed and sonicated at each stage. The supernatant was discarded and the SiNP sediment was re-dispersed in distilled water (H_2O), physiological salt solution (PSS) or endothelial cell culture medium (MV2) prior to characterisation. Three batches of SiNPs were produced and subsequently functionalised over the course of these studies. Further information regarding the underlying chemistry of the Stöber sol-gel method may be found in Appendix 10.1.

2.1.2 Cerium oxide nanoparticle synthesis

Briefly, a 200 mM cerium(III) nitrate hexahydrate ($Ce(NO_3)_3\ 6H_2O$) solution was made by dissolving $Ce(NO_3)_3\ 6H_2O$ (4.34 g) in distilled H_2O (50 ml). The solution was stirred and heated to 70 ºC, before the gradual addition of NH_4OH (5 ml; 1 M) over 5-minutes. The solution was subsequently stirred at 100 rpm for 20-hours. A progressive colour change from light purple to yellow was observed, indicating the solution had become oxidized (Ce^{3+}). Three batches of CeNPs were produced over the course of these studies.

2.1.3 Nanostructured lipid carrier synthesis

Blank (non-loaded) NLCs, RV and RV-dye-loaded NLCs were prepared using hot melt emulsification technique by probe sonication. Water phase containing surfactants, sodium cholate (0.25 g/100 ml) and Tween-80 (1 g/ 100 ml) was heated to 70 ºC, prior to

amalgamation with melted lipid phase comprising of trimyristin (1.5 g/100 ml), triolein (0.5 g/ 100 ml), phosphatidylcholines (0.5 g /100 ml) and RV (1 mg/ml). The dispersion was mixed under magnetic stirring for 5-minutes. The pre-emulsion was sonicated using a probe sonicator (Fisherbrand™ Q700) for 15-minutes. The resulting emulsion was allowed to cool down at ambient temperature overnight to form the NLCs. For the dye-loaded RV-NLCs, coumarin-6 dye (15 µg/ ml) was dissolved in the lipid phase with RV, allowing entrapment within the NLCs. The RV-NLC dispersion was centrifuged at 1,200 g for 5-minutes at 25 °C, in order to remove the residual titanium produced during probe sonication. RV-NLCs were filtered through a 0.22 µM membrane and diluted as appropriate prior to use. Three batches of NLCs were produced over the course of these studies.

2.1.4 Liposomal carrier synthesis

Liposomes were synthesised by collaborators at the University of Manchester (UoM). Briefly, liposomes were synthesised using the thin lipid film process as previously described (King et al., 2016; Cureton et al., 2017). The constituent lipids 1,2-distearoyl-sn-glycero-3-phosphocholine (DSPC; 32.5 mM), 1,2-distearoyl-sn-glycero-3-phosphoethanolamine-N-[methoxy(polyethylene glycol)-2000] ammonium salt (DSPE-PEG (200); 1.875 mM) and cholesterol (15 mM) were dissolved in 5 ml of chloroform in a round-bottomed flask. Subsequent rotary evaporation (40 °C, 270 mbar) removed excess chloroform, and the lipid film was placed in a vacuum oven overnight (25 °C, 0 mbar). The thin film was rehydrated with 1 ml of with calcium and magnesium-free phosphate-buffered saline (DPBS; BE17-161F, Lonza), vortexed for 10-minutes, heated to 55 °C, and vortexed for 5-minutes at 1-hour intervals for a minimum of 4-hours. The suspension containing large multilamellar vesicles was then extruded 11-times using a 1 ml Mini-Extruder (Avanti Polar Lipids)

through a 200 nm polycarbonate membrane to produce unilamellar liposomes ~200 nm in diameter. Fluorescent brain targeting peptides (RLSSVDSDLSGC) bearing a cysteine residue on the N-terminus were added to the liposome suspension, allowing covalent coupling with maleimide groups overnight at room temperature via a Michael type addition reaction. To remove impurities, dialysis against PBS (8 × 500 ml; 24-hours) in a Slide-A-Lyzer cassette with a molecular weight cut-off of 3.5 kD (Thermo Fisher Scientific, USA) was performed. Liposomes were then stored at 4 °C until use. For TMS-loaded liposomes, the lipid film was rehydrated with 1 ml TMS (2 mM; SMB00388, Sigma), heated to 55 °C and extruded/dialysed as above, to give a final encapsulated concentration of approximately 0.1 mM. Three batches of liposomes were produced over the course of these studies.

2.2 Nanoparticle Characterisation

2.2.1 Dye and/or drug loading

Dye/drug loading was determined using ultra-violet visible spectroscopy (UV-VIS) and fluorescence spectroscopy. Undiluted samples (approximately 2 ml) were loaded into a quartz cuvette (can be used in both the UV and visible region, in comparison to glass or plastic). The optical absorbance of nanoparticles was recorded using an ultra-violet visible spectrophotometer (Jenway 7305, Cole-Palmer) in the wavelength range 200-600 nm. Fluorescence spectra were recorded using a fluorescence spectrometer (F-7000, Hitachi) in the 450-700 nm range.

2.2.2 Particle composition

Compositional information was obtained using fourier-transform infrared spectroscopy (FTIR). Background correction was initially performed to exclude non-specific spectra. Next, desiccated sample (approximately 1 mg) was loaded onto the infra-red crystal stage (Nicolet 380 FT-IR Spectrometer, Thermo Scientific) and transmission spectra (inversely proportional to absorbance) collected (resolution: 8 cm^{-1}; scans: 16; range: 500-4,000 cm^{-1}). Thermogravimetric analysis (TGA) was used to assess the thermal stability (composition & degradation kinetics) of samples. Desiccated sample (approximately 10 mg) was transferred into the sample holder (TGA 4000, Perkin Elmer); thermogravimetry and derivative thermogravimetry analysis were performed between 20 °C and 900 °C, at a heating rate of 10 °C/minute under an inert nitrogen atmosphere.

2.2.3 Hydrodynamic size and zeta potential

Nanoparticle size and zeta potential were determined by dynamic light scattering (DLS) and laser doppler micro-electrophoresis (LDME), respectively (25 °C; scattering angle of 173° Zetasizer Nano ZS, Model ZEN3600, Malvern, UK). SiNP and NLC stock solutions were vortexed and sonicated for 5- and 2-minutes, respectively; producing monodisperse samples. Samples were diluted 1:100 (20 µl into 1,980 µl) in distilled H_2O (pH 6.8), PSS (pH 7.2 – 7.4) or endothelial cell culture medium MV2 (pH 7.2 – 7.4) and transferred into a cuvette. For zeta potential measurements, samples were transferred into a folded capillary zeta-cell (DTS1070, Malvern); specialised cuvettes equipped with gold plated copper electrodes, allowing the administration of an electrical current to measure the electrophoretic mobility of samples directly (runs: 40; duration: 10-seconds; measurements: 3; temperature: 37.5 ºC).

SiNP stability was assessed immediately following dilution. RV-NLC size and stability was assessed at predetermined time points (0, 0.5, 1, 2 and 4-hours), by collaborators at the University of Central Lancashire (UCLAN).

2.2.4 Physical size and morphology

Nanoparticle size was determined by scanning electron microscopy (SEM; Supra 40VP, Zeiss Ltd). Samples were dispersed (1 mg/ml) in industrially methylated spirit (IMS; Fisher Scientific), sonicated for 5-minutes and transferred onto aluminium specimen stubs. Stubs were dried at 60 ^{o}C for 30-minutes to promote solvent evaporation and transferred onto an SEM platform for imaging. In order to obtain higher resolution images and gain structural information, samples underwent transmission electron microscopy (TEM; FEI-T12 Biotwin, Tecnai). Inorganic samples (SiNPs) were prepared in the same manner as for SEM but were positioned on palladium-coated holey carbon films (300 mesh).

Organic samples (NLCs, liposomes) were diluted (1 mg/ml) in 4-(2-hydroxyethyl)-1-piperazineethanesulfonic acid) buffer (HEPES; 0.1 M; pH 7.2-7.4) and dried for 1-hour on holey carbon-coated film (300 mesh). Samples were rapidly fixed using osmium tetroxide (1%; 0.1 M HEPES) for 10-minutes and negatively stained with uranyl acetate (1%; 0.1 M HEPES) for 2-minutes in order to improve contrast. Samples were air-dried for 30-minutes prior to imaging. Average nanoparticle size and distribution was determined by manually measuring particle diameters, with reference to the scale bars on micrographs.

2.2.5 Drug release profile

Drug release studies were performed by collaborators at the UCLAN. To determine the release rate of RV from NLCs, a dialysis tubing diffusion method was employed. Dialysis bags (Spectra/Por® 3 Dialysis Tubing, molecular weight cut off 3.5 kD) were washed with distilled water and saturated overnight in release medium. 5 ml of RV-solution/RV-NLC dispersion (4.38 mM) was added to the dialysis bag and placed in a glass vessel (ERWEKA® dissolution tester, D-63150 Heusenstamm/Germany) containing 900 ml of dissolution media (pH 7.4) at 37 ± 0.5 °C. 1 ml samples were withdrawn at predetermined time intervals and analysed using high-performance liquid chromatography (HPLC) using a C18 Luna column [mobile phase - acetonitrile: water], detected at 306 nm (Ratola et al., 2004).

2.2.6 Oxidative capacity of nanoparticles in solution

The oxidative capacity of SiNPs was determined using a dichlorofluorescin diacetate (DCFH-DA) reagent, following a modified protocol (Zhao and Riediker, 2014). Briefly, DCFH-DA powder (2.5 mg) was dissolved in IMS (5 ml; 21.4 M), producing a 1 mM stock solution. The DCFH-DA solution was deacetylated using a strong base solution of sodium hydroxide (NaOH; 1 ml; 10 mM) and kept in the darkness at room temperature (22 ºC) for 30-minutes. A working solution was produced by diluting the deacetylated stock solution (1:100) with sodium phosphate buffer (25 µM/pH 7.2-7.4). Nanoparticles were desiccated and transferred (3 mg) into Eppendorfs, along with 600 µl of working solution (5 mg/ml). Samples were sonicated for 15-minutes at 37 ºC to aid nanoparticle dispersal and transferred into 96-well plates (200 µl/well). Horseradish peroxidase (HRP; 0.5U/ ml^{-1}) catalyst was added into each well (18.2 µl), initiating the reaction. Plates were transferred into the plate

reader (Biotek, HT Synergy) and fluorescence measured after 15-minutes (*exc.* 485 nm; *em.* 530 nm).

The antioxidant capacity of nanoparticles was determined using an Amplex™ Red Hydrogen Peroxide/Peroxidase Assay Kit (A22188, ThermoFisher Scientific) following manufacturer's instructions. Briefly, the Amplex red reagent was dissolved in 60 µl of dimethyl sulfoxide (DMSO; 10 mM) and kept in darkness. Initially, a H_2O_2 standard curve was produced (0 – 10 µM; 100 µl/well) in reaction buffer. Nanoparticle samples were diluted in reaction buffer (5 mg/ml) containing H_2O_2 (10 µM), sonicated for 15-minutes at 37 ºC and transferred into a 96-well plate (100 µl/well). A working solution was produced by combining 50 µl of Amplex red reagent, 100 µl of HRP solution (0.2 U/ml^{-1}) and 4.85 ml of reaction buffer; and adding to each well (100 µl/well), initiating the reaction. Plates were incubated at 37 ºC for 30-minutes inside the plate reader (Biotek, HT Synergy) and fluorescence measured (*exc.* 530 nm; *em.* 590 nm).

2.3 Cell culture studies

2.3.1 Endothelial Cell Culture

Human coronary artery endothelial cells (HCAECs; single donors (3-batches); C-12221) were obtained from PromoCell (Heidelberg, Germany). Cells were grown in Endothelial Cell Growth Medium (MV2; C-22022, PromoCell) supplemented with growth medium MV2 supplement pack (C-39221, PromoCell), 100 µl/ml penicillin and 100 µl/ml streptomycin (Lonza) prior to incubation at 37 ºC with 4 % CO_2. Cells were passaged 1:3 after reaching 90 % confluency. In order to passage cells, firstly they were washed with PBS and incubated with TrypLE express (12605-028, ThermoFisher Scientific) for 5-minutes at

37 ºC until dislodged. Cells were centrifuged at 300 g for 10-minutes and resuspended in culture medium (2-3 ml). The resulting suspension was mixed at a 1:1 ratio with 0.4 % trypan blue (T8154, Sigma), transferred into counting slides (145-0011, Bio-Rad) and analysed using the automatic cell counter (Bio-Rad, TC10); providing an estimate of average cell number/ml. Cells were subsequently diluted and seeded as appropriate into new flasks/plates. For expansion, cells were passaged at a 1:3 ratio. Cells were used at passages 3-6.

Excess cells were resuspended in cell culture medium (2 x 10^6 cells/ml; supplemented with 30 % FBS and 10 % DMSO; Lonza) following trypsinisation, transferred into freezing capsules and frozen at -80 ºC for 24-hours. Cells were subsequently transferred into liquid nitrogen for storage (-196 ºC).

2.3.2 Preparation of nanoparticles

The final concentration of inorganic (silica) nanoparticles was calculated as described in Appendix 10.2. SiNPs were centrifuged at 7,000 g for 5-minutes and washed (x 3) with IMS (70%) to remove contaminants. Nanoparticles were sonicated (FB15048, Fisherbrand) for 3-minutes between washes to aid the dispersal of the nanoparticle pellet. Following centrifugation, the nanoparticle pellets were resuspended in cell culture medium (MV2) and passed through a 0.45 µm filter. Organic nanoparticles (NLCs/liposomes) were diluted as appropriate from the stock solution and passed through a 0.45 µm filter.

2.3.3 Oxidative capacity of nanoparticles *in vitro*

The generation of mitochondrial and cytosolic $O_2^{\bullet-}$ was quantified using MitoSOX™ Red Mitochondrial Superoxide Indicator (M36008, ThermoFisher Scientific) and dihydroethidium (DHE), respectively (D11347, ThermoFisher Scientific). Briefly, HCAECs were cultured in 96-well plates at a density of 1 x 10^4 cells/well for 24-hours. Initially, cells were exposed to H_2O_2 (0 - 500 µM) in cell culture medium for 30-minutes. Cells were washed with PBS (x 3) and fresh culture medium containing alamar blue (1:10 ratio) added. HCAECs were incubated in the dark at 37 °C for 4-hours. Fluorescence was measured at *exc.* 570 /*em.* 590 using a BioTek Synergy™ HT microplate reader. Cell viability was calculated by normalising treatment samples against negative controls. Based upon HCAEC tolerances to H_2O_2, cells were exposed to H_2O_2 (100 µM) in media for 30-minutes to stimulate ROS generation, as previously described (Coyle and Kader, 2007). Cells were washed with PBS, followed by addition of fresh medium in the presence/absence of RV-NLCs for 30-minutes (0.45 µM). Following treatment, cells were washed and incubated with MitoSOX (5 µM) or DHE (10 µM) for 15-minutes (200 µl/well). Fluorescence was measured at *exc.* 530 /*em.* 590 using a BioTek Synergy™ HT microplate reader. Fluorescence values were normalised against negative controls.

2.3.4 Cell viability

The viability of HCAECs was assessed using the fluorometric assay, alamar blue, according to the manufacturer's instructions (DAL1025, ThermoFisher). Briefly, cells were cultured on 96-well plates at a density of 1 x 10^4 cells/well for 24-hours. Cells were exposed to cumulative concentrations of SiNPs (1 x 10^{10} - 10^{13} NPs/ml); NLCs/solution (0.045 – 90

μM); liposomes/solution (0.01 – 1000 nM) for 24-, 48- or 72-hours. Untreated cells were included as negative controls (i.e. 100 % viable). Positive controls were incubated with 0.1 % Triton-X100 (T8787, Sigma). Following treatment, cells were washed with PBS and alamar blue added to fresh cell culture medium at a 1:10 ratio. HCAECs were incubated in the dark at 37 °C for 4-hours. Fluorescence was measured at *exc.* 570 /*em.* 590 using a BioTek Synergy™ HT microplate reader and cell viability calculated by normalising fluorescence values against negative controls.

2.4 Nanoparticle uptake

2.4.1 Fluorescence microscopy

To determine nanoparticle uptake into cells, HCAECs were cultured on glass slides mounted with ProPlate® multi-well chambers at a density of 1 x 10^4/well. Cells were incubated in media supplemented with dye-loaded SiNPs (1 x 10^{11} NPs/ml) or NLCs (0.45 μM) for 24-hours and 30-minutes, respectively. Control wells received standard media. Following exposure, cells were washed with PBS and fixed using paraformaldehyde (PFA; 4 %) at room temperature for 20-minutes. Cells were washed and incubated in PBS-tween (0.05 %) for 10-minutes in order to permeabilise cells, followed by incubation in 1 % bovine serum albumin (BSA)-PBS for 1-hour. Cells were washed and incubated in the phalloidin conjugate (1:10,000; P1951, Sigma) for 1-hour to stain the actin filaments. SiNP co-localisation was assessed by washing and incubating in LysoTracker™ Deep Red (50 nM; L12492, ThermoFisher Scientific) for 30-minutes. Slides were mounted in ProLong Gold antifade mounting medium containing DAPI as a nuclear counterstain; and sealed using a coverslip and then stored at 4 ºC in the dark (P36931, Invitrogen). Slides were imaged using a fluorescent (Axioscope 5, Zeiss) or confocal microscope (TCS SP5, Leica).

2.4.2 Transmission electron microscopy

HCAECs were seeded onto 60 mm culture dishes at a density of 1.2 x 10^6 and grown to 90% confluency. Cells were exposed to SiNPs (1 x 10^{11} NPs/ml) for 1-, 2- and 4-hours. Untreated cells were included as negative controls. Cells were washed with PBS and fixed [4 % formaldehyde + 2.5 % glutaraldehyde in 0.1 M HEPES (pH 7.2-7.4)]. Samples were taken for TEM processing and imaging (FEI-T12 Biotwin, Tecnai) at the University of Manchester imaging suite.

2.5 Vascular function studies

The physiological functional experiments in this study were performed using coronary arteries (100-200 µm) and middle cerebral arteries (100-200 µm) excised from euthanised animals (Male Wistar rats, 150-250g in weight, aged 8-9 weeks), obtained from the Biomedical Science Unit, University of Manchester. The Wistar rats were housed under standardised conditions (12-hour light/ dark cycles at 24 ºC). All animals were euthanised by stunning and cervical dislocation following institutional guidelines and in accordance with guidelines issued by the European Commission Directive 86/609/EEC. A total of 85 rodents were used over the course of these studies. All procedures were conducted in accordance with institutional guidelines of Manchester Metropolitan University, the University of Manchester and the United Kingdom Animals (Scientific Procedures) Act of 1986 (schedule 1). A risk assessment for the use and handling of animal tissue was conducted.

Septal coronary arteries (Figure 2.1A, B) and middle cerebral arteries (Figure 2.1C) were excised and had the perivascular adipose and connective tissue layer surrounding each vessel removed in order to improve visual clarity. Arteries were mounted between two glass cannulae in a pressure myograph chamber (Living Systems, USA; Figure 2.2) and pressurised to an intravascular pressure of 60 mmHg using a servo-control unit (Living Systems Instrumentation, USA). Vessels were secured in place by tying two knots at either end of the cannulae. Arteries were continuously superfused with PSS [composition [mM]: 119 NaCl, 4.7 KCl, 1.2 $MgSO_4.7H_2O$, 25 $NaHCO_3$, 1.17 KH_2PO_4, 0.03 K_2EDTA, 5.5 glucose, 1.6 $CaCl_22H_2O$; pH 7.4] supplemented with 95 % O_2 and 5 % CO_2 at 37 ^oC, and diameters (lumen and wall) constantly recorded using a video dimension analyser (Living Systems) on an inverted Nikon microscope (ECLIPSE Ti2; 10 x magnification) using LabChart 6 (Powerlab, AD Instruments, UK).

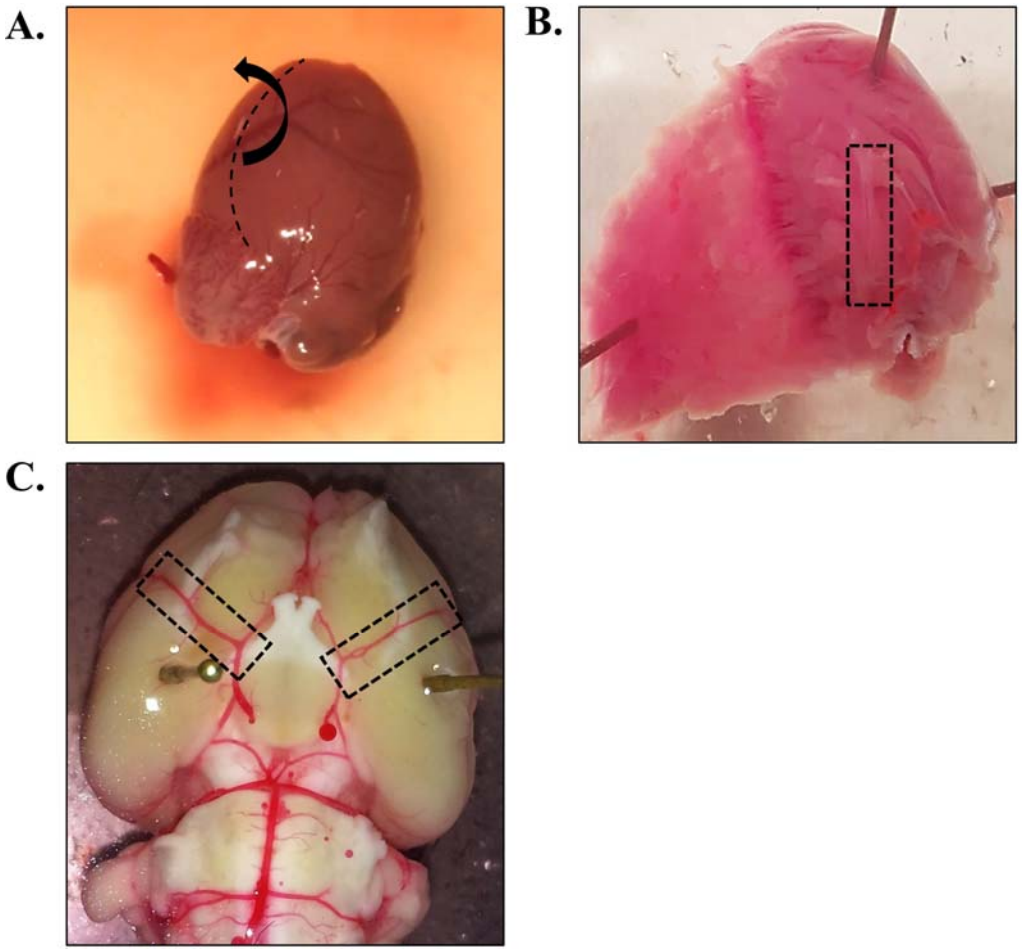

Figure 2.1. The anatomical structure of the isolated rat heart and brain vasculature. *(A) An image of the anterior heart. A superolateral incision is made into the left ventricle, allowing reflection of the ventricular wall. (B) Once reflected, the septal coronary artery becomes visible. (C) The anatomical structure of the dorsal brain; highlighting the vascular architecture following immediate removal from the cranial cavity. Coronary and middle cerebral arteries are highlighted by the dashed boxes.*

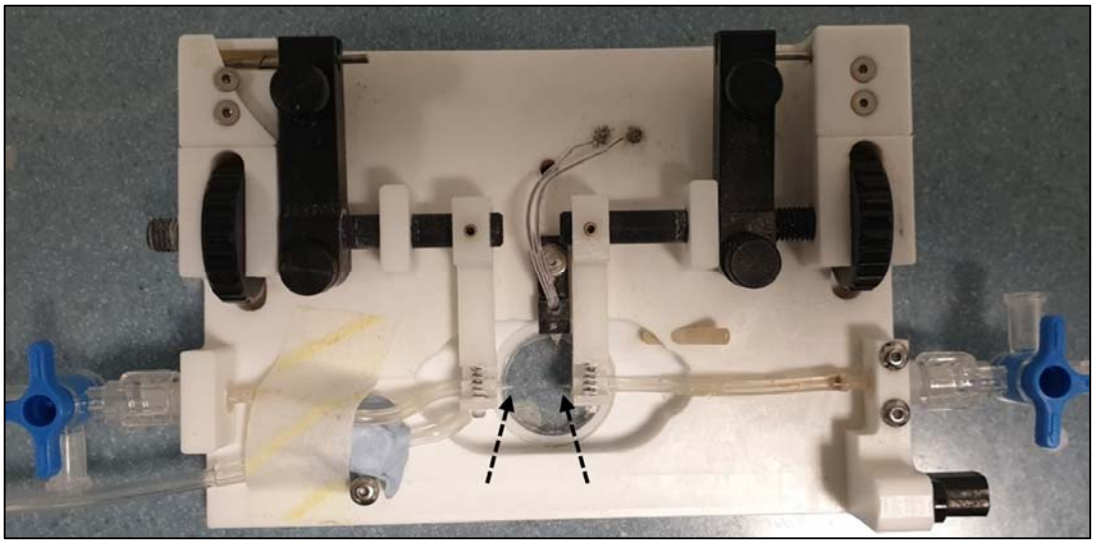

Figure 2.2. Pressure myography chamber. *An image of the pressure myography vessel chamber illustrating the position of the glass cannulae (indicated by dashed arrows).*

2.5.1 Experimental protocol

After a 20-minute equilibration period, viability was assessed by ascertaining initial responses to high potassium solution (KPSS) [composition [mM]: 78.2 NaCl, 60 KCl, 1.2 $MgSO_4.7H_2O$, 25 $NaHCO_3$, 1.17 KH_2PO_4, 0.03 K_2EDTA, 5.5 glucose, 1.6 $CaCl_2.2H_2O$; pH 7.4].

Initially, 5-HT (H9523, Sigma) dose responses were performed to assess vessel contractility (10^{-10} M - 10^{-3} M). In subsequent studies, all arteries were pre-constricted in 5-HT (5-HT, 10^{-6} - 10^{-7} M). Endothelial-dependent (ACh, 10^{-9}-10^{-3} M; A6625, Sigma) responses and were assessed prior to, following or 1-hour after acute pressure elevation. Vessels were exposed to elevated pressure (150mmHg) for 30-minutes, and then returned down to 60mmHg for a further 30-minutes, in the presence/absence of RV-NLCs (0.45 µM); RV-solution (0.45 µM); TMS-liposomes (1 nM) or TMS-solution (10 µM). In order to minimise the depletion of samples, superfusion was ceased for the duration of the incubation period and samples were added directly into the oxygenated chamber; with temperature maintained at 37.5 ºC using an external temperature controller (TC-02, Living Systems). In order to evaluate the possible contribution of ROS in endothelial-dependent dilation, vessels were co-incubated with superoxide dismutase (SOD, 300 U^{-}ml; S7571, Sigma), catalase (CAT, 500 U^{-}ml; C4963, Sigma) or apocynin (NADPH oxidase inhibitor; 30 µM; ab120615, Abcam).

Inhibition studies were used to determine the influence of RV-NLCs on the vasodilator pathways. Responses were assessed in a separate set of experiments, following incubation in; the NO synthase inhibitor Nω-nitro-*L*-arginine (L-NNA, 100 µM; N5501, Sigma), the small (SK) and intermediate (SK) calcium-activated potassium channel blockers apamin (100 µM; A1289, Sigma) and TRAM-34 (1 µM; T6700, Sigma), as well as the COX inhibitor, indomethacin (10 µM; I7378, Sigma). The effect of inhibitors on vessel function

was assessed alone, in combination or in the presence/absence of RV-NLCs. Responses were assessed in the continued presence of inhibitors in the superfusate. The mechanistic contributions of AMPK and SIRT-1 were assessed following incubation with the inhibitors dorsomorphin (10 μM; Ab144821, Abcam) and EX-527 (10 μM; E7034, Sigma), respectively. In order to assess whether RV-NLCs act via endothelial-independent mechanisms, the endothelium was denuded via the introduction of three air-bubbles prior to beginning the experiments. Endothelial-independent responses were assessed using PAPA (100 μM; P3510, Sigma) and SNP (100 μM; 71778, Sigma). At the end of the experiment, arteries were superfused with calcium-free PSS for 30-minutes in order to obtain passive diameters (VSMC hyperpolarisation).

2.6 Ultrastructural Analysis

Following treatment, vessels were dismounted and transferred into a fixative solution [4 % formaldehyde + 2.5 % glutaraldehyde in 0.1 M HEPES (pH 7.2-7.4)]. Samples were taken for TEM processing and imaging (FEI-T12 Biotwin, Tecnai) at the University of Manchester imaging suite.

2.7 Statistical Analysis

All statistical analysis was performed using Prism version 8.3.1 for Windows, GraphPad Software, La Jolla California, USA. DLS and LDME measurements were analysed using an unpaired t-test or a one-way analysis of variance (ANOVA) followed by Tukey's multiple comparison or Bonferroni correction. Drug release was analysed by a two-way ANOVA.

Cell viability was calculated by normalising values to control wells (i.e. 100% viable) and expressing as a percentage. Data was analysed by a one or two-way ANOVA followed by Bonferroni or Tukey's multiple comparison, respectively. Oxidative reactivity was analysed using an unpaired t-test or a one/two-way ANOVA followed by Dunnett's or Tukey's Multiple Comparison. Constrictor responses elicited by 5-HT are expressed as percentage constriction corresponding to the decrease from the passive diameter value. Responses were assessed using unpaired t-test or two-way ANOVA followed by Tukey's multiple comparison. The dilator responses elicited by ACh are expressed as percentage relaxation corresponding to the increase from the pre-constricted value. The Shapiro-Wilk test was used to assess the conformity of the data to normal distribution. Dilator responses were analysed using a two-way ANOVA followed by Tukey's multiple comparisons. In order to calculate EC_{50} values, data were normalised, transformed and plotted using a nonlinear regression model. $LogEC_{50}$ values were calculated and compared using an extra-sum-of-squares F test. Dilator responses elicited by PAPA and SNP were assessed using an unpaired t-test or one-way ANOVA followed by Tukey's multiple comparisons. Values of $P < 0.05$ were considered statistically significant. Asterisks used denote: * $P < 0.05$, ** $P < 0.01$, *** $P < 0.001$, and **** $P < 0.0001$. Experiments were performed in triplicate where appropriate and repeated three times. Data are represented as means ± standard error of the mean (SEM) unless stated otherwise.

Chapter 3: Synthesis and characterisation of inorganic nanoparticles

As discussed in the introductory chapter, SiNPs are a promising platform for the release of vasoactive compounds, offering a potential delivery modality for the treatment of CVD; however, their surface reactivity and oxidative capacity may preclude their use. The objective of this part of the study is to synthesise SiNPs and assess the effects of surface functionalisation on their oxidative capacity and *in vitro* biocompatibility, offering a potential mechanism for antioxidant delivery. The hypothesis of this part of the study is that CeO_2 functionalisation of SiNPs will improve SiNP biocompatibility in isolated endothelial cells. This hypothesis will be addressed through the following specific objective:

- Synthesise and characterise inorganic (silica) nanoparticles and determine their effect on endothelial cell viability, *in vitro*.

SiNPs were prepared using the Stöber technique. Dye-loading was determined using ultra-violet visible spectroscopy (UV-VIS) and composition assessed using fourier transform infrared spectroscopy (FTIR) and thermogravimetric analysis (TGA). Nanoparticle zeta potential was determined by laser doppler micro-electrophoresis (LDME), whilst size and morphology were assessed using scanning electron microscopy (SEM) and transmission electron microscopy (TEM). The oxidative capacity of SiNPs in solution was determined using 2'-7 dichlorofluorescein diacetate (DCFH-DA) and amplex red, respectively. The effects of SiNP on viability and uptake were assessed *in vitro* using alamar blue, fluorescence/confocal microscopy and TEM, respectively.

3.1 Results

3.1.1 SiNPs were successfully synthesised and characterised

SiNPs were synthesised and characterised in aqueous media. Using UV-VIS, FITC-loading within SiNPs was confirmed, with a characteristic absorbance peak at 490 nm (Figure 3.1).

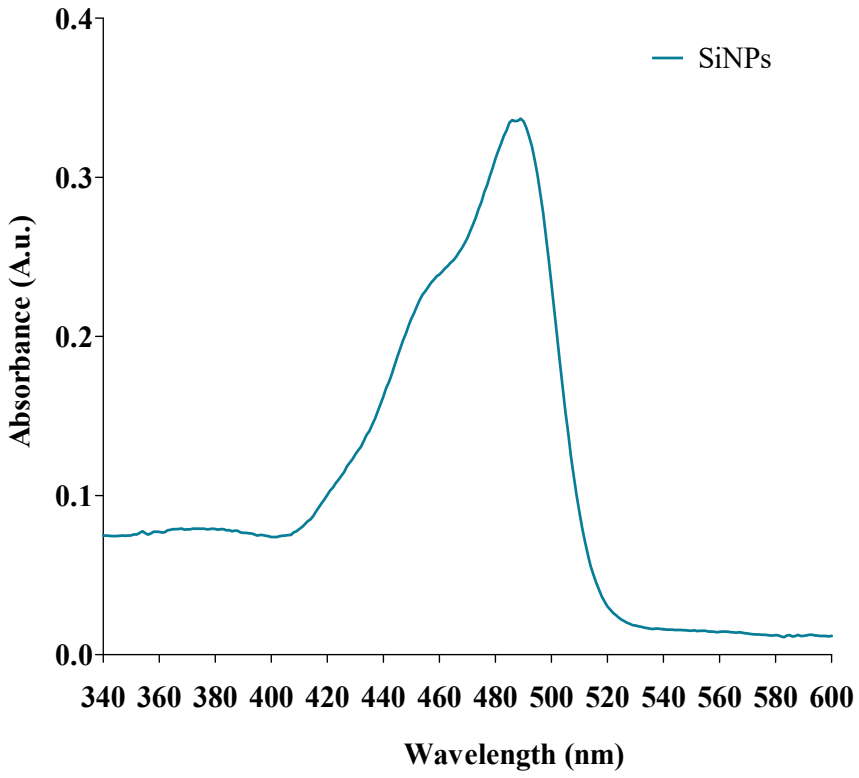

Figure 3.1. Confirmation of dye-encapsulation within SiNPs. *Ultraviolet-visible spectroscopy (UV-Vis) displaying absorbance spectra between 340-600 nm. An absorbance peak was observed at approximately 490 nm, confirming FITC-loading.*

FTIR was used to confirm the molecular structure of the SiNPs. The characteristic position and shape of the vibrational band at 1085 cm^{-1} (Si-O), in addition to the bands at 940 cm^{-1} (Si-O-Si symmetric stretching) and 800 cm^{-1} (O-Si-O symmetrical stretching), confirm the presence of a stoichiometric SiO_2 structure. The peak at 1630 cm^{-1}, as well as the broad absorption bands between 2550 and 3730 cm^{-1}, were assigned to the stretching and bending of physisorbed water molecules, as well as hydrogen-bonded and partially hydrated silanols (Si-OH). Bands in the 1680–1620 cm^{-1} region are also associated with primary amine groups (N-H). The band at 2330 cm^{-1} is attributable to absorption of aqueous and gaseous CO_2 (Figure 3.2). The presence of PEG and CeO_2 was not apparent in the SiNP samples using FTIR, due to the absence of corresponding peaks; hence, TGA was next used to assess the degradation kinetics of the nanoparticles as a function of temperature.

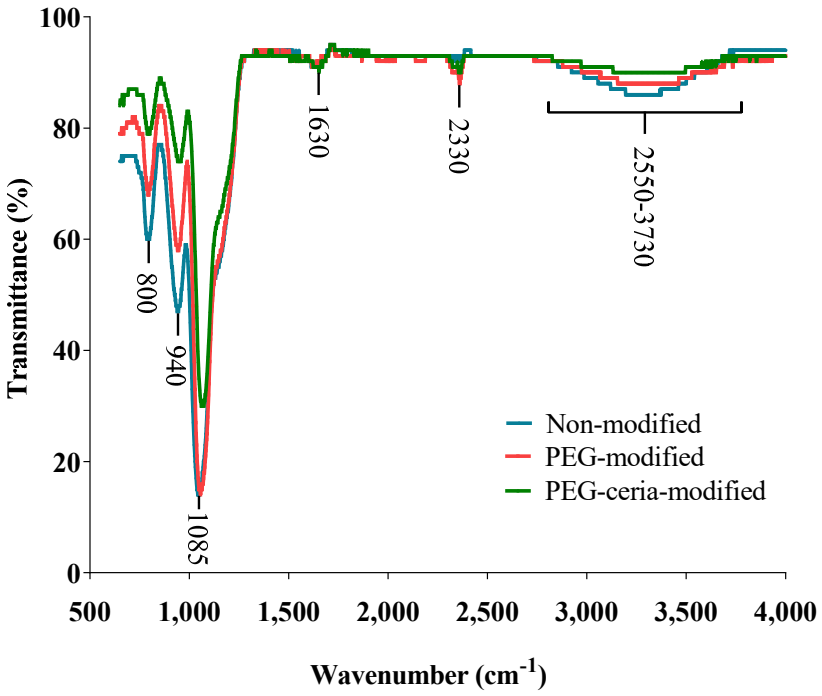

Figure 3.2. Confirmation of SiNP molecular structure. *Fourier transform infrared spectroscopy (FTIR) spectra of non-modified (blue), PEG-modified (red) and PEG-ceria-modified (green) SiNPs, displaying transmittance (%) between 500-4000 cm^{-1}. Characteristic transmittance peaks are indicated on the figure itself (for interpretation of the reference values, refer to main text).*

An analysis of cumulative weight loss identified a gradual reduction in percentage weight as a function of increasing temperature in each sample (Figure 3.3A). The initial weight loss observed between 0 and 200 ºC can be attributed to dehydration; the removal of physisorbed water from the surface of silica. The gradual weight loss at temperatures above 200 ºC is attributable to dehydroxylation; the removal of surface silanol groups via condensation reactions, in which siloxane bonds are formed. Analysis of derivative weight loss allows for the precise identification of constituent chemical evaporation temperatures; defining the point at which weight loss is most apparent (Figure 3.3B).

As noted above, the initial mass reduction observed between 0 and 200 ºC is due to the loss of bulk and hydrate water. Independent analysis of FITC powder identified two prominent areas of weight loss, occurring at 290 ºC and 500 ºC (Figure 3.4A, B). Subsequent analysis identified two troughs at the corresponding temperatures in non-modified SiNPs, the shallowness of the peaks being indicative of the low encapsulated quantity. Due to its small degradation profile, it is not apparent in PEG- and PEG-ceria-modified SiNPs due to obfuscation by other elements. In PEG- and PEG-ceria-modified SiNPs, a trough is identifiable between 450 ºC and 600 ºC, attributable to PEG-maleimide. A distinct trough was observed between 250 ºC and 500 ºC in PEG-ceria-modified SiNPs, confirming the presence of cerium nitrate hexahydrate, the predominant component of CeNPs (Figure 3.3B).

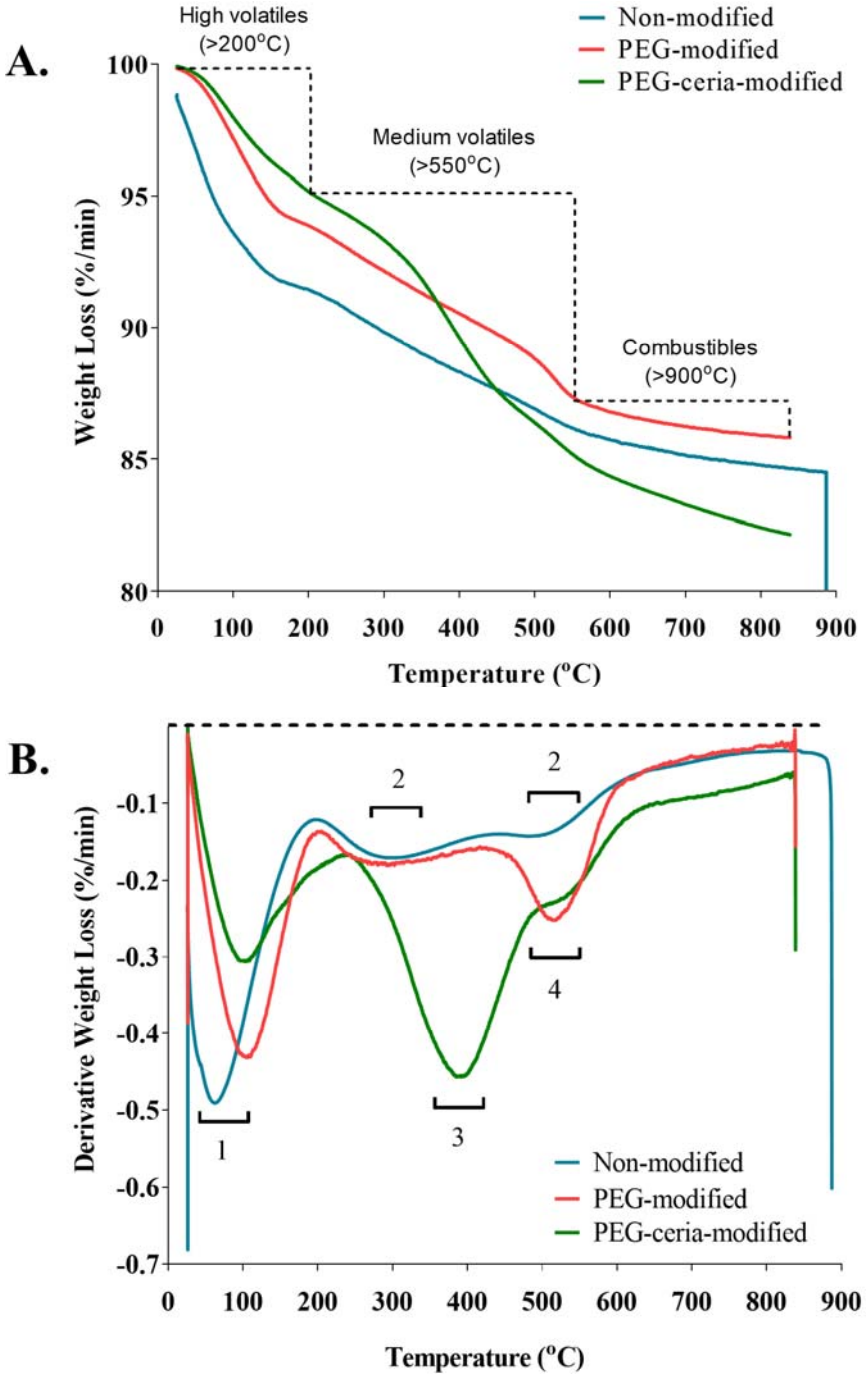

Figure 3.3. Thermal stability of SiNPs. *(A) Cumulative (%) and (B) derivative weight loss (%/min) of non-modified (blue), PEG-modified (red) and PEG-ceria modified (green) SiNPs as a function of increasing temperature (0 - 900 °C) using thermogravimetric analysis. Analysis of derivative weight loss enabled the evaporation temperatures of water (1; 100 °C), FITC (2; 290 °C and 500 °C), cerium nitrate (3; 390 °C) and PEG (4; 510 °C) to be identified.*

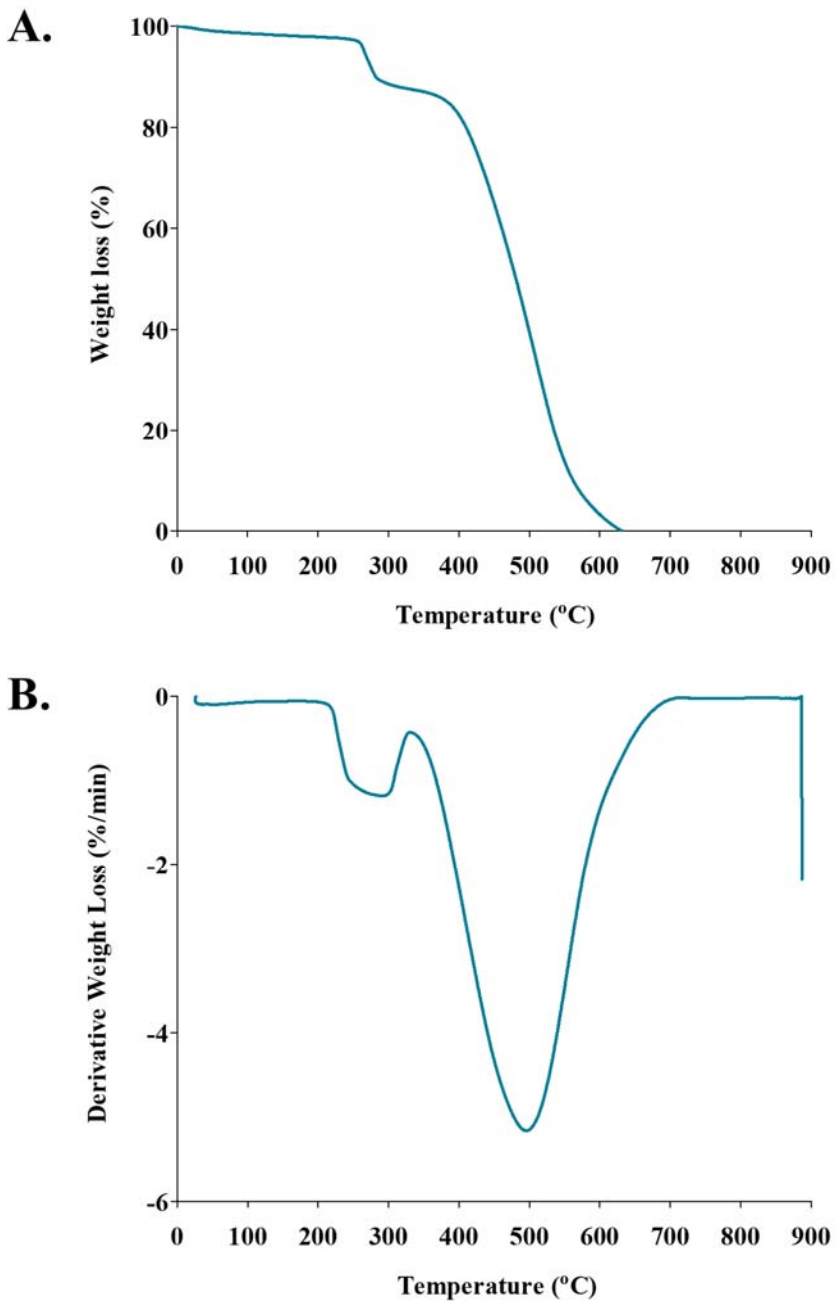

Figure 3.4. Thermal stability of FITC dye. *(A) Cumulative (%) and (B) derivative weight loss (%/min) of fluorescein isothiocyanate (FITC) as a function of increasing temperature (0 - 900 °C) using thermogravimetric analysis. Analysis of derivative weight loss enabled the evaporation temperatures of FITC to be identified, with significant reductions observed at 290 °C and 500 °C.*

The next characteristic assessed was the stability and electrophoretic mobility of the SiNPs. The zeta potential of non-modified SiNPs in water, PSS and media was -35.8 ± 1.15 mV, -31 ± 1.13 mV and -19.1 ± 1.32 mV, respectively. Amine-modified SiNPs in water, PSS and media was -43.7 ± 2.67 mV, -2.55 ± 0.22 mV and -10.7 ± 1.16 mV, respectively. PEG-modified SiNPs in water, PSS and media was -48.53 ± 3.56 mV, -24.3 ± 2.19 mV and -18.7 ± 1.19 mV, respectively. PEG-ceria-modified SiNPs in water, PSS and media was -36.13 ± 2.32 mV, -19.9 ± 2 mV, and -21.9 ± 1.12 mV, respectively (Figure 3.5).

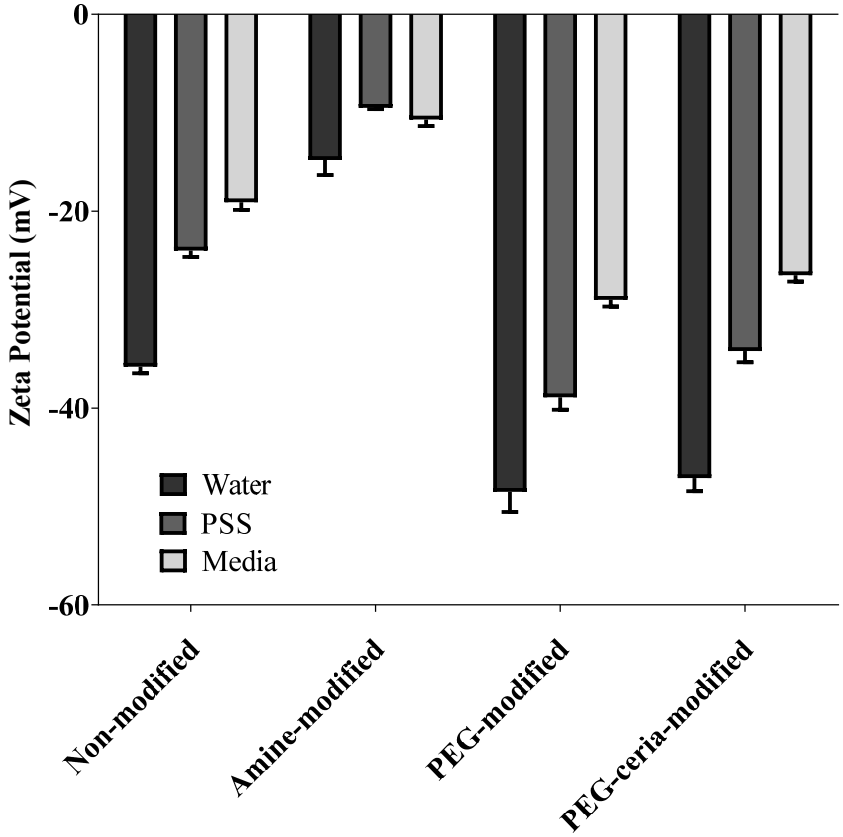

Figure 3.5. Stability and electrophoretic mobility of SiNPs in aqueous medium. *SiNP stability was immediately assessed in water, physiological salt solution (PSS) and endothelial cell growth medium MV2 using laser doppler micro-electrophoresis. Zeta potential measurements for non-modified SiNPs in water, PSS and media were -35.8 ± 1.15 mV, -31 ± 1.13mV and -19.1 ± 1.32mV, respectively. Amine-modified SiNPs in water, PSS and media were -43.7 ± 2.67 mV, -2.55 ± 0.22 mV and -10.7 ± 1.16 m, respectively. PEG-modified SiNPs in water, PSS and media were -48.53 ± 3.56 mV, -24.3 ± 2.19mV and -18.7 ± 1.19mV, respectively. PEG-ceria-modified SiNPs in water, PSS and media were -36.13 ± 2.32 mV, -19.9 ± 2 mV, and -21.9 ± 1.12mV, respectively (n = 3). Data are presented as mean ± SEM.*

Electron microscopy was used to determine the morphological structure and size of the SiNPs. SEM successfully confirmed them to be spherical and monodispersed, with an average size of 63.2 ± 8.5 nm (Figure 3.6). TEM identified non-, amine-, PEG- and PEG-ceria-modified SiNPs as polydisperse (Figure 3.7A-D); surface functionalisation with PEG-ceria was confirmed morphologically, with CeNPs encompassing the SiNP periphery (Figure 3.7D). The size distribution of SiNPs ranged between 50 and 190 nm, with an average size of 105 ± 30.5 nm and were therefore deemed suitable for characterisation and use (Figure 3.7E).

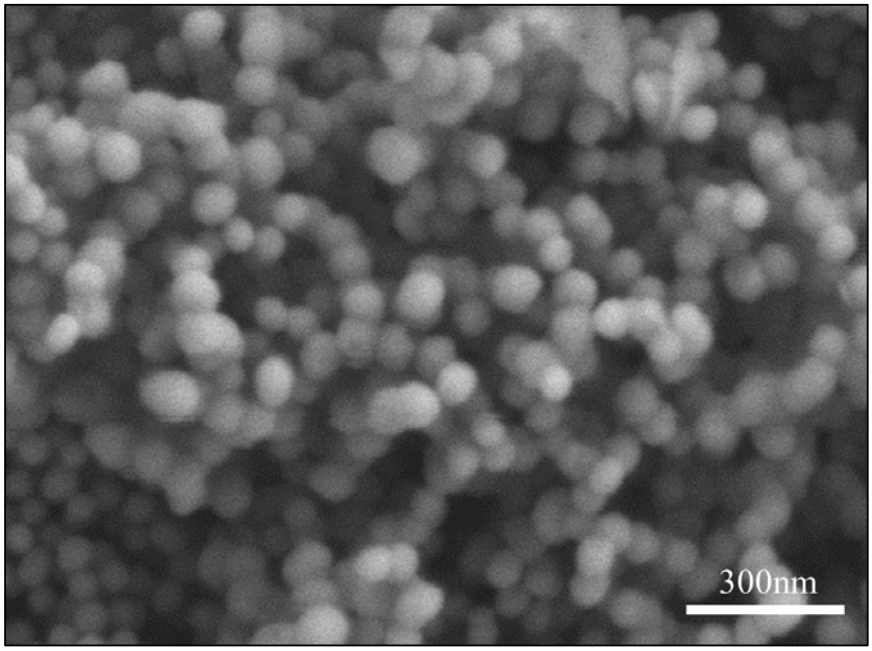

Figure 3.6. Morphological structure of SiNPs. *Representative scanning electron (SEM) micrographs of non-modified SiNPs. SiNPs were dried and imaged. SiNPs are seen as spherical and monodispersed, with an average particle size of 63.2 ± 8.5 nm. Magnification 100,000 x. Scale bar = 300 nm.*

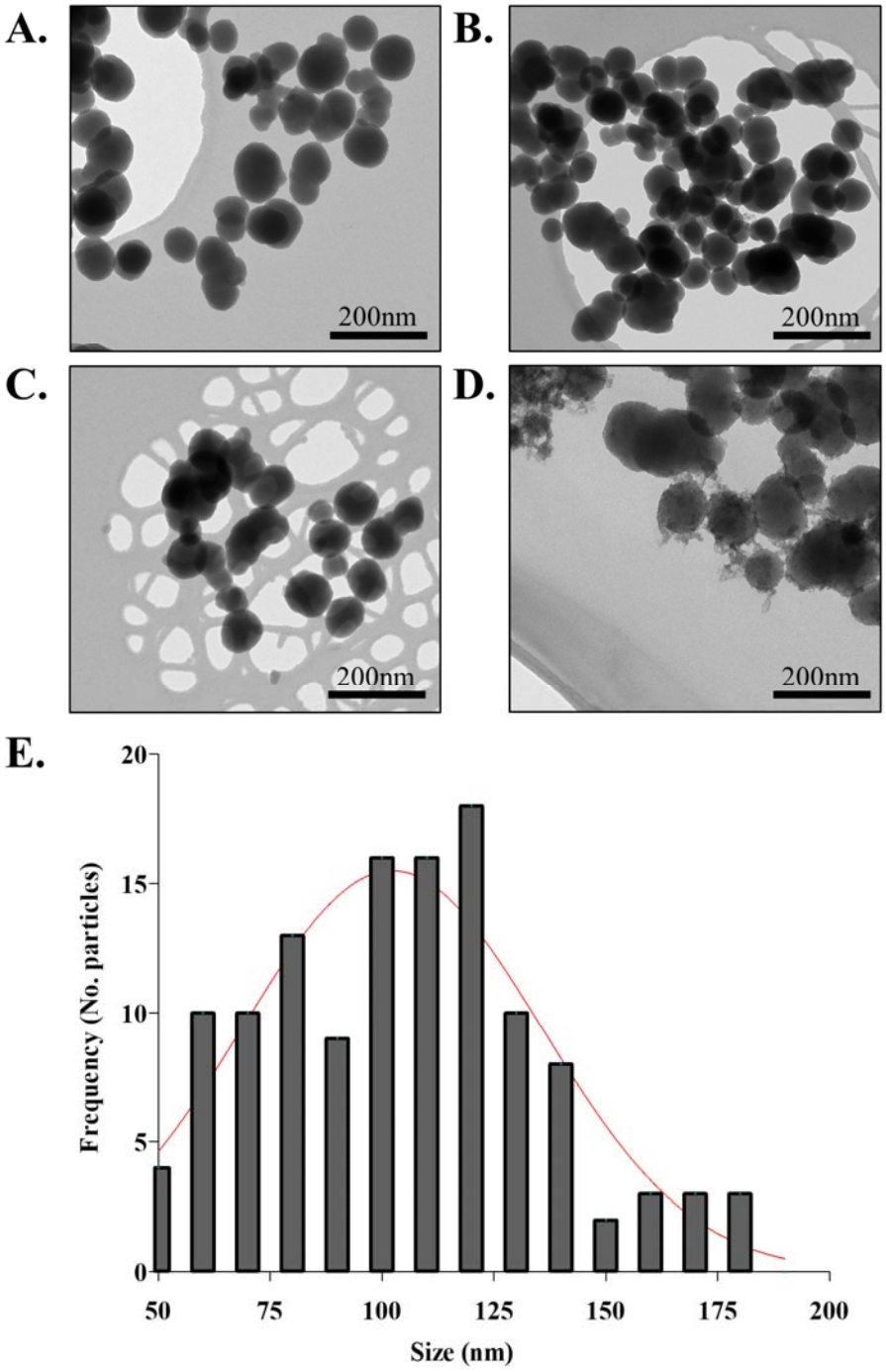

Figure 3.7. Morphological structure and size distribution of SiNPs. *Representative transmission electron (TEM) micrographs of (A) non-modified, (B) amine-modified, (C) PEG-modified and (D) PEG-ceria-modified SiNPs. Particle size distribution acquired from representative TEM micrographs (E). Random measurement sampling (n = 60) from non-modified, amine-modified, PEG-modified and PEG-ceria-modified SiNP micrographs (ImageJ). SiNPs are polydispersed, with an average size of 105 ± 30.5 nm. Magnification 23,000 x. Scale bar = 200 nm.*

3.1.2 PEG-ceria-modified SiNPs reduce hydroxyl radical generation

To ascertain the intrinsic reactivity of SiNPs, dichlorodihydrofluorescein diacetate (DCFH-DA) was used to quantify $^{\bullet}OH$ and peroxyl (HOO^{-}) radical generation in solution. Amine-modification of SiNPs significantly increased $^{\bullet}OH$ and HOO^{-} generating capacity in comparison to non-modified SiNPs ($P = < 0.05$); Figure 3.8); PEG-modification had no effect. PEG-ceria-modification resulted in a significant reduction in $^{\bullet}OH$ and HOO^{-} generating capacity in comparison to non-modified SiNPs ($P = < 0.05$). MSNs were included as a negative control, displaying significantly reduced $^{\bullet}OH$ and HOO^{-} generating capacity in solution compared to non-modified SiNPs ($P = < 0.001$).

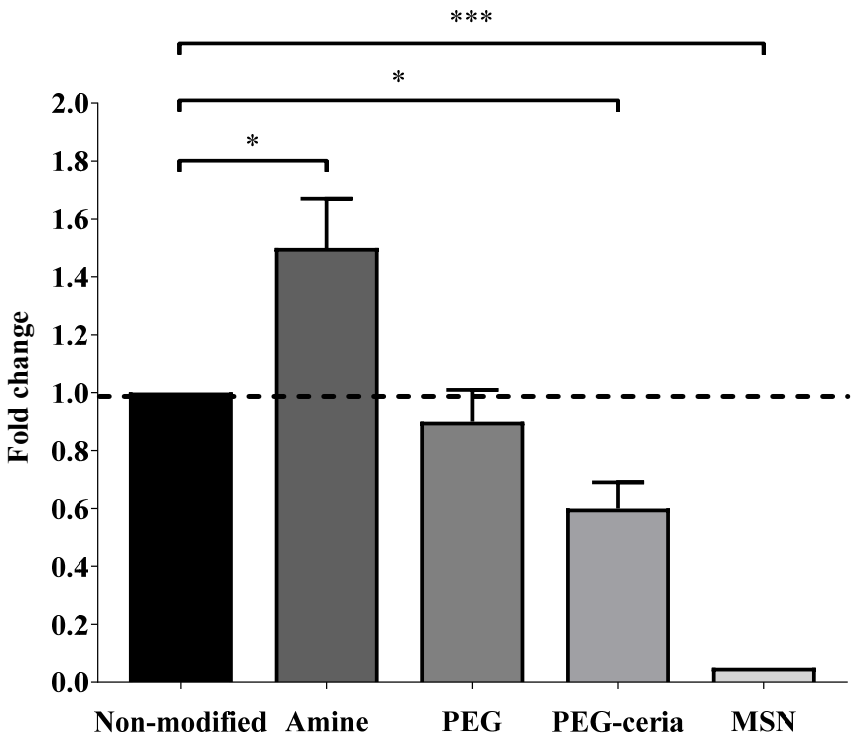

Figure 3.8. Effect of SiNP surface functionalisation on hydroxyl and peroxyl radical generation. *DCFH-DA fluorescence quantification highlighting hydroxyl radical generation in solution following 15-minutes incubation with SiNPs (5 mg/ml; non-modified, amine-modified, PEG-modified, PEG-ceria-modified) and mesoporous silica nanoparticles (MSNs) (n = 3). Data expressed as fold change from control (non-modified). Amine-modified*

*SiNPs significantly increased hydroxyl and peroxyl generating capacity in comparison to non-modified SiNPs (P = < 0.05); PEG-modification had no effect. PEG-ceria-modification significantly reduced the hydroxyl and peroxyl generating capacity of SiNPs, compared to non-modified (P = < 0.05). MSNs were included as a negative control, displaying significantly reduced hydroxyl and peroxyl generating capacity in solution compared to non-modified SiNPs (P = < 0.001). Experiment performed in triplicate and repeated three times. One-way ANOVA followed by a Dunnett's multiple comparison. Data are presented as mean ± SEM. * P < 0.05. *** P < 0.001.*

Amplex red was used to quantify H_2O_2 and other peroxide activity, allowing a determination of the antioxidant capacity of SiNPs. Following 30-minutes incubation with H_2O_2 (0-10 μM), a concentration-response curve was produced (Figure 3.9A). A significant reduction in H_2O_2 and peroxidase activity was observed in solution following 30-minutes incubation with PEG-ceria-modified SiNPs, in comparison to its non-modified counterpart (Figure 3.9B; $P = < 0.001$).

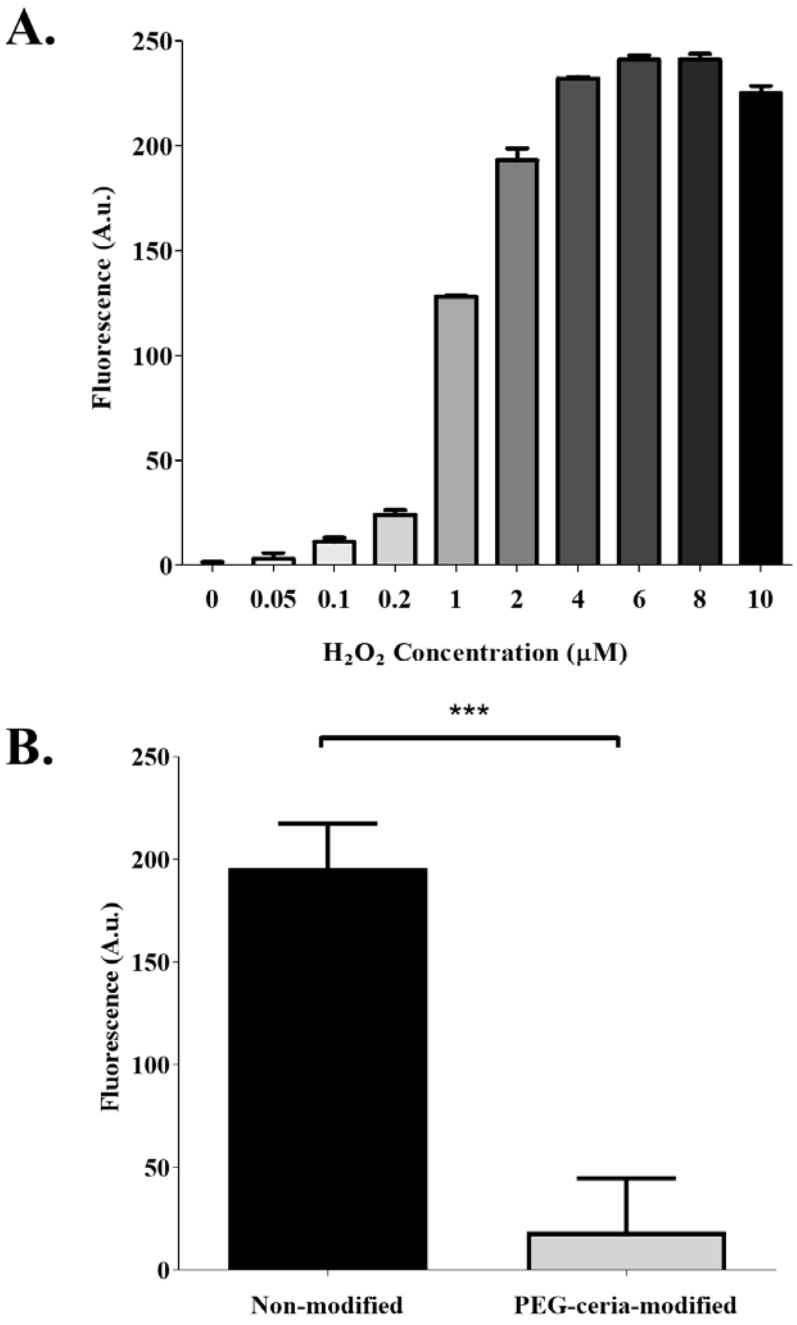

Figure 3.9. Effect of SiNP functionalisation on antioxidant capacity in solution. *(A) Dose-response effect of hydrogen peroxide (H_2O_2; 0 – 10 μM; n = 3) on amplex red fluorescence following 30-minutes incubation. (B) PEG-ceria-modification significantly reduced H_2O_2 and peroxidase activity in solution, in comparison to non-modified SiNPs (5 mg/ml; P = < 0.001; n = 3) following 30-minutes incubation in a H_2O_2 solution (10 μM). Experiment performed in triplicate and repeated three times. Data was analysed using an unpaired t-test. Data are presented as mean ± SEM. *** P < 0.001.*

3.1.3 PEG-ceria-modified SiNPs maintain and improve endothelial cell viability

Having characterised the properties of each of the modified and non-modified SiNPs, it was next of interest to assess their effects on endothelial cells *in vitro*. Following 24-hours co-incubation with SiNPs (non-, PEG-, PEG-ceria-modified), no significant change in HCAEC viability was observed, other than at 1 x 10^{12} and 10^{13} NPs/ml (Figure 3.10). At 1 x 10^{12} and 1 x 10^{13} NPs/ml, PEG- and PEG-ceria-modification significantly improved viability compared to non-modified SiNPs, respectively ($P = < 0.01$; $P = < 0.001$).

3.1.4 SiNPs are successfully taken up by endothelial cells

Having identified the most biocompatible concentrations for use, it was of interest to assess SiNP uptake and localisation within cells. Confocal microscopy demonstrated that non-modified SiNPs (1 x 10^{11} NPs/ml) were taken up by HCAECs after 24-hours (Figure 3.11); whilst fluorescence microscopy demonstrated the apparent localisation of SiNPs within endosomal structures (Figure 3.12).

TEM demonstrated uptake of SiNPs (1 x 10^{11} NPs/ml) into HCAECs over a 4-hour period. In control cells (untreated; Figure 3.13A), the cytoplasmic compartment did not appear to have any significant alterations. Although after 1-hour incubation, SiNPs were observed localised in small clusters within cytoplasmic endosomes (Figure 3.13B), with further uptake observed after 2- and 4-hours; with apparent fusion and degradation occurring (Figure 3.13C, D).

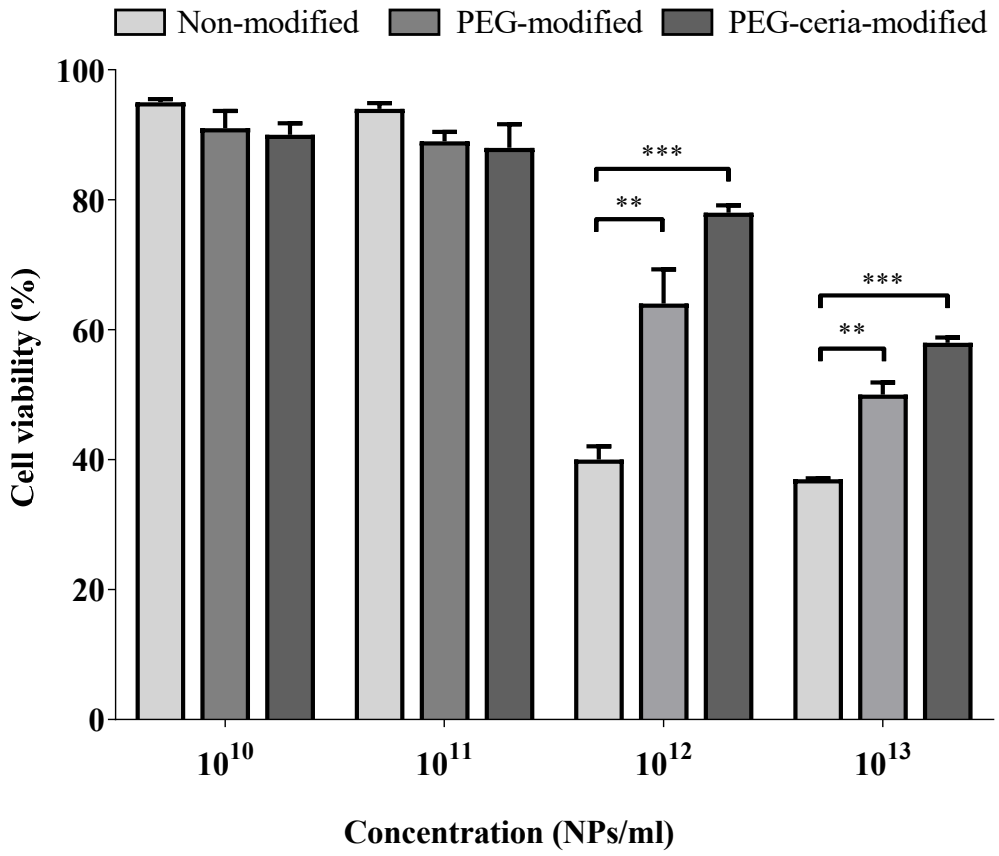

Figure 3.10. Effect of SiNP functionalisation on cell viability. *Human coronary artery endothelial cell (HCAEC) viability following exposure to SiNPs (non-modified, PEG-modified and PEG-ceria modified) at concentrations of 10^{10}, 10^{11}, 10^{12}, 10^{13} NPs/ml over 24-hours. Cell viability determined using an Alamar blue assay (n = 3). Data normalised to control wells (untreated). SiNPs had no significant effects on cell viability, other than at 1 x 10^{12} and 10^{13} NPs/ml. At 1 x 10^{12} NPs/ml, PEG- and PEG-ceria-modification significantly improved viability compared to non-modified SiNPs (P = < 0.01; P = < 0.001, respectively). At 1 x 10^{13} NPs/ml, PEG- and PEG-ceria-modification significantly improved viability compared to non-modified SiNPs (P = < 0.01; P = < 0.001, respectively). Experiment performed in triplicate and repeated three times. Cell viability was analysed by a two-way ANOVA followed by a Tukey's multiple comparison. Data are presented as mean ± SEM. ** P < 0.01. *** P < 0.001.*

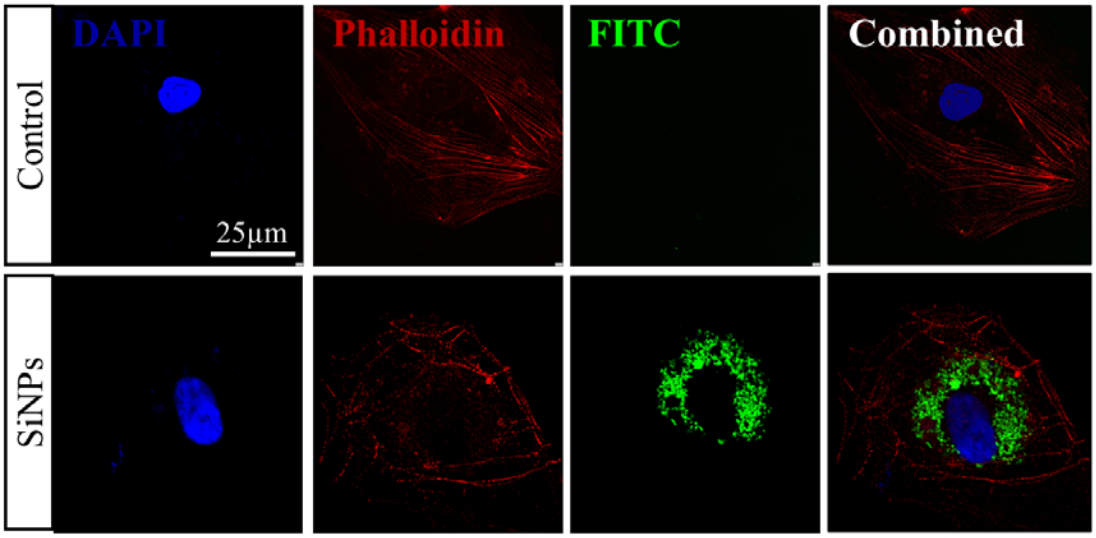

Figure 3.11. SiNP uptake by HCAECs in culture. *Representative confocal fluorescence micrographs of human coronary artery endothelial cells (HCAECs). Cultured cells were incubated with growth medium in the presence/absence of non-modified SiNPs (FITC-loaded; 1 x 10^{11} NPs/ml) for 24-hours, followed by DAPI (nuclear) and phalloidin (actin) staining. Magnification 40 x. Scale bar = 25 µm. Images acquired from 1 of 5 representative slides.*

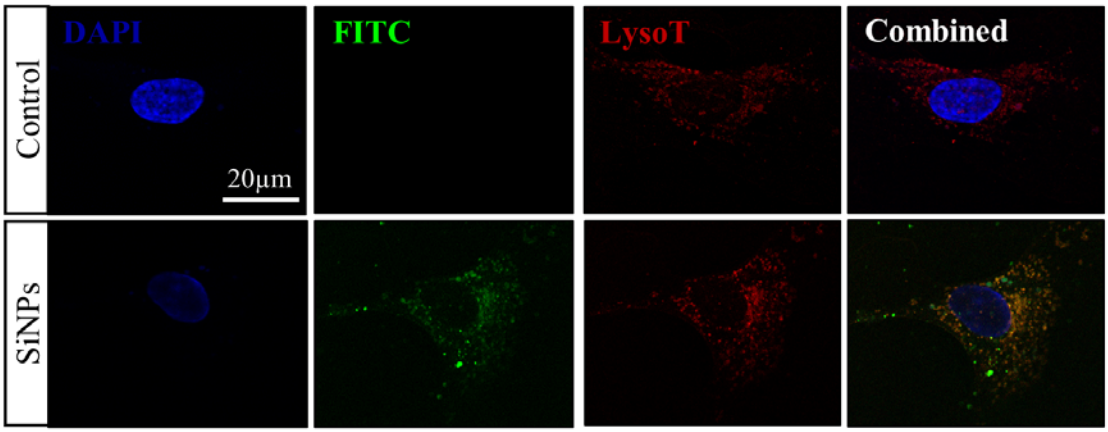

Figure 3.12. Endosomal SiNP uptake within HCAECs in culture. *Representative fluorescence micrographs of human coronary artery endothelial cells (HCAECs) incubated with growth medium in the presence/absence of non-modified SiNPs (FITC-loaded; 1 x 10^{11} NPs/ml) for 24-hours, followed by DAPI (nuclear) and lysotracker (lysosomal/endosomal) staining. Magnification 65 x. Scale bar = 20 µm. Images acquired from 1 of 5 representative slides.*

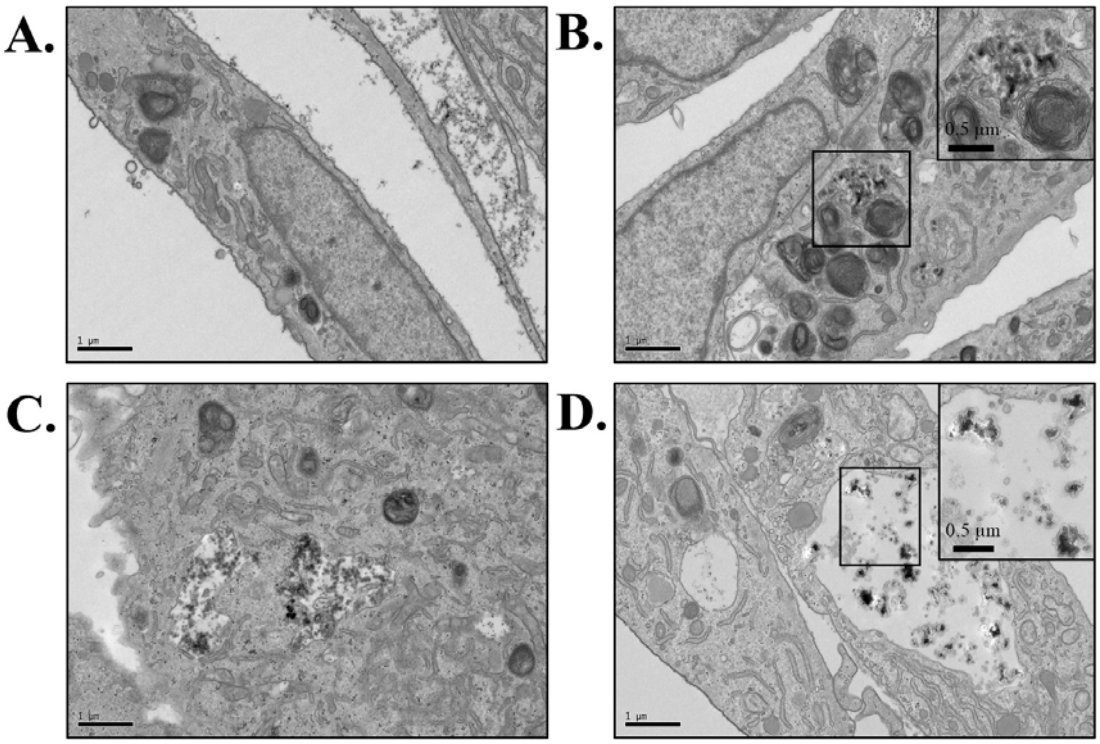

Figure 3.13. Time-dependent uptake of SiNPs by HCAECs in culture. *Representative transmission electron micrographs illustrating the uptake of non-modified SiNPs (1 x 10^{11} NPs/ml) at (A) 0-hours; (B) 1-hour; (C) 2-hours and (D) 4-hours. Following 1-hour incubation, SiNPs were localised in small clusters within cytoplasmic endosomes. After 2- and 4-hours, an increased number of SiNPs could be observed within endosomal structures; with apparent fusion and degradation occurring. SiNPs are represented by black structures. Magnification 1,200 x. Scale bars = 1 µm and 0.5 µm, respectively.*

3.2 Discussion

3.2.1 SiNPs were successfully synthesised and characterised

Inorganic SiNPs of various functionalities were synthesised and characterised, with drug and dye entrapment confirmed using UV-VIS and fluorescence spectroscopy. While the FTIR confirmed the presence of characteristic silanol groups, the spectrographic profile of CeO_2 was not distinguishable, due to the lack of sensitivity of this approach; incapable of observing Ce-O stretching bands expected at 400-600 cm^{-1} (Zamiri et al., 2015). Peaks observed at 2330 cm^{-1} correlate with atmospheric CO_2 (Kauffman et al., 2011). Appropriate background correction should mitigate the presence of such peaks; however, high-resolution acquisition over prolonged/extended periods of time may result in CO_2 adsorption onto the particle. These 'artificial' peaks may substantially impact the interpretation of spectra at various wavelengths, e.g. vibrational bands at 1680–1620 cm^{-1} are frequently associated with H_2O and Si-OH groups; however, adsorption of CO_2 onto the silica surface can lead to the formation of carboxylic compounds, with absorbance found in the same range (Basyuk, 1994). Therefore, further characterisation of the SiNPs was necessary. TGA confirmed successful surface modification and dye-entrapment, including that of the CeO_2 component, cerium-nitrate. PEG is a hygroscopic compound and has been shown to marginally retard water loss in hydrogels, delaying its evaporation (Hackl et al., 2015); attributable to the presence of ether oxygen atoms (-O-) and hydroxyl end groups which can form multiple hydrogen bonds with water (Hsu et al., 2015). Similar observations are made in both PEG and PEG-ceria-modified SiNPs, reflected by a rightward shift (derivative) in the evaporation temperatures of volatile compounds (e.g. water) below 200 ^{o}C. Next, the stability of SiNPs was assessed.

The zeta potential measurements confirmed the stability of non-, PEG- and PEG-ceria-modified SiNPs in water, indicative of low agglomeration and flocculation capacity (Večeř and Pospíšil, 2012). The conjugation of positively charged amino groups onto the particle surface is commonly associated with a net positive charge. The negative charge observed in amine-modified SiNPs, although to a lesser extent than others, is suggestive of incomplete surface functionalisation and hence the reason why these nanoparticles were not used in further experimentation. In each instance, an increase in zeta potential was observed in PSS and media, signifying a reduction in nanoparticle stability; attributable to ion and protein adsorption on the nanoparticle surface, consistent with previous findings (Krętowski et al., 2017). Briefly, following suspension in an aqueous medium such as water, molecules engulf the nanoparticulate surface to produce a structured hydration layer, otherwise known as a Stern layer. The resulting electrostatic forces generate low-level attraction, drawing additional ions inward towards the Stern layer; producing an area termed as the diffuse layer. The electrical potential between these two layers is frequently referred to as the zeta potential; with values in excess of +30 mV or −30 mV being indicative of stable suspensions, whereby particles are not liable to aggregation or flocculation (Bhattacharjee, 2016). The introduction of a highly ionic medium such as PSS or culture media often results in the displacement of water molecules from the particle surface, reducing the integrity of the hydration layer and elevating zeta potential. Furthermore, the presence of serum proteins in culture medium has been observed to reduce particulate stability, following absorption and subsequent corona formation (Hao et al., 2012; Kurtz-Chalot et al., 2017). The reduced stability observed was to a lesser extent in PEG-modified SiNPs. Conventionally, particles rapidly aggregate via van der Waals and/or hydrophobic forces in high-ionic aqueous conditions. As a result of its hydrophilic nature, surface modification with PEG produces a large exclusion zone that sterically precludes SiNPs from interacting with adjacent SiNPs

and/or ions/proteins, retaining their colloidal stability (Kurtz-Chalot et al., 2017), making them a favourable model for the further studies undertaken within this project.

SEM identified SiNPs as spherical in structure with an approximate size of 63.2 ± 8.5 nm. Despite the popularity of SEM for the analysis of sub-micron materials, the technique is hindered by limited resolution and magnification. However, TEM provided images of much higher clarity; identifying spherical, polydisperse SiNPs with an average size of 105 ± 30 nm. In colloid science, LaMer's nucleation theory is used to describe the generation and growth of colloidal materials (LaMer and Dinegar, 1950). The process undergoes three stages: 1) monomer formation and accumulation, reaching critical supersaturation; 2) rapid self-nucleation of monomers; 3) end of self-nucleation, and growth by diffusion of the remaining monomers in solution towards the particle surface. One possibility which may account for the polydispersity observed is the premature cessation of the reaction, with SiNPs still being in the self-nucleation phase and not fully developed. Polydisperse nanoparticles can be problematic in relation to their use as a treatment strategy for a number of reasons. Most notably, several studies have demonstrated the size, uptake and toxicity dependent relationship of SiNPs in a variety of cell types; whereby smaller particles exhibit increased levels of toxicity (Napierska et al., 2009; Gramatke, 2014). Furthermore, nanoparticle surface area has been shown to be integral in determining reactivity with the local environment, with smaller particles having a larger surface area (i.e. larger surface area to volume ratio)(Farooq, 2014). It has been reported that SiNP surface groups have the potential to generate $^{\bullet}OH$ radicals, which may contribute to cellular damage and toxicity (Shang et al., 2009). Consequently, the resulting variation in size produces an inability to accurately calculate the total surface area available, making predictions of treatment efficacy or downstream side-effects difficult.

3.2.2 PEG-ceria modification reduces hydroxyl radical generation

The oxidative capacity of SiNPs was assessed in solution. Following PEG-ceria-modification, a significant reduction in $^{\bullet}OH$ generation and/or release was observed, compared to non-modified controls. The surface chemistry and reactivity of SiNPs are recognised as being integral in regulating their biological responses, with means of synthesis and density of surface silanol groups (−Si-O-H) being an important factor in the modulation of toxicity (Nash et al., 1966). However, the specific mechanism by which surface silanol groups induce toxicity is unclear. Surface groups have been shown to encourage ROS generation, lipid peroxidation and DNA damage upon interaction with biological components *in vitro* (Duan et al., 2013a). However, these findings are contentious, with some demonstrating ROS-independent impairment of cell viability and vascular function following SiNP exposure (Shukur et al., 2016). In some instances, silica has been shown to be chemically reactive in the absence of a biological environment. In the case of fumed silica, researchers demonstrated that the cleavage of strained siloxane rings was responsible for the production of $^{\bullet}OH$ from the SiNP surface (Zhang et al., 2012). In contrast, this study has focused on the use of colloidal silica prepared via sol-gel. Despite differences in their respective modes of synthesis, similar underlying mechanisms of action may be present. Our data are consistent with previously observed results, with SiNPs generating ROS in a cell-free system, implicating an underlying chemical reaction/mechanism of action. CeO_2 has repeatedly demonstrated SOD and CAT catalytic activity in a range of *in vitro* and *in vivo* models (Rzigalinski et al., 2006; Korsvik et al., 2007); attributable to the active absorption and release of oxygen and effective redox cycling between Ce^{3+} and Ce^{4+} oxidation states. Furthermore, it has also been shown to be highly effective at reducing $^{\bullet}OH$ via direct scavenging (Xue et al., 2011; Filippi et al., 2019). Findings from this study are consistent

with previously observed results, with PEG-ceria- modification resulting in a 40 % average reduction in radical generation. In addition to the inherent antioxidant activity of CeO_2, it is likely that particle attachment to the SiNP surface reduces the total surface area, obscuring reactive silanol groups. The conjugation of surface groups onto nanoparticles has been shown to modulate toxicity, with PEG having been shown to sterically hinder the particle surface (Pozzi et al., 2014). As a result of this steric hindrance, PEG-modification would be expected to reduce interaction with surface groups, limiting reactivity (Mohammadi et al., 2018). Surprisingly, however, PEG-modification resulted in a small yet non-significant reduction in ROS generation. In order to establish a monodisperse, heterogeneous dispersion and expose the total nanoparticle surface area in our studies, samples were sonicated. However, previous research has revealed that PEG is highly sensitive to sonolytic degradation, with a 25 % reduction in total PEG observed within as little as 15-minutes (Murali et al., 2015). Such alterations in surface chemistry may negate the beneficial effects that PEG-modification may confer. In contrast to PEG-modification, which is ordinarily used to limit cellular uptake and biological interaction, APTES conjugation is utilised as a means of increasing cellular uptake; a result of electrostatic interactions between positively charged amino groups and the negatively charged cell membrane. Some studies have suggested that amine-modification reduces innate reactivity in a similar capacity to that of PEG, reducing the number of exposed silanol moieties on the surface (via replacement with aminopropyl functional groups), whilst also sterically hindering surface interactions (Lehman et al., 2016; Morris et al., 2016). Our findings differ from previous studies, with amine-modification significantly elevating reactivity. Differences in experimental design may account for the varied observations between studies. In addition to the damaging effect on surface groups, it is well documented that the inertial collapse of cavitation bubbles during sonication are capable of inducing sonochemical reactions, generating ROS, e.g. the

generation of $^{\bullet}OH$ and H_2O_2 in pure water (Makino et al., 1983). Although these phenomena would be consistent across all samples, the formation of highly reactive aminoxyl radical is noted in the literature to occur under oxidising conditions and thus, may account for the elevated reactivity observed in amine-modified SiNPs (Lind and Merényi, 2006). Furthermore, the incomplete surface functionalisation, as denoted by zeta potential measurements, would likely leave surface silanol groups exposed and open to reactivity. Incubation with mesoporous nanoparticles (MSNs) resulted in significantly lower reactivity compared to amphorous SiNPs. This is surprising, given the increased total surface area of MSNs, increased reactivity with surface silanol groups would be expected. Similar findings have been observed using electron spin resonance spectroscopy, identifying a 7-fold reduction in $^{\bullet}OH$ formation from MSNs compared to non-porous SiNPs (Lehman et al., 2016). These observations may be related to the isotropic motion of molecules (radicals), limiting diffusion; resulting in flux through the porous network being heavily reliant on concentration gradients. Hence, whilst MSNs possess a much larger surface area, the majority is located within the pores; thus, the surface area in direct contact per unit time with the reactive molecules is much lower in the porous material and may explain why mesoporous material gives rise to lower reactivity than that of the nonporous material. Despite the prevalence of DCFH for the quantification of ROS, several notable limitations must be considered. DCFH is a multi-stage reaction and thus does not operate as a direct measure of H_2O_2 and/or $^{\bullet}OH$, introducing the possibility of external interference. Secondly, the intermediate radical, DCF, formed via the one-electron oxidation of DCFH, reacts with O_2 to form $O_2^{\bullet-}$. The SOD mimetic activity of CeO_2 leads to the dismutation of $O_2^{\bullet-}$, yielding additional H_2O_2. This redox-cycling mechanism has the potential for artefactual amplification of fluorescence signal intensity, confounding findings (Folkes et al., 2009). Finally, DCFH-DA is conventionally used as a cell-based assay, with activation requiring

esterase cleavage. In order to adapt the protocol to work in a cell-free system, chemical cleavage is required; hence, it is not directly comparable to other studies and impurities in chemical reagents might introduce artefacts.

The antioxidant capacity of the SiNPs was also assessed using a direct measurement technique. Amplex red was able to successfully confirm the antioxidant capacity of PEG-ceria-modified SiNPs, with a similar trend to DCFH identified. Following its addition into a H_2O_2 solution, ceria-modified SiNPs were capable of quenching significantly more H_2O_2 in comparison to its non-modified counterpart, highlighting the CAT mimetic activity and ROS quenching capacity of CeO_2. Previous studies have also demonstrated similar CAT mimetic activity using Amplex red in a cell-free system (Baldim et al., 2018). In contrast to DCFH, oxidation of the Amplex red probe is catalysed by HRP in the presence of H_2O_2 and is highly efficient, vastly increasing the yield of resorufin.

3.2.3 SiNPs are successfully taken up by endothelial cells

Uptake into HCAECs was confirmed within 24-hours of exposure of the cell to the SiNPs, which were observed throughout the cytosol, appearing to localise around the nucleus. Previous literature has observed the localisation of SiNPs within endosomal/lysosomal structures in the cytoplasm of the cell, with none present within the nucleus (Pritz et al., 2013; Shukur et al., 2016). In contrast to the highly organised actin filaments of control cells, SiNP treated cells appeared to have a disorganised actin structure. Nanoparticles (e.g. silica, silver) have previously been shown to cause cytoskeletal disturbances, causing disruption and disorganisation of F-actin fibres in primary human endothelial cells (Xu et al., 2013; Duan et al., 2014); potentially explaining the altered distribution and/or inadequate staining of actin within cells. Fluorescence imaging would be beneficial in assessing the time-

dependent uptake of SiNPs, as well as expulsion at later time-points. However, in the case of polydisperse samples, fluorescence should be avoided as a reliable means of quantification, with variations in SiNP size likely resulting in variable FITC loading capacity which may result in over or under-representation of SiNP uptake. SiNP uptake was successfully demonstrated over 4-hours using TEM, localising within endosomal structures; consistent with fluorescence data. SiNPs are endocytosed by cells and stored in small clusters within cytoplasmic endosomes, providing further evidence that an endocytic pathway of uptake may be involved (Pritz et al., 2013; Shukur et al., 2016). However, internalisation of SiNPs resulted in the apparent fusion and degradation of SiNPs after several hours. SiNP degradation is known to be dependent on several factors, including pH (Yang et al., 2018; Hadipour et al., 2019). The pH of endosomes/lysosomes (6.5 to 4.5*)* is significantly lower than that of the surrounding cytoplasm (pH 7.0), which may partially account for the degradation observed (Yang et al., 2018). SiNP degradation products have been studied extensively, with orthosilicic acid, ($Si(OH)_4$) identified as a major by-product (Quignard et al., 2017). $Si(OH)_4$ is soluble, non-toxic and has been shown to be distributed throughout tissues, blood vessels before excretion through the urinary system (Jurkić et al., 2013).

3.2.4 PEG-ceria-modification improves endothelial cell viability

Consistent with studies investigating the effects of SiNPs exposure on endothelial cells, SiNPs had no effect at lower concentrations, whilst reducing viability at higher concentrations (Nemmar et al., 2014; Guo et al., 2016). Conventionally, SiNP dosages are calculated as μg/ml; however, reactions mediated at the nanoparticle surface have been shown to be the predominant factor involved in ROS mediated toxicity, propagated by their

high surface area to volume ratio (Duan et al., 2013b, 2014). In light of this, the use of µg/ml does not reflect the total surface area of the nanoparticles; hence, in our studies, concentrations were calculated and displayed as NPs/ml, as opposed to mass (Shin et al., 2015). PEG-modification significantly improved cell viability at high SiNP concentrations, which may be attributed to its reduced uptake, steric hindrance, and repulsion forces exerted by surface chains against surrounding contents. In addition to the benefits conferred by PEG, functionalisation with cerium-oxide facilitates antioxidant reactions following their eventual uptake, minimising ROS mediated damage to cellular proteins and lipids (Rzigalinski et al., 2006; Korsvik et al., 2007)

3.3 Chapter summary

In summary, this part of the study aimed to develop a nanoparticle-based delivery platform for the potential loading and release of antioxidant compounds, with the ultimate goal being the development of a potential therapeutic tool for the treatment of diseases associated with elevated ROS in future applications. CeO_2 functionalisation of SiNPs successfully attenuated surface reactivity, and demonstrated antioxidant capacity, resulting in heightened biocompatibility *in vitro*. However, several limitations were identified that would preclude their further use in this study; notably, their polydispersity and rapid degradation, which would result in inaccurate loading and uncontrolled release of drug. Consequently, it was concluded that subsequent work in this study would next investigate the effects of organic nanodelivery modalities to determine if they had improved drug delivery capacity, as will be described in the next chapter.

Chapter 4: Synthesis and characterisation of organic nanoparticles

CeO_2 functionalised SiNPs displayed promising antioxidant potential and improved biocompatibility in the previous chapter; however, due to the limitations associated with their synthesis, this chapter will focus on the use of organic nanolipid carriers (NLCs) and liposomes for the sustained delivery of antioxidant compounds for the treatment of CVD. The hypothesis of this part of study is that RV-loaded NLCs will enhance the delivery and release of drug, reducing oxidative stress *in vitro.* This hypothesis will be addressed through the following specific objective:

- Characterise organic lipid nanoparticles and define their antioxidant capacity and effect on endothelial cell viability *in vitro*.

RV-NLCs were supplied by our collaborators from the University of Central Lancashire (Prof. Singh, UCLAN). TMS-liposomes were supplied by our collaborators from the University of Manchester (Dr. Harris, UoM). They were prepared using a hot melt emulsification technique and thin film process, respectively. Dye and drug-loading were determined in the present study using ultra-violet visible spectroscopy (UV-VIS) and fluorescence-spectroscopy; composition was assessed using fourier transform infrared spectroscopy (FTIR). Hydrodynamic size and zeta potential were determined by dynamic light scattering (DLS) and laser doppler micro-electrophoresis (LDME). Size and morphology were also assessed using transmission electron microscopy (TEM). The *in vitro* release profile of RV-NLCs was assessed using the dialysis bag diffusion method. The effect of organic lipid nanoparticles on viability and uptake were assessed *in vitro* using alamar blue and fluorescence microscopy, respectively. The effects of RV-NLCs on HCAEC mitochondrial and cytosolic $O_2^{\bullet-}$ were determined using MitoSOX and dihydroethidium (DHE), respectively.

4.1 Results

4.1.1 RV-NLCs were successfully characterised

RV-loaded NLCs were synthesised and characterised in PSS solution. Using UV-VIS and fluorescence spectroscopy, RV- and RV-dye-loaded NLCs each displayed characteristic absorbance peaks at approximately 304 nm, confirming the presence of RV which was characteristically absent from the blank-NLCs (Figure 4.1A); a fluorescence peak was detected at 500 nm in RV-dye-loaded NLCs, confirming coumarin-6 loading (Figure 4.1B).

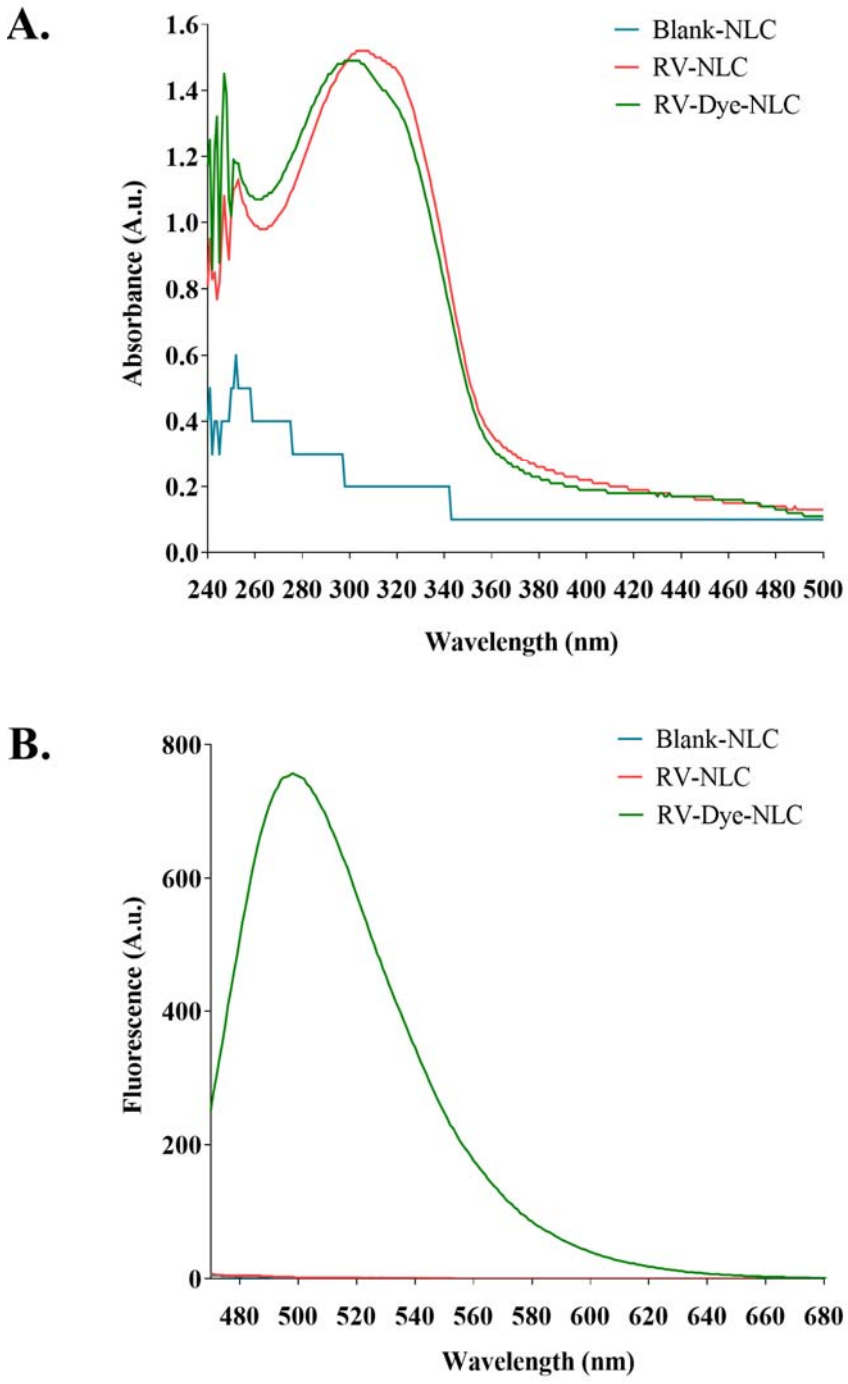

Figure 4.1. Confirmation of drug and dye-encapsulation within NLCs. *Characterisation of blank-, RV- and RV-dye-loaded nanolipid carriers (NLCs). (A) Ultraviolet-visible spectroscopy (UV-Vis) displaying absorbance spectra between 240-500 nm. Absorbance peaks were observed at 304nm in RV- and RV-dye-loaded NLCs, confirming the presence of RV; which was characteristically absent from the blank-NLCs. (B) Fluorescence-spectroscopy displaying spectra between 460-680 nm. A fluorescence peak was detected at 500 nm in RV-dye-loaded NLCs, confirming coumarin-6 loading.*

FTIR was used to confirm the molecular structure of the RV-NLCs. The strong, broad band characteristic for *trans*-RV can be observed between 3550-3200 cm^{-1}, originating from the OH valence vibrations of phenolic groups (Figure 4.2A). The bands 3021 cm^{-1} and 2924 cm^{-1} are a result of the valence vibration of ethenyl groups (=C-H) and C-H bonds, respectively. Phenolic compounds are consistently accompanied by characteristic aromatic hydrocarbons (benzene). The valence vibrations of the benzene ring (C=C) were observable at 1601, 1587, 1512 and 1444 cm^{-1}. The presence of RV could not be confirmed in the RV-NLCs using FTIR, due to the absence of corresponding peaks (Figure 4.2B). However, the infrared spectrum of NLCs highlight peaks corresponding to its parent lipid constituents, with peaks at 2950-2850 and 1730 cm^{-1} corresponding with the presence of alkane (C-H) and carbonyl ester groups (C=O), consistent to the lipid components trimystrin and glyceryl trioleate, respectively. The weak, broad band observed at 3400 cm^{-1} is attributed to OH stretching.

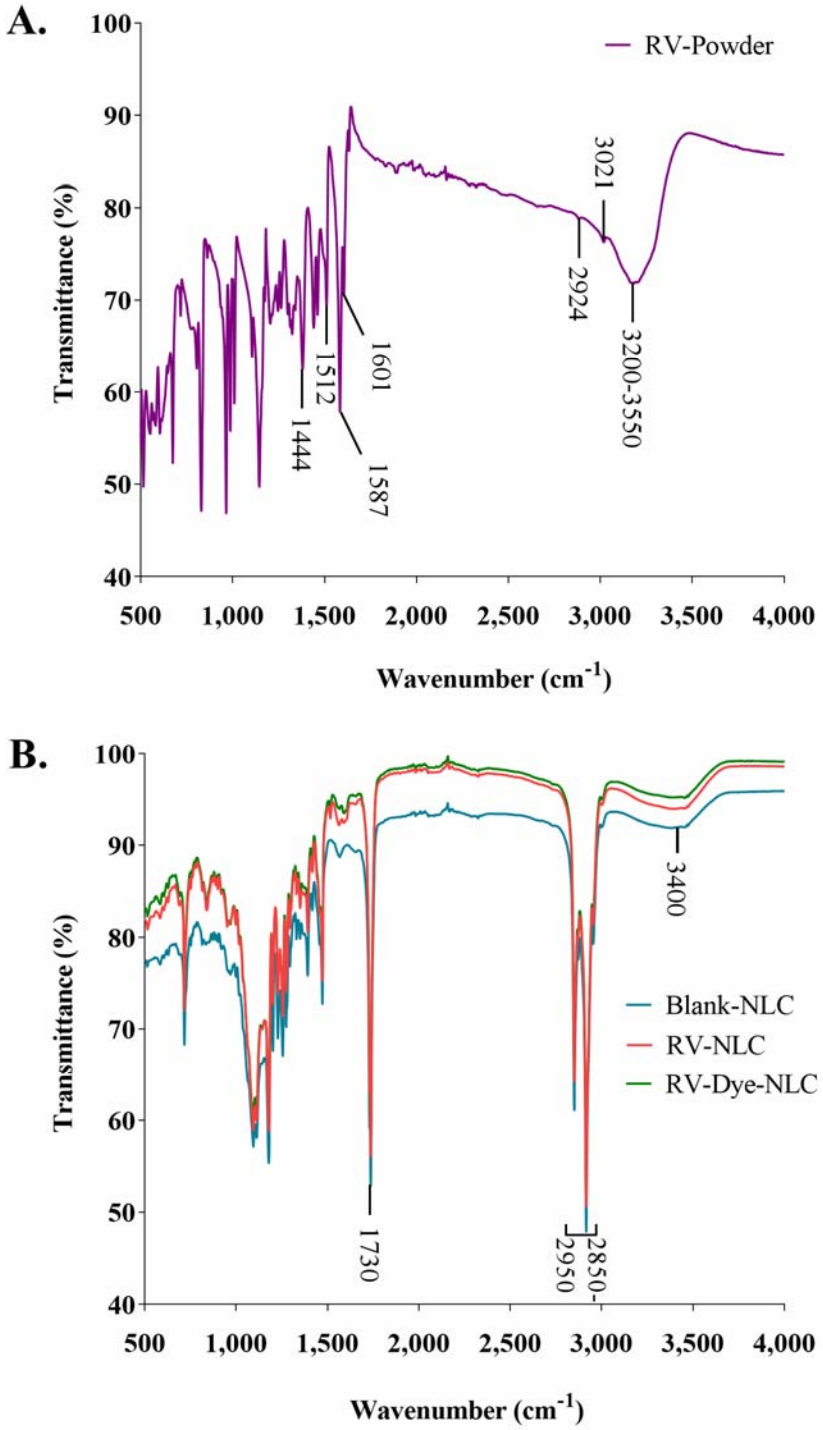

Figure 4.2. Confirmation of NLC molecular structure. *Fourier transform infrared spectroscopy (FTIR) spectra of (A) RV-powder (purple), and (B) blank- (blue), RV- (red), and RV-dye-NLCs (green) respectively, displaying transmittance (%) between 500-4000 cm^{-1}. Characteristic transmittance peaks are indicated on the figure itself (for interpretation of the reference values, refer to main text).*

Having confirmed the molecular structure of the RV-NLCs, the next characteristics to be assessed were size, stability and electrophoretic mobility. Following sonication, RV-NLCs were significantly reduced in size, characterised as having a size of 55.78 ± 2.964 nm and polydispersity index of 0.244 ± 0.003, demonstrating that the particles were monodispersed in comparison to their pre-sonicated, polydispersed state (996 ± 206 nm; $P = < 0.01$; Figure 4.3A). Sonication had a negligible effect on surface charge, with an average zeta potential of 25.6 ± 0.251 mV and a PDI of 0.252, indicating good stability (Figure 4.3B). Incubation of RV-NLCs (0.45 μM) in PSS led to an increase in size after 30-minutes, from 68.97 ± 1.36 nm to 98.7 ± 4.5 nm ($P = < 0.0001$; Figure 4.3C); incubation in media had no effect. Surface charge after incubation in PSS and media is similar over the 4-hour period, indicating stability of the RV-NLCs (Figure 4.3D).

TEM was used to determine the morphological structure and size of the NLCs, successfully confirming them to be spherical and monodispersed, with an average particle size of 82.5 ± 4.65 nm (Figure 4.4).

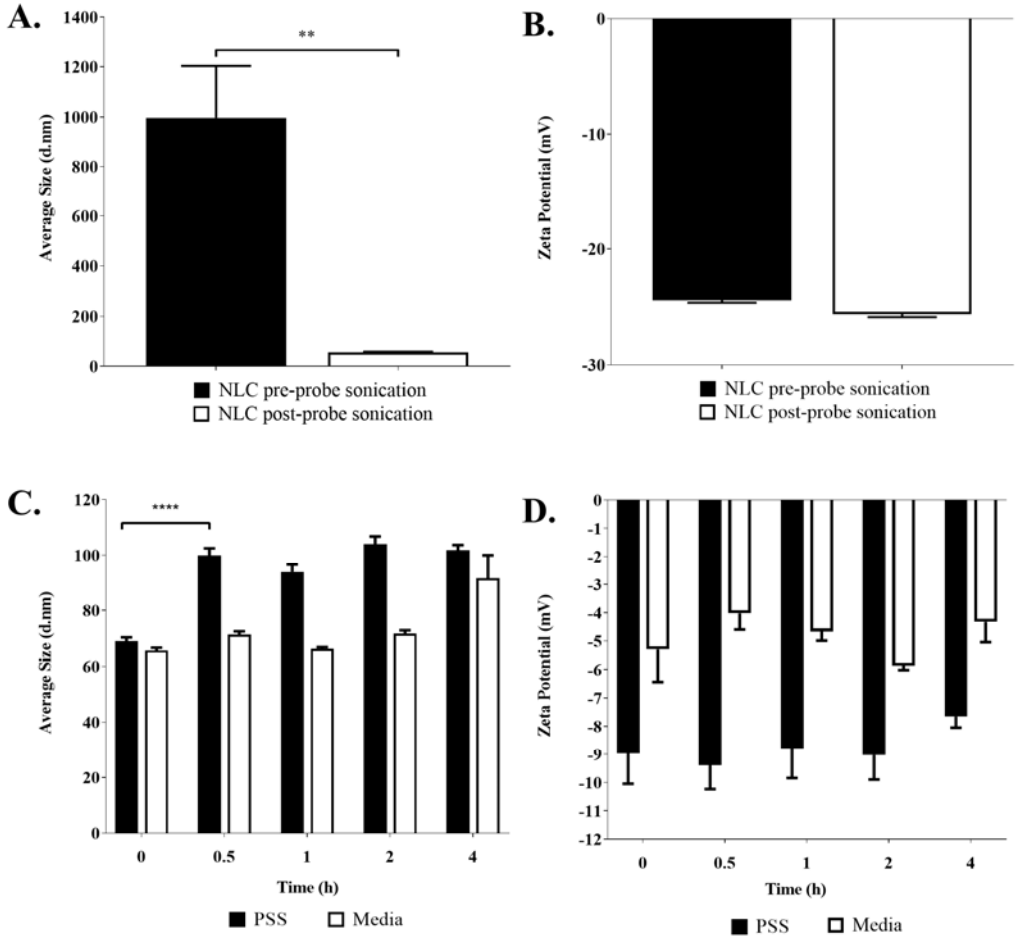

Figure 4.3. Stability and electrophoretic mobility of RV-NLCs in aqueous medium. *Resveratrol-loaded nanolipid carrier (RV-NLC) stability was assessed in water using dynamic light scattering and laser doppler micro-electrophoresis, pre- and post-sonication. (A) Sonication led to a significant decrease in size (996 ± 206 nm to 55.78 ± 2.964 nm; P = < 0.01) and had a negligible effect on surface charge, with an average zeta potential of 25.6 ± 0.251 mV (B). (C) RV-NLC size and zeta potential were assessed in PSS and cell culture medium over 4-hours (0-, 0.5-, 1-, 2- and 4-hours). Incubation of RV-NLCs (0.45 μM) in PSS led to a significant increase in size after 30-minutes (68.97 ± 1.36 nm to 98.7 ± 4.5 nm; P = < 0.0001); size was unaffected in media. (D) Surface charge was unaffected over the 4-hour period, indicating stability of the RV-NLCs in PSS and media. Experiment performed in triplicate and repeated three times. The effects of sonication and time-dependent stability of RV-NLCs were analysed using an unpaired t-test and two-way ANOVA followed by Tukey's multiple comparisons, respectively (n = 3). Data are presented as mean ± SEM. * P < 0.05.**** P < 0.0001.*

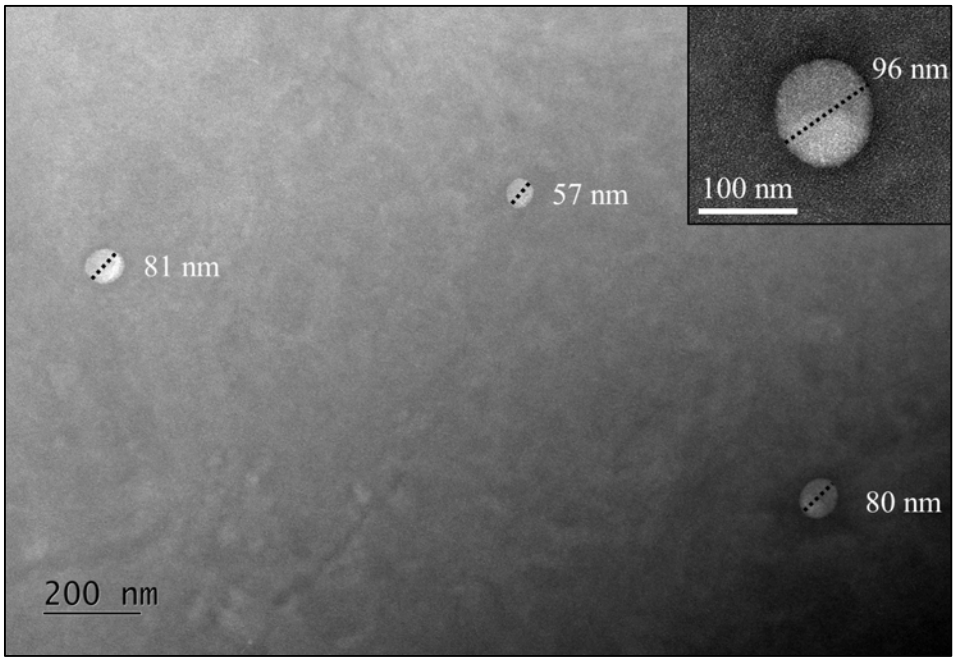

Figure 4.4. Morphological structure of NLCs. *Representative transmission electron (TEM) micrographs of nanolipid carriers (NLCs). NLCs were fixed with osmium tetroxide and stained with uranyl acetate, dried and imaged. NLCs are seen as spherical and monodispersed, with an average particle size of 82.5 ± 4.65 nm. Random measurement sampling (n = 31) from micrographs (ImageJ). Magnification 13,000 x. Scale bars = 200 nm and 100 nm, respectively.*

Next, the pharmacokinetic release profile of RV-NLCs and RV-solution were determined in order to assess the effects of encapsulation on RV diffusion. RV-loading within NLCs significantly reduced the release of RV into the surrounding medium, with maximum release (27.7 %) observed after 12-hours; significantly less than the maximal release observed from the RV-solution after 11-hours (71.5 %; $P = < 0.0001$). This confirms the ability of NLCs to hold the entrapped drug and protect it, reducing its release and degradation in the outer media (Figure 4.5) (Khurana et al., 2017).

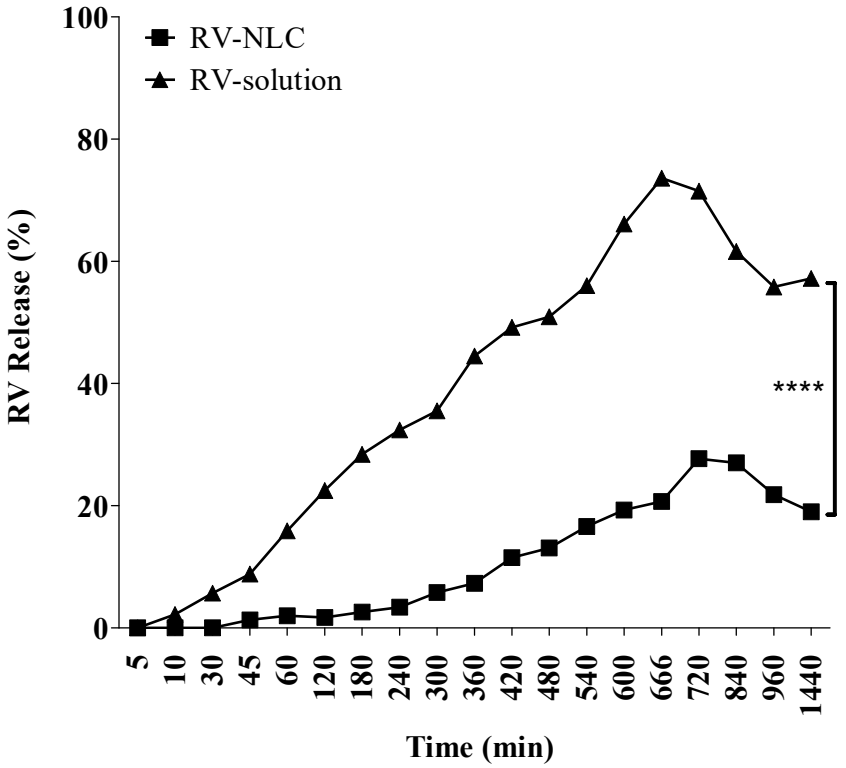

Figure 4.5. Dissolution of RV-NLCs and RV-solution in vitro. *The in vitro release profile was determined using a dialysis bag diffusion method (37 °C, pH 7.4) over 24-hours. Samples were taken at predetermined time intervals and analysed using high-performance liquid chromatography. RV-loading within NLCs significantly reduced the drug release into the surrounding medium, with a maximum release (27.7 %) observed after 12-hours; significantly less than the maximal release observed from the RV-solution after 11-hours (71.5 %; P = < 0.0001). Drug release was analysed by a two-way AVONA. Data are presented as mean ± SEM. **** P < 0.0001.*

4.1.2 RV-NLCs maintain endothelial cell viability and diminish H_2O_2 induced superoxide generation, *in vitro*

Having characterised the properties of the RV-NLCs, it was next of interest to assess their effects on endothelial cells *in vitro*. Following 24-hours co-incubation of NLCs or RV-solution with HCAECs, no significant change in cell viability was observed (Figure 4.6A); however, at the highest dose (90 µM), a significant reduction in viability of 23 % was detected between blank- and RV-dye- NLCs ($P = < 0.01$). Continued exposure over 48- and 72-hours resulted in a significant reduction in viability in cells exposed to NLCs (< 40 %), in comparison to those treated with the RV-solution at concentrations of 90 µM and 45 µM ($P = < 0.0001$; Figure 4.6B and C, respectively).

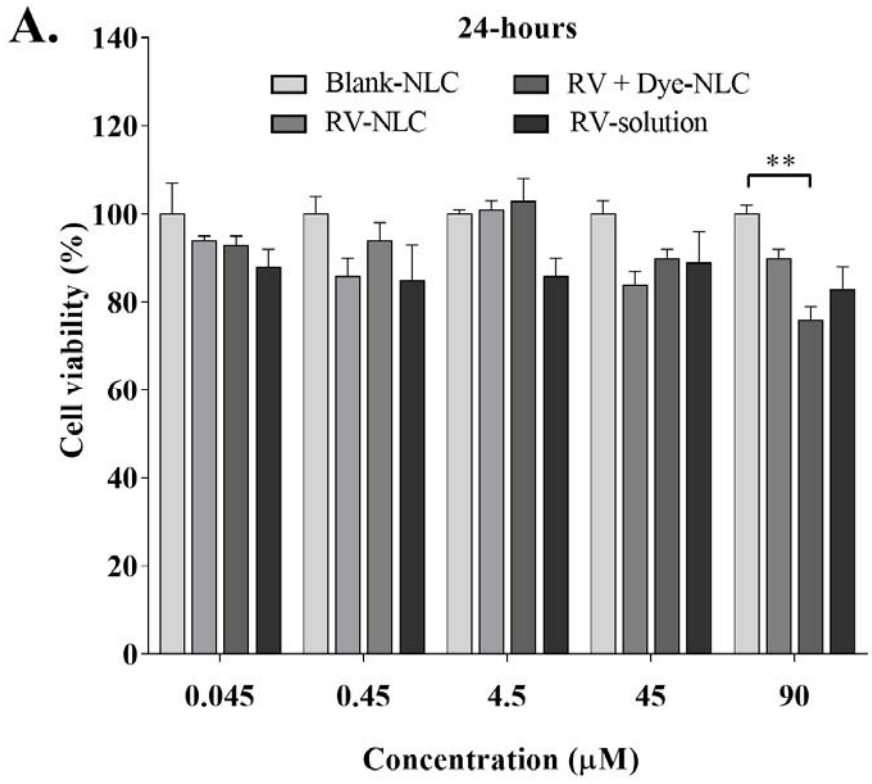

Continued…

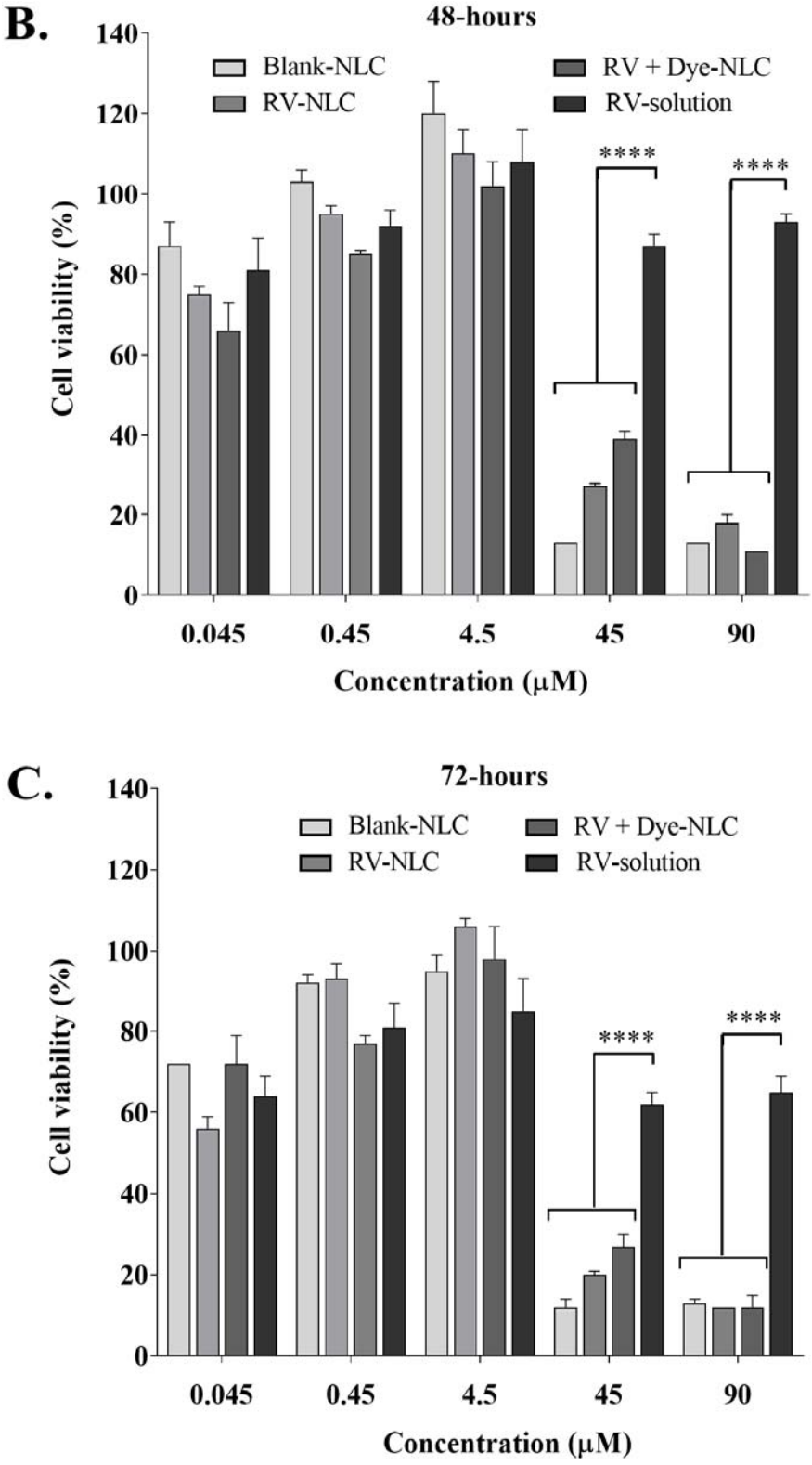

Figure 4.6. Effect of RV-NLCs on cell viability. *Human coronary artery endothelial cell (HCAEC) viability following exposure to NLCs (blank-, RV-, RV- dye-loaded) and RV-solution at concentrations ranging between 0.045-90 μM over (A) 24-, (B) 48- and (C)*

*72-hours. RV-NLCs had no significant effect on cell viability, other than at 90µM (P = < 0.01) after 24-hours. After 48- and 72-hours, NLCs (blank-, RV- and RV-dye) significantly reduced cell viability at 90 µM and 45 µM, in comparison to RV-solution (P < 0.0001). Cell viability was determined using an Alamar blue assay (n = 3). Data normalised to control wells (untreated). Experiment performed in triplicate and repeated three times. Cell viability was analysed by a two-way ANOVA followed by a Tukey's multiple comparison. Data are presented as mean ± SEM.** P < 0.01. **** P < 0.0001.*

Having identified the most biocompatible concentrations for use, it was of interest to assess RV-NLC uptake and localisation within cells. Fluorescence microscopy demonstrated that RV-dye-loaded NLCs (0.45 µM) were taken up by >90 % of HCAECs after 30-minutes (Figure 4.7).

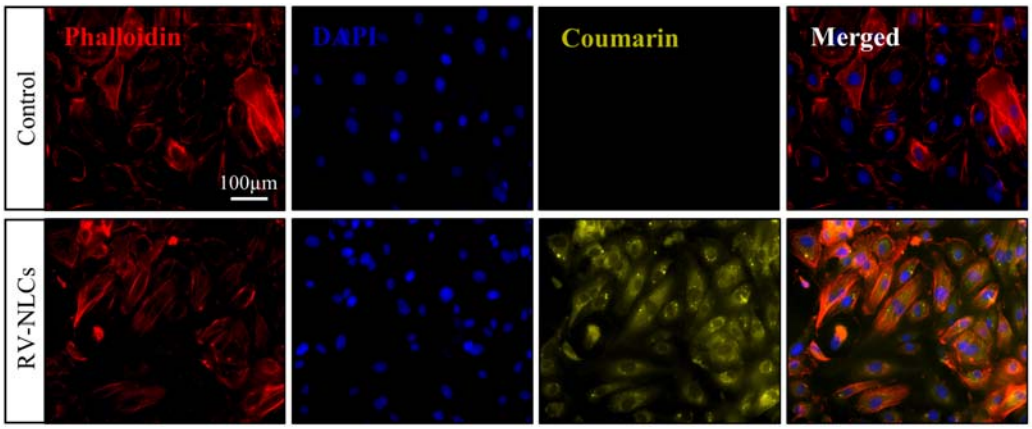

Figure 4.7. RV-NLC uptake within HCAECs. *Representative fluorescence micrographs of human coronary artery endothelial cells (HCAECs) incubated with growth medium or RV-dye-loaded (coumarin-6) NLCs for 30-minutes, followed by DAPI (nuclear) and phalloidin (actin) staining. RV-NLCs (0.45 µM) displayed good uptake following 30-minutes incubation. Magnification 20 x. Scale bar = 100 µm. Images acquired from 1 of 5 representative slides.*

After confirming the biocompatibility and uptake of RV-NLCs (0.45 μM), their antioxidant potential within an oxidative environment was assessed *in vitro*. Initially, HCAEC tolerances were determined following 30-minutes exposure to H_2O_2 (0-500 μM), whereby a significant reduction in cell viability was observable at 500 μM (P = < 0.001; Figure 4.8A). Exposure to H_2O_2 (100 μM; 30-minutes) followed by fresh media (30-minutes) significantly elevated mitochondrial and cytosolic $O_2^{\bullet-}$ levels in HCAECs (P = < 0.001; < 0.01; Figure 4.8B). Incubation with RV-NLCs significantly reduced mitochondrial and cytosolic superoxide levels compared to treatment with media alone (P = < 0.01; < 0.001, respectively). *In vitro* studies demonstrated that NLCs are well tolerated across a range of concentrations, whilst also displaying good uptake and antioxidant capability following 30-minutes incubation with 0.45 μM RV-NLCs. To mitigate potential future pharmatoxicological effects, *ex vivo* studies were conducted using this concentration.

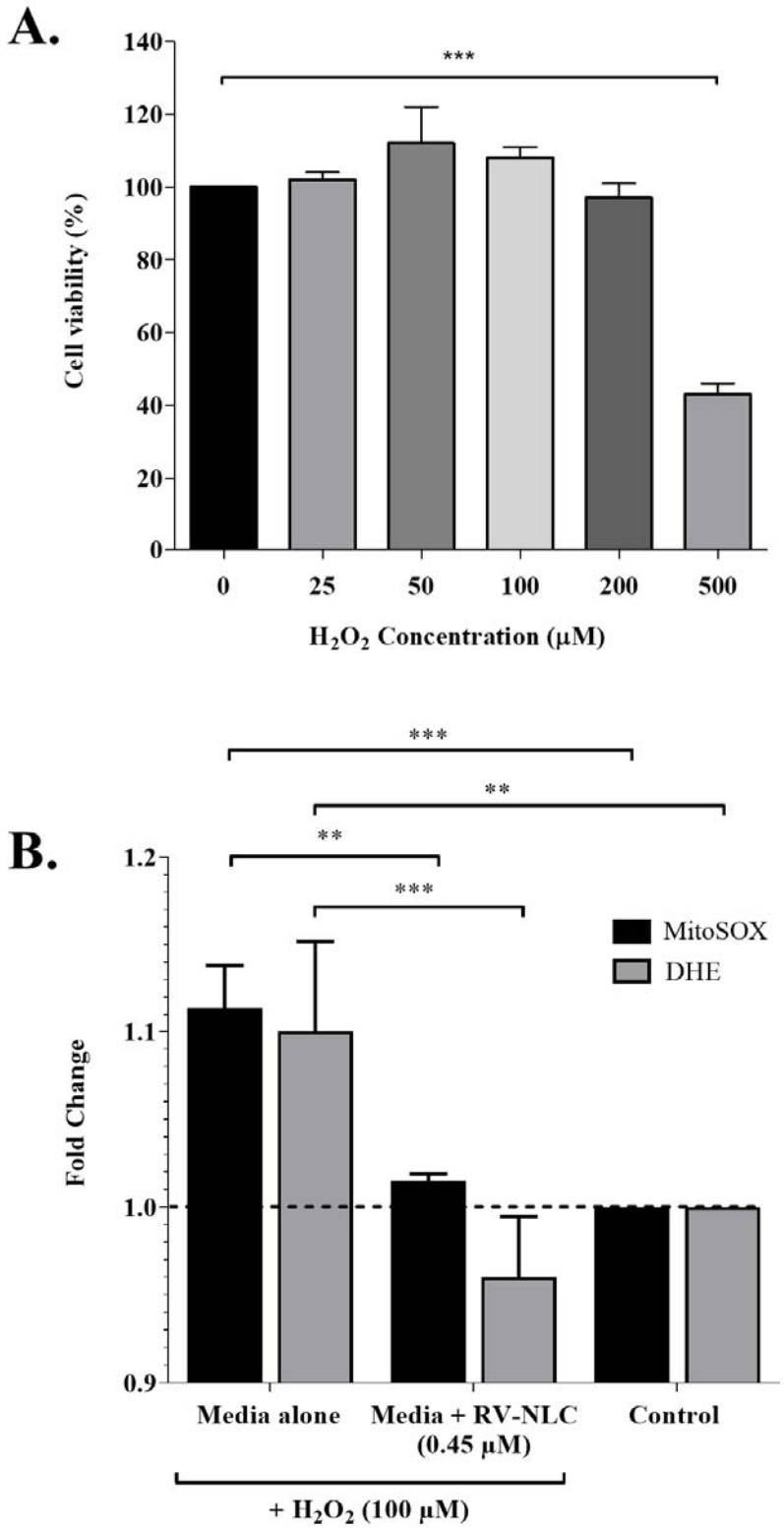

Figure 4.8. Effect of H_2O_2 and RV-NLCs on oxidative reactivity in vitro. *(A) Human coronary artery endothelial cell (HCAEC) viability following exposure to hydrogen peroxide (H_2O_2; 0-500μM) for 30-minutes. H_2O_2 exposure had no significant effects on cell viability, other than at 500 μM (P = < 0.001). Cell viability determined using an*

*Alamar blue assay (n = 3). Data normalised to control wells (untreated). (B) Exposure to H_2O_2 (100 µM; 30-minutes) followed by fresh media (30-minutes) significantly elevated mitochondrial (MitoSOX) and cytosolic (dihydroethidium; DHE) superoxide levels in HCAECs (P = < 0.001; < 0.01) compared to control cells (untreated). Incubation with RV-NLCs (0.45 µM) significantly reduced mitochondrial and cytosolic superoxide levels compared to treatment with media alone (P = < 0.01; < 0.001, respectively). Data expressed as a fold-change change from control (untreated cells – no H_2O_2/RV; n = 3). Experiment performed in triplicate and repeated three times. Cell viability and oxidative reactivity were analysed using a one-way ANOVA followed by Bonferroni correction and two-way ANOVA followed by Tukey's multiple comparisons, respectively. Data are presented as mean ± SEM. ** P < 0.01. *** P < 0.001.*

4.1.3 TMS-liposomes were successfully characterised

TMS-loaded liposomes were characterised in PSS solution. Using UV-VIS and fluorescence spectroscopy, TMS-solution showed two characteristic absorbance peaks at 315 nm and 341 nm (Figure 4.9A). No corresponding peaks were observable in blank-, TMS- or TMS-dye-liposomes. TMS-dye-liposomes had an absorbance peak at 492 nm, characteristic of the 5'6 carboxyfluorescein dye. A fluorescence peak was detected at 517 nm in TMS-dye-liposomes, further confirming dye loading. No peaks were detectable from blank- or TMS-liposomes, confirming the absence of dye-loading (Figure 4.9B).

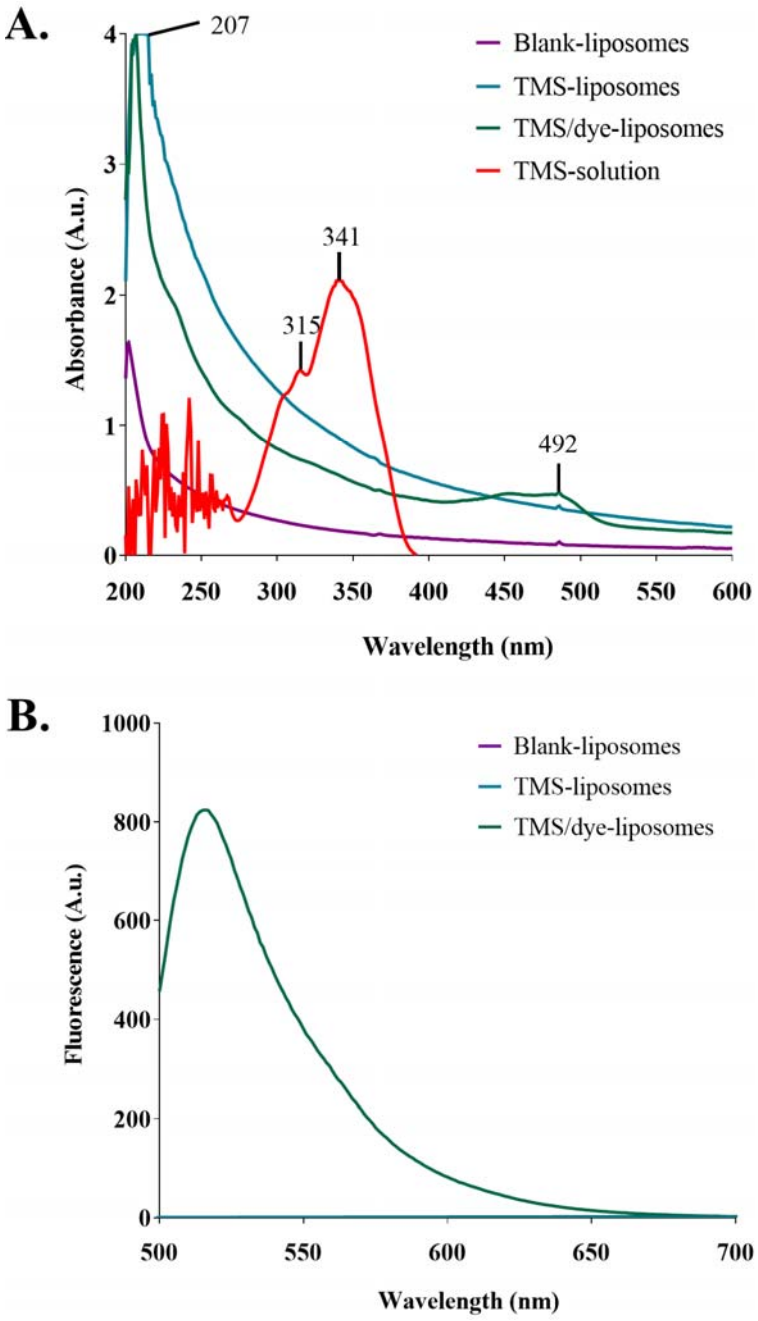

Figure 4.9. Confirmation of drug and dye-encapsulation within liposomes. *Characterisation of blank-, TMS-, TMS-dye-liposomes and TMS-solution. (A) Ultraviolet-visible spectroscopy (UV-Vis) displaying absorbance spectra between 200-600 nm. Absorbance peaks were identified at 315 nm and 341 nm in TMS-solution but was absent from other samples. TMS-dye-liposomes had an absorbance peak at 492 nm, associated with the 5'6 carboxyfluorescein dye. Blank-, TMS-, and TMS-dye-liposomes had a spectral peak identifiable at 207 nm, attributable to cholesterol. (B) Fluorescence-spectroscopy displaying spectra between 500-700 nm. A fluorescence peak was detected at 500 nm in RV-dye-loaded NLCs, confirming coumarin-6 loading.*

FTIR was used to confirm the molecular structure of the TMS-liposomes. FTIR revealed that TMS has a similar infra-red profile to its well-characterised parent compound RV, with characteristic benzene valence (C=C) vibrations identifiable at 1587 and 1570 cm-1 (Figure 4.10A). The strong, broad band characteristics of *trans*-RV are noticeably absent between 3550-3200 cm^{-1}; however, several bands are identifiable at 2850, 2952 and 3000 cm^{-1}, corresponding to the valence vibration of $O\text{-}CH_3$ bonds within synthetically conjugated methyl groups. At 1444 cm^{-1}, additional CH_3 bending is observed. Ether bonds (C-O-C) originating from phenolic groups are identifiable at 1026, 1154, and 1248 cm^{-1} (Figure 4.10B). The bands at 675 cm^{-1} and 831 cm^{-1} correspond to the deformational vibration of OH groups and C-H bonds, originating from the benzene ring.

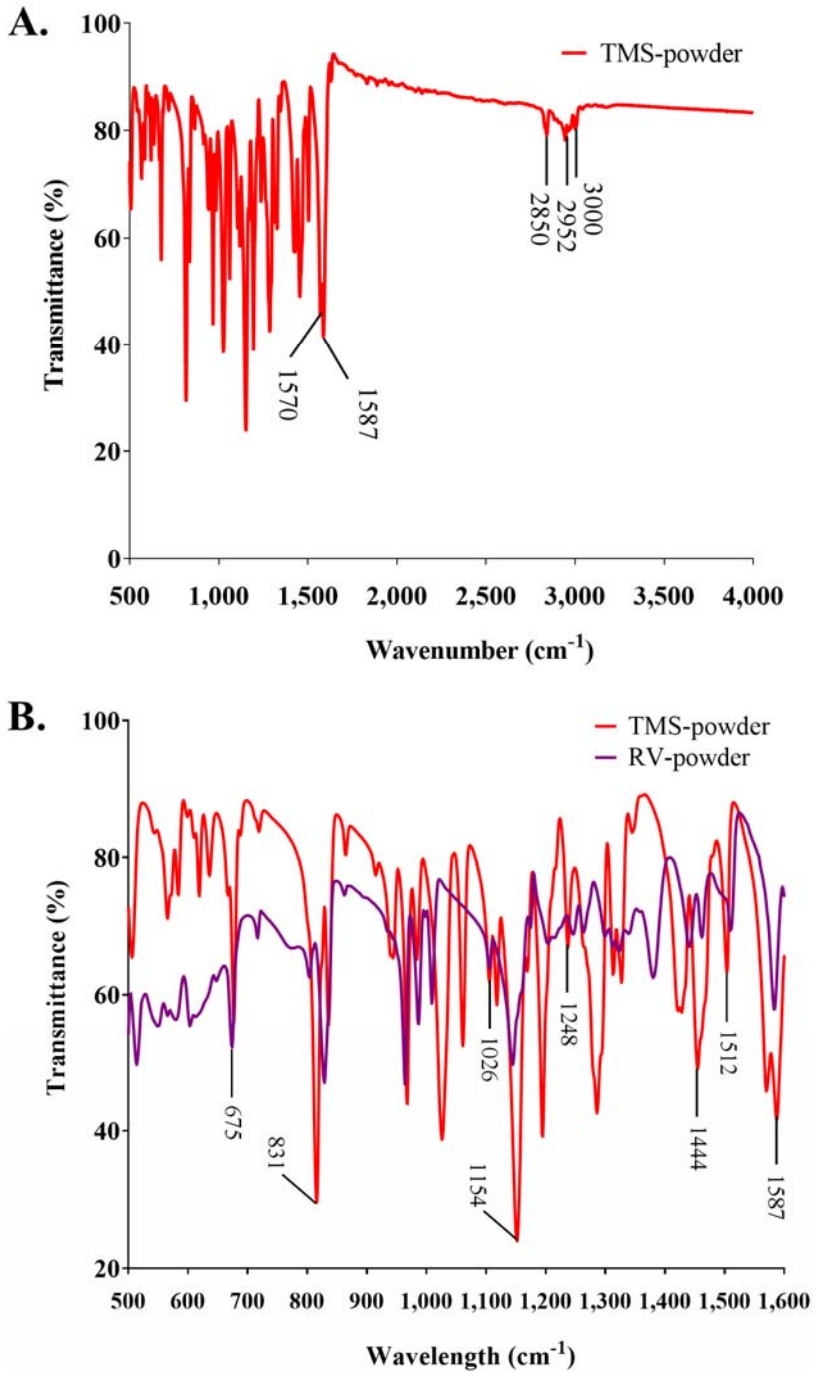

Figure 4.10. Confirmation of TMS and RV molecular structure. *(A) Fourier transform infrared spectroscopy (FTIR) spectra of TMS-powder (red), displaying transmittance (%) between 500-4000 cm^{-1}. (B) Juxtapositional comparison of the 'fingerprint' region of the spectra (500-1600 cm^{-1}) between TMS- and RV-powder. Characteristic transmittance peaks are indicated on the figure itself (for interpretation of the reference values, refer to main text).*

The presence of TMS could not be identified in the liposomes due to the absence of corresponding peaks (Figure 4.11). The individual components of the liposomal structure, 1,2-distearoyl-sn-glycero-3-phosphocholine and 1,2-distearoyl-sn-glycero-3-phosphoethanolamine-N-[methoxy(polyethylene glycol)-2000] ammonium salt were identifiable with peaks between 2950-2850 and 1750 cm^{-1}, corresponding with the presence of alkane (C-H) and carbonyl ester groups (C=O). The broad peak observed between 3550-3200 cm^{-1} is a result of OH groups found within fatty acids (cholesterol).

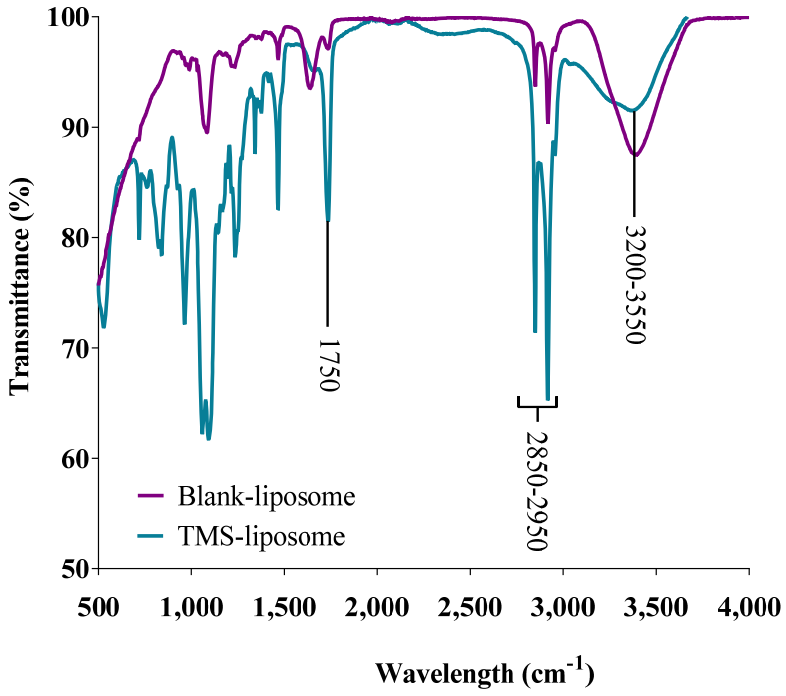

Figure 4.11. Confirmation of entrapment and molecular structure. *Fourier transform infrared spectroscopy (FTIR) spectra of blank- (purple) and TMS-loaded liposomes (blue), displaying transmittance (%) between 500-4000 cm^{-1}. Characteristic transmittance peaks are indicated on figures (for interpretation of the references, refer to main text).*

Next, the size, stability and electrophoretic mobility of TMS-liposomes were assessed. TMS-liposomes incubated in PSS were stable over 4-hours, with an average size, PDI and zeta potential of 157 ± 3 nm, 0.097 and 13.13 ± 0.67 mV, respectively (Figure 4.12A, B).

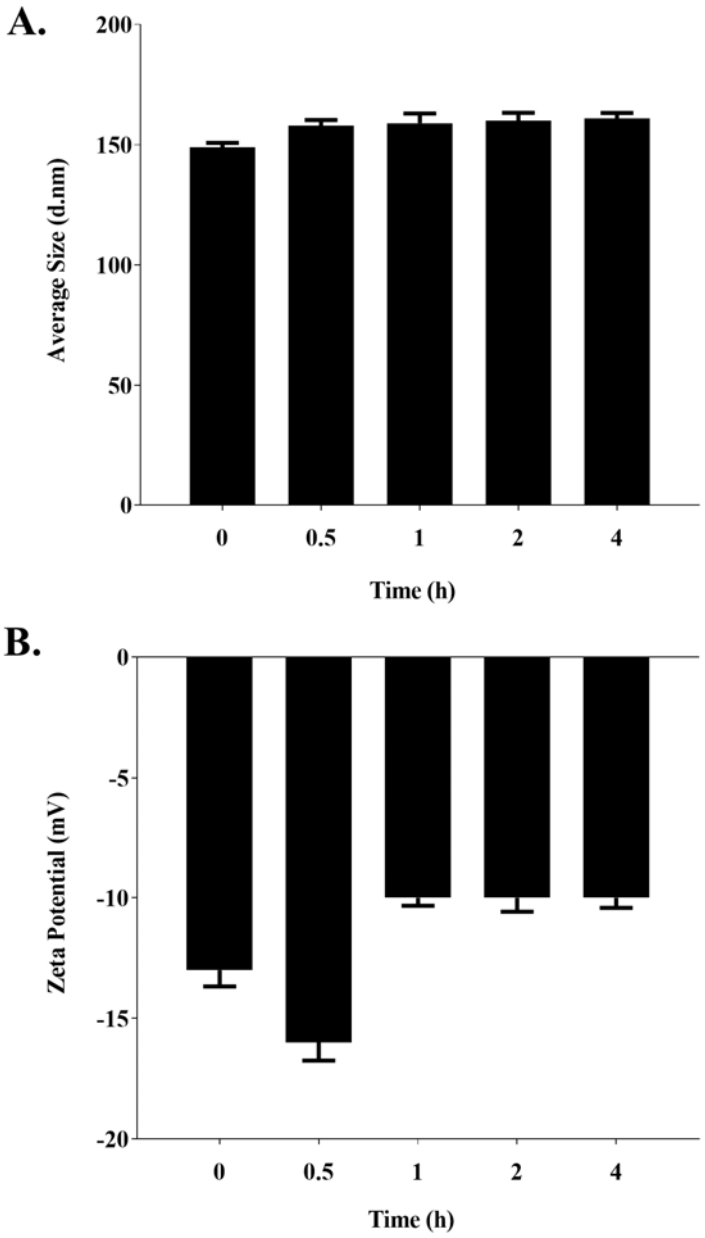

Figure 4.12. Stability and electrophoretic mobility of TMS-liposomes in aqueous medium. *TMS-liposome size and zeta potential were assessed in PSS over 4-hours (0-, 0.5-, 1-, 2- and 4-hours) using dynamic light scattering and laser doppler micro-electrophoresis, respectively (n = 3). Incubation of TMS-liposomes (1000 nM) in PSS had no effect on (A) size or (B) zeta potential over the 4-hour period, indicating stability of*

the TMS-liposomes. Experiment performed in triplicate and repeated three times. Data analysed using a one-way ANOVA followed by Bonferroni correction.

TEM was used to determine the morphological structure and size of the liposomes, successfully confirming them to be spherical and monodispersed, with an average size of 148.3 ± 7.9 nm (Figure 4.13).

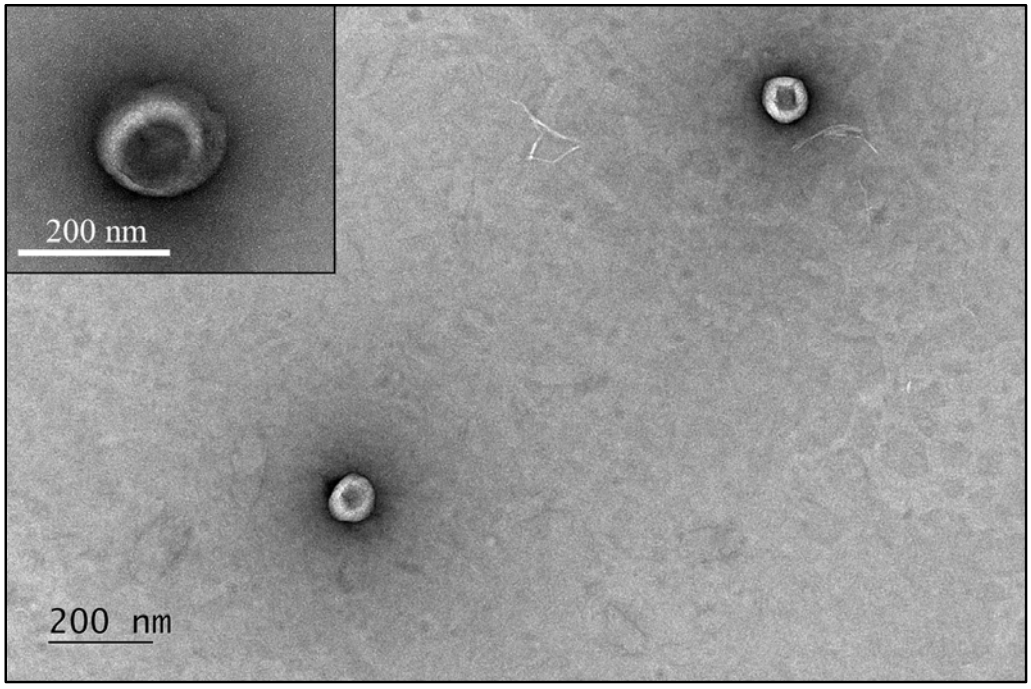

Figure 4.13. Morphological structure of liposomes. *Representative transmission electron (TEM) micrographs of liposomes. Liposomes were fixed with osmium tetroxide and stained with uranyl acetate, dried and imaged. Liposomes are seen as spherical and monodispersed, with an average particle size of 148.3 ± 7.9 nm. Random measurement sampling (n = 26) from micrographs (ImageJ). Magnification 13,000 x. Scale bar = 200 nm.*

4.1.4 TMS-liposomes maintain endothelial cell viability

Having characterised the properties of the TMS-liposomes, it was next of interest to assess their effects on endothelial cells *in vitro*. Following 24-hours co-incubation of TMS-liposomes or TMS solution with HCAECs, no significant change in cell viability was observed at concentrations ranging between 1000 nM and 1 nM; however, at 0.01 nM and 0.1 nM, TMS-solution resulted in significant reductions in viability of 26 % and 21 %, respectively ($P = < 0.05$; Figure 4.14A). Continued exposure over 48-hours resulted in further reductions in viability at 0.01 nM in TMS-, TMS-dye-liposomes and TMS-solution ($P = < 0.001$; Figure 4.14B). After 72-hours, blank-, TMS-, TMS-dye-liposomes and TMS-solution each led to significant reductions in viability at 0.01 nM ($P = < 0.05$; $P = < 0.001$ and $P = < 0.0001$, respectively; Figure 4.14C).

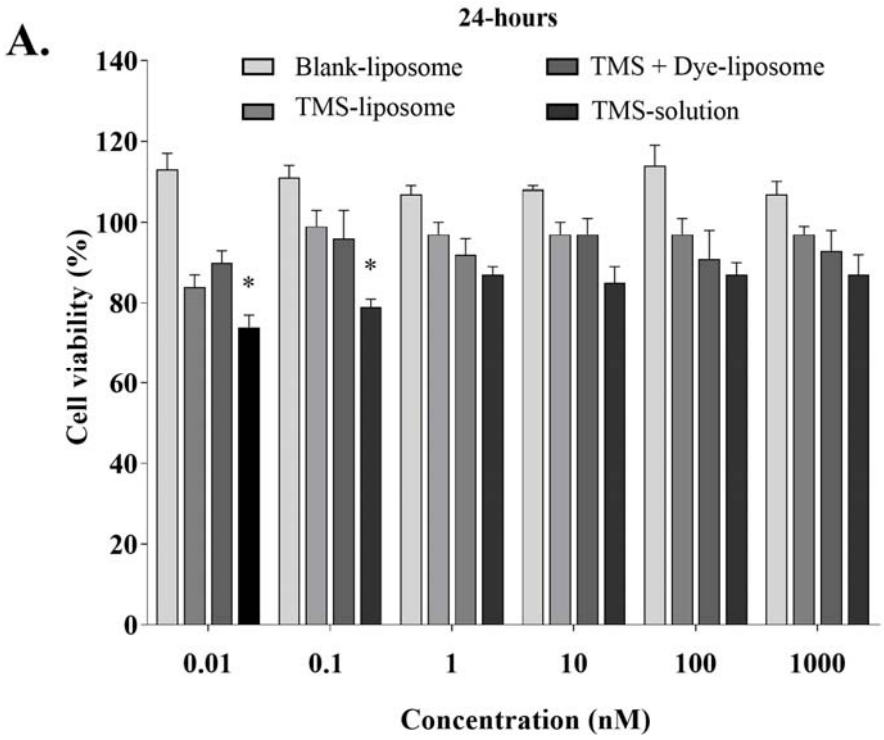

Continued…

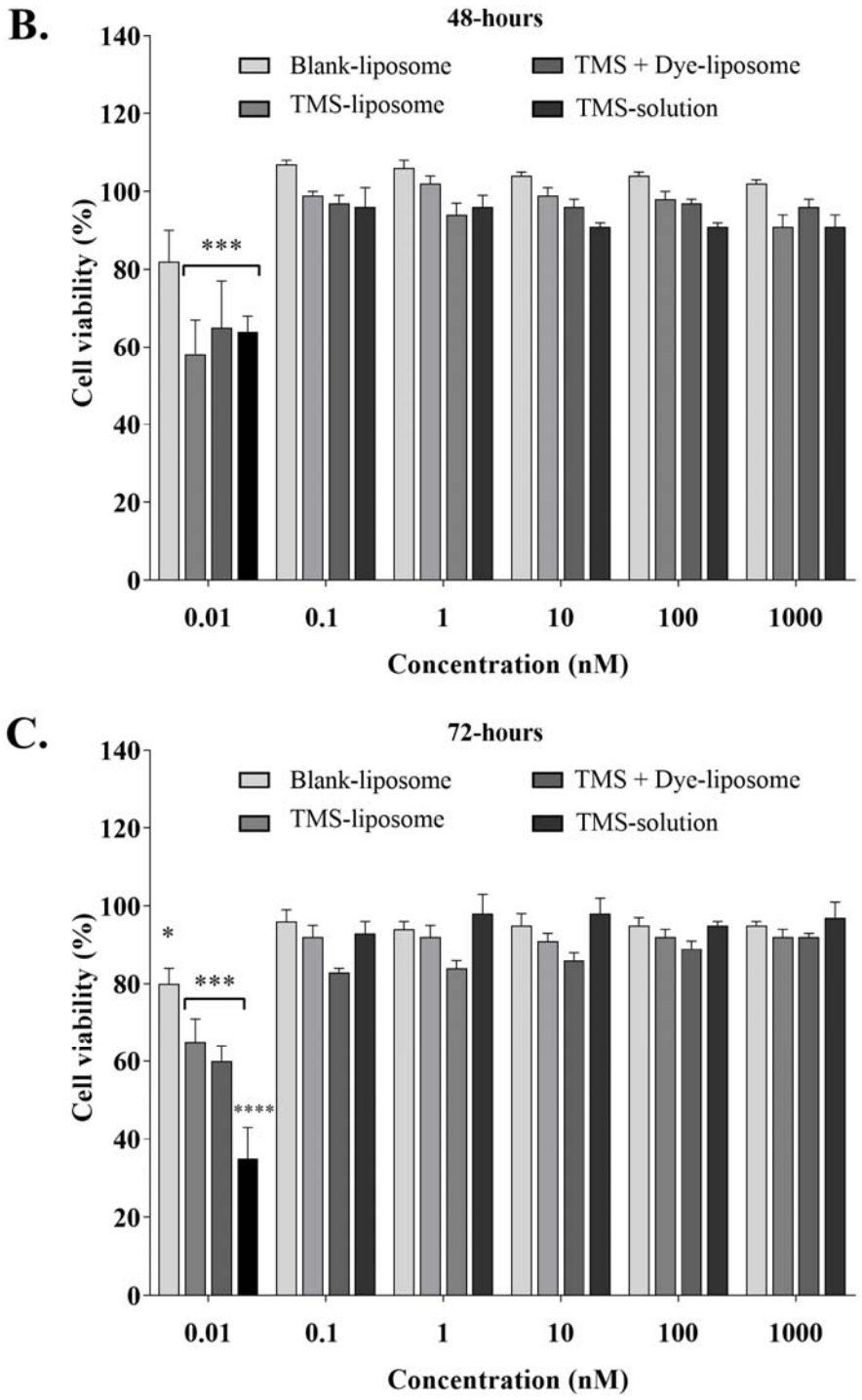

Figure 4.14. Effect of TMS-liposomes on cell viability. *Human coronary artery endothelial cell (HCAEC) viability following exposure to liposomes (blank-, TMS-, TMS + dye-loaded) and TMS-solution at concentrations ranging between 0.01-1000 nM over (A) 24-, (B) 48- and (C) 72-hours. No overall change in cell viability was observed at concentrations ranging between 1000 nM and 1 nM after 24-hours; however, at 0.01 nM and 0.1 nM, TMS-solution resulted in a significant reduction in viability (P = < 0.05). After 48-hours, further reductions in viability were observed in liposomes (TMS-, TMS-*

*dye) and TMS-solution at 0.01 nM (P = < 0.001). After 72-hours, liposomes (blank-, TMS-, TMS-dye) and TMS-solution each led to significant reductions in viability at 0.01 nM (P = < 0.05; P = < 0.01 and P = < 0.0001, respectively). Cell viability was determined using an Alamar blue assay (n = 3). Data normalised to control wells (untreated). Experiment performed in triplicate and repeated three times. Data was analysed by comparing to control wells (untreated (i.e. 100% viable); not shown) using a two-way ANOVA followed by a Tukey's multiple comparison. Data are presented as mean ± SEM. * P = < 0.05. *** P < 0.001. **** P < 0.0001.*

4.2 Discussion

4.2.1 RV-NLCs were successfully characterised

Organic NLCs were synthesised and characterised using the same range of analytical techniques as described in the previous chapter, with drug and dye entrapment confirmed using UV-VIS and fluorescence spectroscopy. The absorption spectra confirmed the presence of the *trans*-RV isomer at approximately 304 nm, defining it from its less characterised, less potent *cis*-isomer, which has a characteristic absorbance peak at 285 nm (Camont et al., 2009). FTIR was able to successfully confirm the presence of constituent compounds used to synthesise the NLCs; however, the spectrographic profile for RV was not distinguishable. Despite the popularity of FTIR, the sensitivity of the technique is often limited, particularly for materials with poor infrared absorption or when the spectral bands of major components overlap. Similar observations have been reported previously by several research groups, where nanoparticles are capable of obscuring the absorption peaks of encapsulated drugs, showing only the predominant parent compounds (Pople and Singh, 2011). In addition, the lack of any additional new peaks observed in the RV-NLC spectra suggests no strong/adverse interactions or incompatibility.

Given the translational goal of this project to develop a clinical tool for drug delivery in patients, it is of great importance to consider the nanoparticle absorption and their interdependence with physicochemical properties of drug carrier systems, which currently are not well understood. Size has been postulated as a crucial determinant of nanoparticle efficacy, with studies identifying improved stability, uptake, and permeation ability in both the gastrointestinal system and blood with nanoparticles of smaller size (< 100 nm) (Li et al., 2016). The 10-fold reduction in size observed in our samples are

indicative of the importance and significant effects of sonication prior to administration; whilst maintenance of surface charge confirms it has no detrimental effect on nanoparticle stability (Al-Kaysi et al., 2005).

A rapid increase in particle size was identified following incubation in PSS, attributable to ionic adsorption on the nanoparticle surface. This is also reflected in the higher zeta potential values observed in PSS (pH 7.2-7.4; -9 mV) when compared to stock solution pre- and post-sonication (water, pH 6.8; -25 mV). No increase in size was observed for several hours in the culture medium, likely due to the low percentage of serum proteins (<5 %) present within the culture medium (leading to time-dependent corona formation). Not much change in zeta potential was observed over several hours due to the absence of any ions in the culture media (pH 7.2 - 7.4; -5 mV); however, the surface charge was still higher relative to zeta potential measurements in water, suggesting interaction. It should be noted that in aqueous media, the pH of the sample is directly related to its zeta potential. Many nanoparticles exhibit an effective charge change in aqueous conditions, from positive (at low pH) to negative (at high pH) with an isoelectric point (0 mV, unstable) in between (Salgin et al., 2013). Variations in pH e.g. water, pH 6.8 vs PSS, pH 7.4, are likely to account, in part, for the observed fluctuation in zeta potential between solutions. NLCs incubated in PSS showed an increased PDI over several hours, with a maximum PDI of 0.377. Similarly, NLCs in media resulted in progressively increasing PDI over time, however, in each instance to a lower extent than in PSS with a maximum PDI of 0.274. These results demonstrated that NLCs were within acceptable levels of monodispersity.

Despite its overarching popularity in the nanomaterial field, DLS is still considered a low-resolution technique; several limitations are affiliated with its use, including the inability to accurately determine nanoparticle size in biologically relevant environments. Due to

their high surface free energy, nanoparticles adsorb ions (electrostatic attraction) upon interaction with abiotic environments, forming a diffuse electrical double layer. Ions trapped within this electrical double layer otherwise referred to as the 'slipping plane', lead to size overestimation when measured using techniques such as DLS. Due to the limited capability of DLS, measuring the hydrodynamic diameter of the particle, as opposed to the particle itself; SEM or TEM are utilised to provide a more accurate representation of nanoparticle diameter. TEM identified an average size of 82.5 nm, a 17 % reduction when compared to DLS, highlighting the techniques ability to mitigate the artificial increases in size.

The drug release profile of RV-NLCs was measured *in vitro*. RV-NLCs displayed an extended, slow-release of RV over 12-hours with no burst effect. In comparison, non-encapsulated RV resulted in a much faster release. The sustained release observed is likely attributable to the slow diffusion of RV entrapped within the lipid matrix, with a maximal release of RV observed following 12-hours (27.7 %) compared to the diffusion of the non-encapsulated RV alone (maximum diffusion 71.5 % at 11-hours). The three bent carbon chains of triolein disrupt the packing of trimyristin crystals, offering better stability and higher drug loading (Yang et al., 2014). This confirms the ability of NLC to hold the entrapped drug and protect it, reducing its release and degradation in the outer media (Khurana et al., 2017).

4.2.2 RV-NLCs maintain endothelial cell viability

While the exposure to RV encapsulated-NLCs had no overall effect on endothelial cell viability, incorporation of the dye within RV-NLCs led to reduced viability at higher concentrations. The toxic effects of fluorophores have been previously investigated, which may account for this reduction in viability (Farooq, 2014). Previous studies have

demonstrated the dose-dependent effects of the unencapsulated form of RV on endothelial proliferation and apoptosis, with concentrations above 50 μM resulting in 20-50 % cell death following 24-hours incubation (Szende and Tyihák, 2000; In et al., 2006; Maria et al., 2015). These findings contrast with the data obtained from this study, suggesting that the improved biocompatibility of our RV-NLCs may be attributable to encapsulation, resulting in a slower, sustained release of RV over time. Prolonged exposure (48- and 72-hours) to blank- and RV-NLCs led to a significant reduction in viability at higher concentrations, which was not observed with the RV-solution. High concentrations of RV have been shown to induce pro-oxidant effects, dependant on exposure time, dose and cell type (Giordo et al., 2013; Martins et al., 2014). The RV mediated generation of $O_2^{\bullet-}$ and $^{\bullet}OH$ can result in the formation of lipid peroxides via interactions with, e.g. membrane lipids; these lipid peroxides are ultimately degraded into alkoxyl and peroxyl radicals, initiating further oxidation and cytotoxicity (Gutteridge, 1984). In cells treated with NLCs, the particle capsule provides a rich source of lipid available for oxidation. In contrast, in cells treated with RV-solution, the primary source of lipid resides within the cell membrane only. At high concentrations, a more substantial reduction in viability might be expected following incubation with RV-solution; however, our laboratory has previously demonstrated the rapid degradation of unencapsulated-RV over a one-hour test period (Diaz et al., 2019). Additionally, limited information is available regarding the degradation products of RV and their long-term toxicological effects. Elevated accumulation of these products may account for the increased toxicity observed at high concentrations. However, this is unlikely to be the case as a more substantial reduction in viability would be expected following exposure to an RV-solution.

Interestingly, a subtle trend is observed at lower concentrations (0.045 - 4.5 μM), with the lowest concentration resulting in reduced viability too. Several reasons may account for these changes. RV is known to have concentration-dependent biphasic effects (e.g. inducer of apoptosis vs proliferation). This hormetic response has been observed across a broad range of biological models (Calabrese et al., 2010). Additionally, RV has been shown to be a regulator of metabolic activity, mediated via AMPK/SIRT-1 and subsequent peroxisome proliferator-activated receptor gamma coactivator 1-alpha (PGC-1) modulation. However, despite the frequent use of alamar blue as a cell viability assay, it is, in fact, an indicator of cellular metabolism and may, therefore, be influenced by metabolic modulation by RV. Uptake into HCAECs was confirmed within 30-minutes of exposure of the cell to the RV-NLCs, which were observed throughout the cytosol; the presence of the triglyceride triolein within the NLCs likely contributing to its improved uptake via modulation of the cell membrane (Prades et al., 2003). RV-NLCs were identified diffusely throughout the cytoplasmic compartment and were notably absent within the nucleus, which is consistent with findings previously reported in HUVEC and HepG2 cells following RV exposure (Lançon et al., 2004; Chen et al., 2013). This accumulation and retention of RV within the cytoplasm of endothelial cells might explain the paradoxical observations that RV has low bioavailability in humans while exerting noticeable bioactivities (Magyar et al., 2012). The apparent lack of nuclear uptake demonstrated by us and others suggests the indirect effects of RV are mediated by second messengers within the cytosol, modulating gene expression. Amongst the cytoplasmic compartment, RV-NLCs appeared to form clusters which may be indicative of clathrin-dependent or clathrin-independent (caveolin-dependent) endocytic uptake. Previous research investigating the uptake mechanics of intestinal epithelial cells observed reduced cellular uptake of NLCs when performed at 4 ^{o}C and in the presence of energy inhibitors

such as sodium azide; with a dependency on cellular energy potentially indicative of an endocytic mechanism. This was further corroborated following inhibition of clathrin- and caveolin-dependent endocytosis, each limiting uptake; however, clathrin-mediated uptake was identified as the predominant pathway (Neves and Queiroz, 2016; Piazzini et al., 2018). In each instance, however, the NLCs were >180 nm in diameter. Endocytic processes are highly regulated, with nanoparticle size being heavily influential on respective uptake pathways (He et al., 2010). Although variation exists, clathrin-coated vesicles have an approximate diameter of 100-200 nm, whilst caveosomes are smaller measuring between 60-100 nm (Rejman et al., 2004; Wang et al., 2009). As the average size of our NLCs was 82.5 ± 4.65 nm (based on TEM), preferential uptake of NLCs by caveolin-dependent endocytosis would be expected.

4.2.3 RV-NLCs diminish H_2O_2 induced superoxide generation

The generation of mitochondrial and cytosolic $O_2^{\bullet-}$ in HCAECs exposed to H_2O_2 was significantly reduced in the presence of RV-NLCs compared to untreated controls. Mitochondrial and cytosolic $O_2^{\bullet-}$ is a significant contributor to NO quenching and has previously been found to be increased in isolated arteries following elevated pressure, interfering with flow mediated-dilation and endothelial-dependent dilation in multiple vascular beds (Ungvari et al., 2003; Christensen et al., 2007; Peluffo et al., 2009). As a means of replicating the elevated $O_2^{\bullet-}$ levels observed in the vasculature following pressure elevation, cells were stimulated with H_2O_2. Previous studies have observed elevated intracellular $O_2^{\bullet-}$ generation following brief periods of exposure (< 10-minutes) to H_2O_2, potentially mediated via the NADPH oxidase and xanthine oxidase pathways, as well as through NOS uncoupling (Carter et al., 1994; Coyle et al., 2006; Coyle and Kader,

2007). Our findings are consistent with previously observed results, whereby RV resulted in attenuated mitochondrial $O_2^{\bullet-}$ in HCAECs following hyperglycaemia-induced mitochondrial ROS generation (Ungvari et al., 2009). However, differences in the mode of ROS generation, means of RV delivery and varied exposure times make direct comparisons difficult. RV has been found to reduce $O_2^{\bullet-}$ through both direct and indirect mechanisms and has demonstrated a strong ability to directly remove free radicals. This property is primarily attributed to the presence of hydroxyl groups in both phenyl rings of the stilbene scaffold, promoting hydrogen-atom transfer (HAT) from hydroxyl groups to surrounding reactive oxidants, a common feature amongst phenolic compounds (Cao et al., 2003; Caruso et al., 2004; Iuga et al., 2012). In addition to its direct antioxidant ability, RV has been associated the activation and upregulation of several molecular targets involved in the propagation of dilation and regulation of basal antioxidant activity including eNOS, SOD, CAT, and nuclear factor erythroid 2-related factor 2 (Nrf2) (Xia et al., 2017). However, due to the limited/short incubation period, it is unlikely that these effects relate to the upregulation of antioxidant genes, but are attributable to post-translational modification, e.g. increased phosphorylation of eNOS.

Whilst the effects of RV-loaded NLCs appear to be beneficial in reducing intracellular $O_2^{\bullet-}$, the effect of blank-NLCs were not investigated. In the absence of RV and its antioxidant benefit, elevated $O_2^{\bullet-}$ may be expected as the particle capsule provides a rich source of lipid available for oxidation. However, the administration of exogenous lipid has also been shown to be beneficial, promoting the release of EDRF and EDHF in the vasculature, as well as demonstrating antioxidant capacity, although, this is highly dependent of the type of lipid utilised (Ruisanchez et al., 2014; Limbu et al., 2018). There are a limited number of studies that have investigated the antioxidant activity of the constituent lipid capsule components, trimystrin and triolein. A study by Luo *et al.,*

demonstrated the indirect antioxidant capacity of triolein following oxidative LDL stimulated ROS generation over 24-hours, significantly improving cell viability and increasing the expression of SOD. However, at 10 μM, the concentration was several fold-higher than that utilised in our studies; whilst 0.45 μM RV-NLCs were used in our studies, triolein accounts for only a small proportion of the total contents. Moreover, our studies have focused on acute exposure to RV-NLCs over 30-minutes, due to the limited/short incubation period, it is unlikely that these effects relate to the upregulation of antioxidant genes; which in combination with the limited concentration, may explain the apparent lack of benefit. Furthermore, whilst successfully demonstrating upregulation of SOD, $O_2^{\bullet-}$ levels were not directly assessed and is therefore not a direct reflection of antioxidant ability (Luo et al., 2014). A further study by Chan *et al.* demonstrated the direct ability of triolein to scavenge oxygen-derived free radicals, resulting in up to a 31.9% reduction at concentrations ranging between 1 μM and 10 nM, however, this was performed using pure triolein extract (Chan et al., 1996). Whilst trimystrin is another major constituent component of the lipid capsule, a review of the literature has not revealed any reports of antioxidant capacity. No definitive conclusions can be drawn pertaining to the potential effects of blank-NLCs from the literature, however given the concentrations and length of exposure used in these studies it is unlikely the effects we observe could be caused by the lipid components alone. To confirm this, future studies would need to evaluate the response to blank-NLCs.

Due to its successful uptake *in vitro* and impressive $O_2^{\bullet-}$ reducing capacity at a minimal dose of 0.45 μM RV-NLCs, this dosage was used for subsequent *ex vivo* studies.

4.2.4 TMS-liposomes were successfully characterised

Drug and dye entrapment were assessed using UV-VIS and fluorescence spectroscopy. Independent analysis of TMS-solution identified two absorbance peaks at 315 nm and 341 nm, similar to that of the parent compound RV. This is not unexpected for synthetic analogues; following the synthetic conjugation of methyl groups, heightened delocalisation of pi bonding orbitals within the molecule in response to photonic stimulation would be observed, reducing the energy required to induce chromophoric absorption and thus, producing a rightward shift towards the visible wavelength region (Suzuki, 1967). Despite the successful detection of TMS-solution, no peaks relating to TMS were distinguishable in either of the TMS-loaded samples. Due to the limited content encapsulated within liposomes, a substantial absorptance peak would not be expected and may, therefore, become obscured by more prominent absorption peaks, as seen at 207 nm. Intense absorption peaks in the high-frequency range have previously been documented in liposomes and have been attributed to the presence of cholesterol. Cholesterol and other well-known oxysterols have been shown to absorb light in the vacuum-UV region (< 200 nm). However, light scattering results in the λ max (peak absorbance) shifting rightwards towards a lower energy state, producing an effect commonly referred to as false energy. This results in a spectral 'redshift', with the λ max now appearing in the 207 nm region (Gupta et al., 2014).

FTIR identified several peaks which corresponded with the parent compound RV, confirming its derived nature. FTIR confirmed the presence of constituent compounds used to synthesise the liposomes; however, the spectrographic profile for TMS was not distinguishable. Similar observations have been reported previously by several research groups, where nanoparticles can obscure the absorption peaks of encapsulated drugs,

showing only the predominant parent compounds (Pople and Singh, 2011). In the context of polyphenolic compounds, the presence of OH groups are commonplace and would be expected at around 3500 cm^{-1}. Despite originating from a polyphenolic compound, it is crucial to note that in TMS, OH groups have been substituted for synthetically conjugated methyl groups, and as a result would not expect valance vibration bands at 3500 cm^{-1}. Consequently, the presence of a broad peak on both blank and TMS-liposomes at approximately 3500 cm^{-1} may be solely attributed to the lipid components; not TMS. An in-depth examination of the fingerprint region (500-1600 cm^{-1}); an area characterised by its high specificity for a given compound, identified several similarities between the spectral profile of RV and TMS; they are, however, distinctly unique. The distribution and intensity of absorption (% transmission) bands (blank vs TMS- loaded liposome) are a direct reflection of the range and quantity of chemical bonds present within a given sample. In some instances, this may reflect an increase or decrease in band intensity, as a result of sample modification and altered chemical composition. In this case, however, the varied intensities observed between samples can be attributed to different dilution ratios of stock samples.

Incubation in PSS over several hours had no effect on size, with small, yet non-significant fluctuations in zeta potential, indicating the stability of the colloidal system. TEM determined an average size of 148.3 ± 7.9 nm. Closer inspection of the liposomes highlighted aberrant morphology, appearing concave in structure. Similar observations have been documented previously, with a large dependency on the mode of processing and technical implementation employed (e.g. scanning-, cryo-, low-voltage-). Due to the limited contrast of lipids, samples were rapidly fixed using osmium tetroxide and negatively stained with uranyl acetate, an electron-dense metal with the ability to embed directly into the membrane. Exclusion of the stain from the volume occupied by the

sample provides contrast to the surrounding membrane. During staining and subsequent drying, liposomes lose their hydration shell and are prone to collapse, leading to an accumulation of negative stain around the periphery of the liposomes; resulting in the 'halo' effect observed in our samples. In future, the use of cryo-TEM in conjunction with perforated carbon supports should be used to mitigate the processing artefacts discussed above.

4.2.5 TMS-liposomes maintain endothelial cell viability

Limited information exists on the potential effects of TMS on endothelial cells, with a primary focus to date being placed on cancer cells as a result of its potent antiproliferative potential. Exposure to TMS and TMS-liposomes had no effect on cell viability at higher concentrations. In our studies, TMS-liposomes showed improved viability at each concentration in comparison to TMS-solution after 24-hours, although, this was not significant. Liposomes have been found to improve overall uptake and reduce systemic drug toxicity in a multitude of studies; liposome-enveloped substances are protected from enzyme-mediated degradation or inactivation by the immune system and similar to NLCs, result in the sustained release of internalised contents (Szoka Jr et al., 1987; Mehta, 1996; Raj et al., 2013). After 48- and 72-hours, viability was maintained (>80 %), other than at 0.01 nM. The increased toxicity observed at lower concentrations is consistent with observations made in RV.

4.3 Chapter summary

This part of the study aimed to assess the potential of RV loaded within trimyristin-triolein NLCs, and TMS loaded within liposomes as a therapeutic platform for the treatment of ROS-associated disease. Using chemi-analytical techniques, stable NLCs

with the ability to entrap and release RV (as a model organic molecule) over sustained periods of time were successfully characterised. Furthermore, RV-NLCs have demonstrated their ability to successfully deliver and release *in vitro*, reducing both cytosolic and mitochondrial $O_2^{\bullet-}$ anion levels; highlighting their potential use as an antioxidant in future applications. Stable TMS-liposomes were synthesised, with no effect on cell viability. The effects of RV-NLCs and TMS liposomes on the coronary and/or cerebral vasculature will be assessed in the subsequent chapters.

Chapter 5: Development of an ex vivo model of acute hypertension for the evaluation of novel treatment strategies

Having successfully identified NLCs as a suitable delivery platform that may be loaded with an antioxidant, the next objective was to develop an *ex vivo* model of acute hypertension as a means of replicating the oxidative environment associated with hypertension mediated endothelial dysregulation; allowing an evaluation of novel treatment strategies, their efficacy and mechanisms of action within the vasculature in future applications. The hypothesis of this part of the study is that acute pressure elevation will significantly attenuate endothelial-dependent dilator responses, which will be restored following exposure to antioxidant compounds. This hypothesis will be addressed through the following specific objective:

- Establish alterations in vascular function in coronary and cerebral arteries following acute pressure elevation using an *ex vivo* model of acute hypertension, via pressure myography.

First-order septal coronary arteries and middle cerebral arteries were excised and mounted on a pressure myograph system. Endothelial-dependent and independent responses were assessed prior to, following or one hour after acute pressure elevation. The contribution of ROS was assessed using SOD, CAT or apocynin. The dilator component was assessed in coronary arteries using pharmacological inhibitors of NO-, PGI- and EDHF-pathways.

5.1 Results

5.1.1 Coronary artery

5.1.1.1 Control responses

Initial studies were conducted to establish the viability of tissues and the repeatability of vascular responses. The repeatability of responses is an integral component in experimental design as it informs the appropriate methodological approach. Coronary vessels were isolated and exposed to pressure at 60mmHg for 30-minutes. All vessels (resting diameter = 192 ± 8 µm; n = 18) constricted in response to high potassium (KCl, 60 mM; 48 ± 5 %; n = 18) and also to 5-HT in a dose-dependent manner, confirming the viability of vessels and identifying the sub-maximal concentrations of 5-HT as 10^{-5} - 10^{-6} M (Figure 5.1).

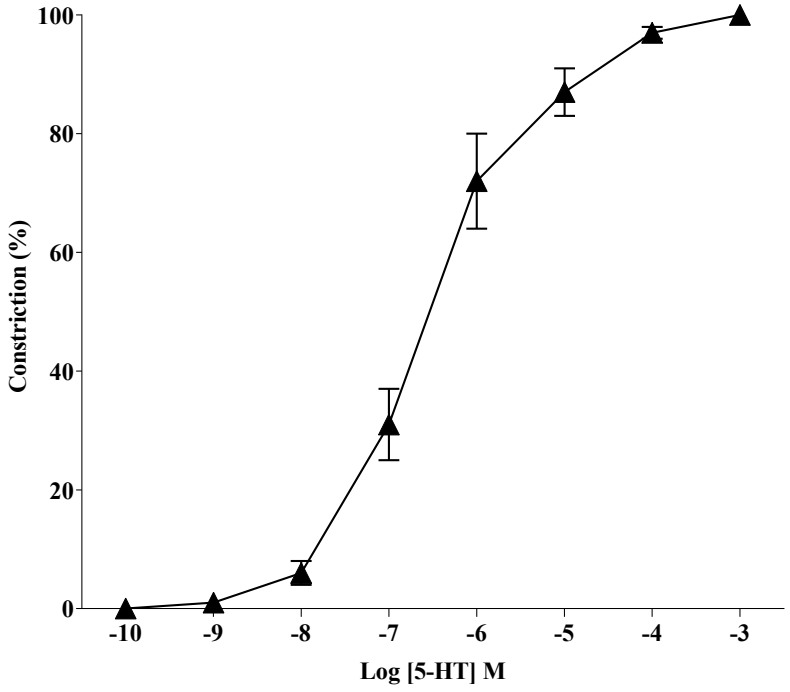

Figure 5.1. Constrictor response to 5-HT in coronary arteries. *The dose-response effect of serotonin (5-HT; 10^{-10} M – 10^{-3} M) in coronary arteries of young Wistar rats (2-month) under normotensive pressure (60 mmHg). All vessels constricted to 5-HT in a dose-dependent manner (n = 8). Repeats represent vessels from different animals. Data are presented as mean ± SEM.*

Pressure elevation (150mmHg; 30-minutes) had no effect on 5-HT-mediated constriction compared to control vessels maintained at 60mmHg (maximal constriction: 58 ± 2 % and 57 ± 7 %, respectively; 10^{-6} M; Figure 5.2).

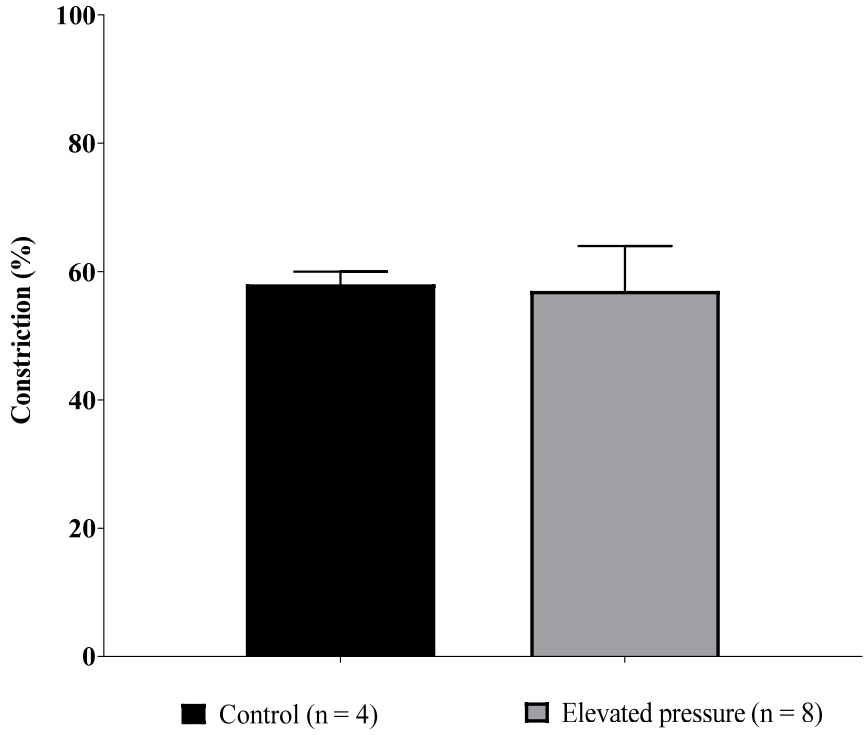

Figure 5.2. Effect of elevated pressure on the constrictor response to 5-HT. *Serotonin (5-HT; sub-maximal; 10^{-6} M) induced constrictor responses in the coronary arteries of young Wistar rats (2-month). Elevated pressure (150mmHg; 30-minutes) had no effect on 5-HT induced constrictor responses. Control (n = 4); elevated pressure (n = 8). Repeats represent vessels from different animals. Data analysed using an unpaired t-test. Data are presented as mean ± SEM.*

All 5-HT pre-constricted (sub-maximal; 10^{-6}M) vessels dilated to ACh (10^{-9} – 10^{-3} M) in a dose-dependent manner. Responses to incremental ACh administration pre- and post-incubation (60 mmHg/1-hour) in PSS resulted in dose-dependent dilation, with a similar magnitude of dilation observed (maximal dilation: 74 ± 4 % and 70 ± 6 %, respectively; Figure 5.3).

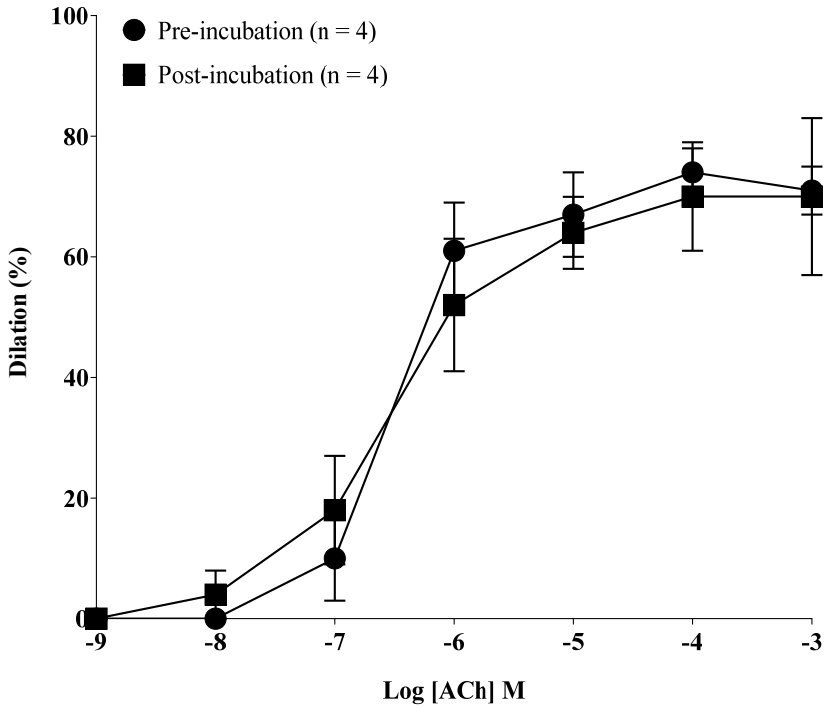

Figure 5.3. Effect of repeated ACh exposure on the dilator response to ACh. *Endothelial-dependent acetylcholine (ACh) induced dilator responses in the coronary arteries of young Wistar rats (2-month), pre- and post-incubation (60 mmHg/1-hour). Repeated exposure to ACh had no effect on endothelial-dependent dilator responses. Pre-incubation (n = 4); post-incubation (n = 4). Repeats represent vessels from different animals. Data analysed using a two-way ANOVA followed by Tukey's multiple comparisons. Data are presented as mean ± SEM.*

5.1.1.2 Acute pressure elevation attenuates endothelial-dependent dilator responses via NADPH oxidase mediated ROS generation

Initial studies were conducted to assess the influence of acute pressure elevation on the magnitude of dilator responses in isolated coronary arteries. Following pressure elevation (150 mmHg; 30-minutes), a significant reduction in ACh responses (10^{-9} – 10^{-3} M) was observed (P = < 0.01 Figure 5.4A). Co-incubation with SOD (500 U^{-}ml; P = < 0.0001; Figure 5.4A) or apocynin (30 µM; P = < 0.0001; Figure 5.4B) significantly improved endothelial-dependent dilation, suggesting that NADPH mediated ROS generation may play an important role in attenuating the dilator responses, after pressure elevation.

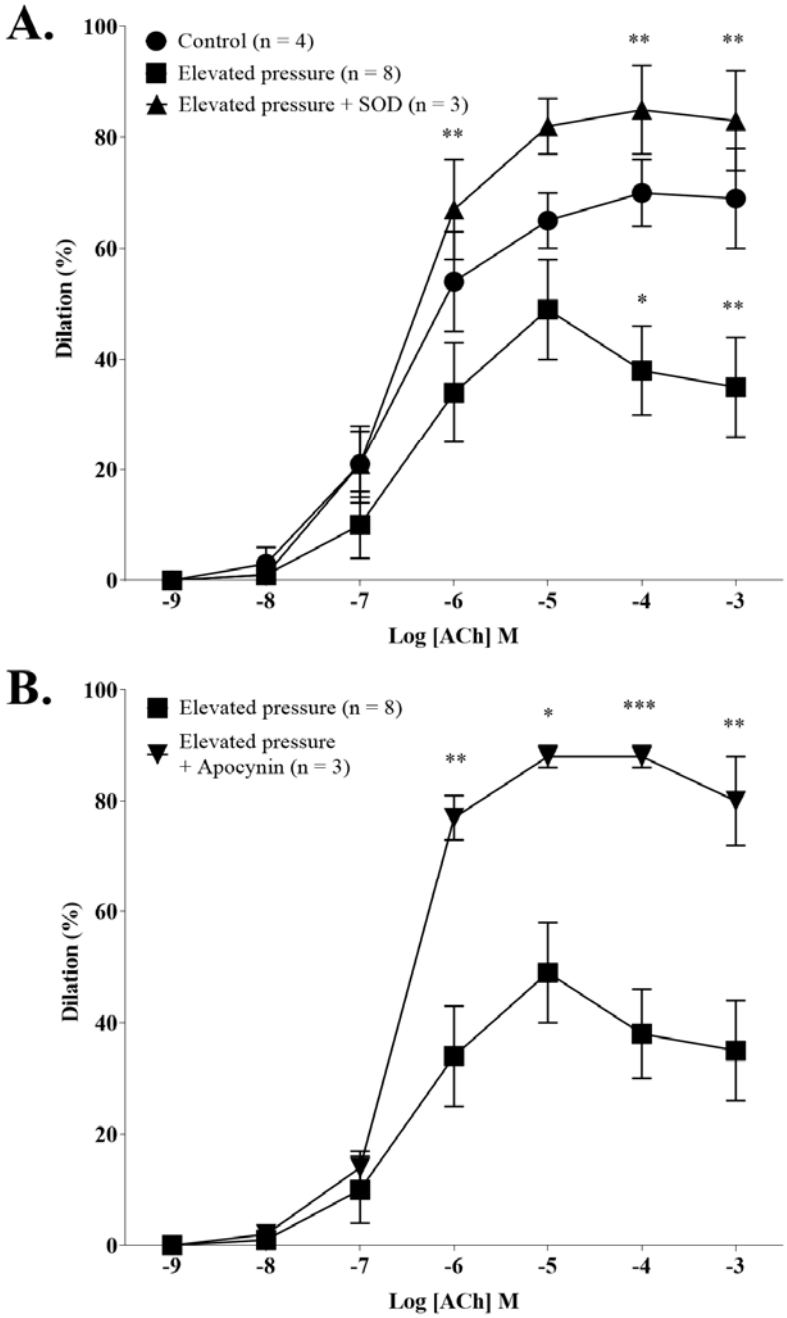

Figure 5.4. Effect of acute pressure elevation on the dilator response to ACh. *Endothelial-dependent acetylcholine (ACh) induced dilator responses in the coronary arteries of young Wistar rats (2-month). (A) Elevated pressure (150mmHg; 30-minutes) significantly attenuated dilator responses (P = < 0.01), which were restored following co-incubation with superoxide dismutase (SOD; 500 U ml; P = < 0.0001). (B) Incubation with the NADPH oxidase inhibitor apocynin (30 µM) resulted in restoration of dilation (P = < 0.0001). Control (n = 4); elevated pressure (n = 8); elevated pressure + SOD (n = 3); elevated pressure + apocynin (n = 3). Repeats represent vessels from different animals. Data analysed using a two-way ANOVA followed by Tukey's multiple comparisons test. * P < 0.05. ** P < 0.01. *** P < 0.001.*

5.1.1.3 Following acute pressure elevation, endothelial-dependent dilator responses are mediated by NO in coronary arteries

In order to establish the relative contribution of each vasodilator pathway to the dilator component following acute pressure elevation (150mmHg; 30-minutes), inhibitors of the respective pathways were used. Incubation with L-NNA (100 μM), a NO synthase inhibitor, resulted in a reduction in dilation ($P = < 0.0001$; Figure 5.5A), while incubation with the nonselective inhibitor of COX 1 and 2, indomethacin (10 μM), a significant potentiation of dilation is observed ($P = < 0.0001$; Figure 5.5B). Incubation with the small and intermediate calcium-activated potassium channel blockers apamin (100 nM) and TRAM-34 (1 μM) resulted in the potentiation of dilation ($P = < 0.0001$; Figure 5.5C). Co-incubation of vessels with L-NNA and EDH inhibitors (apamin and TRAM-34) resulted in attenuation, suggesting the potentiation observed following incubation with EDH inhibitors may be a compensatory dilator mechanism, involving mediators such as NO ($P = < 0.0001$; Figure 5.5D). Incubation with L-NNA, apamin, TRAM-34 and indomethacin resulted in the loss of the dilator component ($P = < 0.0001$; Figure 5.5E).

5.1.1.4 Endothelial-independent dilator responses are maintained following elevated pressure

Following elevated pressure (150mmHg; 30-minutes), endothelial-independent responses to papaverine (PAPA; cAMP inhibitor; 100 μM) and sodium nitroprusside (SNP; NO donor; 100 μM) were unaffected (PAPA: 85 ± 8 % and 74 ± 10 %, respectively; SNP: 66 ± 10 % and 69 ± 7 %, respectively) and comparable to control vessels maintained at 60mmHg (Figure 5.6A and B, respectively).

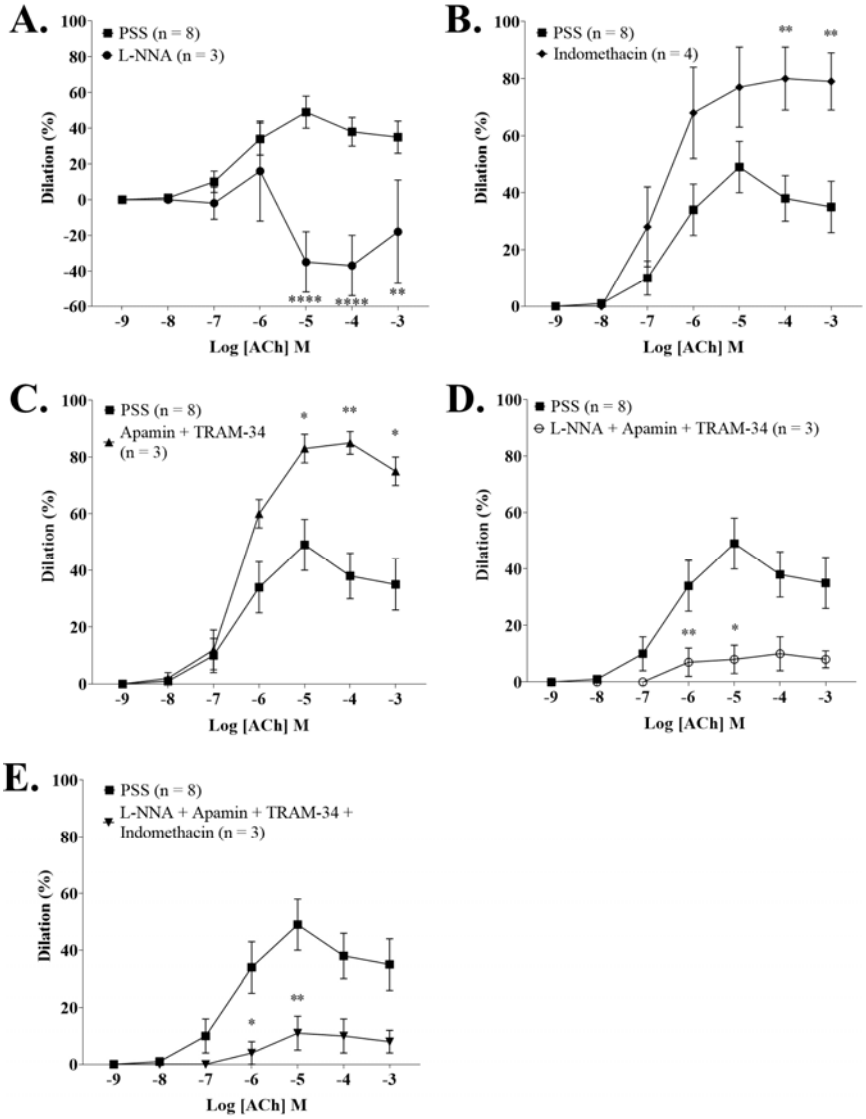

Figure 5.5. Characterisation of the dilator response to ACh following acute pressure elevation. *The influence of the inhibitors NΩ-nitro-L-arginine (A; 100 μM; n = 3), indomethacin (B; 10 μM; n = 4), apamin (100 nM) and TRAM-34 (1 μM) C; n = 3), L-NNA, apamin and TRAM-34 (D; n = 3) or L-NNA, indomethacin, apamin and TRAM-34 in combination (E; n = 3) on endothelial-dependent acetylcholine (ACh) induced dilator responses in the coronary arteries of young Wistar rats (2-month) following elevated pressure (150mmHg; 30-minutes). Incubation with L-NNA resulted in a significant constriction (P = < 0.0001). Incubation with indomethacin resulted in a significant potentiation of dilation (P = < 0.0001). Incubation with apamin and TRAM-34 resulted in the potentiation of dilation (P = < 0.0001). Co-incubation of vessels with L-NNA and EDHF inhibitors (apamin and TRAM-34) resulted in attenuated dilation (P = < 0.0001). Incubation with L-NNA, apamin, TRAM-34 and indomethacin resulted in the loss of dilator component (P = < 0.0001). Repeats represent vessels from different animals. Data analysed using a two-way ANOVA followed by Tukey's multiple comparisons. Data are presented as mean ± SEM.* P < 0.05. ** P < 0.01. **** P < 0.0001.*

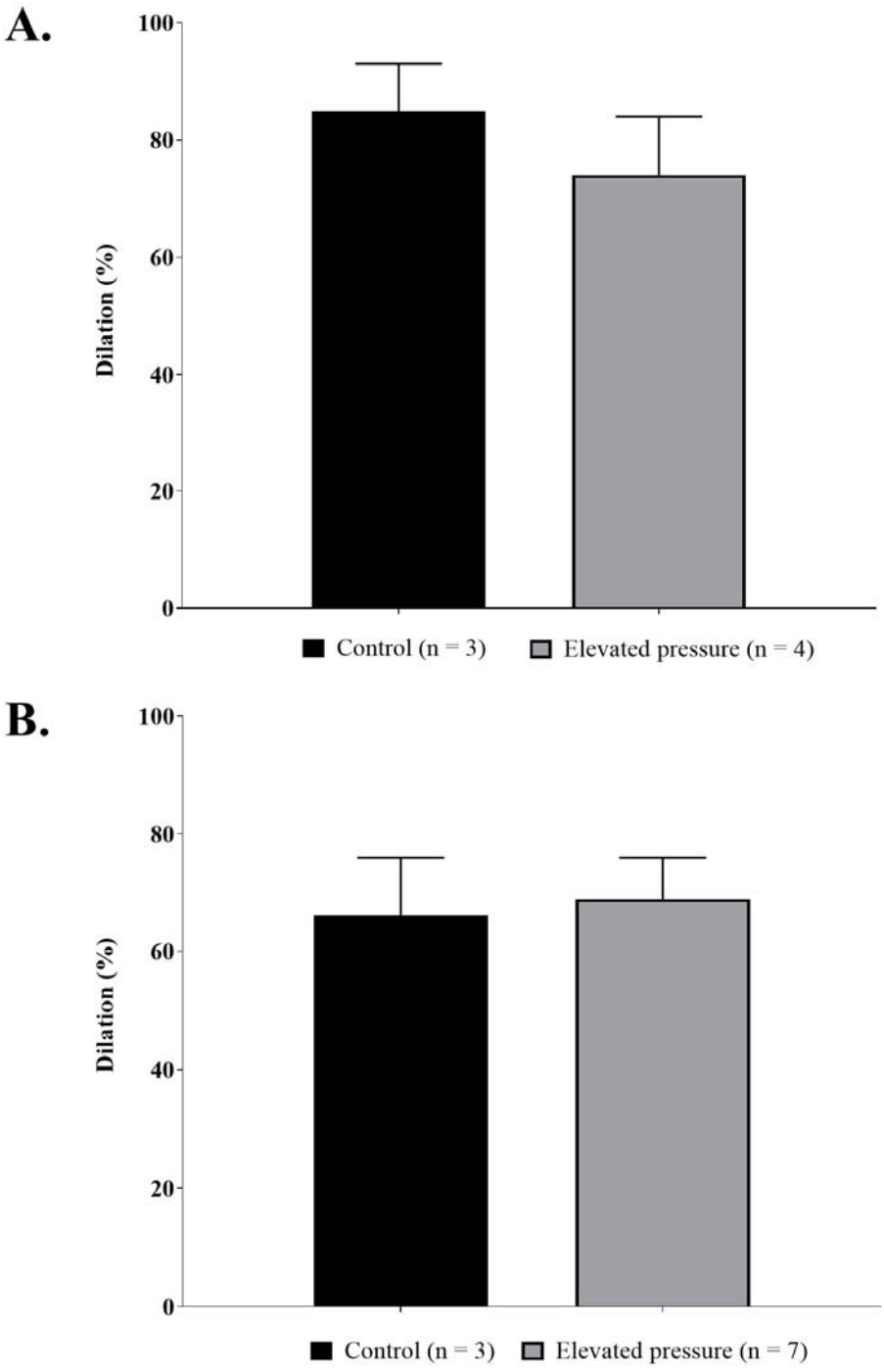

Figure 5.6. Effect of elevated pressure on the dilator response to PAPA and SNP. *Endothelial-independent papaverine (PAPA) and sodium nitroprusside (SNP) induced dilator responses in the coronary arteries of young Wistar rats (2-month). Elevated pressure (150mmHg; 30-minutes) had no effect on PAPA (A; 100 µM; Control (n = 3); elevated pressure (n = 4)) or SNP (B; 100 µM; Control (n = 3); elevated pressure (n = 7)) induced dilator responses. Repeats represent vessels from different animals. Data analysed using an unpaired t-test. Data are presented as mean ± SEM.*

5.1.1.5 Acute elevation in pressure has no effect on the structural integrity of the vessel wall

In order to establish whether acute pressure elevation was capable of affecting the structural integrity of the vessels, the structural morphology of vessels was assessed using TEM. Pressure elevation had no overall effect on the structural integrity of vessels maintained under normotensive (60 mmHg), or hypertensive (150 mmHg) pressure, with minor endothelial detachment observable (Figure 5.7A and B, respectively).

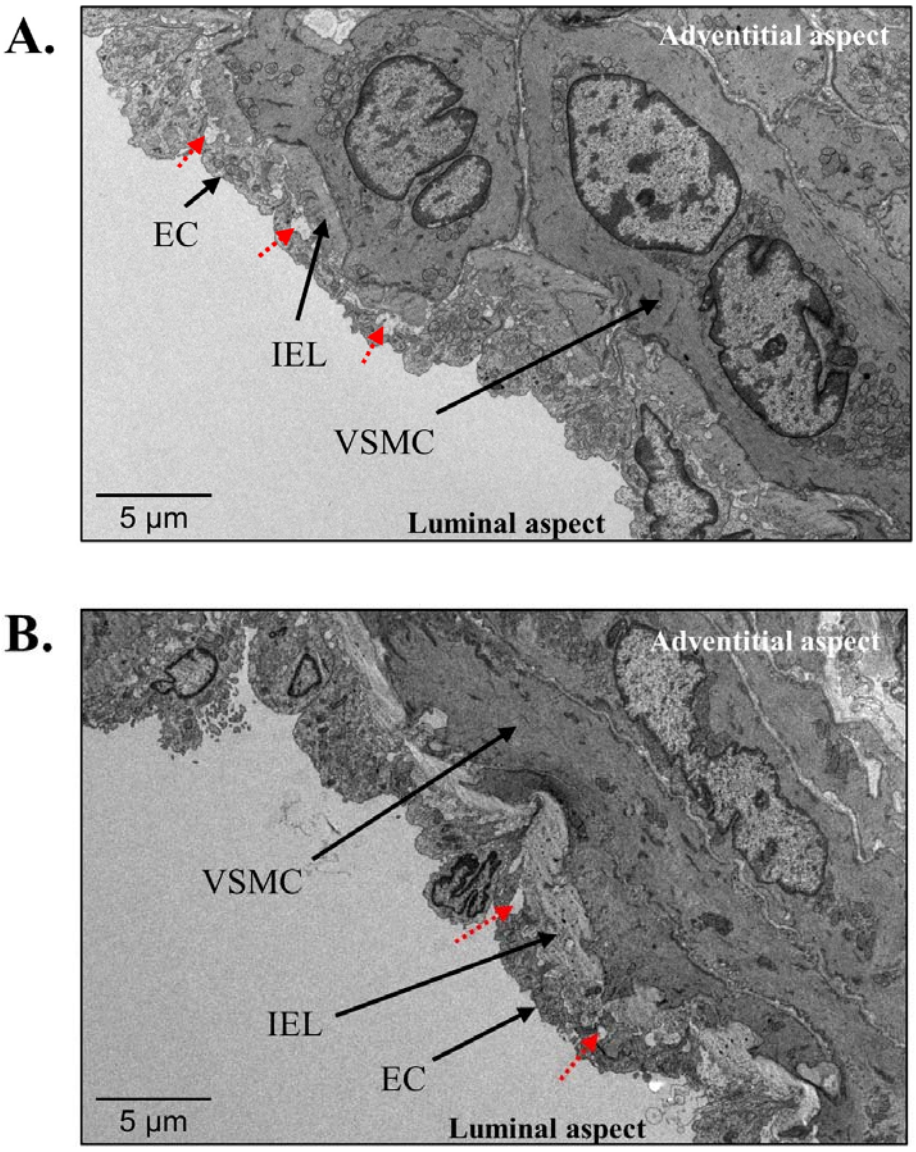

Figure 5.7. The effect of elevated pressure on the vascular integrity of the coronary artery. *Representative transmission electron (TEM) micrographs of the rat coronary artery. Maintaining vessels under normotensive pressure (A; 60 mmHg) and elevated pressure (B; 150 mmHg) had no overall effect of endothelial or smooth muscle cell integrity. However, minor endothelial detachment is observable. Control (n = 3), elevated (n = 3). Magnification 690 x. Scale bar = 5 µm. Micrograph legend: endothelial cell (EC); internal elastic lamina (IEL); vascular smooth muscle cell (VSMC). Red arrows indicate sites of endothelial detachment.*

5.1.2 Cerebral artery

5.1.2.1 Control responses

Initial studies were conducted to establish the viability of tissues and the repeatability of vascular responses. Cerebral vessels were isolated and exposed to pressure at 60mmHg for 30-minutes. All vessels (resting diameter = 169 ± 8 μm; n = 21) constricted in response to high potassium (KCl, 60 mM; 49 ± 4 %; n = 21) and also to 5-HT in a dose-dependent manner, confirming the viability of vessels and identifying the sub-maximal concentrations of 5-HT as 10^{-6} - 10^{-7} M (n = 6) (Figure 5.8).

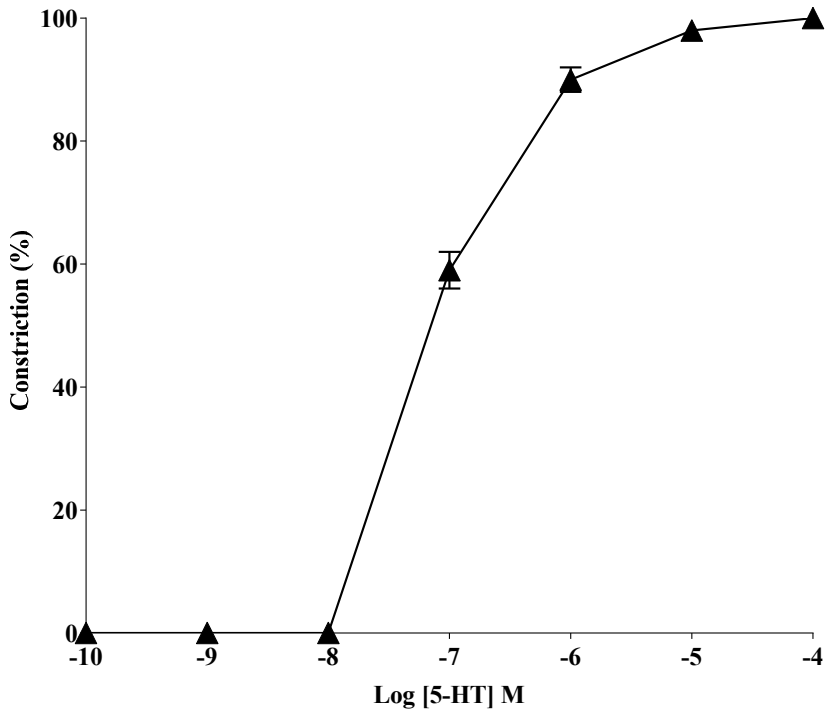

Figure 5.8. Constrictor response to 5-HT in cerebral arteries. *The dose-response effect of serotonin (5-HT; 10^{-10} M – 10^{-4} M) in cerebral arteries of young Wistar rats (2-month) under normotensive pressure (60 mmHg). All vessels constricted to 5-HT in a dose-dependent manner (n = 6). Repeats represent vessels from different animals. Data are presented as mean ± SEM.*

Pressure elevation (150mmHg; 30-minutes) had no effect on 5-HT-mediated constriction compared to control vessels maintained at 60mmHg (maximal constriction: 60 ± 7% and 66 ± 16%, respectively 10^{-7} M; Figure 5.9).

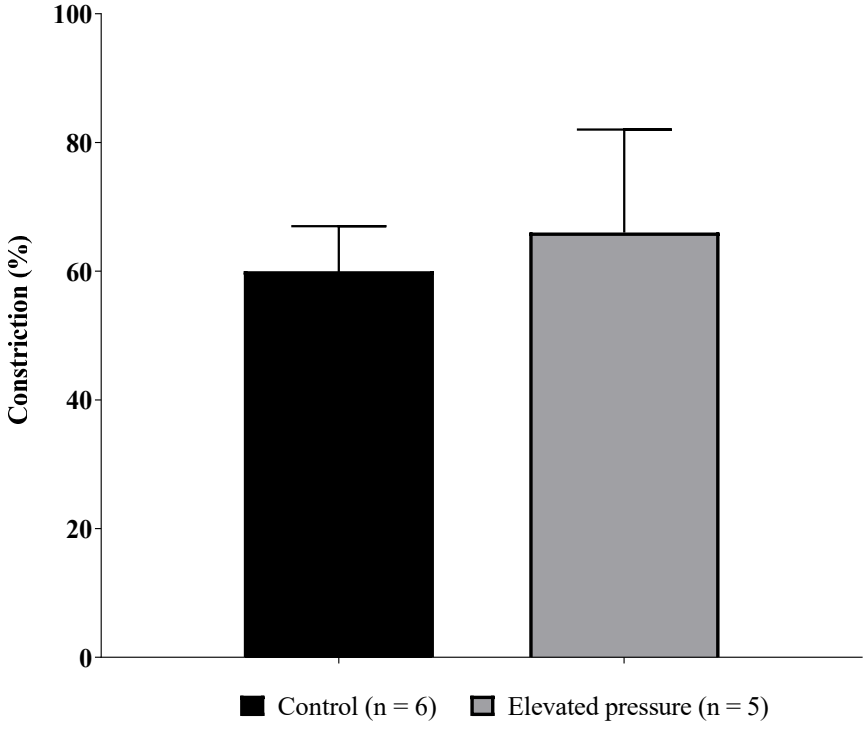

Figure 5.9. Effect of elevated pressure on the constrictor response to 5-HT. *Serotonin (5-HT; sub-maximal; 10^{-7} M) induced constrictor responses in the cerebral arteries of young Wistar rats (2-month). Elevated pressure (150mmHg; 30-minutes) had no effect on 5-HT induced constrictor responses. Control (n = 6); elevated pressure (n = 5). Repeats represent vessels from different animals. Data analysed using an unpaired t-test. Data are presented as mean ± SEM.*

All 5-HT pre-constricted (sub-maximal; 10^{-7} M) vessels dilated to ACh (10^{-9} – 10^{-3} M) in a dose-dependent manner. Responses to ACh pre- and post-incubation (60 mmHg/1-hour) resulted in dose-dependent dilation, which was significantly reduced post-incubation (maximal dilation: 62 ± 7 % and 38 ± 7 %, respectively; $P = < 0.001$; Figure 5.10). Consequently, only post-incubation responses were evaluated.

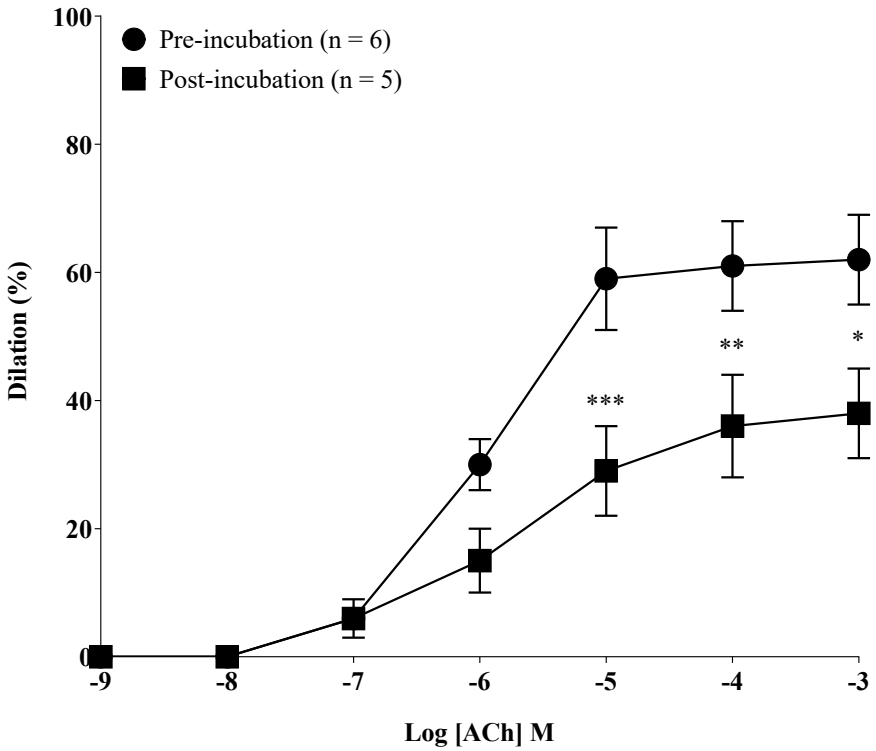

Figure 5.10. Effect of repeated ACh exposure on the dilator response to ACh. *Endothelial-dependent acetylcholine (ACh) induced dilator responses in the cerebral arteries of young Wistar rats (2-month), pre- and post-incubation (60 mmHg/1-hour). Repeated exposure to ACh significantly attenuated ACh induced dilation (P = < 0.001). Pre-incubation (n = 6); post-incubation (n = 5). Repeats represent vessels from different animals. Data analysed using a two-way ANOVA followed by Tukey's multiple comparisons. Data are presented as mean ± SEM. * P < 0.05. ** P < 0.01. *** P < 0.001.*

5.1.2.2 Acute pressure elevation attenuates endothelial-dependent dilator responses

Following elevated pressure (150 mmHg; 30-minutes), a significant reduction in ACh responses was observed (P = < 0.0001). Co-incubation with SOD (500 U^{-}ml) in the absence or presence of CAT (300 U^{-}ml) had no effect on attenuated dilator responses (Figure 5.11).

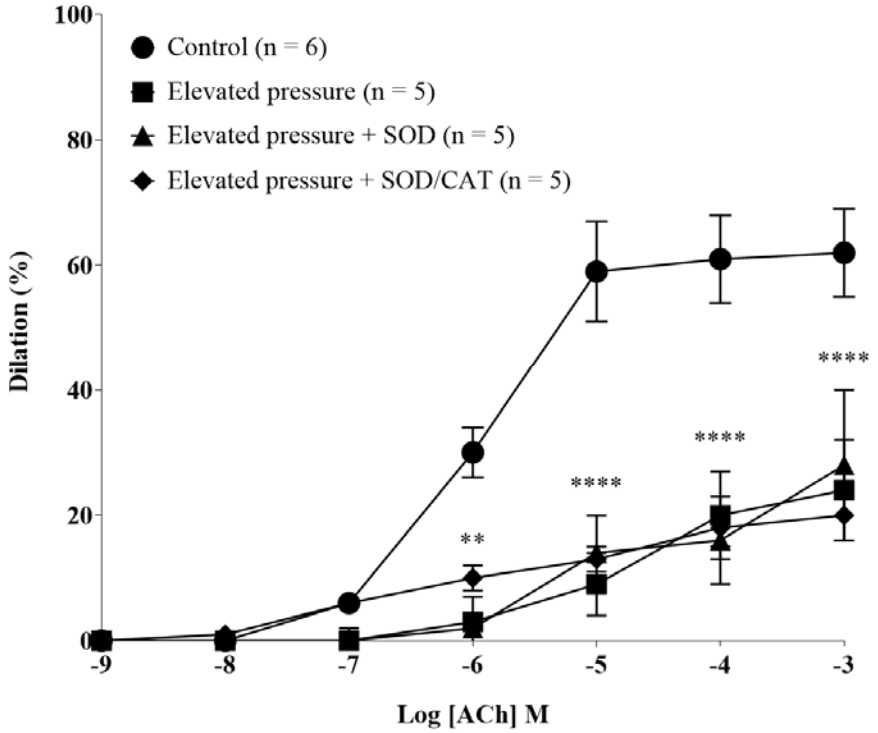

Figure 5.11. Effect of acute pressure elevation ± SOD/CAT on the dilator response to ACh. *Endothelial-dependent acetylcholine (ACh) induced dilator responses in the cerebral arteries of young Wistar rats (2-month). Elevated pressure (150mmHg; 30-minutes) significantly attenuated dilator responses (P = < 0.0001). Co-incubation with superoxide dismutase (SOD; 500 U·ml) had no effect on attenuated dilator responses. Co-incubation with SOD and catalase (CAT; 300U·ml) had no effect on attenuated dilator responses. Control (n = 6); elevated pressure (n = 5); elevated pressure + SOD (n = 5); elevated pressure + SOD/CAT (n = 5). Repeats represent vessels from different animals. Data assessed using a two-way ANOVA followed by Tukey's multiple comparisons. Data are presented as mean ± SEM. ** P < 0.01. **** P < 0.0001.*

5.1.2.3 Endothelial-independent dilator responses are affected by H_2O_2

Endothelial-independent responses to PAPA were unaffected, with dilator responses comparable to control vessels maintained at 60mmHg (Figure 5.12A). Following acute pressure elevation (150mmHg; 30-minutes), SNP mediated dilation was comparable to that of control vessels (normotensive pressure @ 60 mmHg). Co-incubation with SOD (500 $U^{-}ml$) significantly attenuated dilator responses ($P = < 0.05$), which were restorable in the presence of SOD/CAT ($P = < 0.05$; Figure 5.12B).

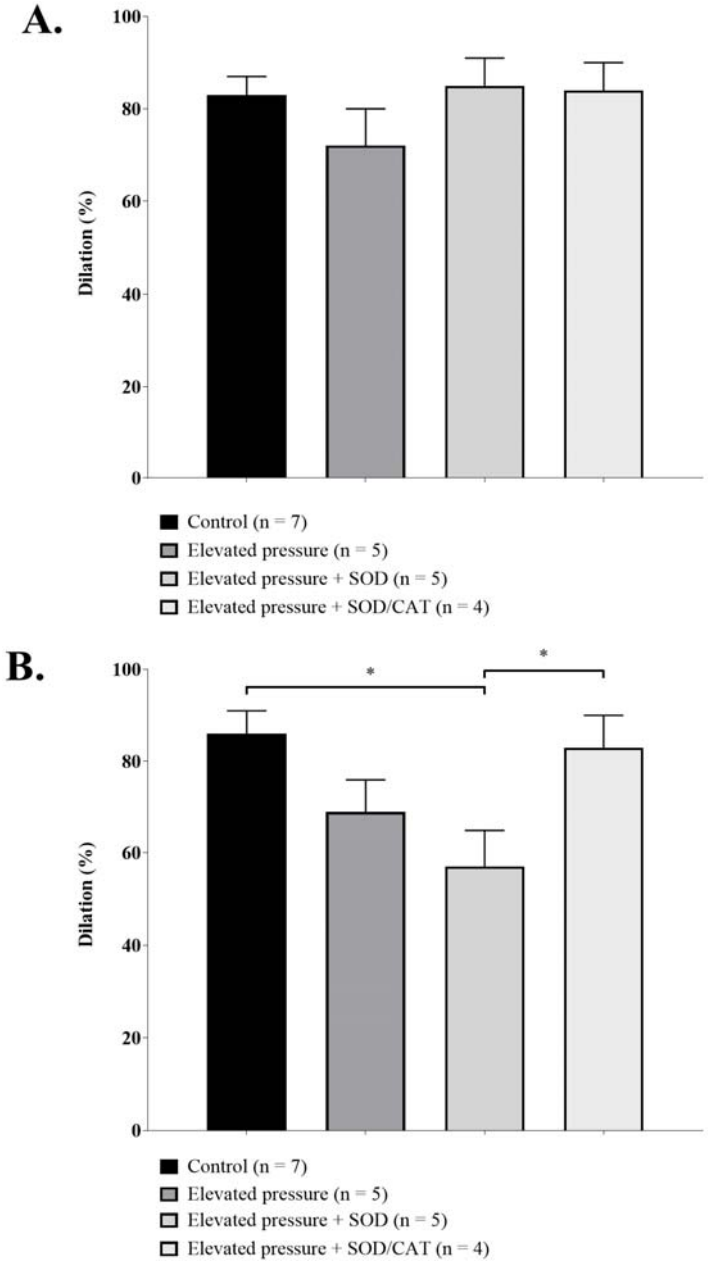

Figure 5.12. Effect of elevated pressure on the dilator response to PAPA and SNP. *Endothelial-independent papaverine (PAPA) and sodium nitroprusside (SNP) induced dilator responses in the cerebral arteries of young Wistar rats (2-month) following elevated pressure (150mmHg; 30-minutes). (A) Treatment had no effect on PAPA (100 µM) induced dilator responses. (B) Co-incubation with superoxide dismutase (SOD; 300U΄/ml) significantly attenuated SNP (100 µM) mediated dilator responses (P = < 0.05). Co-incubation with SOD and catalase (CAT; 500U΄/ml) significantly improved dilator responses, compared to SOD alone. Control (n = 7); elevated pressure (n = 5); elevated pressure + SOD (n = 5); elevated pressure + SOD/CAT (n = 4). Repeats represent vessels from different animals. Data analysed using a one-way ANOVA followed by Dunnett's comparison. Data are presented as mean ± SEM. * P < 0.05.*

5.1.2.4 Acute elevation in pressure has no effect on the structural integrity of the vessel wall

In order to establish whether acute pressure elevation was capable of affecting the structural integrity of the vessels, the structural morphology of vessels was assessed using TEM. Pressure elevation had no overall effect on the structural integrity of vessels maintained under normotensive (60 mmHg), or hypertensive (150 mmHg) pressure, with minor endothelial detachment observable (Figure 5.13A and B, respectively).

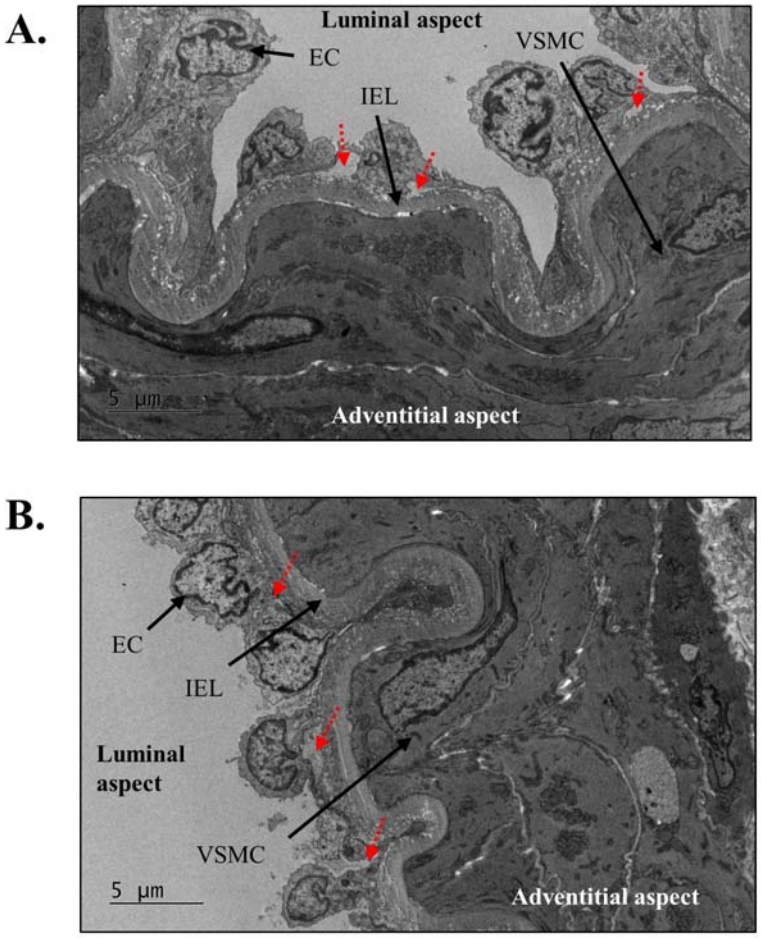

Figure 5.13. Effect of elevated pressure on the vascular integrity of the cerebral artery. *Representative transmission electron (TEM) micrographs of the rat middle cerebral artery. Maintaining vessels under normotensive pressure (A; 60 mmHg) and elevated pressure (B; 150 mmHg) had no overall effect of endothelial or smooth muscle cell integrity. However, minor endothelial detachment is observable. Control (n = 3), elevated (n = 3). Magnification 690 x. Scale bar = 5 µm. Micrograph legend: endothelial cell (EC); internal elastic lamina (IEL); vascular smooth muscle cell (VSMC). Red arrows indicate sites of endothelial detachment.*

5.2 Discussion

5.2.1 Acute pressure elevation attenuates endothelial-dependent dilator responses via activation of NADPH oxidase in coronary arteries

Following acute pressure elevation, a significant reduction in endothelial-dependent dilation in isolated coronary arteries *ex vivo* was observed. Previous *in vivo* and *ex vivo* studies employing experimental models of hypertension (pharmacological-, genetically-, pressure-induced) using isolated arteries have attributed the impairment of endothelial-dependent dilation in several vascular beds (cerebral, coronary, femoral) to increased $O_2^{\bullet-}$ generation (Wei et al., 1985; De Bruyn et al., 1994; Ungvari et al., 2003); affirmed following incubation of vessels with SOD and CAT, reducing endogenously-derived ROS and restoring attenuated responses. Several sources of ROS have been identified in the vasculature following hypertension, with inhibition studies identifying NADPH oxidase as the predominant candidate (leading to the generation of $O_2^{\bullet-}$). In order to ascertain whether coronary vessels subjected to elevated pressure possess similar mechanisms and sources of ROS generation, vessels were incubated with SOD or apocynin to assess the contribution of $O_2^{\bullet-}$ and NADPH oxidase, respectively (Guillermo et al., 2000; Cooke and Davidge, 2003). Consistent with previous studies, SOD incubation following pressure elevation lead to the restoration and potentiation of dilation (Huang et al., 1998; Ungvari et al., 2004). Similarly, co-incubation with apocynin resulted in the restoration of dilation, implicating NADPH oxidase in the generation of vascular $O_2^{\bullet}$.

5.2.2 Following acute pressure elevation, endothelial-dependent dilator responses are mediated by NO in coronary arteries

Stimulation of endothelial cells leads to endothelial-dependent dilation via NO-, PGI- and EDH-mediated pathways; however, considerable heterogeneity exists among vascular beds and species. Both NO and EDH play an integral role in regulating dilation in the coronary arteries, whereby patients administered NO inhibitors observe active upregulation of EDH, suggesting potential cross-talk and dynamic compensatory mechanisms between pathways (Urakami et al., 1997; Miura et al., 2001; Ozkor et al., 2011). The disruptive potential of hypertension on NO and EDHF-mediated dilator pathways has been demonstrated *in vivo* and *ex vivo* (Dunn et al., 2017). Consequently, in order to assess the influence of potential treatment strategies, an accurate understanding of the mechanistic pathways mediating endothelial-dependent dilation and their relative contributions under an elevated pressure environment was required.

Our inhibition studies demonstrate that following acute pressure elevation, NO is the major dilator component in coronary arteries with modulation by the COX and EDHF pathways, as previously documented in vessels from aged mice (Vessieres et al., 2010). Inhibition using L-NNA significantly compromised dilation, resulting in constriction of the vessel. This is likely attributable to a global reduction in dilator bioavailability, resulting in constrictor prostanoids (such as thromboxane A2 (TXA_2) and prostaglandin H_2 (PGH_2)) having a more pronounced effect on the vasculature. These observations suggest that the release of NO from the endothelium following acute pressure elevation has a significant dilator influence on the coronary vasculature. This is in agreement with previous studies, where NO was identified as playing an integral role in maintaining vasomotor tone in both conduit and resistance vessels in the coronary circulation

(Quyyumi et al., 1995; Nishikawa and Ogawa, 1997). Nonetheless, these findings were unexpected, given the exacerbated production of $O_2^{\bullet-}$ observed in hypertensive environments and its potential inhibitory effects on NO, limiting its bioavailability and dilator capacity. However, the agonist-induced dilation of pre-constricted vessels has been shown to be reduced or eliminated by inhibitors of eNOS in isolated coronary vessels from hypertensive human and murine models, suggesting that NO continues to play an important role in the regulation of dilation, despite its bioavailability being reduced in hypertension (Pourageaud and Freslon, 1995; Quyyumi et al., 1995). Whilst a body of evidence supports the principal contribution of NO, several studies contest this notion, arguing that EDHFs are of greater significance in the regulation of coronary dilation (Nishikawa et al., 1999; Miura et al., 2001).

In our *ex vivo* model, a potentiation of dilation was observed following inhibition of EDH. As previously described, studies have demonstrated the ability of the vasculature to actively compensate for the loss of normal dilator responses, minimising disruption to the systemic circulation. In order to ascertain whether the potentiated response was attributable to EDH, or a possible compensatory mechanism facilitated by NO, vessels were co-incubated in both apamin, TRAM-34 and L-NNA. The addition of L-NNA resulted in the loss of the dilator response, confirming compensation by NO. The apparent lack of EDH response differs from observations produced by some studies, identifying EDHF as the major dilator component in human and murine coronary arteries (Miura and Gutterman, 1998; Simone et al., 2003). However, this discrepancy can be attributed to experimental design. The influence of vessel size on the distribution and expression of EDRFs is well documented, with studies identifying a proportional increase in EDHF activity as vessel size decreases within the arterial network, with predominant EDHF activity in the resistance vessels (Nagao et al., 1992; Nishikawa et al., 1999). In studies

documenting prominent EDHF activity, isolated vessels with an average diameter < 100 μm were used; associated with elevated EDHF localisation. In contrast, vessels utilised in our studies were > 100 μm, and hence, preferentially subject to NO-mediated dilation. The differing dilator components reported are therefore, unsurprising. The decision to use vessels > 100 μm is related to arterial pressure. Pressure distribution within the arterial network is well documented, with elevated pressure associated with larger vessels. Hence, superior (larger) segments of the coronary arteries were isolated, as opposed to the inferior (smaller), as these would be expected to undergo elevated pressure during systole.

In addition to NO- and EDH-mediated dilator pathways, other dilators include prostanoids such as PGI_2, a COX derived metabolite. The effects of COX derived products were investigated using indomethacin, which significantly potentiated dilation; likely attributable to its inhibitory effect on downstream COX constrictors such as PGH_2 and TXA_2 (Brace et al., 1985). Similar responses have been observed in the mesenteric arteries of clinically hypertensive rats (i.e. spontaneously hypertensive/co-morbidity associated) following the administration of indomethacin, suggesting the involvement of vasoconstrictor prostanoids (Watt and Thurston, 1989; Vessieres et al., 2010). The complex interplay between COX-mediated dilator and constrictor generation has generated considerable ambiguity in the interpretation of experimental data, whereby several studies have revealed conflicting results, noting enhanced constriction in the absence of functional COX. In isolated murine aortic rings incubated with COX inhibitors, a significant enhancement of phenylephrine-induced constriction was found, but only in the presence of L-NAME (NOS inhibitor), implicating NO in the suppression of vasoconstrictive prostanoid generation (Anning et al., 2006). Hence, it is possible that our observations are a consequence of having a partially intact NO-dilator pathway, preventing adverse effects of constrictors on the vasculature and promoting dilation.

It is unclear why incubation with inhibitors of NO-, PGI -and EDHF-pathways were incapable of abolishing dilation, retaining only a minimal dilator influence (< 8 ± 3 %); however, it could suggest the presence of a possible further dilator pathway in the coronary artery. In small coronary resistance size arteries, it has been reported that stimulation of Ca^{2+} permeable cation channels such as transient receptor potential vanilloid 4 (TRPV4), contribute to and perpetuate signalling mechanisms mediating smooth muscle cell hyperpolarisation and dilation. To date, members of the TRP family have been identified in numerous tissues, including coronary arterioles, with the TRPV4 subtype being highly expressed in vascular endothelial cells (Mendoza et al., 2010; Bubolz et al., 2012). TRPV4 activation and signal transduction is subject to a broad range of mechanical (e.g. membrane distension and shear stress) and chemical stimuli, including endogenous lipid activators such as arachidonic acid (AA) and downstream metabolically derived products of CYP450 epoxygenases; such as EETs (Zheng et al., 2013; Cao et al., 2016). Despite the ability of indomethacin to successfully inhibit the production of downstream AA metabolic products, AA production is itself upstream of COX 1/2 and is consequently not subject to inhibition, and may therefore, account for the modest dilator influence observed.

Whilst the dilator component under normotensive conditions were not characterised in this study, previous work conducted by our group has characterised the effects of intravascular and extravascular pressure on myogenic responses in the coronary arteries of rats (Azzawi and Austin, 2004, 2006). However, it would be important to evaluate the effect of potential therapeutics on normal vessels and vessels undergoing hypertension (see Chapter 6) in to develop a comprehensive understanding of the mechanisms underlying potential therapeutics.

5.2.3 Endothelial-independent dilator responses are maintained following elevated pressure

In order to ascertain whether the effects observed were localised to the endothelium or were also affecting the VSMCs, endothelial-independent responses were assessed. Endothelial-independent dilator responses following PAPA and SNP were unaffected, suggesting that VSMC integrity and responsiveness were not influenced by acute elevation in pressure. This was also shown by some (Fresquet et al., 2006; Agostino et al., 2013), but not all models of hypertension (Huang et al., 1998; Ungvari et al., 2003), suggesting that in our case, $O_2^{\bullet-}$ generation may be localised to the endothelial cells.

5.2.4 Acute elevation in pressure has no effect on the structural integrity of the vessel wall

In addition to the molecular impairment associated with ROS, physical damage to the endothelium is known to impair dilator responses and, in some cases, (e.g. endothelial denudation), promote constriction due to the reduction of basal NO (Azzawi and Austin, 2006). TEM was performed to assess the integrity of the endothelial and smooth muscle layers following exposure to normotensive and hypertensive pressures. Overall, pressure elevation had no effect on vessel integrity, suggesting the impaired dilator function observed is the result of aberrant mechanistic control, rather than structurally related damage. The lack of pressure-induced damage is unsurprising, given the high, sustained perfusion pressures expected of intramuscular blood vessels (Ramanathan and Skinner, 2005). Many studies using experimental models of hypertension have documented

remodelling of the vasculature; however, these are chronic models and alterations would therefore be expected (Hamasaki et al., 2000; Arnalich-Montiel et al., 2014).

TEM imaging shows that in the case of both normotensive and hypertensive vessels, minor detachment of endothelial cells from the basement membrane is evident. There are several possible explanations, the most likely being processing artefacts, involving the shrinkage of the elastin layer underneath the endothelium, in addition to some damage (maybe hypoxia or mechanical action). Elastin shrinkage occurs when vessels are fixed with aldehydes without sufficient pressure inside to counteract this shrinkage (McDonald and Chandler, 1981). Following treatment, vessels were preserved via immersion fixation, requiring removal and depressurisation of the vessel. Retrospectively, perfusion fixation of pressurised vessels would be a more appropriate technique, mitigating the hypertonic effects of fixatives on tissue specimens. Collectively, these observations suggest that impaired dilator function is a result of mechanistic dysregulation mediated via ROS and not a result of hypertension-induced structural damage.

5.2.5 Acute pressure elevation attenuates endothelial-dependent dilator responses in cerebral arteries

Constriction of cerebral arteries showed a higher potency to 5-HT compared to coronary ($LogEC_{50}$: 0.78 μM and 3.12 μM, respectively) and is likely attributable to the varied expression and density of 5-HT receptors in the cerebral and peripheral vasculature. Repeated exposure to ACh significantly attenuated dilator responses. ACh receptors are subject to agonist-mediated desensitisation and sequestration, as demonstrated with M_5 receptors following acute exposure to cholinomimetic compounds (Tsuga et al., 1998). The prominence of the M_5 receptor in the cerebral vasculature has been documented,

whereby deletion of genes encoding the M_5 receptor subtype abolished the dilator response to ACh in cerebral blood vessels but did not affect dilation of coronary arteries (Yamada et al., 2001; Araya et al., 2006). Hence, incremental exposure to ACh may result in partial M_5 receptor desensitisation, limiting second messenger generation and accounting for the impaired dilator response observed in the cerebral arteries, and not the coronary.

Acute pressure elevation significantly attenuated ACh-dependent dilation. Analogous to the coronary artery, $O_2^{\bullet-}$ generation has been associated with impaired dilator function in genetic, pharmacological and pressure-induced models of hypertension in cerebral arteries (Wei et al., 1985; Didion and Frank, 2003; Faraci et al., 2006). In order to determine whether $O_2^{\bullet-}$ contributes to impaired dilation in our own acute hypertension model, vessels were co-incubated with SOD. In contrast to previous studies performed in the coronary artery, co-incubation with SOD did not improve ACh-induced dilation. Several possibilities may account for these observations; 1) metabolic by-products of $O_2^{\bullet-}$ dismutation, i.e. H_2O_2, may themselves be causing toxicity or elevated constriction. The generation of $O_2^{\bullet-}$ and its subsequent impairment of vascular responses have previously been observed using a pharmacological model of hypertension in feline cerebral arteries, which demonstrated dilation was restorable following co-incubation with SOD and CAT, implicating $O_2^{\bullet-}$ as well as and H_2O_2 in impaired dilation (Wei et al., 1985). However, the effects of H_2O_2 on the cerebral vasculature vary with the artery and species studied, with the paradoxical effects of H_2O_2 being well documented (Wei et al., 1996; Sobey et al., 1997). In murine MCAs, H_2O_2 has been identified as an inducer of constriction, mediating the oxidant-dependent stimulation of cerebral arterial smooth muscle L-type calcium channels (Chaplin and Amberg, 2012). In order to assess whether by-products of $O_2^{\bullet-}$ dismutation, specifically H_2O_2, were causing and or contributing to impaired dilation,

vessels were co-incubated with SOD and CAT. Co-incubation did not result in improved dilation, seemingly absolving the influence of H_2O_2.

5.2.6 Endothelial-independent dilator responses are affected by H_2O_2

VSMCs contain the contractile apparatus and are paramount in regulating constrictor and dilator responses, with pressure-induced damage/injury having been shown to compromise VSMC function (Ungvari et al., 2003; Gündüz et al., 2008). To determine whether acute pressure elevation might have compromised smooth muscle cell integrity, endothelial-independent dilator responses to PAPA and SNP were assessed. The ability of PAPA to induce relaxation of smooth muscle cells (via inhibition of cAMP-dependent phosphodiesterase) suggests that acute pressure had no overall effect on the contractile machinery or the integrity of the VSMCs. In contrast, the responsiveness of vessels to the NO donor SNP was varied. Co-incubation of vessels with SOD resulted in attenuated dilator responses, which were restored following co-incubation with CAT; implicating H_2O_2 in the impairment of endothelial-independent responses. As with most cell types, the primary sources of H_2O_2 in VSMCs include NADPH oxidase enzyme complexes and the mitochondrial electron transport chain, generated by SODs (Lennicke et al., 2015); catalysing the dismutation of $O_2^{\bullet-}$ anions into the less chemically reactive H_2O_2 and O_2. Despite its comparatively low reactivity, H_2O_2 is a mild oxidant with the ability to diffuse freely through cellular membranes due to its solubility in both lipid and aqueous environments. The capacity of H_2O_2 to induce alterations in the activity and function of molecules has been reported previously, with incubation alongside NO propagating the generation of singlet oxygen species and reducing NO bioavailability (Noronha-Dutra et al., 1993). The significance of SOD as a source of H_2O_2 was further established following

the exogenous administration of SOD, enhancing the generation of ROS, whilst CAT inhibited the reaction; affirming the detrimental effects of exogenous antioxidant administration. These observations differ significantly from those of the coronary vasculature following incubation with SOD. This is unsurprising, given the abundance of polyunsaturated fatty acids susceptible to oxidation, and the increased concentration of transition metals such as iron or copper liable to Fenton-like reactions ($^{\bullet}OH$ generation) in cerebral tissues (Crichton and Ward, 2013). Following an assessment of endothelial-dependent and independent responses, evidence has arisen vindicating but also implicating the influence of H_2O_2. However, it should be noted that whilst endothelial-independent SNP responses suggest H_2O_2 is affecting VSMCs, it provides no indication of endothelial viability/integrity. The endothelium could, therefore, be damaged, accounting for the limited dilator response. TEM was performed to assess the integrity of the endothelial and smooth muscle layers following exposure of vessels to normotensive and hypertensive pressure. Pressure elevation had no overall effect on vessel integrity. Similar to observations made on coronary arteries, fixation resulted in minor endothelial detachment.

5.3 Chapter summary

In summary, this part of the study aimed to develop an *ex vivo* model of acute hypertension and determine the mechanisms underlying attenuated dilation, as a means of replicating the oxidative environment observed in hypertension. Using the *ex vivo* model, NADPH-oxidase derived $O_2^{\bullet-}$ was shown to play an integral role in attenuating dilator responses in the coronary artery; with inhibition studies identifying NO as the principal dilator component, despite the presence of elevated $O_2^{\bullet-}$. In contrast, pressure

mediated attenuated dilation in cerebral vessels was not restored by incubation with SOD or CAT, suggesting a role for other ROS moieties. Consideration of anatomical, functional and physiological differences between vascular beds are important in the development and implementation of safe, effective and innovative treatments for the strategic improvement of cardiovascular health. Consequently, the *ex vivo* model was deemed suitable as a means of replicating an oxidative environment, allowing an investigation into the use of novel strategies for treating ROS-mediated impairment.

Chapter 6: The influence of organic nanoparticles on coronary artery function

The objective of this next part of the study was to utilise the *ex vivo* model of hypertension described in chapter 5 and use the organic RV-NLCs characterised and described in chapter 4 to establish their capacity to ameliorate oxidative injury. The hypothesis of this part of the study is that RV-NLCs will restore attenuated endothelial-dependent dilator responses which will be maintained over sustained time-periods. This hypothesis will be addressed through the following specific objective:

- Determine whether RV-NLCs have the capacity to restore attenuated dilation following acute pressure elevation.

First-order septal coronary arteries were excised and mounted on a pressure myograph system. Endothelial-dependent and independent responses were assessed following and one hour after acute pressure elevation in the presence of RV-NLCs or RV-solution. The dilator component was investigated using inhibitors of NO, PGI and EDHF-mediated relaxation. Mechanisms leading to dilation were investigated using inhibitors of SIRT-1 and AMPK.

6.1 Results

6.1.1 Control responses

Coronary vessels were isolated and exposed to pressure at 60mmHg for 30-minutes. The viability of vessels was assessed by ascertaining initial responses to KPSS. All vessels (resting diameter = 187 ± 7 µm; n = 40) constricted to high potassium, confirming the viability of vessels (KCl, 60 mM; 49 ± 7 %; n = 40). Pressure elevation (150mmHg; 30-minutes) + RV-NLC/RV-solution (0.45 µM) had no effect on 5-HT-mediated constriction (10^{-6} M; Figure 6.1).

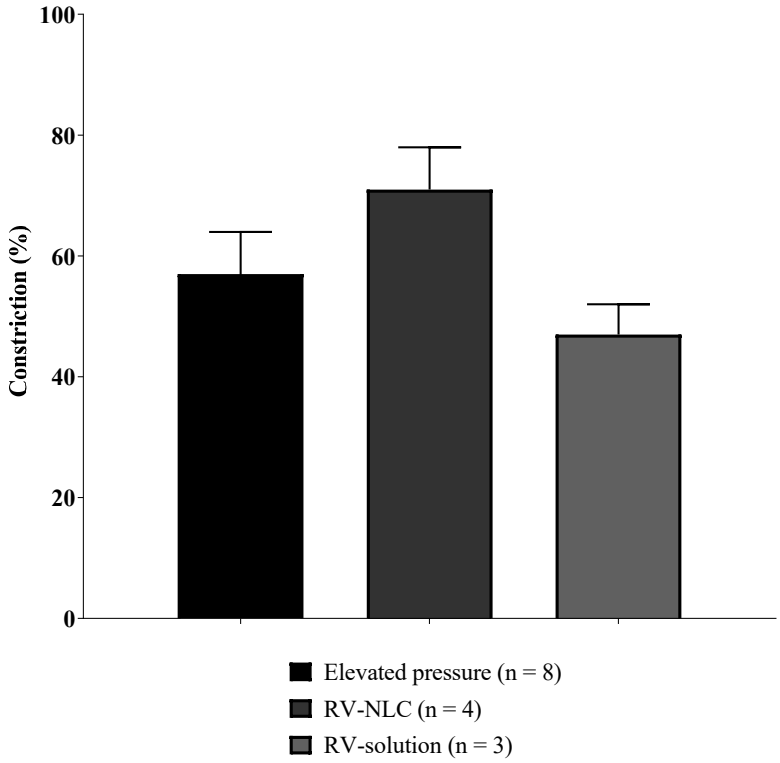

Figure 6.1. Effect of RV-NLCs on the constrictor response to 5-HT. *Serotonin (5-HT; sub-maximal; 10^{-6} M) induced constrictor responses in the coronary arteries of young Wistar rats (2-month). Pressure elevation (150mmHg; 30-minutes) ± RV-NLCs/RV-solution (0.45 µM; 30-minutes) had no effect on 5-HT induced constrictor responses. Elevated pressure (n = 8); elevated pressure + RV-NLC (n = 4); elevated pressure + RV-solution (n = 3). Repeats represent vessels from different animals. Data analysed using a one-way ANOVA followed by a Dunnett's multiple comparison. Data are presented as mean ± SEM.*

6.1.2 RV-NLCs restore the magnitude of dilation following acute pressure elevation

The influence of RV-NLCs on the magnitude of dilator responses following acute pressure elevation was examined. Acute pressure elevation (150mmHg; 30-minutes) followed by incubation with 0.45 μM RV-NLCs resulted in significant improvement in endothelium-dependent (ACh; 10^{-9} – 10^{-3} M) dilation in comparison to incubation in PSS alone ($P = < 0.0001$). Similar responses were observed following incubation with a 0.45 μM RV-solution ($P = < 0.0001$). In order to define the respective contributions of the entrapped RV and surrounding lipid capsule, vessels were incubated with blank-NLCs. Acute pressure elevation followed by incubation with 0.45 μM blank-NLCs had no overall effect on attenuated dilator responses (Figure 6.2A).

A significant shift in $LogEC_{50}$ values were observed between initial RV-NLC and RV-solution responses, with mean values of 4.73 x 10^{-7} M (0.47 μM) and 1.16 x 10^{-7} M (0.16 μM), respectively ($P = < 0.0001$; Figure 6.2B). Sustained dilator responses were reduced for both RV-NLCs and RV-solution, one-hour post-incubation when compared to initial responses. Blank NLCs had no effect on sustained dilator responses, with results comparable to control. Endothelium-dependent responses were significantly higher following RV-NLC incubation, in comparison to RV-solution, but not significantly different from control ($P = < 0.0001$; Figure 6.2C). A significant rightward shift in $LogEC_{50}$ values was observed, with RV-NLCs displaying increased potency in comparison to RV-solution, with values of 1.13 x 10^{-6} M (1.13 μM) and 5.33 x 10^{-6} M (5.33 μM), respectively ($P = < 0.01$; Figure 6.2D).

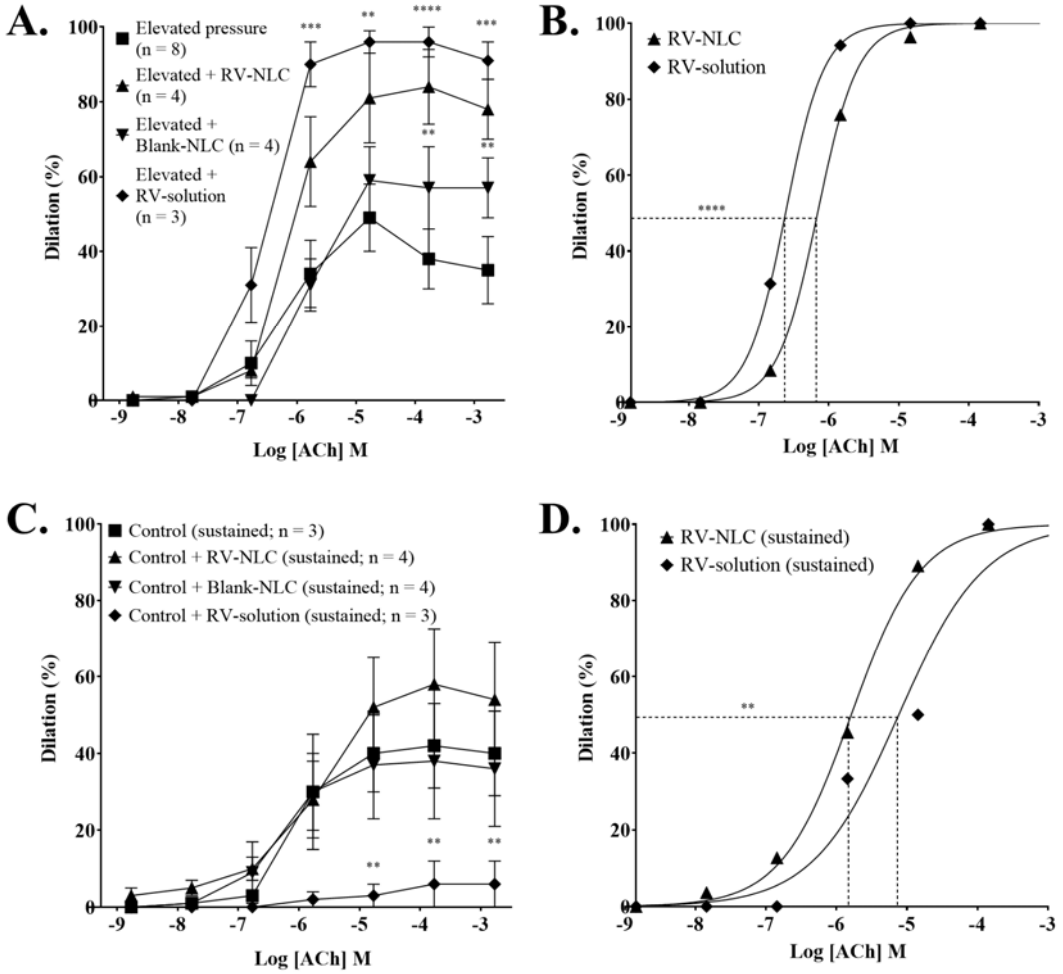

Figure 6.2. Effect of RV-NLCs on initial and sustained dilator responses to ACh. *The influence of resveratrol-loaded nanostructured lipid carriers (RV-NLCs; 0.45 μM; 30-minutes) on initial and sustained endothelial-dependent acetylcholine (ACh) induced dilator responses in the coronary arteries of young Wistar rats (2-month) following acute pressure elevation (150mmHg; 30-minutes). (A) RV-NLCs and RV-solution (0.45 μM; 30-minutes) significantly improved attenuated dilation (P = < 0.0001 and P = < 0.0001, respectively), whereas Blank-NLCs (0.45 μM; 30-minutes) had no effect. (B) A significant shift in LogEC$_{50}$ values was observed between responses to RV-NLCs and RV-solution, with mean values of 4.73 x 10^{-7} M (0.47 μM) and 1.64 x 10^{-7} M (0.16 μM) respectively (P = < 0.0001). (C) Sustained dilator responses of RV-NLCs and Blank-NLCs were maintained to comparable levels as control tissue, in comparison to RV-solution (P = < 0.0001). (D) A significant shift in LogEC$_{50}$ values were observed between sustained responses to RV-NLCs and RV-solution, with mean values of 1.13 x 10^{-6} M (1.13 μM) and 5.33 x 10^{-6} M (5.33 μM), respectively (P = < 0.01). Elevated pressure (n = 8); elevated pressure + RV-NLC (n = 4); elevated pressure + Blank-NLC (n = 4); elevated pressure + RV-solution (n = 3); control (sustained; n = 3); control + RV-NLC (sustained; n = 4); control + Blank-NLC (sustained; n = 5); control + RV-solution (sustained; n = 3). Repeats represent vessels from different animals. Dilator responses analysed using a two-*

*way ANOVA followed by Tukey's multiple comparisons. $LogEC_{50}$ values calculated by normalising, transforming and plotting data using a nonlinear regression model; $LogEC_{50}$ values were compared using an extra-sum-of-squares F test. Data are presented as mean ± SEM.** P < 0.01. *** P < 0.001. **** P < 0.0001.*

Initial and sustained $LogEC_{50}$ values for RV-NLC and RV-solution responses were independently assessed. RV-NLCs and RV-solution each observed significant reductions in potency over time, with $LogEC_{50}$ values of RV-NLCs shifting from 4.73×10^{-7} M (0.47 μM) to 1.13×10^{-6} M (1.13 μM; $P = < 0.05$; Figure 6.3A); and RV-solution from 1.64×10^{-7} M (0.16 μM) to 5.33×10^{-6} M (5.33 μM), respectively ($P = < 0.0001$; Figure 6.3B).

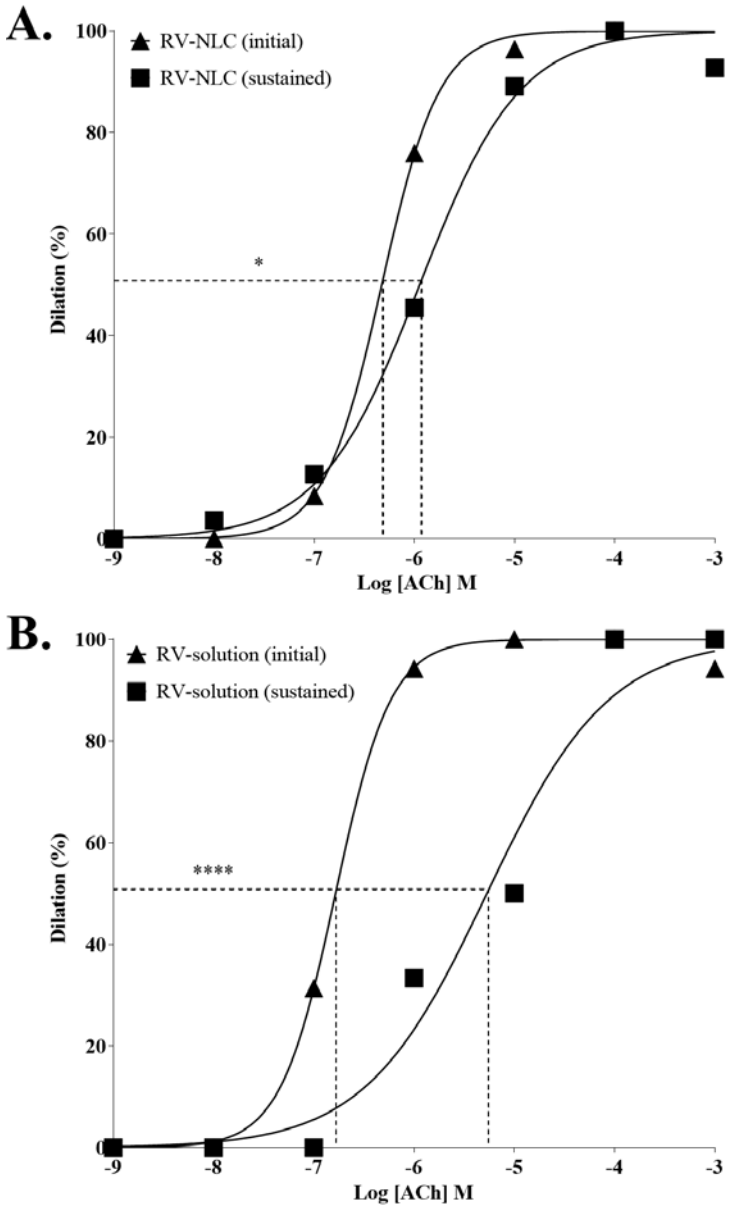

Figure 6.3. Comparison of initial and sustained potency effects of the RV-NLCs and RV-solution. *The effect of resveratrol (RV) loading within nanolipid carriers (NLCs) on the maintenance of potency. (A) The potency (LogEC$_{50}$) of the RV-NLCs was assessed by comparing initial and sustained responses. A significant shift in LogEC$_{50}$ values was observed between initial and sustained RV-NLC responses, with mean values of 4.73 x 10^{-7} M (0.47 µM) and 1.13 x 10^{-6} M (1.13 µM), respectively (P = < 0.05). (B) A significant shift in LogEC$_{50}$ values was observed between initial and sustained RV-solution responses, with mean values of 1.64 x 10^{-7} M (0.16 µM) and 5.33 x 10^{-6} M (5.33 µM) respectively (P = < 0.0001). LogEC$_{50}$ values calculated by normalising, transforming and plotting data using a nonlinear regression model; LogEC$_{50}$ values were compared using an extra-sum-of-squares F test. * P < 0.05. **** P < 0.0001.*

6.1.3 RV-NLCs restore dilation via NO and COX following elevated pressure, mediated via AMPK.

To define the dilator pathways that RV-NLCs may be stimulating to potentiate endothelial-dependent dilation, inhibition studies were carried out in the presence of RV-NLCs (0.45 μM). Incubation with L-NNA (100 μM) resulted in significant attenuation of dilation (P = < 0.0001; Figure 6.4A). Similarly, co-incubation of vessels with indomethacin (10 μM) resulted in a significant attenuation of dilation (P = < 0.01; Figure 6.4B). Incubation with apamin (100 nM) and TRAM-34 (1 μM) had no influence on dilation, suggesting the RV-NLCs may be acting via EDHF independent mechanisms (Figure 6.4C). L-NNA, apamin, TRAM-34 and indomethacin resulted in a further reduction of the dilator component (P = < 0.0001; Figure 6.4D). Co-incubation with dorsomorphin (AMPK inhibitor; 20 μM) led to a significant reduction in dilation (P = < 0.001), resulting in a dilator capacity similar to that observed following acute pressure elevation, without intervention (Figure 6.4E). In contrast, incubation with EX-527 (SIRT-1 inhibitor; 10 μM) did not influence dilator responses (Figure 6.4F). Denudation resulted in the complete abolishment of dilation, confirming that RV-NLCs potentiate dilation via endothelial-dependent mechanisms (P = < 0.0001; Figure 6.4G).

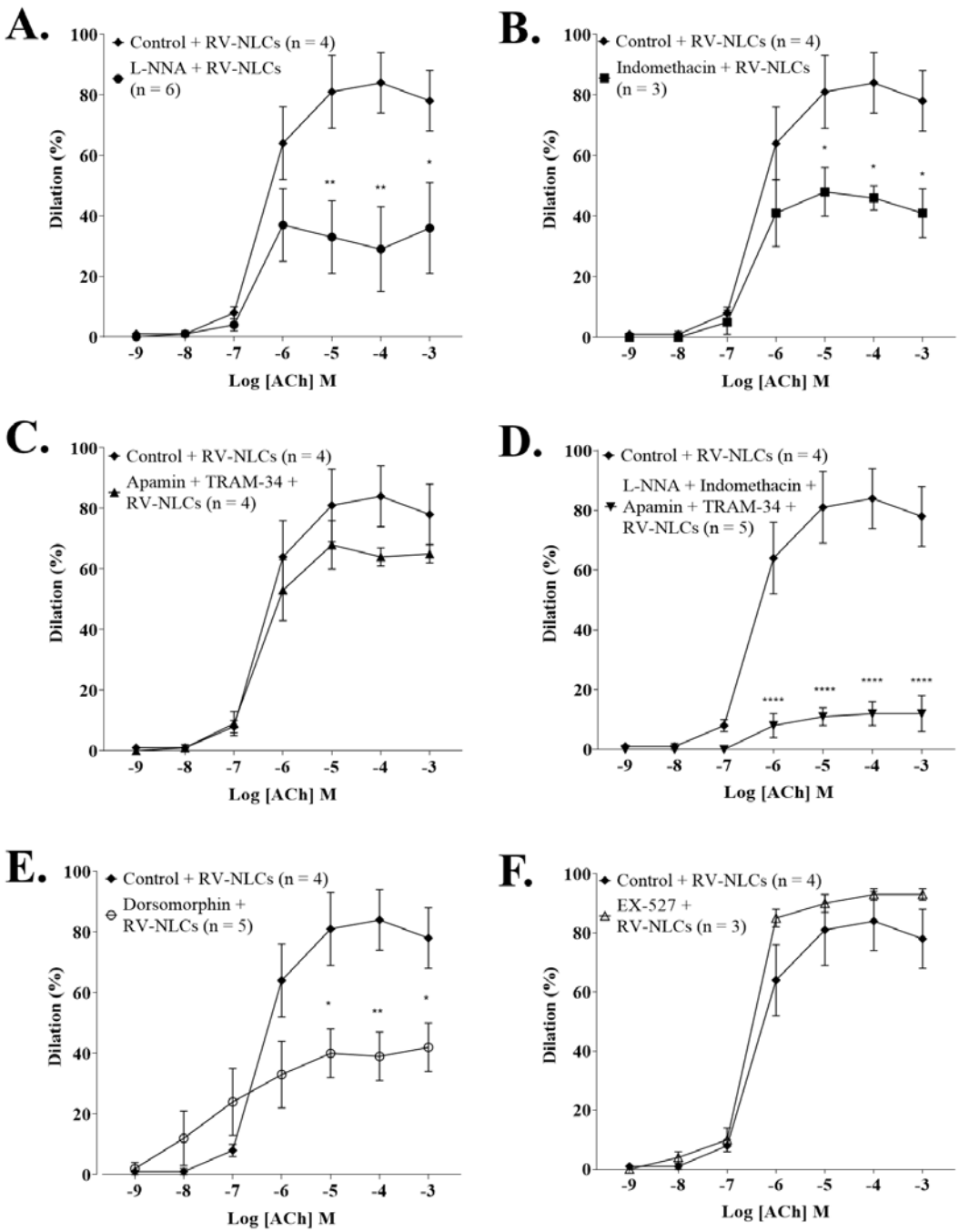
A.
Control + RV-NLCs (n = 4)
L-NNA + RV-NLCs (n = 6)
Dilation (%)
Log [ACh] M
B.
Control + RV-NLCs (n = 4)
Indomethacin + RV-NLCs (n = 3)
Dilation (%)
Log [ACh] M
C.
Control + RV-NLCs (n = 4)
Apamin + TRAM-34 + RV-NLCs (n = 4)
Dilation (%)
Log [ACh] M
D.
Control + RV-NLCs (n = 4)
L-NNA + Indomethacin + Apamin + TRAM-34 + RV-NLCs (n = 5)
Dilation (%)
Log [ACh] M
E.
Control + RV-NLCs (n = 4)
Dorsomorphin + RV-NLCs (n = 5)
Dilation (%)
Log [ACh] M
F.
Control + RV-NLCs (n = 4)
EX-527 + RV-NLCs (n = 3)
Dilation (%)
Log [ACh] M

Continued…

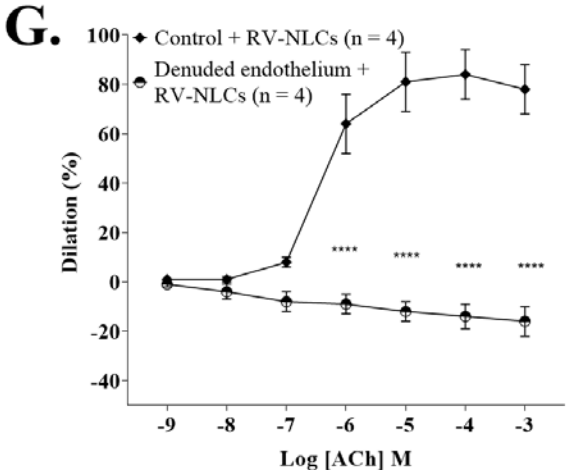

Figure 6.4. Characterisation of the dilator response to ACh following acute pressure elevation in the presence of RV-NLCs. *The influence of the inhibitors NΩ-nitro-L-arginine (A; 100 µM; n = 6), indomethacin (B; 10 µM; n = 3), apamin (100 nM) and TRAM-34 (C; 1 µM; n = 4), L-NNA, indomethacin, apamin and TRAM-34 (D; n = 5), dorsomorphin (E; 20 µM; n = 5), and EX-527 (F; 10 µM; n = 3) on endothelial-dependent acetylcholine (ACh) induced dilator responses in the coronary arteries of young Wistar rats (2-month) following elevated pressure (150mmHg; 30-minutes) and incubation with resveratrol-loaded nanostructured lipid carriers (RV-NLCs; 0.45uM; 30-minutes). Incubation with L-NNA or indomethacin resulted in significant attenuation (P = < 0.0001 and P = < 0.01, respectively). Incubation with apamin and TRAM-34 had no influence on dilator responses. Co-incubation of vessels with L-NNA, indomethacin, apamin and TRAM-34 resulted in attenuated dilation (P = < 0.0001). Incubation with dorsomorphin resulted in attenuated dilation (P = < 0.001), whilst EX-527 had no effect. Endothelial denudation resulted in loss of the dilator component (P = < 0.0001), (G; n = 4). Repeats represent vessels from different animals. Data analysed using a two-way ANOVA followed by Tukey's multiple comparisons. Data are presented as mean ± SEM.* P < 0.05. ** P < 0.01. **** P < 0.0001.*

6.1.4 Endothelial-independent dilator responses to SNP are influenced by RV

Endothelial-independent responses to PAPA were unaffected, with responses comparable to elevated pressure (150mmHg) alone (Figure 6.5A). Responses to SNP were varied, with RV-NLCs or L-NNA, apamin, TRAM-34 and indomethacin leading to a significant improvement in dilation ($P = < 0.05$; Figure 6.5B).

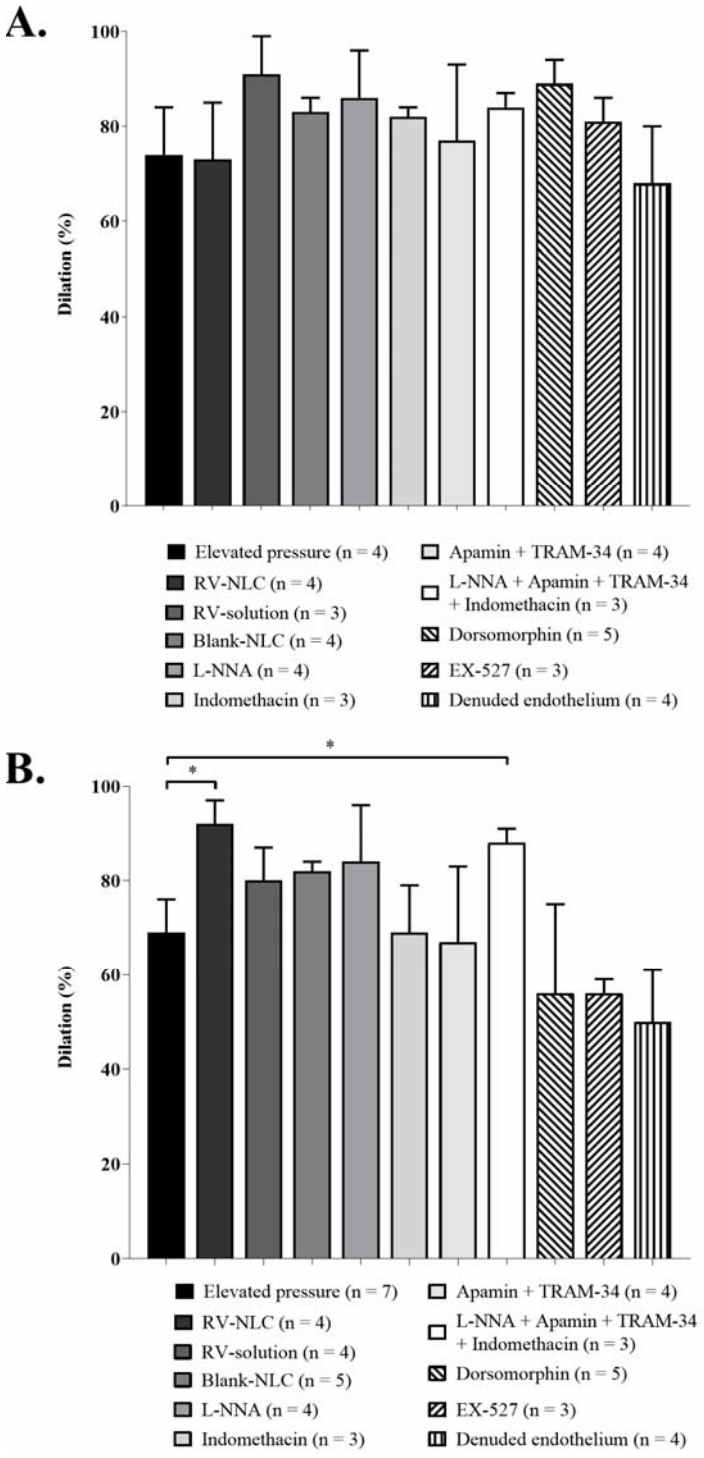

Figure 6.5. Effect of treatment on the dilator response to PAPA and SNP. *Endothelial-independent papaverine (PAPA) and sodium nitroprusside (SNP) induced dilator responses in the coronary arteries of young Wistar rats (2-month) following elevated pressure (150mmHg; 30-minutes). Treatment had no effect on PAPA (A; 100 μM) induced dilator responses. RV-NLCs and L-NNA + apamin + TRAM-34 + indomethacin significantly improved SNP (B; 100 μM) induced dilator responses (P < 0.05 and P <*

*0.05, respectively; B). Elevated pressure (n = 4/7, respectively); RV-NLC (n = 4); RV-solution (n = 3/4, respectively); blank-NLC (n = 4/5, respectively); L-NNA (n = 4); indomethacin (n = 3); apamin + TRAM-34 (n = 4); L-NNA + apamin + TRAM-34 + indomethacin (n = 5); dorsomorphin (n = 5); EX-527 (n = 3); denuded endothelium (n = 4). Repeats represent vessels from different animals. One way-ANOVA followed by Dunnett's comparison. Data are presented as mean ± SEM. * P < 0.05.*

6.2 Discussion

6.2.1 RV-NLCs restore the magnitude of dilation following acute pressure elevation

RV-NLCs significantly improved the attenuated dilation after acute pressure elevation, to a similar magnitude as that following SOD treatment (see previous chapter). These findings are maybe attributable to RV's antioxidant properties (Burns et al., 2002), replicating the role of endogenous enzymes by scavenging a range of ROS moieties (Leonard et al., 2003; Iuga et al., 2012). In addition to its direct antioxidant ability, RV has been associated with the activation and upregulation of several molecular targets involved in the prorogation of dilation and regulation of basal antioxidant activity including eNOS, SOD, CAT, and nuclear factor erythroid 2-related factor 2 (Nrf2) (Thomas et al., 2002; Sayin et al., 2012; Xia et al., 2017). However, due to the limited/short incubation period in the present study, it is unlikely that the observed effects relate to the upregulation of antioxidant genes, but maybe attributable to post-translational modification, e.g. increased phosphorylation of eNOS. Consistent with liposomes and solid lipid nanoparticles, encapsulation of content within NLCs has been associated with enhanced stability and protection from metabolic degradation (Cirri et al., 2018). In order to assess this, the non-encapsulated RV-solution was used for comparison. Although RV-solution displayed increased efficacy and magnitude of dilation, likely attributable to superior diffusion kinetics over time in comparison to RV-NLCs, sustained responses were significantly less than that induced by RV-NLCs, with a nearly 5-fold improvement in potency demonstrated by the RV-NLCs (as shown by the $LogEC_{50}$ data). A comparative examination of initial and sustained responses (i.e. RV-NLC initial vs RV-NLC sustained) from each treatment allowed the assessment of treatment potency as a measure of time. Incubation with RV-NLCs over the one-hour test period resulted in a

2.4-fold reduction in potency, in comparison to the much larger 32-fold reduction demonstrated by RV-solution; confirming the ability of NLCs to successfully entrap and release RV over sustained time-periods. This is consistent with previous findings, whereby studies have demonstrated NLCs increase the bioavailability of poorly soluble antihypertensive drugs (Cirri et al., 2018; Son et al., 2019) and vasoprotective nutraceutical products such as RV (Magyar et al., 2012; Theodotou et al., 2017), protecting it from rapid metabolism, whilst also allowing fine manipulation of release kinetics (Burns et al., 2002; Teskac and Kristl, 2010; Neves et al., 2013; Khan et al., 2018).

The reduced potency of RV-solution in comparison to RV-NLCs may be attributable to RV's degradation. This is supported by previous observations in the Azzawi laboratory whereby the concentration of RV was reduced by 27 % one-hour after circulation in the *ex vivo* pressure myography setup (Diaz et al., 2019). This may partially be due to the high sensitivity of RV to photochemical and photocatalytic degradation, leading to UV light-induced *trans*-*cis* isomerization (Silva et al., 2013); with *cis*-RV having been shown to have reduced stability and potency in comparison to its *trans*- counterpart. Lipid encapsulation, on the other hand, has been found to stabilise contents, reducing the effects of UV-damage (Bandak et al., 1999; Tursilli et al., 2006). Additionally, the degradation of RV has been shown to produce several ill-investigated breakdown products, including aldehydes and carboxylic acids; many of which are highly toxic and may accumulate resulting in modulation of vascular activity (Bader et al., 2008). These may account for the loss of sustained dilator response observed following incubation with the RV-solution, as opposed to RV-NLCs; releasing contents over a prolonged period, mitigating any detrimental effects.

In addition to the documented benefits of RV, exposure to exogenous lipid has been found to promote vascular function in several tissue beds. The generation of endothelium-dependent vasodilator substance following lipid exposure has been demonstrated via NO and EDHF generation in conduit and resistance size arteries, respectively (Ruisanchez et al., 2014; Limbu et al., 2018). Replacement of oxidised phospholipids via incorporation/integration of the lipid carrier, as well as usage of catabolised products (e.g. ATP) may potentially restore aberrant membrane functionality. In order to assess whether constituent components of the phospholipid-capsule may contribute to improved dilation, vessels were incubated with blank-NLCs. Co-incubation with blank-NLCs did not improve initial or sustained responses, confirming the restorative effects were attributable to RV. Potentially, the lack of apparent benefit observed following blank-NLC administration may be due to the specificity of lipids involved, their relative concentrations and overall ratios. Thus, the results of the present study support the notion that encapsulation of RV leads to increased potency in the coronary artery over sustained periods of time, and encapsulation protects from degradation when compared to RV-solution alone.

6.2.2 RV-NLCs restore dilation via NO and COX following elevated pressure, mediated via AMPK.

In the present study, dilator pathway inhibition studies suggest that RV-NLCs can potentiate dilation (after acute pressure elevation) by modulating the NO and COX pathways. Potentiation of the NO pathway has been extensively reported across several species and vascular beds, including the coronary artery (Naderali et al., 2000; El-Mowafy, 2002; Rakici et al., 2005; Li et al., 2006). In contrast, the influence on

indomethacin-sensitive prostaglandins are sparse. Previous studies using human internal mammary arteries and guinea pig uterine arteries, suggest that RV may reduce levels of vasoconstrictor prostaglandins (PGH_2 and TXA_2) (Naderali et al., 2000; Rakici et al., 2005). In porcine coronary arteries, however, indomethacin did not influence RV-mediated dilation (Li et al., 2006). In the latter study, vessels were pre-incubated with indomethacin for only 20-minutes, suggesting insufficient inhibition (> 45-minutes utilised in our study and others). It is also likely that the influence of vasoconstrictor prostanoids on vascular reactivity in response to RV is tissue-dependent and requires further investigation.

The vasodilator component induced by RV-NLCs after acute pressure elevation was not influenced by incubation with apamin and TRAM-34, suggesting that RV has a minimal effect on the EDH pathway. In the murine femoral artery exposed to normal pressure, RV potentiated dilation via NO and EDHF (Diaz et al., 2019). Also, a study characterising the dilator component of the porcine coronary artery following administration of red wine polyphenols identified EDHF as a primary contributor to dilation alongside NO, whereby inhibiting channels associated with potassium entry significantly attenuated responses (Dell'Agli et al., 2004). These findings suggest that RV's mechanism of potentiated dilation may differ, following normal or elevated pressure, given that ROS has previously been shown to inactivate potassium channels (hence EDH responses) (Brzezinska et al., 2000; Yanping et al., 2002). Following incubation with all four inhibitors in the presence of RV-NLCs, a small dilator component remained. Consistent with previously noted observations during the characterisation of the *ex vivo* model, this residual dilation may be attributable to TRPV4 activation.

In order to investigate the mechanisms involved in RV-NLC mediated dilator responses, further inhibition studies were carried out. RV has been associated with the activation of several cell surface receptors, and is widely thought to convey its beneficial characteristics via the activation/upregulation of SIRT-1 and/or AMPK (Schmitt et al., 2010). However, NLCs are capable of being endocytosed into cells and releasing RV into the cytosol, thus, it was of interest to assess whether RV delivery via NLCs, potentiated dilation via an alternate mechanism. Incubation with dorsomorphin resulted in a partial reduction in dilation, suggesting a limited involvement of AMPK in mediating the effects of RV. In contrast, co-incubation with the SIRT-1 inhibitor EX-527 did not influence dilator responses, suggesting the absent participation of SIRT-1 in RV-mediated dilation. These data contrast previous findings which have attributed the effects of RV to SIRT-1; however, *in vitro* studies in which the effects of SIRT-1 have been observed in the coronary artery are often performed following several days/weeks' exposure to agonistic stimulus and/or treatment with RV, which is likely to modulate SIRT-1/AMPK activity. Finally, there is considerable variability in the experimental concentrations used; with AMPK activation being found to be cell-type and concentration-dependent (Lan et al., 2017). Interestingly, AMPK is known to be an upstream signalling mediator of COX-2, with the capacity to regulate its function (Hou et al., 2008). Inhibition of AMPK resulted in observations consistent with those using indomethacin, whereby inhibition of COX resulted in attenuated dilation. However, indomethacin is a non-selective COX inhibitor, and it has a preferential affinity for COX-1. Our data show that endothelial denudation abolished the vasodilation induced by RV, after acute pressure elevation, and promoted constriction, ascribed to the binding of ACh to the muscarinic acetylcholine receptors (M_3) present in smooth muscle cells; suggesting that RV-NLCs exert an endothelial-dependent response. Although previous studies have

examined the contribution of the endothelium in RV-mediated responses, the effects of endothelial-denudation on RV-induced dilation has been inconsistently reported. Some studies observed partial or complete endothelial dependency in the coronary artery and aorta under normotensive pressure (El-Mowafy, 2002; Li et al., 2006), respectively, whereas a shifting from partial endothelium-dependent to complete endothelium-independent was reported in rat mesenteric arteries following dietary-induced obesity or humans with coronary artery disease (Naderali et al., 2001; Cruz et al., 2006). It appears that the role of the endothelium in RV-induced dilation depends on the tissue, species, and perhaps disease states.

6.2.3 Endothelial-independent dilator responses to SNP are influenced by RV

Interestingly, RV-NLCs significantly improved SNP mediated dilation. The lack of endothelial-dependent dilator response following denudation, and improved dilation in the presence of a NO donating agent (simulating endothelial-dependent responses) suggest RV-NLCs may increase SMC sensitivity to NO.

6.3 Chapter summary

The experiments performed in this part of the study aimed to assess the potential of RV loaded within NLCs to restore dilator responses in an *ex vivo* model of acute hypertension. Using this model, RV-NLCs demonstrated the ability to restore and potentiate attenuated dilator responses to comparable levels as that observed by endogenous antioxidants (e.g. SOD), highlighting their successful delivery into tissues and antioxidant capacity in the coronary vasculature. These responses were sustained over a more prolonged period, in

comparison to a RV-solution alone; confirming the ability of NLCs to protect internalised contents. Through inhibition studies, RV-NLCs were found to potentiate dilation via the modulation of NO and COX pathways, partially mediated by AMPK; as opposed to the conventionally accepted SIRT-1. In the following chapter, an investigation of the effects of RV-NLCs in the cerebral vasculature will be described.

Chapter 7: The influence of organic nanoparticles on cerebral artery function

In the preceding chapter, RV-loaded NLCs successfully demonstrated their capacity to restore attenuated dilator responses in the coronary artery; however, differential receptivity to EDRF might not make these findings applicable across vascular beds. Using the same *ex vivo* model of hypertension described, the objective of this study was to assess the use of antioxidant-loaded organic nanoparticles in the cerebral vasculature. The hypothesis of this study is that RV-NLCs and TMS-liposomes will restore attenuated endothelial-dependent dilator responses of cerebral arteries after acute pressure elevation. This hypothesis will be addressed through the following specific objective:

- Determine whether RV-NLCs and TMS-liposomes have the capacity to restore attenuated dilation following acute pressure elevation.

First-order middle cerebral arteries were excised and mounted on a pressure myograph system. Endothelial-dependent and independent responses were assessed following acute pressure elevation in the presence of organic nanoparticles (as described in the previous chapter). Additionally, TMS-liposomes were supplied by our collaborators from the University of Manchester (Dr. Harris, UoM); potentially offering improved uptake efficiency in the cerebral vasculature due to functionalisation with a brain targeting peptide, compared to RV-NLCs. They were prepared using a thin film process and characterised in the present study using the same analytical techniques described in chapters 3 and 4.

7.1 Results

7.1.1 Control responses

Coronary vessels were isolated and exposed to pressure at 60mmHg for 30-minutes. The viability of vessels was assessed by ascertaining initial responses to KPSS. All vessels (resting diameter = 187 ± 9 µm; n = 10) constricted to high potassium, confirming the viability of vessels (KCl, 60 mM; 47 ± 9 %; n = 10). Pressure elevation (150mmHg; 30-minutes) ± RV-NLCs (0.45 µM) had no effect on 5-HT-mediated constriction compared to vessels subjected to pressure elevation alone (maximal constriction: 66 ± 6 % and 75 ± 8 %, respectively; 10^{-7} M; Figure 7.1).

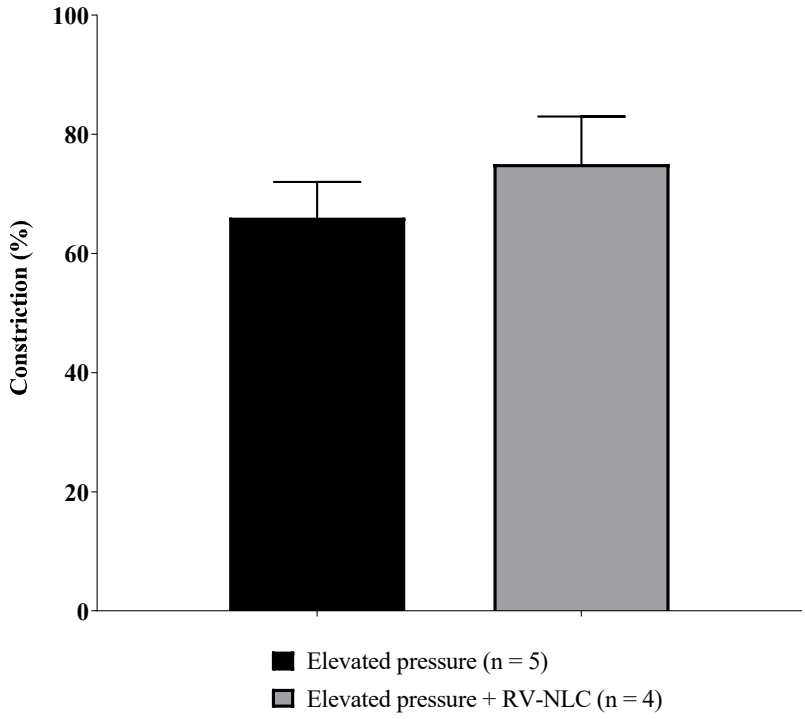

Figure 7.1. Effect of RV-NLCs on the constrictor response to 5-HT in cerebral arteries. *Serotonin (5-HT; sub-maximal; 10^{-7} M) induced constrictor responses in the cerebral arteries of young Wistar rats (2-month). Pressure elevation (150mmHg; 30-minutes) ± RV-NLCs (0.45 µM; 30-minutes) had no effect on 5-HT induced constrictor responses. Elevated pressure (n = 5); elevated pressure + RV-NLCs (n = 4). Repeats represent vessels from different animals. Data analysed using an unpaired t-test. Data are presented as mean ± SEM.*

7.1.2 RV-NLCs do not restore attenuated dilation following acute pressure elevation

The influence of RV-NLCs on the magnitude of dilator responses following acute pressure elevation was examined. Acute pressure elevation (150mmHg; 30-minutes) followed by incubation with 0.45 μM RV-NLCs had no effect on attenuated dilator responses (Figure 7.2).

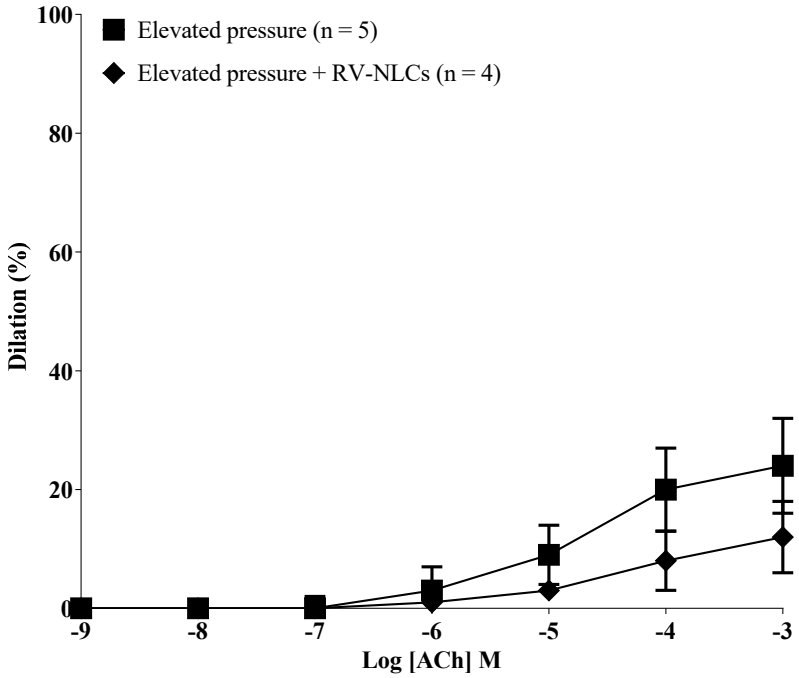

Figure 7.2. Effect of RV-NLCs on the dilator response to ACh. *Endothelial-dependent acetylcholine (ACh) induced dilator responses in the cerebral arteries of young Wistar rats (2-month) following elevated pressure (150mmHg; 30-minutes). RV-NLCs (0.45 μM; 30-minutes) had no effect on attenuated dilator responses. Elevated pressure (n = 5); elevated pressure + RV-NLCs (n = 4). Repeats represent vessels from different animals. Data analysed by a two-way ANOVA followed by Tukey's multiple comparison. Data are presented as mean ± SEM.*

7.1.3 Control responses

The viability of vessels was assessed by ascertaining initial responses to KPSS. All vessels (resting diameter = 169 ± 12 µm; n = 11) constricted to high potassium, confirming the viability of vessels (KCl, 60 mM; 48 ± 7 %; n = 15). Pressure elevation (150mmHg; 30-minutes) ± TMS-liposomes/solution (1 nM and 10 nM, respectively) had no effect on 5-HT-mediated constriction (10^{-7} M; Figure 7.3).

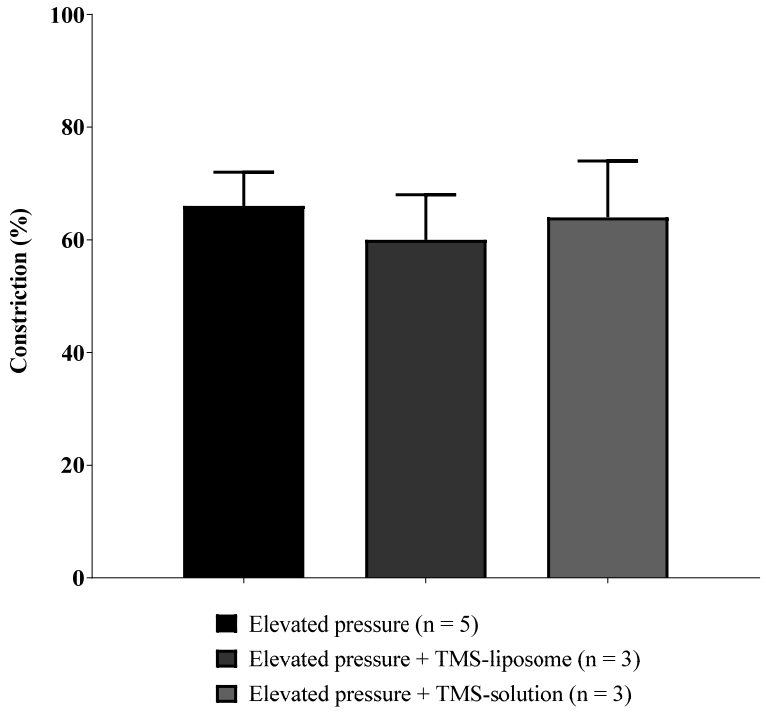

Figure 7.3. Effect of treatment on the constrictor response to 5-HT. *Serotonin (5-HT; sub-maximal; 10^{-7} M) induced constrictor responses in the cerebral arteries of young Wistar rats (2-month) following elevated pressure (150mmHg; 30-minutes). Elevated pressure ± TMS-liposomes/solution (1 nM and 10 nM, respectively; 30-minutes) had no effect on 5-HT induced constrictor responses. Elevated pressure (n = 5); elevated pressure + TMS-liposome (n = 3); elevated pressure + TMS-solution (n = 3). Repeats represent vessels from different animals. One way-ANOVA followed by Dunnett's comparison. Data are presented as mean ± SEM.*

7.1.4 TMS-liposomes do not restore attenuated dilation following acute pressure elevation

The influence of TMS-liposomes and TMS-solution on the magnitude of dilator responses following acute pressure elevation was examined. Acute pressure elevation (150mmHg; 30-minutes) followed by incubation with TMS-liposomes (1 nM, Figure 7.4A) or TMS-solution (10 nM; Figure 7.4B) had no effect on attenuated dilator responses.

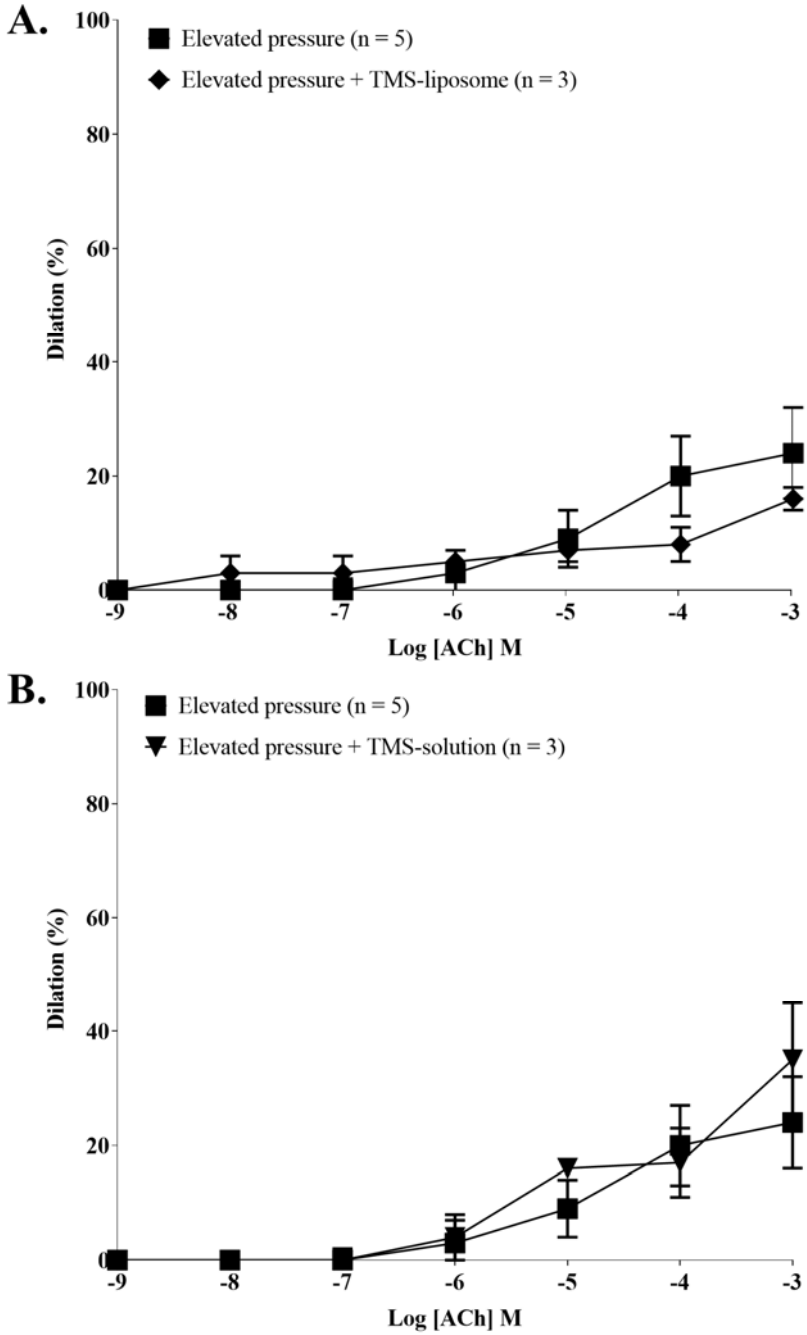

Figure 7.4. Effect of TMS-liposomes on the dilator response to ACh. *Endothelial-dependent acetylcholine (ACh) induced dilator responses in the cerebral arteries of young Wistar rats (2-month) following elevated pressure (150mmHg; 30-minutes). TMS-liposomes (A; 1 nM) and TMS-solution (B; 10 nM) had no effect on attenuated dilator responses after 30-minutes incubation. Elevated pressure (n = 5); elevated pressure + TMS-liposome (n = 3); TMS-solution (n = 3). Repeats represent vessels from different animals. Data analysed by a two-way ANOVA followed by Tukey's multiple comparison. Data are presented as mean ± SEM.*

7.1.5 RV-NLCs attenuate endothelial-independent SNP responses, but are unaffected by TMS-liposomes

Endothelium-independent responses to PAPA (100 μM) remained unchanged, despite RV-NLCs (0.45 μM) showing a tendency for reduction (Figure 7.5A). In contrast, SNP (100 μM) responses were varied (Figure 7.5B). Co-incubation with RV-NLCs resulted in significantly attenuated SNP responses ($P = < 0.0001$). SNP responses following incubation with TMS-liposomes (1 nM) and TMS-solution (10 nM) were significantly higher in comparison to RV-NLCs, respectively ($P = < 0.001$).

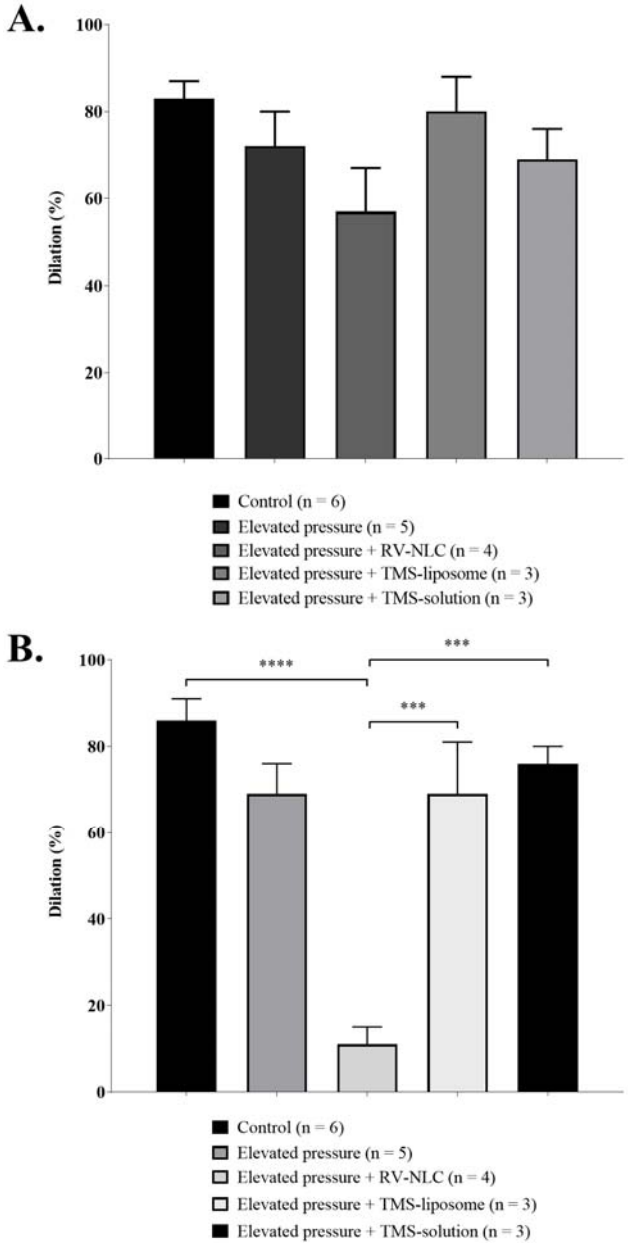

Figure 7.5. Effect of treatment on the dilator response to PAPA and SNP. *Endothelial-independent papaverine (PAPA) and sodium nitroprusside (SNP) induced dilator responses in the cerebral arteries of young Wistar rats (2-month) following elevated pressure (150mmHg; 30-minutes). (A) Treatment had no effect on PAPA (100 µM) induced dilator responses. (B) RV-NLCs significantly attenuated SNP (100 µM) induced dilator responses (P = < 0.0001); dilator responses were unaffected following incubation with TMS-liposomes or TMS-solution, and significantly higher compared to RV-NLCs (P = < 0.001). Control (n = 6); elevated pressure (n = 5); elevated pressure + RV-NLC (n = 4); elevated pressure + TMS-liposome (n = 3); elevated pressure + TMS-solution (n = 3). Repeats represent vessels from different animals. One way-ANOVA followed by Tukey's multiple comparison. Data are presented as mean ± SEM. *** P < 0.001. **** P < 0.0001.*

7.2 Discussion

7.2.1 RV-NLCs do not restore attenuated dilation following acute pressure elevation in cerebral arteries

Whilst the effects of RV-solution were not assessed in this study due to the limited availability of tissue, the effects of RV on the cerebral vasculature has been extensively studied, with RV having been shown to be effective at improving impaired cerebral function across a range of *in vivo* disease models (diabetes, focal ischemia, hypertension-induced oxidative stress) and species (Sinha et al., 2002; Toth et al., 2015; Wong et al., 2016; Xu et al., 2018). Furthermore, NLCs are considered to be promising delivery mechanisms for the treatment of cerebrovascular dysfunction, owing to their lipophilicity and ability to enter the cerebral vasculature *in vivo* (Fang et al., 2012). These findings differ significantly from our own observations, whereby RV-NLCs were incapable of restoring attenuated dilator responses after acute pressure elevation, with responses comparable to that of control tissue. One potential variable that may account for these observations is the length of exposure. In contrast to the acute exposure (30-minutes) utilised in our studies, these studies have focused on chronic exposure to RV over days or weeks, whereby RV has been associated with the activation and upregulation of several molecular targets involved in the prorogation of dilation and regulation of basal antioxidant activity.

In order to assess whether the RV or NLC delivery modality may be limiting factors, 2,3',4,5'-tetramethoxystilbene (TMS), a potent RV-derived analogue, was encapsulated within liposomes; tagged with a specific brain peptide which has demonstrated an ability

to cross the blood-brain barrier and bind to cerebral vasculature (Jennings et al., 2014; Urich et al., 2015).

7.2.2 TMS-liposomes do not restore attenuated dilation following acute pressure elevation in cerebral arteries

Previous work in our laboratory has demonstrated the capacity of TMS-liposomes (1 nM) to restore ROS-mediated attenuation of dilator responses in rat aortic vessels *ex vivo*, following 30-minutes incubation (Zaabalawi et al., 2019). In the cerebral arteries, however, responses were unaffected. In order to assess whether the concentration and/or release of drug from the liposomal carrier might be the limiting factor, vessels were incubated with a TMS-solution (10 nM). Previous experiments conducted on the coronary artery (see Chapter 6) demonstrated that exposure to the non-encapsulated drug had greater efficacy than encapsulated counterparts over the one-hour test period, likely attributable to superior diffusion kinetics. However, incubation with TMS-solution had no effect. These findings, in conjunction with information obtained following the characterisation of our cerebral *ex vivo* model (see chapter 5), whereby attenuated dilator responses were not restored following incubation with SOD and CAT; may suggest that ROS generation following acute pressure elevation may be less prevalent in the cerebral architecture, with attenuated endothelial-dependent responses underlined by another, unknown mechanism. One example may be the effect of circumferential stretching (pressure-mediated) on endothelial mechanics; with previous studies demonstrating the detrimental effects of axial stretching, observing actin remodelling which correlated with impaired endothelial-dependent dilation, yet intact endothelial-independent dilation (Sipkema et al., 2003).

7.2.3 RV-NLCs attenuate endothelial-independent SNP responses, but an unaffected by TMS-liposomes

In order to ascertain whether treatment was also affecting the VSMCs, endothelial-independent responses were assessed. Endothelium-independent responses to PAPA were unaffected, suggesting the cAMP pathway remains intact. In contrast, SNP responses were varied. Co-incubation of vessels with RV-NLCs significantly attenuated dilator responses. Despite RV's standing as a promising antioxidant, previous research has demonstrated its ability to induce pro-oxidant effects. One mechanism postulated to account for these observations involves transition metal-mediated oxidation. Transition metals, such as iron and copper (Cu), are unique in their ability actively redox-cycle between reduced and oxidised states (i.e. Cu^{2+}, Cu^{1+}); however, this electron-donating ability can result in the indiscriminate oxidisation of surrounding molecules, generating ROS (Popescu and Nichol, 2011). In the presence of Cu^{2+}, RV has been demonstrated to undergo oxidation; generating phenoxyl radicals capable of propagating the further reduction of Cu^{2+}, inducing DNA damage and cell death (Ahmad et al., 2000). The oxidation likely occurs with surface hydroxyl groups on the benzene scaffold of RV; these observations were confirmed in later studies, whereby the reactivity of *trans*-stilbene (no hydroxyl groups) and RV was compared in the presence of Cu^{2+}. *Trans*-stilbene showed little to no reactivity in comparison to its hydroxylated counterpart (Azmi et al., 2005). Furthermore, copper-mediated oxidation reactions were found to be promoted in the presence of biological chelators and reductants, such as ascorbate (Vidrio et al., 2008).

The brain is a major metal repository and has a high density of transition metals which are integral in maintaining normal function, acting as essential co-factors in regulating a wealth of physiological processes including; gene expression and neurotransmission. The

abundance of transition metals and reductants (i.e. ascorbate (Harrison and May, 2009)) in cerebral tissues are likely to foster a supportive and propagative environment for the oxidation of RV, which in its oxidised state may have the capacity to quench NO; potentially accounting for the impaired SNP-mediated dilator response observed in our study. In contrast to the attenuated dilator response observed following RV-NLC incubation, SNP-mediated dilator responses following incubation with TMS-liposomes and TMS-solution were unremarkable, with responses similar to control; yet significantly improved compared to RV-NLCs. Despite originating from a polyphenolic compound (RV-analogue), it is crucial to note that in TMS, OH groups have been substituted for synthetically conjugated methyl groups. This substitution may account for the vast differences in response observed. Some reactions may be tissue-specific, depending on complex interplay with surrounding environmental factors. Although interaction with methoxy groups are possible, it may be that the cerebral environment is not conducive to such reactions.

7.3 Chapter summary

The experiments performed in this part of the study aimed to assess the influence of RV loaded within NLCs to restore dilator responses in an *ex vivo* model of acute hypertension using cerebral arteries. RV-NLCs were incapable of restoring attenuated responses; furthermore, incubation with TMS, an analogue of higher potency, was also unable to restore responses in solution or following liposomal encapsulation; highlighting tissue bed dependent variability in the vasculature. In conjunction with information from chapter 5, it is conceivable that ROS generation following acute pressure elevation may be less prevalent in the cerebral architecture, with attenuated-endothelial dependant

responses underlined by another, unknown mechanism. Additionally, RV-NLCs appear detrimental to VSMC reactivity, in comparison to the synthetically modified TMS. These studies highlight the need for accurate, in-depth, comparative studies to develop an understanding of tissue-bed and time-specific effects whilst generating novel treatment strategies for clinical use.

Chapter 8: General Discussion and Conclusions

Given the global burden of hypertension, there is an unmet clinical need for alternative/complementary therapy. While RV is promising, it suffers low stability and bioavailability. Encapsulation of RV within nanoparticles may preserve drug stability, resulting in improved bioavailability and clinical outcome. The hypothesis of the present study is that RV (and analogues), delivered via NPs, will enable the restoration of attenuated dilation after acute pressure elevation *ex vivo*, and will provide a more sustained dilator response than the unencapsulated form. NPs (inorganic and organic) were characterised and their antioxidant capacity assessed in solution, within cells and/or isolated vessels using an *ex vivo* model of acute hypertension.

8.1 Cerium oxide modification of SiNPs attenuates their surface reactivity and demonstrates antioxidant capacity, improving their biocompatibility *in vitro*.

SiNPs (inorganic) are considered an attractive delivery modality for drugs in the treatment of CVD; however, oxidative reactivity at the particle surface is associated with attenuated vascular responses that may preclude their use (Corbalan et al., 2012; Ahamed, 2013; Duan et al., 2013a; Farooq et al., 2014b). The work reported in this thesis demonstrates that functionalisation of SiNPs with CeO_2 (with its unique redox cycling activity) provides a means of attenuating surface reactivity and promoting antioxidant capacity, resulting in heightened biocompatibility *in vitro*. Whilst the effects of CeO_2 functionalised silica have been documented in the context of stability enhancement/*ex vivo* (Farooq et al., 2014b; Munusamy et al., 2014); we are the first to document the physiochemical effects of CeO_2 functionalisation in solution. Whilst deemed unsuitable for further investigation in this thesis, these studies highlight the importance of understanding the fundamental mechanisms underlying the use of nanomaterials, to

promote research into the development of safer, silica-based delivery modalities for the release of drugs.

8.2 Novel RV-NLCs reduce ROS in human coronary artery endothelial cells *in vitro*.

Lipidic delivery systems (organic) are an alternate delivery platform, with noted benefits over inorganic strategies including improved biocompatibility, and the ability to traverse challenging physiological barriers. The findings presented in Chapter 3 demonstrate the potential of novel trimyristin-triolein NLCs to entrap and release RV over sustained periods of time, within an oxidative environment *in vitro*, reducing both cytosolic and mitochondrial $O_2^{\bullet-}$ anion levels. This data is consistent with previous observations, whereby RV-solution reduced mitochondrial $O_2^{\bullet-}$ in HCAECs following hyperglycaemia-induced mitochondrial ROS generation (Ungvari et al., 2009); highlighting the potential of RV-NLCs as an antioxidant in future therapeutic applications. Whilst several studies have documented the effects of RV in solution and in encapsulated forms (e.g. solid lipid nanoparticles) on endothelial viability and oxidative capacity (Leonard et al., 2003; Neves et al., 2016), this study is the first to document the effects of these novel NLCs composed of trimyristin-triolein (which incurs enhanced stability, RV entrapment and uptake) using physiologically relevant HCAECs.

8.3 Acute pressure elevation attenuates endothelial-dependent dilator responses via the activation of NADPH oxidase in isolated arteries

Elevated oxidative stress is a crucial contributor to the pathogenesis of endothelial dysfunction in hypertension (Higashi et al., 2002; Mollnau et al., 2002). Several experimental models have attempted to simulate hypertensive environments *ex vivo*, with studies demonstrating that high pressure itself could lead to the production of oxidative stress in the absence of neurohumoral factors (Ungvari et al., 2003). I have used this *ex vivo*, acute pressure model, throughout this thesis to examine the potential of RV to restore dilator capacity using isolated vessels. The findings presented in Chapter 5 confirm that acute pressure is an appropriate model for replicating the oxidative environment observed in hypertension in the coronary artery, demonstrating that NADPH-oxidase derived $O_2^{\bullet-}$ plays an integral role in attenuating dilator responses, as previously described in femoral and aortic arteries (Ungvari et al., 2003, 2004). In addition, inhibition studies identified NO as the principal dilator component, under elevated pressure, despite the presence of elevated $O_2^{\bullet-}$, which usually quenches NO. The role of NO as a key vasodilator in hypertension has also been confirmed by studies demonstrating that agonist-induced dilation of pre-constricted vessels is reduced or eliminated by inhibitors of eNOS in isolated coronary vessels from hypertensive human and murine models (Pourageaud and Freslon, 1995; Quyyumi et al., 1995). In contrast to findings in coronary arteries, notable ROS moieties such as $O_2^{\bullet-}$ and H_2O_2 do not appear to contribute to attenuated endothelial-dependent dilator responses in cerebral arteries; highlighting the disparity between potential mechanisms of action between tissue beds. These studies are integral in understanding and interpreting functional responses in the vasculature in disease states and developing appropriate treatment strategies.

8.4 RV-NLCs restore the magnitude of dilation via NO following acute pressure elevation, mediated via AMPK.

A number of studies have shown that polyphenols such as RV and its analogues have antioxidant potential but are hindered by poor bioavailability (Cottart et al., 2010; Chachay et al., 2014; van der Made et al., 2015; Zortea et al., 2016). The findings from Chapter 6 confirmed the ability of RV loaded within NLCs to restore dilator responses in the *ex vivo* model of acute hypertension. Using this model, RV-NLCs restored and potentiated attenuated dilator responses to comparable levels as that observed by endogenous antioxidants (e.g. SOD), highlighting their successful delivery into tissues and antioxidant capacity in the coronary vasculature. These responses were sustained over a more prolonged period, in comparison to RV-solution alone; confirming the ability of NLCs to protect encapsulated content. Through inhibition studies, RV-NLCs were found to potentiate dilation via the modulation of NO and COX pathways, partially mediated by AMPK; as opposed to the conventionally accepted SIRT-1 pathway (Figure 8.1) (Ma et al., 2017). Whilst studies have investigated the use of NLC-encapsulated RV; to our knowledge, this is the first time that novel trimystrin-trioleate NLCs have been used for the delivery of RV into the vasculature using pressure myography. Thus, differences in mode of delivery and uptake of RV may reflect different regulatory pathways and have implications on treatment efficacy and outcome. These findings have important implications for the future design and implementation of anti-hypertensive treatment strategies.

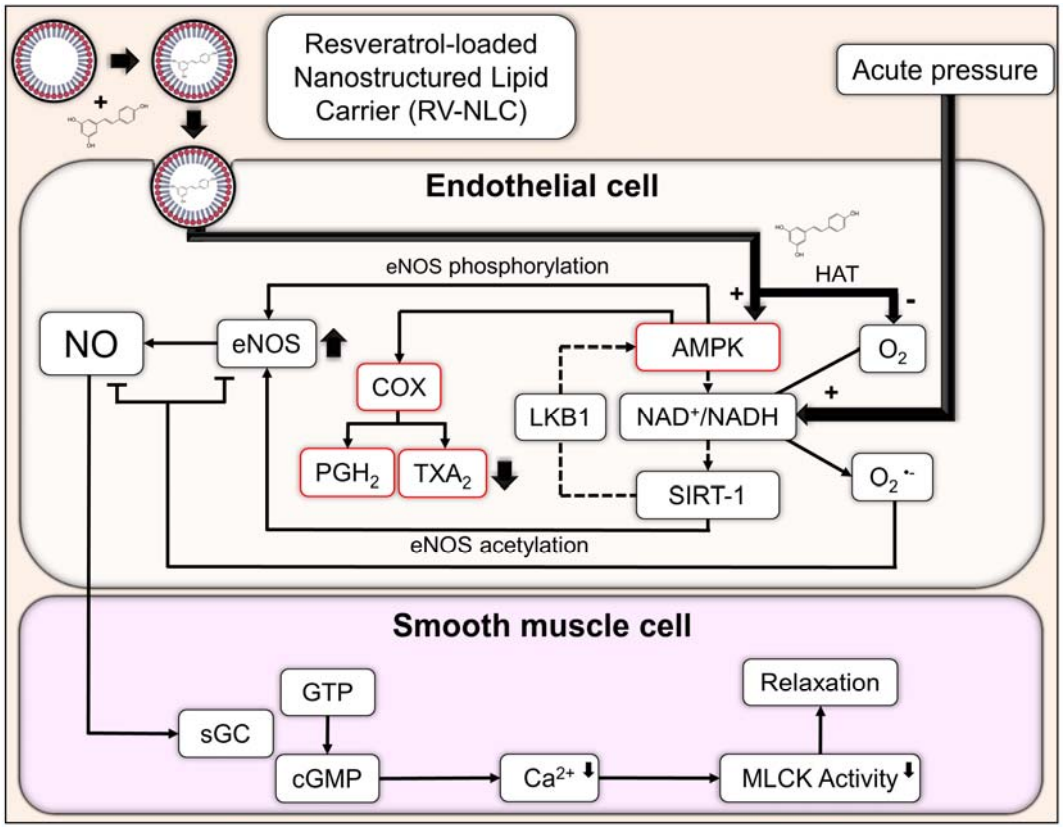

Figure 8.1. Potential mechanisms mediating endothelial dependent dilation in the coronary artery following acute pressure elevation. *Acute pressure elevation results in the activation of NAD/NADPH and subsequent generation of $O_2^{\bullet-}$, which indiscriminately oxidises NO and downregulates eNOS, impairing dilation. Following release into the coronary vasculature, RV may exhibit a range of mechanisms including direct antioxidant activity via the promotion of HAT, and indirect activity via the activation of AMPK. The activation of AMPK results in the generation of NO, potentially via eNOS phosphorylation. Concurrently, AMPK may also modulate COX activity, reducing levels of vasoconstrictors such as PGH_2 and TXA_2, resulting in improved dilator responses. Whilst no direct evidence implicating a relationship between SIRT-1 and RV was found, it remains to be seen whether AMPK and SIRT-1 act in a compensatory manner via mediation by LKB1; potentially contributing further via eNOS acetylation. Resveratrol (RV); nitric oxide (NO); endothelial nitric oxide synthase (eNOS); 5′ adenosine monophosphate-activated protein kinase (AMPK); liver kinase B1 (LKB1); cyclooxygenase (COX); prostaglandin H2 (PGH_2); thromboxane A2 (TXA_2); hydrogen atom transfer (HAT); nicotinamide adenine dinucleotide (NAD); sirtuin (silent mating type information regulation 2 homolog) 1 (SIRT1); oxygen (O2), superoxide ($O_2^{\bullet-}$); soluble guanylate cyclase (sGC); guanosine triphosphate (GTP); cyclic guanosine monophosphate (sGMP); calcium (Ca^{2+}); myosin light chain kinase (MCLK).*

8.5 Organic nanoparticles (RV-NLCs and TMS-liposomes) are incapable of restoring elevated pressure induced attenuated dilation in cerebral arteries

The findings from Chapter 7 demonstrate the inability of organic nanoparticles (RV-NLCs and TMS-liposomes) to restore attenuated dilator responses in the cerebral arteries following acute pressure elevation; differing significantly from findings using coronary arteries, suggesting tissue-specific variability in the control of vessel diameter. Furthermore, RV-NLCs appear detrimental to VSMC reactivity, potentially acting as a pro-oxidant and quenching NO, compared to the synthetically modified TMS-liposomes. The pro-oxidant effects of RV have previously been documented; whilst TMS is an analogue of RV, the disparity between responses are likely a result of its synthetic modification, resulting in reduced chemical reactivity (Ahmad et al., 2000; Azmi et al., 2005). However, this differs from current literature, whereby prolonged RV exposure has demonstrated antioxidant and restorative abilities in the cerebral vasculature subjected to hypertension-induced oxidative stress (Toth et al., 2015); suggesting treatment may be time-dependent and thus, RV may be unsuitable for treating acute vascular damage (Figure 8.2).

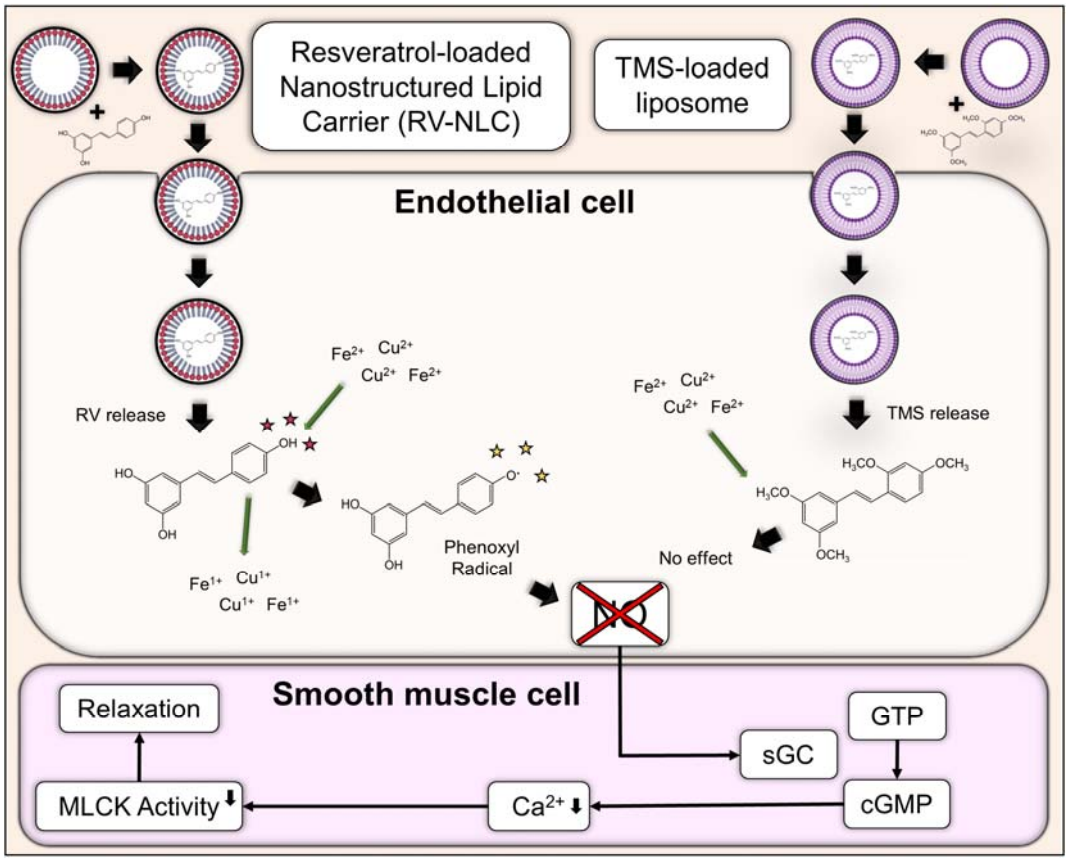

Figure 8.2. Potential mechanisms of disparity between RV and TMS mediated effects in the cerebral vasculature. *Following release into the cerebral vasculature, RV may be subject to transition metal mediated (Fe^{2+} and Cu^{2+}) oxidation of surface hydroxyl groups (OH), resulting in the generation of highly reactive phenoxyl radical; leading to the indiscriminate oxidisation of surrounding molecules such as NO, impairing dilation. In contrast, TMS has had OH groups substituted for synthetically conjugated methyl groups which are not subject to oxidation, thus leaving NO intact. Resveratrol (RV); iron (Fe); copper (Cu); nitric oxide (NO); soluble guanylate cyclase (sGC); guanosine triphosphate (GTP); cyclic guanosine monophosphate (sGMP); calcium (Ca^{2+}); myosin light chain kinase (MCLK). Active redox cycling between reduced and oxidised states (i.e. Cu^{2+}, Cu^{1+}; red stars). Phenoxyl radical oxidative reactivity (yellow stars).*

8.6 Translatability of experimental findings

To date, there are a limited number of publications that have conducted *ex vivo* studies using human tissue. Due to the requirements for live and healthy vessels in these *ex vivo* experiments, obtaining them ethically is a major hurdle. This makes translating findings from rat coronary and cerebral arteries to human very challenging.

However, various studies have demonstrated fundamental mechanisms are evolutionary conserved between rat and human and is considered an acceptable model for the evaluation of cardiovascular disease. Toth *et al.* investigated the effects of intraluminal pressure and flow on constrictor responses and underlying mechanism of action in both the human and rat cerebral arteries. In response to a progressive increase in flow and/or pressure, increased constriction was observed; incubation with inhibitors of 20-HETE and COX abolished constriction in both species, implicating ROS and COX activity in flow-induced constriction (Toth et al., 2011).

Similarities in the mechanisms underlying endothelial-dependent dilation mimic our own observations in the coronary artery, whereby NO continues to play an important role in the regulation of dilation, despite its bioavailability being reduced in hypertension. Quyyumi *et al.* investigated the dilator component in the coronary arteries of healthy and hypertensive patients undergoing coronary angiography. Following inhibition of NO, ACh-mediated dilator responses were supressed, suggesting NO may play an important role in maintaining dilation even in a hypertensive state (Quyyumi et al., 1995, 1997). These findings were recapitulated by Nishikawa *et al.* in patients suffering from atherosclerosis, whereby NO synthesis maintained basal vasomotor tone in both conduit and resistance vessels in the normal human coronary circulation; although NO release

was impaired in the large epicardial coronary arteries in patients with atherosclerosis, NO still regulated vascular tone in the small epicardial coronary arteries and arterioles.

Whilst these studies appear to confirm the translatability of rodent and human studies, there are currently no studies that compare the responses seen in healthy rodent and human coronary or cerebral arteries. The removal of healthy tissue from essential organs is not commonplace and is largely associated with underlying disease, which may directly or indirectly influence the vasculature and thus, may not accurately reflect normal vascular responses. A more detailed understanding of the similarity of the human vasculature response compared to the rodent would be necessary before these potential therapeutics could be translated. Due to the difficulty in obtaining tissue for *ex vivo* experiments but the comparative ease in obtaining cells, in future work the molecular responses could be compared in a flow culture system utilising primary human or rodent arterial cells.

8.7 Study Limitations

Several limitations were identified and considered when interpreting the experimental data, along with the potential implications for the conclusions drawn. Firstly, whilst our model was well characterised and considered suitable for use to study elevated oxidative stress; hypertension is a multifactorial disease, with well-documented interactions with other physiological components (e.g. humoral factors) which may influence vascular responses and/or may alter treatment outcome when assessed *in vivo.* Affirmation of findings would require assessment using *in vivo* animal models of hypertension, then in patients. Furthermore, with the use of any experimental animal, there will be innate variability within groups. This could be improved in future by increasing n numbers in all experimental conditions. Secondly, the nature of working with small size arteries make these experiments technically difficult; requiring microdissection and tissue manipulation performed underneath a dissection microscope. This manipulation may cause small amounts of endothelial and/or smooth muscle stress and damage. Furthermore, an accurate assessment of vascular reactivity *ex vivo* requires the removal of perivascular adipose tissue (PVAT); however, in addition to providing structural support, PVAT has demonstrated an ability to modulate vascular contractility and its removal may thus, influence responses (Won et al., 2019). Lastly, after mounting tissue on the glass cannulae, vessels must be stretched; it is difficult to standardise stretch, which may affect signalling due to the presence of mechanoreceptors. Whilst there is a possibility this may have had an effect; it may be assumed that this was largely mitigated due to the relatively low variability observed with experiments.

Furthermore, whilst evidence on the EDRF component on small size arteries exists, considering the tissue-bed and size-specific distribution of EDRFs, it would be prudent

to investigate the dilator component of coronary arteries under normotensive pressure in order to observe how these components are modulated following acute pressure elevation in our *ex vivo* model.

In these studies, acute pressure elevation has been implicated in the generation of ROS and subsequent attenuation of endothelial-dependent dilator responses, with SOD restoring and potentiating dilation in the coronary artery; implicating the presence of basal ROS. In order to confirm the presence and extent of basal ROS, SOD experiments should also be performed under normotensive pressure (60mmHg). For the design of sustained drug release strategies, it would be beneficial to observe the effects of treatment on vessel reactivity over prolonged periods of time lasting days, not hours. However, this is not currently possible due to limitations of the pressure myography technique; although vessels can be maintained, the endothelium becomes unresponsive when incubated over days.

8.8 Future Directions

Whilst this *ex vivo* study has convincingly shown that oxidative stress plays a critical role in promoting hypertension-mediated endothelial dysfunction and the restorative effects of RV-NLCs (in the coronary artery); it is evident that several key questions remain to be answered.

Firstly, whilst these data demonstrate the predominant influence of AMPK (approximately 50 %) in mediating RV-NLC-mediated dilation in the coronary artery, as opposed to the conventionally accepted SIRT-1 pathway; it remains to be seen whether AMPK and SIRT-1 act in a compensatory manner. Inhibition of both would likely result in total abolishment of RV-NLC-mediated dilation. This would be consistent with unpublished observations conducted with aortic tissue *ex vivo* within the Azzawi laboratory; however, substantial differences in vessel size and distribution of EDRF signalling do not make these experimental findings readily comparable. Furthermore, whilst many reports have documented the effects of RV and its modulatory effects on SIRT-1, little is known about its molecular mechanism of action. The effects of RV are known to be receptor-mediated, with several potential candidates identified to date (e.g. androgen-, estrogen-, troponin-c-receptor) (Wang et al., 2010; Pineda-Sanabria et al., 2011; Nwachukwu et al., 2014); in contrast, RV-NLCs are capable of being endocytosed into cells, releasing RV directly into the cytoplasmic compartment (Neves and Queiroz, 2016; Piazzini et al., 2018). Activation of these cell surface receptors inherently implicates multiple signalling pathways, the mechanisms of which may express preferential aversion or affinity towards downstream targets (e.g. SIRT-1 vs AMPK). An accurate understanding of the respective pathways activated and modulated by RV and

RV-NLCs is essential, as the mode of delivery and uptake may have implications on treatment efficacy and outcome.

Whilst a precise understanding of cell signalling in disease states is vital in the development of therapeutic treatment strategies, an accurate understanding of pathways in untreated tissue is essential and arguably of greater importance. Following acute pressure elevation in the coronary artery (in the presence and absence of treatment), an intact dilator component was demonstrated in the presence of EDRF inhibitors L-NNA, indomethacin, apamin and TRAM-34. TRPV4 channels have attracted interest in recent years and have been reported to contribute to dilation in the coronary artery (Bubolz et al., 2012; Cao et al., 2018). Given that TRPV4-mediated dilation is predominantly mediated by NO, PGI and EDH; the mechanisms of which are inhibited, the contribution of TRPV4 would be unexpected. However, much is still unknown about EDHF signalling.

In small-sized arteries, endothelial SK_{Ca} and IK_{Ca} channels are thought to be the primary mediators of hyperpolarisation. Whilst studies have also demonstrated the presence of BKCa channels in coronary artery VSMCs; evidence suggests their threshold for activation is x10 higher and likely do not contribute to the maintenance of vessel diameter in small size arteries; hence, BK_{Ca} channels are not inhibited experimentally. However, circumferential stretching of vessels (such as when elevating pressure) has been demonstrated to alter the sensitivity of BK_{Ca} channels (Hill et al., 2010). Therefore, it may be that AA (which is not subject to COX inhibition) activates TRPV4, resulting in ryanodine receptor activation and Ca^{2+} release from the sarcoplasmic reticulum; the now sensitive BK_{Ca} channels detect elevated intracellular Ca^{2+} and open, resulting in Ca^{2+} efflux and relaxation. It would be of interest to pharmacologically inhibit TRPV4 and/or BK_{Ca} channels in order to assess their contribution to endothelial-dependent dilation.

Although this potential mechanism may not appear to be influenced by current treatment, it may be a pathway that can be exploited using future treatment strategies.

In this thesis, acute pressure elevation has been implicated in the generation of ROS and subsequent attenuation of endothelial-dependent dilator responses, with SOD restoring and potentiating dilation in the coronary artery; implicating the presence of basal ROS. In order to confirm the presence and extent of basal ROS, SOD experiments should also be performed under normotensive pressure (60 mmHg).

Given the haemodynamics of the *in vivo* environment, where the nanoparticles would ultimately be used, it would be logical to investigate the uptake and influence of the RV-loaded nanoparticles on cell viability and dilator function under flow conditions. Generally, it would be expected that assays performed following the continuous circulation of nanoparticles would have improved biocompatibility, as opposed to stagnant conditions observed under conventional static assays; this is consistent with observations by researchers investigating the toxicological impact of SiNPs (Yazdimamaghani et al., 2018). These findings have important clinical implications, allowing the optimisation of therapeutic dosing to enhance treatment outcome whilst maintaining acceptable levels of toxicity.

8.9 Concluding Statements

CVDs are associated with oxidative stress and dysfunction of the vascular endothelium. Acute pressure elevation provides a means of replicating the oxidative environment and vascular dysregulation associated with hypertension; providing a useful model for the development of novel treatment strategies. The use of nanoparticles for encapsulation of drugs (e.g. novel antioxidants) offer tissue-bed specific means of improving impaired vascular function. Nanoparticles demonstrate excellent potential as delivery platforms for the sustained release of metabolically unstable compounds improving their bioavailability for the amelioration of CVDs associated with oxidative stress and restoration of cardiovascular health. Our findings have important implications for the future design and implementation of anti-hypertensive treatment strategies.

List of References

Adler, S. and Huang, H. (2002) ‘Impaired Regulation of Renal Oxygen Consumption in Spontaneously Hypertensive Rats.’ *Journal of the American Society of Nephrology*, 13(7) pp. 1788 LP – 1794.

Agostino, V., Alessandra, B., Rocchina, C., Emiliano, D., Matteo, F., Gabriele, M., Chiara, I., Nunzia, B., Corrado, B., Giampaolo, B. and Stefano, T. (2013) ‘Endothelial Dysfunction in Small Arteries of Essential Hypertensive Patients.’ *Hypertension*. American Heart Association, 62(2) pp. 337–344.

Ahamed, M. (2013) ‘Silica nanoparticles-induced cytotoxicity, oxidative stress and apoptosis in cultured A431 and A549 cells.’ *Human & experimental toxicology*. England, 32(2) pp. 186–195.

Ahmad, A., Farhan Asad, S., Singh, S. and Hadi, S. M. (2000) ‘DNA breakage by resveratrol and Cu(II): reaction mechanism and bacteriophage inactivation.’ *Cancer letters*. Ireland, 154(1) pp. 29–37.

Akbar, N., Mohamed, T., Whitehead, D. and Azzawi, M. (2011) ‘Biocompatibility of amorphous silica nanoparticles: Size and charge effect on vascular function, in vitro.’ *Biotechnology and Applied Biochemistry*, 58(5) pp. 353–362.

Al-Kaysi, R. O., Müller, A. M., Ahn, T.-S., Lee, S. and Bardeen, C. J. (2005) ‘Effects of Sonication on the Size and Crystallinity of Stable Zwitterionic Organic Nanoparticles Formed by Reprecipitation in Water.’ *Langmuir*. American Chemical Society, 21(17) pp. 7990–7994.

Alister, M., Shaun, S., Craig, N., Mark, C., Kim, D. and Christopher, G. (2006) ‘Evidence for Involvement of Both IKCa and SKCa Channels in Hyperpolarizing Responses of the Rat Middle Cerebral Artery.’ *Stroke*. American Heart Association, 37(5) pp. 1277–1282.

Anning, P. B., Coles, B., Morton, J., Wang, H., Uddin, J., Morrow, J. D., Dey, S. K., Marnett, L. J. and O’Donnell, V. B. (2006) ‘Nitric oxide deficiency promotes vascular side effects of cyclooxygenase inhibitors.’ *Blood*, 108(13) pp. 4059–4062.

Araya, R., Noguchi, T., Yuhki, M., Kitamura, N., Higuchi, M., Saido, T. C., Seki, K., Itohara, S., Kawano, M., Tanemura, K., Takashima, A., Yamada, K., Kondoh, Y., Kanno, I., Wess, J. and Yamada, M. (2006) ‘Loss of M5 muscarinic acetylcholine

receptors leads to cerebrovascular and neuronal abnormalities and cognitive deficits in mice.' *Neurobiology of disease*. United States, 24(2) pp. 334–344.

Arnalich-Montiel, A., Gonzalez, M. C., Delgado-Baeza, E., Delgado-Martos, M. J., Condezo-Hoyos, L., Martos-Rodriguez, A., Rodriguez-Rodriguez, P. and Quintana-Villamandos, B. (2014) 'Short-term esmolol improves coronary artery remodeling in spontaneously hypertensive rats through increased nitric oxide bioavailability and superoxide dismutase activity.' *BioMed research international*. United States, 2014 p. 531087.

Arunachalam, G., Yao, H., Sundar, I. K., Caito, S. and Rahman, I. (2010) 'SIRT1 regulates oxidant- and cigarette smoke-induced eNOS acetylation in endothelial cells: Role of resveratrol.' *Biochemical and biophysical research communications*. United States, 393(1) pp. 66–72.

Asefa, T. and Tao, Z. (2012) 'Biocompatibility of mesoporous silica nanoparticles.' *Chemical Research in Toxicology*, 25(11) pp. 2265–2284.

Azmi, A. S., Bhat, S. H. and Hadi, S. M. (2005) 'Resveratrol–Cu(II) induced DNA breakage in human peripheral lymphocytes: Implications for anticancer properties.' *FEBS Letters*. John Wiley & Sons, Ltd, 579(14) pp. 3131–3135.

Azzawi, M. and Austin, C. (2004) 'Myogenic regulation of isolated small coronary arteries following increases in extravascular pressure.' *Microvascular Research*, 68(1) pp. 71–74.

Azzawi, M. and Austin, C. (2006) 'Extravascular pressure modulates responses of isolated rat coronary arteries to vasodilator, but not vasoconstrictor, stimuli.' *American Journal of Physiology-Heart and Circulatory Physiology*. American Physiological Society, 290(3) pp. H1151–H1156.

Bader, Y., Quint, R. M. and Getoff, N. (2008) 'Resveratrol products resulting by free radical attack.' *Radiation Physics and Chemistry*, 77(6) pp. 708–712.

Baldim, V., Bedioui, F., Mignet, N., Margaill, I. and Berret, J.-F. (2018) 'The enzyme-like catalytic activity of cerium oxide nanoparticles and its dependency on Ce(3+) surface area concentration.' *Nanoscale*. England, 10(15) pp. 6971–6980.

Bandak, S., Ramu, A., Barenholz, Y. and Gabizon, A. (1999) 'Reduced UV-Induced

Degradation of Doxorubicin Encapsulated in Polyethyleneglycol-Coated Liposomes.' *Pharmaceutical Research*, 16(6) pp. 841–846.

Basyuk, V. A. (1994) 'Infrared spectra of carboxylic compounds on silica surfaces at 1500–1800 cm−1.' *Journal of Applied Spectroscopy*, 60(1) pp. 29–33.

Bauersachs, J., Popp, R., Hecker, M., Sauer, E., Fleming, I. and Busse, R. (1996) 'Nitric oxide attenuates the release of endothelium-derived hyperpolarizing factor.' *Circulation*. United States, 94(12) pp. 3341–3347.

Beckman, J. A., Goldfine, A. B., Gordon-Mary, B. and Creager, M. A. (2001) 'Ascorbate Restores Endothelium-Dependent Vasodilation Impaired by Acute Hyperglycemia in Humans.' *Circulation*. American Heart Association, 103(12) pp. 1618–1623.

Bendall, J. K., Douglas, G., McNeill, E., Channon, K. M. and Crabtree, M. J. (2013) 'Tetrahydrobiopterin in Cardiovascular Health and Disease.' *Antioxidants & Redox Signaling*. Mary Ann Liebert, Inc., publishers, 20(18) pp. 3040–3077.

Beswick, R. A., Dorrance, A. M., Leite, R. and Webb, R. C. (2001) 'NADH/NADPH oxidase and enhanced superoxide production in the mineralocorticoid hypertensive rat.' *Hypertension (Dallas, Tex. : 1979)*. United States, 38(5) pp. 1107–1111.

Beverelli, F., Bea, M. L., Puybasset, L., Giudicelli, J. F. and Berdeaux, A. (1997) 'Chronic inhibition of NO synthase enhances the production of prostacyclin in coronary arteries through upregulation of the cyclooxygenase type 1 isoform.' *Fundamental & clinical pharmacology*. England, 11(3) pp. 252–259.

Beyer, A. M., Zinkevich, N., Miller, B., Liu, Y., Wittenburg, A. L., Mitchell, M., Galdieri, R., Sorokin, A. and Gutterman, D. D. (2017) 'Transition in the mechanism of flow-mediated dilation with aging and development of coronary artery disease.' *Basic research in cardiology*. Germany, 112(1) p. 5.

Bhattacharjee, S. (2016) 'DLS and zeta potential - What they are and what they are not?' *Journal of controlled release : official journal of the Controlled Release Society*. Netherlands, 235, August, pp. 337–351.

Biswas, I. and Khan, G. (2019) 'Endothelial Dysfunction in Cardiovascular Diseases [Online First].' *In*. IntechOpen.

Borgos, S. E. F., Cornier, J., Owen, A., Kwade, A. and Van de Voorde, M. (2017) 'Characterization Methods: Physical and Chemical Characterization Techniques.' *In Pharmaceutical Nanotechnology: Innovation and Production*. Wiley-VCH Verlag GmbH & Co. KGaA, pp. 135–156.

Brace, L. D., Venton, D. L. and Le Breton, G. C. (1985) 'Thromboxane A2/prostaglandin H2 mobilizes calcium in human blood platelets.' *American Journal of Physiology-Heart and Circulatory Physiology*. American Physiological Society, 249(1) pp. H1–H7.

De Bruyn, V. H., Nuno, D. W., Cappelli-Bigazzi, M., Dole, W. P. and Lamping, K. G. (1994) 'Effect of acute hypertension in the coronary circulation: role of mechanical factors and oxygen radicals.' *Journal of hypertension*. England, 12(2) pp. 163–172.

Brzezinska, A. K., Gebremedhin, D., Chilian, W. M., Kalyanaraman, B. and Elliott, S. J. (2000) 'Peroxynitrite reversibly inhibits Ca(2+)-activated K(+) channels in rat cerebral artery smooth muscle cells.' *American journal of physiology. Heart and circulatory physiology*. United States, 278(6) pp. H1883-90.

Bubolz, A. H., Mendoza, S. A., Zheng, X., Zinkevich, N. S., Li, R., Gutterman, D. D. and Zhang, D. X. (2012) 'Activation of endothelial TRPV4 channels mediates flow-induced dilation in human coronary arterioles: role of Ca2+ entry and mitochondrial ROS signaling.' *American journal of physiology. Heart and circulatory physiology*. United States, 302(3) pp. H634-42.

Burnham, M. P., Bychkov, R., Félétou, M., Richards, G. R., Vanhoutte, P. M., Weston, A. H. and Edwards, G. (2002) 'Characterization of an apamin-sensitive small-conductance Ca(2+)-activated K(+) channel in porcine coronary artery endothelium: relevance to EDHF.' *British journal of pharmacology*, 135(5) pp. 1133–1143.

Burns, J., Yokota, T., Ashihara, H., Lean, M. E. J. and Crozier, A. (2002) 'Plant Foods and Herbal Sources of Resveratrol.' *Journal of Agricultural and Food Chemistry*. American Chemical Society, 50(11) pp. 3337–3340.

Bychkov, R., Burnham, M. P., Richards, G. R., Edwards, G., Weston, A. H., Félétou, M. and Vanhoutte, P. M. (2002) 'Characterization of a charybdotoxin-sensitive intermediate conductance Ca2+-activated K+ channel in porcine coronary endothelium: relevance to EDHF.' *British journal of pharmacology*, 137(8) pp. 1346–1354.

Calabrese, E. J., Mattson, M. P. and Calabrese, V. (2010) ‘Resveratrol commonly displays hormesis: Occurrence and biomedical significance.’ *Human & Experimental Toxicology*. SAGE Publications Ltd STM, 29(12) pp. 980–1015.

Camont, L., Cottart, C.-H., Rhayem, Y., Nivet-Antoine, V., Djelidi, R., Collin, F., Beaudeux, J.-L. and Bonnefont-Rousselot, D. (2009) ‘Simple spectrophotometric assessment of the trans-/cis-resveratrol ratio in aqueous solutions.’ *Analytica chimica acta*. Netherlands, 634(1) pp. 121–128.

Cao, H., Pan, X., Li, C., Zhou, C., Deng, F. and Li, T. (2003) ‘Density functional theory calculations for resveratrol.’ *Bioorganic & medicinal chemistry letters*. England, 13(11) pp. 1869–1871.

Cao, S., Anishkin, A., Zinkevich, N. S., Nishijima, Y., Korishettar, A., Wang, Z., Fang, J., Wilcox, D. A. and Zhang, D. X. (2018) ‘Transient receptor potential vanilloid 4 (TRPV4) activation by arachidonic acid requires protein kinase A-mediated phosphorylation.’ *The Journal of biological chemistry*. United States, 293(14) pp. 5307–5322.

Cao, S., Nishijima, Y. and Zhang, D. X. (2016) ‘Arachidonic Acid-Induced TRPV4 Activation is Enhanced by Serine Phosphorylation in Human Coronary Artery Endothelial Cells.’ *The FASEB Journal*. Federation of American Societies for Experimental Biology, 30(1_supplement) pp. 1281.2-1281.2.

Cardillo, C., Kilcoyne, C. M., Quyyumi, A. A., Cannon, R. O. 3rd and Panza, J. A. (1998) ‘Selective defect in nitric oxide synthesis may explain the impaired endothelium-dependent vasodilation in patients with essential hypertension.’ *Circulation*. United States, 97(9) pp. 851–856.

Carter, W. O., Narayanan, P. K. and Robinson, J. P. (1994) ‘Intracellular hydrogen peroxide and superoxide anion detection in endothelial cells.’ *Journal of leukocyte biology*. United States, 55(2) pp. 253–258.

Caruso, F., Tanski, J., Villegas-Estrada, A. and Rossi, M. (2004) ‘Structural Basis for Antioxidant Activity of *trans* -Resveratrol: Ab Initio Calculations and Crystal and Molecular Structure.’ *Journal of Agricultural and Food Chemistry*, 52(24) pp. 7279–7285.

Chachay, V. S., Macdonald, G. A., Martin, J. H., Whitehead, J. P., O'Moore-Sullivan, T. M., Lee, P., Franklin, M., Klein, K., Taylor, P. J., Ferguson, M., Coombes, J. S., Thomas, G. P., Cowin, G. J., Kirkpatrick, C. M. J., Prins, J. B. and Hickman, I. J. (2014) 'Resveratrol does not benefit patients with nonalcoholic fatty liver disease.' *Clinical gastroenterology and hepatology : the official clinical practice journal of the American Gastroenterological Association*. United States, 12(12) pp. 2092–2096.

Chan, P., Cheng, J. T., Tsao, C. W., Niu, C. S. and Hong, C. Y. (1996) 'The in vitro antioxidant activity of trilinolein and other lipid-related natural substances as measured by enhanced chemiluminescence.' *Life sciences*. Netherlands, 59(24) pp. 2067–2073.

Chaplin, N. L. and Amberg, G. C. (2012) 'Hydrogen peroxide mediates oxidant-dependent stimulation of arterial smooth muscle L-type calcium channels.' *American journal of physiology. Cell physiology*. United States, 302(9) pp. C1382-93.

Chen, M., Yi, L., Jin, X., Xie, Q., Zhang, T., Zhou, X., Chang, H., Fu, Y., Zhu, J., Zhang, Q. and Mi, M. (2013) 'Absorption of resveratrol by vascular endothelial cells through passive diffusion and an SGLT1-mediated pathway.' *The Journal of Nutritional Biochemistry*, 24(11) pp. 1823–1829.

Chen, S., Hou, Y., Cheng, G., Zhang, C., Wang, S. and Zhang, J. (2014) *Cerium Oxide Nanoparticles Protect Endothelial Cells from Apoptosis Induced by Oxidative Stress*. *Biological trace element research*.

Christensen, F. H., Hansen, T., Stankevicius, E., Buus, N. H. and Simonsen, U. (2007) 'Elevated pressure selectively blunts flow-evoked vasodilatation in rat mesenteric small arteries.' *British journal of pharmacology*. 2006/11/27, Nature Publishing Group, 150(1) pp. 80–87.

Cirri, M., Maestrini, L., Maestrelli, F., Mennini, N., Mura, P., Ghelardini, C. and Di Cesare Mannelli, L. (2018) 'Design, characterization and in vivo evaluation of nanostructured lipid carriers (NLC) as a new drug delivery system for hydrochlorothiazide oral administration in pediatric therapy.' *Drug delivery*. Taylor & Francis, 25(1) pp. 1910–1921.

Cooke, C.-L. M. and Davidge, S. T. (2003) 'Endothelial-dependent vasodilation is reduced in mesenteric arteries from superoxide dismutase knockout mice.' *Cardiovascular Research*, 60(3) pp. 635–642.

Corbalan, J. J., Medina, C., Jacoby, A., Malinski, T. and Radomski, M. W. (2012) 'Amorphous silica nanoparticles aggregate human platelets: potential implications for vascular homeostasis.' *International Journal of Nanomedicine*. Dove Medical Press, 7, February, pp. 631–639.

Cottart, C.-H., Nivet-Antoine, V., Laguillier-Morizot, C. and Beaudeux, J.-L. (2010) 'Resveratrol bioavailability and toxicity in humans.' *Molecular nutrition & food research*. Germany, 54(1) pp. 7–16.

Coyle, C. H. and Kader, K. N. (2007) 'Mechanisms of H2O2-induced oxidative stress in endothelial cells exposed to physiologic shear stress.' *ASAIO Journal*, 53(1) pp. 17–22.

Coyle, C. H., Martinez, L. J., Coleman, M. C., Spitz, D. R., Weintraub, N. L. and Kader, K. N. (2006) 'Mechanisms of H2O2-induced oxidative stress in endothelial cells.' *Free radical biology & medicine*. United States, 40(12) pp. 2206–2213.

Craige, S. (2015) 'Reactive Oxygen Species in Endothelial Function\r– From Disease to Adaptation –.' *Circulation Journal*, 79(June) pp. 1145–1155.

Crichton, R. R. and Ward, R. J. (2013) 'Role of Metal Ions in Brain Function, Metal Transport, Storage and Homoeostasis.' *Metal-based Neurodegeneration*. (Wiley Online Books) pp. 23–50.

Cruz, M. N., Luksha, L., Logman, H., Poston, L., Agewall, S. and Kublickiene, K. (2006) 'Acute responses to phytoestrogens in small arteries from men with coronary heart disease.' *American journal of physiology. Heart and circulatory physiology*. United States, 290(5) pp. H1969-75.

Cureton, N., Korotkova, I., Baker, B., Greenwood, S., Wareing, M., Kotamraju, V. R., Teesalu, T., Cellesi, F., Tirelli, N., Ruoslahti, E., Aplin, J. D. and Harris, L. K. (2017) 'Selective Targeting of a Novel Vasodilator to the Uterine Vasculature to Treat Impaired Uteroplacental Perfusion in Pregnancy.' *Theranostics*. Australia, 7(15) pp. 3715–3731.

Das, S., Singh, S., Dowding, J. M., Oommen, S., Kumar, A., Sayle, T. X. T., Saraf, S., Patra, C. R., Vlahakis, N. E., Sayle, D. C., Self, W. T. and Seal, S. (2012) 'The induction of angiogenesis by cerium oxide nanoparticles through the modulation of oxygen in intracellular environments.' *Biomaterials*, 33(31) pp. 7746–7755.

Davis, C. M., Siler, D. A. and Alkayed, N. J. (2011) 'Endothelium-derived hyperpolarizing factor in the brain: influence of sex, vessel size and disease state.' *Women's health (London, England)*, 7(3) pp. 293–303.

Dell'Agli, M., Buscialà, A. and Bosisio, E. (2004) 'Vascular effects of wine polyphenols.' *Cardiovascular Research*, 63(4) pp. 593–602.

Deng, L.-Y., Jin-Sheng, L. I. and Schiffrin, E. L. (1995) 'Endothelium-Dependent Relaxation of Small Arteries from Essential Hypertensive Patients: Mechanisms and Comparison with Normotensive Subjects and with Responses of Vessels from Spontaneously Hypertensive Rats.' *Clinical Science*, 88(6) pp. 611–622.

Diaz, M., Avila, A., Degens, H., Coeckelberghs, E., Vanhees, L., Cornelissen, V. and Azzawi, M. (2020) 'Acute resveratrol supplementation in coronary artery disease: towards patient stratification.' *Scandinavian cardiovascular journal : SCJ*. England, August, pp. 1–6.

Diaz, M., Ismail, S., Maxamed, R., Tye, E., Austin, C., Dew, T., Graf, B. A., Vanhees, L., Degens, H. and Azzawi, M. (2019) 'Differential effects of resveratrol on the dilator responses of femoral arteries, ex vivo.' *Nitric Oxide*, 92 pp. 1–10.

Didion, S. and Frank, F. (2003) 'Angiotensin II Produces Superoxide-Mediated Impairment of Endothelial Function in Cerebral Arterioles.' *Stroke*. American Heart Association, 34(8) pp. 2038–2042.

Duan, J., Yu, Yongbo, Li, Yang, Yu, Yang, Li, Yanbo, Zhou, X., Huang, P. and Sun, Z. (2013a) 'Toxic Effect of Silica Nanoparticles on Endothelial Cells through DNA Damage Response via Chk1-Dependent G2/M Checkpoint.' *PLOS ONE*. Public Library of Science, 8(4) p. e62087.

Duan, J., Yu, Yongbo, Li, Yang, Yu, Yang, Li, Yanbo, Zhou, X., Huang, P. and Sun, Z. (2013b) 'Toxic Effect of Silica Nanoparticles on Endothelial Cells through DNA Damage Response via Chk1-Dependent G2/M Checkpoint.' *PLoS ONE*, 8(4).

Duan, J., Yu, Yongbo, Yu, Yang, Li, Y., Huang, P., Zhou, X., Peng, S. and Sun, Z. (2014) 'Silica nanoparticles enhance autophagic activity, disturb endothelial cell homeostasis and impair angiogenesis.' *Particle and Fibre Toxicology*, 11(1) p. 50.

Dunn, S. M., Hilgers, R. H. and Das, K. C. (2017) 'Decreased EDHF-mediated

relaxation is a major mechanism in endothelial dysfunction in resistance arteries in aged mice on prolonged high-fat sucrose diet.' *Physiological reports*. John Wiley and Sons Inc., 5(23) p. e13502.

El-Mowafy, A. M. (2002) 'Resveratrol activates membrane-bound guanylyl cyclase in coronary arterial smooth muscle: a novel signaling mechanism in support of coronary protection.' *Biochemical and biophysical research communications*. United States, 291(5) pp. 1218–1224.

Ellinsworth, D. C., Sandow, S. L., Shukla, N., Liu, Y., Jeremy, J. Y. and Gutterman, D. D. (2016) 'Endothelium-Derived Hyperpolarization and Coronary Vasodilation: Diverse and Integrated Roles of Epoxyeicosatrienoic Acids, Hydrogen Peroxide, and Gap Junctions.' *Microcirculation*. John Wiley & Sons, Ltd (10.1111), 23(1) pp. 15–32.

Fang, M., Jin, Y., Bao, W., Gao, H., Xu, M., Wang, D., Wang, X., Yao, P. and Liu, L. (2012) 'In vitro characterization and in vivo evaluation of nanostructured lipid curcumin carriers for intragastric administration.' *International journal of nanomedicine*. New Zealand, 7 pp. 5395–5404.

Faraci, F. M., Lamping, K. G., Modrick, M. L., Ryan, M. J., Sigmund, C. D. and Didion, S. P. (2006) 'Cerebral vascular effects of angiotensin II: new insights from genetic models.' *Journal of cerebral blood flow and metabolism : official journal of the International Society of Cerebral Blood Flow and Metabolism*. United States, 26(4) pp. 449–455.

Farooq, A. (2014) 'Restored Endothelial Dependent Vasodilation in Aortic Vessels after Uptake of Ceria Coated Silica Nanoparticles, ex vivo.' *Journal of Nanomedicine & Nanotechnology*, 05(02).

Farooq, A., Shukur, A., Astley, C., Tosheva, L., Kelly, P., Whitehead, D. and Azzawi, M. (2018) 'Titania coating of mesoporous silica nanoparticles for improved biocompatibility and drug release within blood vessels.' *Acta biomaterialia*. England, 76, August, pp. 208–216.

Farooq, A., Tosheva, L., Azzawi, M. and Whitehead, D. (2016) 'Real-time observation of aortic vessel dilation through delivery of sodium nitroprusside via slow release mesoporous nanoparticles.' *Journal of Colloid and Interface Science*. Elsevier Inc., 478 pp. 127–135.

Farooq, A., Whitehead, D. and Azzawi, M. (2014a) 'Attenuation of endothelial-dependent vasodilator responses, induced by dye-encapsulated silica nanoparticles, in aortic vessels.' *Nanomedicine (London, England)*. England, 9(3) pp. 413–425.

Farooq, A., Whitehead, D. and Azzawi, M. (2014b) 'Attenuation of endothelial-dependent vasodilator responses, induced by dye-encapsulated silica nanoparticles, in aortic vessels.' *Nanomedicine (London, England)*, 9(3) pp. 413–425.

Filippi, A., Liu, F., Wilson, J., Lelieveld, S., Korschelt, K., Wang, T., Wang, Y., Reich, T., Pöschl, U., Tremel, W. and Tong, H. (2019) 'Antioxidant activity of cerium dioxide nanoparticles and nanorods in scavenging hydroxyl radicals.' *RSC Advances*. The Royal Society of Chemistry, 9(20) pp. 11077–11081.

Fiorani, L., Passacantando, M., Santucci, S., Di Marco, S., Bisti, S. and Maccarone, R. (2015) 'Cerium Oxide Nanoparticles Reduce Microglial Activation and Neurodegenerative Events in Light Damaged Retina.' *PLOS ONE*. Public Library of Science, 10(10) p. e0140387.

Flores, A. M., Jianqin, Y., Jarr, K. U., Hosseini, N. N., Bryan, S. and Leeper, N. J. (2019) 'Nanoparticle Therapy for Vascular Diseases.' *Arteriosclerosis, Thrombosis, and Vascular Biology*. American Heart Association, 39(4) pp. 635–646.

Folkes, L. K., Patel, K. B., Wardman, P. and Wrona, M. (2009) 'Kinetics of reaction of nitrogen dioxide with dihydrorhodamine and the reaction of the dihydrorhodamine radical with oxygen: Implications for quantifying peroxynitrite formation in cells.' *Archives of Biochemistry and Biophysics*, 484(2) pp. 122–126.

Forouzanfar, M. H., Liu, P., Roth, G. A., Ng, M., Biryukov, S., Marczak, L., Alexander, L., Estep, K., Hassen Abate, K., Akinyemiju, T. F., Ali, R., Alvis-Guzman, N., Azzopardi, P., Banerjee, A., Bärnighausen, T., Basu, A., Bekele, T., Bennett, D. A., Biadgilign, S., Catalá-López, F., Feigin, V. L., Fernandes, J. C., Fischer, F., Gebru, A. A., Gona, P., Gupta, R., Hankey, G. J., Jonas, J. B., Judd, S. E., Khang, Y.-H., Khosravi, A., Kim, Y. J., Kimokoti, R. W., Kokubo, Y., Kolte, D., Lopez, A., Lotufo, P. A., Malekzadeh, R., Melaku, Y. A., Mensah, G. A., Misganaw, A., Mokdad, A. H., Moran, A. E., Nawaz, H., Neal, B., Ngalesoni, F. N., Ohkubo, T., Pourmalek, F., Rafay, A., Rai, R. K., Rojas-Rueda, D., Sampson, U. K., Santos, I. S., Sawhney, M., Schutte, A. E., Sepanlou, S. G., Shifa, G. T., Shiue, I., Tedla, B. A., Thrift, A. G., Tonelli, M.,

Truelsen, T., Tsilimparis, N., Ukwaja, K. N., Uthman, O. A., Vasankari, T., Venketasubramanian, N., Vlassov, V. V., Vos, T., Westerman, R., Yan, L. L., Yano, Y., Yonemoto, N., Zaki, M. E. S. and Murray, C. J. L. (2017) 'Global Burden of Hypertension and Systolic Blood Pressure of at Least 110 to 115 mm Hg, 1990-2015.' *JAMA*, 317(2) pp. 165–182.

Francis, B. N., Salameh, M., Khamisy-Farah, R. and Farah, R. (2018) 'Tetrahydrobiopterin (BH4): Targeting endothelial nitric oxide synthase as a potential therapy for pulmonary hypertension.' *Cardiovascular therapeutics*. England, 36(1).

Fresquet, F., Pourageaud, F., Leblais, V., Brandes, R. P., Savineau, J.-P., Marthan, R. and Muller, B. (2006) 'Role of reactive oxygen species and gp91phox in endothelial dysfunction of pulmonary arteries induced by chronic hypoxia.' *British journal of pharmacology*. 2006/05/22, Nature Publishing Group, 148(5) pp. 714–723.

Fukai, T. and Fukai, M. U. (2011) 'Superoxide dismutases: role in redox signaling, vascular function, and diseases.' *Antioxidants & redox signaling*, 15(6) pp. 1583–606.

Furchgott, R. F. and Zawadzki, J. V (1980) 'The obligatory role of endothelial cells in the relaxation of arterial smooth muscle by acetylcholine.' *Nature*. England, 288(5789) pp. 373–376.

Giordo, R., Cossu, A., Pasciu, V., Hoa, P. T., Posadino, A. M. and Pintus, G. (2013) 'Different redox response elicited by naturally occurring antioxidants in human endothelial cells.' *The open biochemistry journal*. Bentham Open, 7, April, pp. 44–53.

Gojova, A., Lee, J.-T., Jung, H. S., Guo, B., Barakat, A. I. and Kennedy, I. M. (2009) 'Effect of cerium oxide nanoparticles on inflammation in vascular endothelial cells.' *Inhalation toxicology*, 21(Suppl 1) pp. 123–130.

Goszcz, K., Deakin, S. J., Duthie, G. G., Stewart, D., Leslie, S. J. and Megson, I. L. (2015) 'Antioxidants in Cardiovascular Therapy: Panacea or False Hope?' *Frontiers in Cardiovascular Medicine*, 2 p. 29.

Goto, K. and Kitazono, T. (2019) 'Endothelium-Dependent Hyperpolarization (EDH) in Diabetes: Mechanistic Insights and Therapeutic Implications.' *International journal of molecular sciences*. Switzerland, 20(15).

Gramatke, A. M. (2014) 'Size and Cell Type Dependent Uptake of Silica

Nanoparticles.' Joksimovic, R. (ed.) *Journal of Nanomedicine & Nanotechnology*. OMICS International.,.

Guillermo, Z., J., B. F., San, J. G., Ana, F., A., F. M., C., E. J. and Javier, D. (2000) 'Vascular NADH/NADPH Oxidase Is Involved in Enhanced Superoxide Production in Spontaneously Hypertensive Rats.' *Hypertension*. American Heart Association, 35(5) pp. 1055–1061.

Gündüz, F., Meiselman, H. J. and Bas, K. (2008) 'Responses of Small Mesenteric Arteries in the Rat,' 72(March) pp. 482–486.

Guo, C., Yang, M., Jing, L., Wang, J., Yu, Y., Li, Yang, Duan, J., Zhou, X., Li, Yanbo and Sun, Z. (2016) 'Amorphous silica nanoparticles trigger vascular endothelial cell injury through apoptosis and autophagy via reactive oxygen species-mediated MAPK/Bcl-2 and PI3K/Akt/mTOR signaling.' *International journal of nanomedicine*. New Zealand, 11 pp. 5257–5276.

Gupta, U., Singh, V., Kumar, V. and Khajuria, Y. (2014) 'Spectroscopic Studies of Cholesterol: Fourier Transform Infra-Red and Vibrational Frequency Analysis.' *Materials Focus*, 3(3) pp. 211–217.

Gutteridge, J. M. (1984) 'Lipid peroxidation initiated by superoxide-dependent hydroxyl radicals using complexed iron and hydrogen peroxide.' *FEBS letters*. England, 172(2) pp. 245–249.

Hackl, E. V, Khutoryanskiy, V. V, Tiguman, G. M. B. and Ermolina, I. (2015) 'Evaluation of water properties in HEA–HEMA hydrogels swollen in aqueous-PEG solutions using thermoanalytical techniques.' *Journal of Thermal Analysis and Calorimetry*, 121(1) pp. 335–345.

Hadipour, S. P., Mohammadpour, R. and Ghandehari, H. (2019) 'In vitro and in vivo evaluation of degradation, toxicity, biodistribution, and clearance of silica nanoparticles as a function of size, porosity, density, and composition.' *Journal of controlled release : official journal of the Controlled Release Society*. Netherlands, 311–312, October, pp. 1–15.

Hamasaki, S., Al Suwaidi, J., Higano, S. T., Miyauchi, K., Holmes, D. R. J. and Lerman, A. (2000) 'Attenuated coronary flow reserve and vascular remodeling in

patients with hypertension and left ventricular hypertrophy.' *Journal of the American College of Cardiology*. United States, 35(6) pp. 1654–1660.

Hamilton, C. A., Brosnan, J. M., McIntyre, M., Graham, D. and Dominiczak, A. F. (2001) 'Superoxide Excess in Hypertension and Aging.' *Hypertension*. American Heart Association, 37(2) pp. 529–534.

Hao, N., Liu, H., Li, Linlin, Chen, D., Li, Laifeng and Tang, F. (2012) 'In vitro degradation behavior of silica nanoparticles under physiological conditions.' *Journal of nanoscience and nanotechnology*. United States, 12(8) pp. 6346–6354.

Harrison, F. E. and May, J. M. (2009) 'Vitamin C function in the brain: vital role of the ascorbate transporter SVCT2.' *Free radical biology & medicine*. United States, 46(6) pp. 719–730.

He, C., Hu, Y., Yin, L., Tang, C. and Yin, C. (2010) 'Effects of particle size and surface charge on cellular uptake and biodistribution of polymeric nanoparticles.' *Biomaterials*. Netherlands, 31(13) pp. 3657–3666.

Heckert, E. G., Karakoti, A. S., Seal, S. and Self, W. T. (2008) 'The role of cerium redox state in the SOD mimetic activity of nanoceria.' *Biomaterials*, 29(18) pp. 2705–2709.

Hendre, A. S., Shariff, A. K., Patil, S. R., Durgawale, P. P., Sontakke, A. V and Suryakar, A. N. (2013) 'Evaluation of oxidative stress and anti-oxidant status in essential hypertension.' *Journal of the Indian Medical Association*. India, 111(6) pp. 377-378,380-381.

Higashi, Y., Sasaki, S., Nakagawa, K., Matsuura, H., Oshima, T. and Chayama, K. (2002) 'Endothelial Function and Oxidative Stress in Renovascular Hypertension.' *New England Journal of Medicine*. Massachusetts Medical Society, 346(25) pp. 1954–1962.

Hill, M. A., Yang, Y., Ella, S. R., Davis, M. J. and Braun, A. P. (2010) 'Large conductance, Ca2+-activated K+ channels (BKCa) and arteriolar myogenic signaling.' *FEBS letters*. 2010/02/20, 584(10) pp. 2033–2042.

Hiroto, M. and Gutterman, D. D. (1998) 'Human Coronary Arteriolar Dilation to Arachidonic Acid Depends on Cytochrome P-450 Monooxygenase and Ca2+-Activated K+ Channels.' *Circulation Research*. American Heart Association, 83(5) pp. 501–507.

Hiroto, M., Yanping, L. and Gutterman, D. D. (1999) 'Human Coronary Arteriolar Dilation to Bradykinin Depends on Membrane Hyperpolarization.' *Circulation*. American Heart Association, 99(24) pp. 3132–3138.

Hirst, S. M., Karakoti, A., Singh, S., Self, W., Tyler, R., Seal, S. and Reilly, C. M. (2013) 'Bio-distribution and in vivo antioxidant effects of cerium oxide nanoparticles in mice.' *Environmental toxicology*. United States, 28(2) pp. 107–118.

Hou, C.-H., Tan, T.-W. and Tang, C.-H. (2008) 'AMP-activated protein kinase is involved in COX-2 expression in response to ultrasound in cultured osteoblasts.' *Cellular signalling*. England, 20(5) pp. 978–988.

Hou, L., Zheng, Y., Wang, Y., Hu, Y., Shi, J., Liu, Q., Zhang, H. and Zhang, Z. (2018) 'Self-Regulated Carboxyphenylboronic Acid-Modified Mesoporous Silica Nanoparticles with "Touch Switch" Releasing Property for Insulin Delivery.' *ACS applied materials & interfaces*. United States, 10(26) pp. 21927–21938.

Hozawa, A., Jacobs Jr, D. R., Steffes, M. W., Gross, M. D., Steffen, L. M. and Lee, D.-H. (2007) 'Relationships of circulating carotenoid concentrations with several markers of inflammation, oxidative stress, and endothelial dysfunction: the Coronary Artery Risk Development in Young Adults (CARDIA)/Young Adult Longitudinal Trends in Antioxidants (YALT.' *Clinical chemistry*. 2007/01/18, 53(3) pp. 447–455.

Hsieh, N.-K., Wang, J.-Y., Liu, J.-C., Wang, S.-D. and Chen, H. I. (2004) 'Nitric oxide inhibition accelerates hypertension and induces perivascular inflammation in rats.' *Clinical and experimental pharmacology & physiology*. Australia, 31(4) pp. 212–218.

Hsu, H.-Y., Toth, S., Simpson, G. J. and Harris, M. T. (2015) 'Drop Printing of Pharmaceuticals: Effect of Molecular Weight on PEG Coated-Naproxen/PEG3350 Solid Dispersions.' *AIChE journal. American Institute of Chemical Engineers*, 61(2) pp. 4502–4508.

Huang, A., Sun, D., Kaley, G. and Koller, A. (1998) 'Superoxide Released to High Intra-arteriolar Pressure Reduces Nitric Oxide–Mediated Shear Stress– and Agonist-Induced Dilations.' *Circulation Research*. American Heart Association, 83(9) pp. 960–965.

Huang, X., Teng, X., Chen, D., Tang, F. and He, J. (2010) 'The effect of the shape of

mesoporous silica nanoparticles on cellular uptake and cell function.' *Biomaterials*. Netherlands, 31(3) pp. 438–448.

Ibrahim, I. A. M., Zikry, A. A. F. and Sharaf, M. A. (2010) 'Preparation of spherical silica nanoparticles : Stober silica,' 6(11) pp. 985–989.

Imig, J. D. (2016) 'Epoxyeicosatrienoic Acids and 20-Hydroxyeicosatetraenoic Acid on Endothelial and Vascular Function.' *Advances in pharmacology (San Diego, Calif.)*. United States, 77 pp. 105–141.

In, K., Park, J. and Park, H. (2006) 'Resveratrol at H igh D oses A cts as an A poptotic Inducer in E ndothelial C ells,' 38(1) pp. 48–53.

Iuga, C., Alvarez-Idaboy, J. R. and Russo, N. (2012) 'Antioxidant Activity of trans-Resveratrol toward Hydroxyl and Hydroperoxyl Radicals: A Quantum Chemical and Computational Kinetics Study.' *The Journal of Organic Chemistry*. American Chemical Society, 77(8) pp. 3868–3877.

Jain, A., Mehra, N. and Swarnakar, N. (2015) 'Role of Antioxidants for the Treatment of Cardiovascular Diseases: Challenges and Opportunities.' *Current pharmaceutical design*, 21, August.

Jennings, B. L., Montanez, D. E., May, M. E. J., Estes, A. M., Fang, X. R., Yaghini, F. A., Kanu, A. and Malik, K. U. (2014) 'Cytochrome P450 1B1 contributes to increased blood pressure and cardiovascular and renal dysfunction in spontaneously hypertensive rats.' *Cardiovascular drugs and therapy*. United States, 28(2) pp. 145–161.

Jennings, B. L., Seyhan, S. F., Estes, A. M., Das, K., Farjana, N., Fang, X. R., Gonzalez, F. J. and Kafait, M. (2010) 'Cytochrome P450 1B1 Contributes to Angiotensin II–Induced Hypertension and Associated Pathophysiology.' *Hypertension*. American Heart Association, 56(4) pp. 667–674.

Jurkić, L. M., Cepanec, I., Pavelić, S. K. and Pavelić, K. (2013) 'Biological and therapeutic effects of ortho-silicic acid and some ortho-silicic acid-releasing compounds: New perspectives for therapy.' *Nutrition & Metabolism*, 10(1) p. 2.

Kauffman, K. L., Culp, J. T., Goodman, A. and Matranga, C. (2011) 'FT-IR Study of CO2 Adsorption in a Dynamic Copper(II) Benzoate−Pyrazine Host with CO2−CO2 Interactions in the Adsorbed State.' *The Journal of Physical Chemistry C*. American

Chemical Society, 115(5) pp. 1857–1866.

Khan, A. A., Abdulbaqi, I. M., Abou Assi, R., Murugaiyah, V. and Darwis, Y. (2018) 'Lyophilized Hybrid Nanostructured Lipid Carriers to Enhance the Cellular Uptake of Verapamil: Statistical Optimization and In Vitro Evaluation.' *Nanoscale Research Letters*. Nanoscale Research Letters, 13.

Khoo, J. P., Zhao, L., Alp, N. J., Bendall, J. K., Nicoli, T., Rockett, K., Wilkins, M. R. and Channon, K. M. (2005) 'Pivotal role for endothelial tetrahydrobiopterin in pulmonary hypertension.' *Circulation*. United States, 111(16) pp. 2126–2133.

Khosa, A., Reddi, S. and Saha, R. N. (2018) 'Nanostructured lipid carriers for site-specific drug delivery.' *Biomedicine & Pharmacotherapy*, 103 pp. 598–613.

Khurana, R. K., Bansal, A. K., Beg, S., Burrow, A. J., Katare, O. P., Singh, K. K. and Singh, B. (2017) 'Enhancing biopharmaceutical attributes of phospholipid complex-loaded nanostructured lipidic carriers of mangiferin: Systematic development, characterization and evaluation.' *International journal of pharmaceutics*. Netherlands, 518(1–2) pp. 289–306.

King, A., Ndifon, C., Lui, S., Widdows, K., Kotamraju, V. R., Agemy, L., Teesalu, T., Glazier, J. D., Cellesi, F., Tirelli, N., Aplin, J. D., Ruoslahti, E. and Harris, L. K. (2016) 'Tumor-homing peptides as tools for targeted delivery of payloads to the placenta.' *Science Advances*, 2(5) p. e1600349.

Koller, A. and Huang, A. (1994) 'Impaired nitric oxide-mediated flow-induced dilation in arterioles of spontaneously hypertensive rats.' *Circulation research*. United States, 74(3) pp. 416–421.

Korsvik, C., Patil, S., Seal, S. and Self, W. T. (2007) 'Superoxide dismutase mimetic properties exhibited by vacancy engineered ceria nanoparticles.' *Chemical communications (Cambridge, England)*. England, (10) March, pp. 1056–1058.

Krętowski, R., Kusaczuk, M., Naumowicz, M., Kotyńska, J., Szynaka, B. and Cechowska-Pasko, M. (2017) 'The Effects of Silica Nanoparticles on Apoptosis and Autophagy of Glioblastoma Cell Lines.' *Nanomaterials* .

Krüger-Genge, A., Blocki, A., Franke, R.-P. and Jung, F. (2019) 'Vascular Endothelial Cell Biology: An Update.' *International journal of molecular sciences*. MDPI, 20(18) p.

4411.

Kurtz-Chalot, A., Villiers, C., Pourchez, J., Boudard, D., Martini, M., Marche, P. N., Cottier, M. and Forest, V. (2017) 'Impact of silica nanoparticle surface chemistry on protein corona formation and consequential interactions with biological cells.' *Materials Science and Engineering: C*, 75(Supplement C) pp. 16–24.

Kwon, H. J., Cha, M.-Y., Kim, D., Kim, D. K., Soh, M., Shin, K., Hyeon, T. and Mook-Jung, I. (2016) 'Mitochondria-Targeting Ceria Nanoparticles as Antioxidants for Alzheimer's Disease.' *ACS Nano*. American Chemical Society, 10(2) pp. 2860–2870.

Lai, C.-Y., Trewyn, B. G., Jeftinija, D. M., Jeftinija, K., Xu, S., Jeftinija, S. and Lin, V. S.-Y. (2003) 'A Mesoporous Silica Nanosphere-Based Carrier System with Chemically Removable CdS Nanoparticle Caps for Stimuli-Responsive Controlled Release of Neurotransmitters and Drug Molecules.' *Journal of the American Chemical Society*. American Chemical Society, 125(15) pp. 4451–4459.

LaMer, V. K. and Dinegar, R. H. (1950) 'Theory, Production and Mechanism of Formation of Monodispersed Hydrosols.' *Journal of the American Chemical Society*. American Chemical Society, 72(11) pp. 4847–4854.

Lan, F., Cacicedo, J. M., Ruderman, N. and Ido, Y. (2008) 'SIRT1 modulation of the acetylation status, cytosolic localization, and activity of LKB1. Possible role in AMP-activated protein kinase activation.' *The Journal of biological chemistry*. United States, 283(41) pp. 27628–27635.

Lan, F., Weikel, K. A., Cacicedo, J. M. and Ido, Y. (2017) 'Resveratrol-Induced AMP-Activated Protein Kinase Activation Is Cell-Type Dependent: Lessons from Basic Research for Clinical Application.' *Nutrients*. MDPI, 9(7) p. 751.

Lançon, A., Delma, D., Osman, H., Thénot, J.-P. and Latruffe N, B. J. (2004) 'Human hepatic cell uptake of resveratrol: involvement of both passive diffusion and carrier-mediated process.' *Biochemical and Biophysical Research Communications*, 316(4) pp. 1132–1137.

Lehman, S. E., Morris, A. S., Mueller, P. S., Salem, A. K., Grassian, V. H. and Larsen, S. C. (2016) 'Silica Nanoparticle-Generated ROS as a Predictor of Cellular Toxicity: Mechanistic Insights and Safety by Design.' *Environmental science. Nano*. 2015/11/10,

3(1) pp. 56–66.

Lennicke, C., Rahn, J., Lichtenfels, R., Wessjohann, L. A. and Seliger, B. (2015) 'Hydrogen peroxide – production, fate and role in redox signaling of tumor cells.' *Cell Communication and Signaling*, 13(1) p. 39.

Leonard, S. S., Xia, C., Jiang, B.-H., Stinefelt, B., Klandorf, H., Harris, G. K. and Shi, X. (2003) 'Resveratrol scavenges reactive oxygen species and effects radical-induced cellular responses.' *Biochemical and biophysical research communications*. United States, 309(4) pp. 1017–1026.

Levine, G. N., Frei, B., Koulouris, S. N., Gerhard, M. D., Keaney, J. F. J. and Vita, J. A. (1996) 'Ascorbic acid reverses endothelial vasomotor dysfunction in patients with coronary artery disease.' *Circulation*. United States, 93(6) pp. 1107–1113.

Li, H.-F., Tian, Z.-F., Qiu, X.-Q., Wu, J.-X., Zhang, P. and Jia, Z.-J. (2006) 'A study of mechanisms involved in vasodilatation induced by resveratrol in isolated porcine coronary artery.' *Physiological research*. Czech Republic, 55(4) pp. 365–372.

Li, H., Chen, M., Su, Z., Sun, M. and Ping, Q. (2016) 'Size-exclusive effect of nanostructured lipid carriers on oral drug delivery.' *International journal of pharmaceutics*. Netherlands, 511(1) pp. 524–537.

Li, M., Du, C., Guo, N., Teng, Y., Meng, X., Sun, H., Li, S., Yu, P. and Galons, H. (2019) 'Composition design and medical application of liposomes.' *European Journal of Medicinal Chemistry*, 164 pp. 640–653.

Limbu, R., Cottrell, G. S. and McNeish, A. J. (2018) 'Characterisation of the vasodilation effects of DHA and EPA, n-3 PUFAs (fish oils), in rat aorta and mesenteric resistance arteries.' *PloS one*. Public Library of Science, 13(2) pp. e0192484–e0192484.

Lin, H.-S., Choo, Q.-Y. and Ho, P. C. (2010) 'Quantification of oxyresveratrol analog trans-2,4,3',5'-tetramethoxystilbene in rat plasma by a rapid HPLC method: application in a pre-clinical pharmacokinetic study.' *Biomedical chromatography : BMC*. England, 24(12) pp. 1373–1378.

Lin, H.-S., Zhang, W., Go, M. L., Tringali, C., Spatafora, C. and Ho, P. C. (2011) 'Quantification of trans-3,4,5,4'-Tetramethoxystilbene in rat plasma by HPLC: application to pharmacokinetic study.' *Journal of agricultural and food chemistry*.

United States, 59(4) pp. 1072–1077.

Lind, J. and Merényi, G. (2006) ‘Kinetic and Thermodynamic Properties of the Aminoxyl (NH2O•) Radical.’ *The Journal of Physical Chemistry A*. American Chemical Society, 110(1) pp. 192–197.

Linder, L., Kiowski, W., Buhler, F. R. and Luscher, T. F. (1990) ‘Indirect evidence for release of endothelium-derived relaxing factor in human forearm circulation in vivo. Blunted response in essential hypertension.’ *Circulation*. United States, 81(6) pp. 1762–1767.

Lu, J., Liong, M., Li, Z., Zink, J. I. and Tamanoi, F. (2010) ‘Biocompatibility, Biodistribution, and Drug-Delivery Efficiency of Mesoporous Silica Nanoparticles for Cancer Therapy in Animals.’ *Small (Weinheim an der Bergstrasse, Germany)*, 6(16) pp. 1794–1805.

Lu, J., Liong, M., Zink, J. I. and Tamanoi, F. (2007) ‘Mesoporous Silica Nanoparticles as a Delivery System for Hydrophobic Anticancer Drugs.’ *Small*. WILEY-VCH Verlag, 3(8) pp. 1341–1346.

Luo, T., Deng, Z., Li, X., Rao, H. and Fan, Y. (2014) ‘Triolein and trilinolein ameliorate oxidized low-density lipoprotein-induced oxidative stress in endothelial cells.’ *Lipids*. United States, 49(5) pp. 495–504.

Ma, S., Feng, J., Zhang, R., Chen, J., Han, D., Li, Xiang, Yang, B., Li, Xiujuan, Fan, M., Li, C., Tian, Z., Wang, Y. and Cao, F. (2017) ‘SIRT1 Activation by Resveratrol Alleviates Cardiac Dysfunction via Mitochondrial Regulation in Diabetic Cardiomyopathy Mice.’ *Oxidative Medicine and Cellular Longevity*, 2017 pp. 1–15.

van der Made, S. M., Plat, J. and Mensink, R. P. (2015) ‘Resveratrol Does Not Influence Metabolic Risk Markers Related to Cardiovascular Health in Overweight and Slightly Obese Subjects: A Randomized, Placebo-Controlled Crossover Trial.’ *PLOS ONE*. Public Library of Science, 10(3) p. e0118393.

Magyar, K., Halmosi, R., Palfi, A., Feher, G., Czopf, L., Fulop, A., Battyany, I., Sumegi, B., Toth, K. and Szabados, E. (2012) ‘Cardioprotection by resveratrol: A human clinical trial in patients with stable coronary artery disease.’ *Clinical hemorheology and microcirculation*. Netherlands, 50(3) pp. 179–187.

Makino, K., Mossoba, M. M. and Riesz, P. (1983) ‘Chemical effects of ultrasound on aqueous solutions. Formation of hydroxyl radicals and hydrogen atoms.’ *The Journal of Physical Chemistry*. American Chemical Society, 87(8) pp. 1369–1377.

Maria, A., Cossu, A., Giordo, R. and Zinellu, A. (2015) ‘Resveratrol alters human endothelial cells redox state and causes mitochondrial-dependent cell death.’ *Food and Chemical Toxicology*. Elsevier Ltd, 78 pp. 10–16.

Martins, L. A. M., Coelho, B. P., Behr, G., Pettenuzzo, L. F., Souza, I. C. C., Moreira, J. C. F., Borojevic, R., Gottfried, C. and Guma, F. C. R. (2014) ‘Resveratrol induces pro-oxidant effects and time-dependent resistance to cytotoxicity in activated hepatic stellate cells.’ *Cell biochemistry and biophysics*. United States, 68(2) pp. 247–257.

Massaro, M., Scoditti, E., Carluccio, M. A. and De Caterina, R. (2019) ‘Oxidative stress and vascular stiffness in hypertension: A renewed interest for antioxidant therapies?’ *Vascular pharmacology*. United States, 116, May, pp. 45–50.

McDonald, T. F. and Chandler, A. B. (1981) ‘Connective Tissues in Arterial and Pulmonary Disease.’ *In*. 1st ed., Springer-Verlag New York, pp. 66–72.

Mehta, R. T. (1996) ‘Liposome encapsulation of clofazimine reduces toxicity in vitro and in vivo and improves therapeutic efficacy in the beige mouse model of disseminated Mycobacterium avium-M. intracellulare complex infection.’ *Antimicrobial Agents and Chemotherapy*, 40(8) pp. 1893–1902.

Mendoza, S. A., Fang, J., Gutterman, D. D., Wilcox, D. A., Bubolz, A. H., Li, R., Suzuki, M. and Zhang, D. X. (2010) ‘TRPV4-mediated endothelial Ca2+ influx and vasodilation in response to shear stress.’ *American journal of physiology. Heart and circulatory physiology*. 2009/12/04, American Physiological Society, 298(2) pp. H466–H476.

Minarchick, V. C., Stapleton, P. A., Sabolsky, E. M. and Nurkiewicz, T. R. (2015) ‘Cerium Dioxide Nanoparticle Exposure Improves Microvascular Dysfunction and Reduces Oxidative Stress in Spontaneously Hypertensive Rats.’ *Frontiers in Physiology*. Frontiers Media S.A., 6, November, p. 339.

Mitchell, J. A. and Kirkby, N. S. (2019) ‘Eicosanoids, prostacyclin and cyclooxygenase in the cardiovascular system.’ *British journal of pharmacology*. England, 176(8) pp.

1038–1050.

Miura, H. and Gutterman, D. D. (1998) ‘Human coronary arteriolar dilation to arachidonic acid depends on cytochrome P-450 monooxygenase and Ca2+-activated K+ channels.’ *Circulation research*. United States, 83(5) pp. 501–507.

Miura, H., Wachtel, R. E., Liu, Y., Loberiza, F. R. J., Saito, T., Miura, M. and Gutterman, D. D. (2001) ‘Flow-induced dilation of human coronary arterioles: important role of Ca(2+)-activated K(+) channels.’ *Circulation*. United States, 103(15) pp. 1992–1998.

Mohammadi, M. R., Malkovskiy, A. V, Jothimuthu, P., Kim, K.-M., Parekh, M., Inayathullah, M., Zhuge, Y. and Rajadas, J. (2018) ‘PEG/Dextran Double Layer Influences Fe Ion Release and Colloidal Stability of Iron Oxide Nanoparticles.’ *Scientific reports*. Nature Publishing Group UK, 8(1) p. 4286.

Mollnau, H., Wendt, M., Szocs, K., Lassegue, B., Schulz, E., Oelze, M., Li, H., Bodenschatz, M., August, M., Kleschyov, A. L., Tsilimingas, N., Walter, U., Forstermann, U., Meinertz, T., Griendling, K. and Munzel, T. (2002) ‘Effects of angiotensin II infusion on the expression and function of NAD(P)H oxidase and components of nitric oxide/cGMP signaling.’ *Circulation research*. United States, 90(4) pp. E58-65.

Morris, A. S., Adamcakova-Dodd, A., Lehman, S. E., Wongrakpanich, A., Thorne, P. S., Larsen, S. C. and Salem, A. K. (2016) ‘Amine modification of nonporous silica nanoparticles reduces inflammatory response following intratracheal instillation in murine lungs.’ *Toxicology letters*. 2015/11/10, 241, January, pp. 207–215.

Munusamy, P., Sanghavi, S., Varga, T. and Suntharampillai, T. (2014) ‘Silica supported ceria nanoparticles: a hybrid nanostructure to increase stability and surface reactivity of nano-crystalline ceria.’ *RSC Adv.* The Royal Society of Chemistry, 4(17) pp. 8421–8430.

Murali, V. S., Wang, R., Mikoryak, C. A., Pantano, P. and Draper, R. (2015) ‘Rapid detection of polyethylene glycol sonolysis upon functionalization of carbon nanomaterials.’ *Experimental biology and medicine (Maywood, N.J.)*. England, 240(9) pp. 1147–1151.

Naderali, E. K., Doyle, P. J. and Williams, G. (2000) ‘Resveratrol induces vasorelaxation of mesenteric and uterine arteries from female guinea-pigs.’ *Clinical science (London, England : 1979)*. England, 98(5) pp. 537–543.

Naderali, E. K., Smith, S. L., Doyle, P. J. and Williams, G. (2001) ‘The mechanism of resveratrol-induced vasorelaxation differs in the mesenteric resistance arteries of lean and obese rats.’ *Clinical science (London, England : 1979)*. England, 100(1) pp. 55–60.

Nagao, T., Illiano, S. and Vanhoutte, P. M. (1992) ‘Heterogeneous distribution of endothelium-dependent relaxations resistant to NG-nitro-L-arginine in rats.’ *The American journal of physiology*. United States, 263(4 Pt 2) pp. H1090-4.

Napierska, D., Thomassen, L. C. J., Rabolli, V., Lison, D., Gonzalez, L., Kirsch-Volders, M., Martens, J. A. and Hoet, P. H. (2009) ‘Size-dependent cytotoxicity of monodisperse silica nanoparticles in human endothelial cells.’ *Small (Weinheim an der Bergstrasse, Germany)*. Germany, 5(7) pp. 846–853.

Nash, T., Allison, A. C. and Harington, J. S. (1966) ‘Physico-Chemical Properties of Silica in Relation to its Toxicity.’ *Nature*, 210(5033) pp. 259–261.

Nawaz, W., Zhou, Z., Deng, S., Ma, Xiaodong, Ma, Xiaochi, Li, C. and Shu, X. (2017) ‘Therapeutic Versatility of Resveratrol Derivatives.’ *Nutrients*. Switzerland, 9(11).

Nemmar, A., Albarwani, S., Beegam, S., Yuvaraju, P., Yasin, J., Attoub, S. and Ali, B. H. (2014) ‘Amorphous silica nanoparticles impair vascular homeostasis and induce systemic inflammation.’ *International Journal of Nanomedicine*, 9(1) pp. 2279–2789.

Neves, A. and Queiroz, J. (2016) ‘Cellular uptake and transcytosis of lipid-based nanoparticles across the intestinal barrier: Relevance for oral drug delivery.’ *Journal of colloid and interface science*. United States, 463, February, pp. 258–265.

Neves, A., Queiroz, J. and Reis, S. (2016) ‘Brain-targeted delivery of resveratrol using solid lipid nanoparticles functionalized with apolipoprotein E.’ *Journal of nanobiotechnology*. BioMed Central, 14, April, p. 27.

Neves, A. R., Lucio, M., Martins, S., Lima, J. L. C. and Reis, S. (2013) ‘Novel resveratrol nanodelivery systems based on lipid nanoparticles to enhance its oral bioavailability.’ *International journal of nanomedicine*. New Zealand, 8 pp. 177–187.

Nishikawa, Y. and Ogawa, S. (1997) ‘Importance of Nitric Oxide in the Coronary

Artery at Rest and During Pacing in Humans.' *Journal of the American College of Cardiology*, 29(1) pp. 85–92.

Nishikawa, Y., Stepp, D. W. and Chilian, W. M. (1999) 'In vivo location and mechanism of EDHF-mediated vasodilation in canine coronary microcirculation.' *The American journal of physiology*. United States, 277(3) pp. H1252-9.

Noronha-Dutra, A. A., Epperlein, M. M. and Woolf, N. (1993) 'Reaction of nitric oxide with hydrogen peroxide to produce potentially cytotoxic singlet oxygen as a model for nitric oxide-mediated killing.' *FEBS letters*. England, 321(1) pp. 59–62.

Nwachukwu, J. C., Srinivasan, S., Bruno, N. E., Parent, A. A., Hughes, T. S., Pollock, J. A., Gjyshi, O., Cavett, V., Nowak, J., Garcia-Ordonez, R. D., Houtman, R., Griffin, P. R., Kojetin, D. J., Katzenellenbogen, J. A., Conkright, M. D. and Nettles, K. W. (2014) 'Resveratrol modulates the inflammatory response via an estrogen receptor-signal integration network.' *eLife*, 2014(3).

Ozkor, M. A., Murrow, J. R., Rahman, A. M., Kavtaradze, N., Lin, J., Manatunga, A. and Quyyumi, A. A. (2011) 'Endothelium-derived hyperpolarizing factor determines resting and stimulated forearm vasodilator tone in health and in disease.' *Circulation*. United States, 123(20) pp. 2244–2253.

Ozkor, M. and Quyyumi, A. (2011) 'Endothelium-Derived Hyperpolarizing Factor and Vascular Function.' *Cardiology research and practice*, 2011, August, p. 156146.

Panday, A., Sahoo, M. K., Osorio, D. and Batra, S. (2015) 'NADPH oxidases: an overview from structure to innate immunity-associated pathologies.' *Cell Mol Immunol*. Chinese Society of Immunology and The University of Science and Technology, 12(1) pp. 5–23.

Pattni, B. S., Chupin, V. V and Torchilin, V. P. (2015) 'New Developments in Liposomal Drug Delivery.' *Chemical Reviews*. American Chemical Society, 115(19) pp. 10938–10966.

Paulis, L., Zicha, J., Kunes, J., Hojna, S., Behuliak, M., Celec, P., Kojsova, S., Pechanova, O. and Simko, F. (2008) 'Regression of L-NAME–Induced Hypertension: The Role of Nitric Oxide and Endothelium-Derived Constricting Factor.' *Hypertension Research*, 31(4) pp. 793–803.

Peluffo, G., Calcerrada, P., Piacenza, L., Pizzano, N. and Radi, R. (2009) 'Superoxide-mediated inactivation of nitric oxide and peroxynitrite formation by tobacco smoke in vascular endothelium: studies in cultured cells and smokers.' *American journal of physiology. Heart and circulatory physiology*. 2009/04/10, American Physiological Society, 296(6) pp. H1781–H1792.

Piazzini, V., Lemmi, B., D'Ambrosio, M., Cinci, L., Luceri, C., Bilia, R. A. and Bergonzi, C. M. (2018) 'Nanostructured Lipid Carriers as Promising Delivery Systems for Plant Extracts: The Case of Silymarin.' *Applied Sciences* .

Pineda-Sanabria, S. E., Robertson, I. M. and Sykes, B. D. (2011) 'Structure of trans-resveratrol in complex with the cardiac regulatory protein troponin C.' *Biochemistry*. United States, 50(8) pp. 1309–1320.

Popescu, B. F. G. and Nichol, H. (2011) 'Mapping brain metals to evaluate therapies for neurodegenerative disease.' *CNS neuroscience & therapeutics*. England, 17(4) pp. 256–268.

Pople, P. and Singh, K. (2011) 'Development and evaluation of colloidal modified nanolipid carrier: Application to topical delivery of tacrolimus.' *European journal of pharmaceutics and biopharmaceutics : official journal of Arbeitsgemeinschaft für Pharmazeutische Verfahrenstechnik e.V*, 79, March, pp. 82–94.

Porkert, M., Sher, S., Reddy, U., Cheema, F., Niessner, C., Kolm, P., Jones, D. P., Hooper, C., Taylor, W. R., Harrison, D. and Quyyumi, A. A. (2008) 'Tetrahydrobiopterin: a novel antihypertensive therapy.' *Journal of Human Hypertension*, 22(6) pp. 401–407.

Pourageaud, F. and Freslon, J. L. (1995) 'Endothelial and smooth muscle properties of coronary and mesenteric resistance arteries in spontaneously hypertensive rats compared to WKY rats.' *Fundamental & clinical pharmacology*. England, 9(1) pp. 37–45.

Pozzi, D., Colapicchioni, V., Caracciolo, G., Piovesana, S., Capriotti, A. L., Palchetti, S., De Grossi, S., Riccioli, A., Amenitsch, H. and Laganà, A. (2014) 'Effect of polyethyleneglycol (PEG) chain length on the bio–nano-interactions between PEGylated lipid nanoparticles and biological fluids: from nanostructure to uptake in cancer cells.' *Nanoscale*. The Royal Society of Chemistry, 6(5) pp. 2782–2792.

Prades, J., Funari, S. S., Escriba, P. V and Barcelo, F. (2003) ‘Effects of unsaturated fatty acids and triacylglycerols on phosphatidylethanolamine membrane structure.’ *Journal of lipid research*. United States, 44(9) pp. 1720–1727.

Prasad, S., Gupta, S. C. and Tyagi, A. K. (2017) ‘Reactive oxygen species (ROS) and cancer: Role of antioxidative nutraceuticals.’ *Cancer Letters*. Elsevier, 387, August, pp. 95–105.

Pritz, C. O., Bitsche, M., Salvenmoser, W., Dudas, J., Schrott-Fischer, A. and Glueckert, R. (2013) ‘Endocytic trafficking of silica nanoparticles in a cell line derived from the organ of Corti.’ *Nanomedicine (London, England)*. England, 8(2) pp. 239–252.

Quignard, S., Coradin, T., Powell, J. J. and Jugdaohsingh, R. (2017) ‘Silica nanoparticles as sources of silicic acid favoring wound healing in vitro.’ *Colloids and surfaces. B, Biointerfaces*. Netherlands, 155, July, pp. 530–537.

Quyyumi, A. A., Dakak, N., Andrews, N. P., Gilligan, D. M., Panza, J. A. and Cannon, R. O. 3rd (1995) ‘Contribution of nitric oxide to metabolic coronary vasodilation in the human heart.’ *Circulation*. United States, 92(3) pp. 320–326.

Raj, T. A. S., Smith, A. M. and Moore, A. S. (2013) ‘Vincristine sulfate liposomal injection for acute lymphoblastic leukemia.’ *International journal of nanomedicine*. 2013/11/06, Dove Medical Press, 8 pp. 4361–4369.

Rakici, O., Kiziltepe, U., Coskun, B., Aslamaci, S. and Akar, F. (2005) ‘Effects of resveratrol on vascular tone and endothelial function of human saphenous vein and internal mammary artery.’ *International journal of cardiology*. Netherlands, 105(2) pp. 209–215.

Ramanathan, T. and Skinner, H. (2005) ‘Coronary blood flow.’ *Continuing Education in Anaesthesia Critical Care & Pain*, 5(2) pp. 61–64.

Ratola, N., Faria, J. and Alves, A. (2004) ‘Analysis and Quantification of trans-Resveratrol in Wines from Alentejo Region (Portugal).’ *Food Technology and Biotechnology*, 42, April, pp. 125–130.

Rejman, J., Oberle, V., Zuhorn, I. S. and Hoekstra, D. (2004) ‘Size-dependent internalization of particles via the pathways of clathrin- and caveolae-mediated endocytosis.’ *The Biochemical journal*. England, 377(Pt 1) pp. 159–169.

Rhoads, J. P. and Major, A. S. (2018) 'How Oxidized Low-Density Lipoprotein Activates Inflammatory Responses.' *Critical reviews in immunology*, 38(4) pp. 333–342.

Royaume, U. (2011) 'PAS71-2011-Nanoparticles – Vocabulary.' *BSI Standards Publication*.

Ruisanchez, É., Dancs, P., Kerék, M., Németh, T., Faragó, B., Balogh, A., Patil, R., Jennings, B. L., Liliom, K., Malik, K. U., Smrcka, A. V, Tigyi, G. and Benyó, Z. (2014) 'Lysophosphatidic acid induces vasodilation mediated by LPA1 receptors, phospholipase C, and endothelial nitric oxide synthase.' *FASEB journal : official publication of the Federation of American Societies for Experimental Biology*. 2013/11/18, Federation of American Societies for Experimental Biology, 28(2) pp. 880–890.

Rzigalinski, B. A., Meehan, K., Davis, R. M., Xu, Y., Miles, W. C. and Cohen, C. A. (2006) 'Radical nanomedicine.' *Nanomedicine (London, England)*. England, 1(4) pp. 399–412.

Sahan-Firat, S., Jennings, B. L., Yaghini, F. A., Song, C. Y., Estes, A. M., Fang, X. R., Farjana, N., Khan, A. I. and Malik, K. U. (2010) '2,3',4,5'-Tetramethoxystilbene prevents deoxycorticosterone-salt-induced hypertension: contribution of cytochrome P-450 1B1.' *American journal of physiology. Heart and circulatory physiology*. 2010/09/17, American Physiological Society, 299(6) pp. H1891–H1901.

Sale, S., Verschoyle, R. D., Boocock, D., Jones, D. J. L., Wilsher, N., Ruparelia, K. C., Potter, G. A., Farmer, P. B., Steward, W. P. and Gescher, A. J. (2004) 'Pharmacokinetics in mice and growth-inhibitory properties of the putative cancer chemopreventive agent resveratrol and the synthetic analogue trans 3,4,5,4'-tetramethoxystilbene.' *British journal of cancer*. England, 90(3) pp. 736–744.

Salgin, S., Salgın, U. and Bahadır, S. (2013) 'Zeta Potentials and Isoelectric Points of Biomolecules: The Effects of Ion Types and Ionic Strengths.' *International journal of electrochemical science*, 7, January, p. 12404.

Salheen, S. M., Panchapakesan, U., Pollock, C. A. and Woodman, O. L. (2015) 'The Dipeptidyl Peptidase-4 Inhibitor Linagliptin Preserves Endothelial Function in Mesenteric Arteries from Type 1 Diabetic Rats without Decreasing Plasma Glucose.'

PLOS ONE. Public Library of Science, 10(11) p. e0143941.

de Santi, C., Pietrabissa, A., Mosca, F. and Pacifici, G. M. (2000) 'Glucuronidation of resveratrol, a natural product present in grape and wine, in the human liver.' *Xenobiotica; the fate of foreign compounds in biological systems*. England, 30(11) pp. 1047–1054.

Sayin, O., Arslan, N. and Guner, G. (2012) 'The protective effects of resveratrol on human coronary artery endothelial cell damage induced by hydrogen peroxide in vitro.' *Acta clinica Croatica*. Croatia, 51(2) pp. 227–235.

Schildmeyer, L. A. and Bryan, R. M. (2002) 'Effect of NO on EDHF response in rat middle cerebral arteries.' *American Journal of Physiology-Heart and Circulatory Physiology*. American Physiological Society, 282(2) pp. H734–H738.

Schmitt, C. A., Heiss, E. H. and Dirsch, V. M. (2010) 'Effect of resveratrol on endothelial cell function: Molecular mechanisms.' *BioFactors*, 36(5) pp. 342–349.

El Shaer, S. S., Salaheldin, T. A., Saied, N. M. and Abdelazim, S. M. (2017) 'In vivo ameliorative effect of cerium oxide nanoparticles in isoproterenol-induced cardiac toxicity.' *Experimental and Toxicologic Pathology*.

Shah, N. V, Seth, A. K., Balaraman, R., Aundhia, C. J., Maheshwari, R. A. and Parmar, G. R. (2016) 'Nanostructured lipid carriers for oral bioavailability enhancement of raloxifene: Design and in vivo study.' *Journal of Advanced Research*, 7(3) pp. 423–434.

Shang, Y., Zhu, T., Li, Y. and Zhao, J. (2009) 'Size-dependent hydroxyl radicals generation induced by SiO2 ultra-fine particles: The role of surface iron.' *Science in China Series B: Chemistry*, 52(7) pp. 1033–1041.

Shimokawa, H. (2010) 'Hydrogen peroxide as an endothelium-derived hyperpolarizing factor.' *Pflugers Archiv : European journal of physiology*. Germany, 459(6) pp. 915–922.

Shin, S., Song, I. and Um, S. (2015) 'Role of Physicochemical Properties in Nanoparticle Toxicity.' *Nanomaterials*, 5(3) pp. 1351–1365.

Shukur, A., Whitehead, D., Seifalian, A. and Azzawi, M. (2016) 'The influence of silica nanoparticles on small mesenteric arterial function.' *Nanomedicine*, 11(16) pp. 2131–2146.

Silva, C. G., Monteiro, J., Marques, R. R. N., Silva, A. M. T., Martinez, C., Canle, M. and Faria, J. L. (2013) 'Photochemical and photocatalytic degradation of trans-resveratrol.' *Photochemical & photobiological sciences : Official journal of the European Photochemistry Association and the European Society for Photobiology*. England, 12(4) pp. 638–644.

Simone, G., H., H. R., Dick, de Z. and Hendrik, B. (2003) 'Coronary Myogenic Constriction Antagonizes EDHF-Mediated Dilation.' *Hypertension*. American Heart Association, 41(4) pp. 912–918.

Sinha, K., Chaudhary, G. and Gupta, Y. K. (2002) 'Protective effect of resveratrol against oxidative stress in middle cerebral artery occlusion model of stroke in rats.' *Life sciences*. Netherlands, 71(6) pp. 655–665.

Sipkema, P., Van Der Linden, P. J. W., Westerhof, N. and Yin, F. C. P. (2003) 'Effect of cyclic axial stretch of rat arteries on endothelial cytoskeletal morphology and vascular reactivity.' *Journal of Biomechanics*, 36(5) pp. 653–659.

Sobey, C. G., Heistad, D. D. and Faraci, F. M. (1997) 'Mechanisms of bradykinin-induced cerebral vasodilatation in rats. Evidence that reactive oxygen species activate K+ channels.' *Stroke*. United States, 28(11) pp. 2290–4; discussion 2295.

Son, G.-H., Na, Y.-G., Huh, H. W., Wang, M., Kim, M.-K., Han, M.-G., Byeon, J.-J., Lee, H.-K. and Cho, C.-W. (2019) 'Systemic Design and Evaluation of Ticagrelor-Loaded Nanostructured Lipid Carriers for Enhancing Bioavailability and Antiplatelet Activity.' *Pharmaceutics*. Switzerland, 11(5).

Stewart, J., Manmathan, G. and Wilkinson, P. (2017) 'Primary prevention of cardiovascular disease: A review of contemporary guidance and literature.' *JRSM cardiovascular disease*. SAGE Publications, 6, January, pp. 2048004016687211–2048004016687211.

Stöber, W., Fink, A. and Bohn, E. (1968) 'Controlled growth of monodisperse silica spheres in the micron size range.' *Journal of Colloid and Interface Science*, 26(1) pp. 62–69.

Suk, J. S., Xu, Q., Kim, N., Hanes, J. and Ensign, L. M. (2016) 'PEGylation as a strategy for improving nanoparticle-based drug and gene delivery.' *Advanced drug*

delivery reviews. Netherlands, 99(Pt A) pp. 28–51.

Suzuki, H. (1967) 'Chapter 2 - Molecular Orbital Theory.' *In* SUZUKI, H. B. T.-E. A. S. and G. of O. M. (ed.). Academic Press, pp. 10–34.

Szende, B. and Tyihák, E. (2000) 'Dose-dependent effect of resveratrol on proliferation and apoptosis in endothelial and tumor cell cultures,' 32(2) pp. 88–92.

Szoka Jr, F. C., Milholland, D. and Barza, M. (1987) 'Effect of lipid composition and liposome size on toxicity and in vitro fungicidal activity of liposome-intercalated amphotericin B.' *Antimicrobial agents and chemotherapy*, 31(3) pp. 421–429.

Tejero, J., Shiva, S. and Gladwin, M. T. (2019) 'Sources of Vascular Nitric Oxide and Reactive Oxygen Species and Their Regulation.' *Physiological reviews*. United States, 99(1) pp. 311–379.

Teskac, K. and Kristl, J. (2010) 'The evidence for solid lipid nanoparticles mediated cell uptake of resveratrol.' *International journal of pharmaceutics*. Netherlands, 390(1) pp. 61–69.

Theodotou, M., Fokianos, K., Mouzouridou, A., Konstantinou, C., Aristotelous, A., Prodromou, D. and Chrysikou, A. (2017) 'The effect of resveratrol on hypertension: A clinical trial.' *Experimental and Therapeutic Medicine*. D.A. Spandidos, 13(1) pp. 295–301.

Thomas, W., Göran, D., Thomas, T., Henrik, A., Huige, L., Klaus, W. and Ulrich, F. (2002) 'Resveratrol, a Polyphenolic Phytoalexin Present in Red Wine, Enhances Expression and Activity of Endothelial Nitric Oxide Synthase.' *Circulation*. American Heart Association, 106(13) pp. 1652–1658.

Tong, L., Wei, Q., Wei, A. and Cheng, J.-X. (2009) 'Gold nanorods as contrast agents for biological imaging: optical properties, surface conjugation, and photothermal effects.' *Photochemistry and photobiology*, 85(1) p. 21.

Torok, J. and Kristek, F. (2002) 'Beneficial effect of pentaerythrityl tetranitrate on functional and morphological changes in the rat thoracic aorta evoked by long-term nitric oxide synthase inhibition.' *Vascular pharmacology*, 38, April, pp. 177–182.

Toth, P., Tarantini, S., Springo, Z., Tucsek, Z., Gautam, T., Giles, C. B., Wren, J. D., Koller, A., Sonntag, W. E., Csiszar, A. and Ungvari, Z. (2015) 'Aging exacerbates

hypertension-induced cerebral microhemorrhages in mice: role of resveratrol treatment in vasoprotection.' *Aging cell*. England, 14(3) pp. 400–408.

Toyotaka, Y., Hiroaki, S., Osamu, H., Tatsuya, K., Fumiyuki, S., Masami, G., Yasuo, O. and Fumihiko, K. (2003) 'Hydrogen Peroxide, an Endogenous Endothelium-Derived Hyperpolarizing Factor, Plays an Important Role in Coronary Autoregulation In Vivo.' *Circulation*. American Heart Association, 107(7) pp. 1040–1045.

Tsuga, H., Okuno, E., Kameyama, K. and Haga, T. (1998) 'Sequestration of human muscarinic acetylcholine receptor hm1-hm5 subtypes: effect of G protein-coupled receptor kinases GRK2, GRK4, GRK5 and GRK6.' *The Journal of pharmacology and experimental therapeutics*. United States, 284(3) pp. 1218–1226.

Tursilli, R., Casolari, A., Iannuccelli, V. and Scalia, S. (2006) 'Enhancement of melatonin photostability by encapsulation in lipospheres.' *Journal of pharmaceutical and biomedical analysis*. England, 40(4) pp. 910–914.

Ungvari, Z., Csiszar, A., Huang, A., Kaminski, P. M., Wolin, M. S. and Koller, A. (2003) 'High pressure induces superoxide production in isolated arteries via protein kinase C-dependent activation of NAD(P)H oxidase.' *Circulation*, 108(10) pp. 1253–1258.

Ungvari, Z., Csiszar, A., Kaminski, P. M., Wolin, M. S. and Koller, A. (2004) 'Chronic high pressure-induced arterial oxidative stress: involvement of protein kinase C-dependent NAD(P)H oxidase and local renin-angiotensin system.' *The American journal of pathology*. American Society for Investigative Pathology, 165(1) pp. 219–226.

Ungvari, Z., Labinskyy, N., Mukhopadhyay, P., Pinto, J. T., Bagi, Z., Ballabh, P., Zhang, C., Pacher, P. and Csiszar, A. (2009) 'Resveratrol attenuates mitochondrial oxidative stress in coronary arterial endothelial cells.' *American Journal of Physiology-Heart and Circulatory Physiology*, 297(5) pp. H1876–H1881.

Urakami, L. H., Shimokawa, H., Nakashima, M., Egashira, K. and Takeshita, A. (1997) 'Importance of endothelium-derived hyperpolarizing factor in human arteries.' *The Journal of clinical investigation*. United States, 100(11) pp. 2793–2799.

Urich, E., Schmucki, R., Ruderisch, N., Kitas, E., Certa, U., Jacobsen, H., Schweitzer,

C., Bergadano, A., Ebeling, M., Loetscher, H. and Freskgård, P.-O. (2015) ‘Cargo Delivery into the Brain by in vivo identified Transport Peptides.’ *Scientific Reports*, 5(1) p. 14104.

Vecchione, C., Carnevale, D., Di Pardo, A., Gentile, M. T., Damato, A., Cocozza, G., Antenucci, G., Mascio, G., Bettarini, U., Landolfi, A., Iorio, L., Maffei, A. and Lembo, G. (2009) ‘Pressure-induced vascular oxidative stress is mediated through activation of integrin-linked kinase 1/betaPIX/Rac-1 pathway.’ *Hypertension (Dallas, Tex. : 1979)*. United States, 54(5) pp. 1028–1034.

Večeř, M. and Pospíšil, J. (2012) ‘Stability and Rheology of Aqueous Suspensions.’ *Procedia Engineering*, 42(Supplement C) pp. 1720–1725.

Vessieres, E., Belin De Chantemèle, E., Toutain, B., Guihot, A.-L., Jardel, A., Loufrani, L. and Henrion, D. (2010) ‘Cyclooxygenase-2 Inhibition Restored Endothelium-Mediated Relaxation in Old Obese Zucker Rat Mesenteric Arteries.’ *Frontiers in Physiology*, 1 p. 145.

Vidrio, E., Jung, H. and Anastasio, C. (2008) ‘Generation of hydroxyl radicals from dissolved transition metals in surrogate lung fluid solutions.’ *Atmospheric Environment*, 42(18) pp. 4369–4379.

Wahajuddin and Arora, S. (2012) ‘Superparamagnetic iron oxide nanoparticles: Magnetic nanoplatforms as drug carriers.’ *International Journal of Nanomedicine*, 7 pp. 3445–3471.

Wang, Y., Romigh, T., He, X., Orloff, M. S., Silverman, R. H., Heston, W. D. and Eng, C. (2010) ‘Resveratrol regulates the PTEN/AKT pathway through androgen receptor-dependent and -independent mechanisms in prostate cancer cell lines.’ *Human Molecular Genetics*, 19(22) pp. 4319–4329.

Wang, Z., Tiruppathi, C., Minshall, R. D. and Malik, A. B. (2009) ‘Size and dynamics of caveolae studied using nanoparticles in living endothelial cells.’ *ACS nano*, 3(12) pp. 4110–4116.

Watt, P. A. and Thurston, H. (1989) ‘Endothelium-dependent relaxation in resistance vessels from the spontaneously hypertensive rats.’ *Journal of hypertension*. England, 7(8) pp. 661–666.

Wei, E. P., Kontos, H. A. and Beckman, J. S. (1996) ‘Mechanisms of cerebral vasodilation by superoxide, hydrogen peroxide, and peroxynitrite.’ *The American journal of physiology*. United States, 271(3 Pt 2) pp. H1262-6.

Wei, E. P., Kontos, H. A., Christman, C. W., DeWitt, D. S. and Povlishock, J. T. (1985) ‘Superoxide generation and reversal of acetylcholine-induced cerebral arteriolar dilation after acute hypertension.’ *Circulation research*. United States, 57(5) pp. 781–787.

Willis, A. P. and Leffler, C. W. (1999) ‘NO and prostanoids: age dependence of hypercapniaand histamine-induced dilations of pig pial arterioles.’ *American Journal of Physiology-Heart and Circulatory Physiology*. American Physiological Society, 277(1) pp. H299–H307.

Won, K. H., J., B. de C. E. and L., W. N. (2019) ‘Perivascular Adipocytes in Vascular Disease.’ *Arteriosclerosis, Thrombosis, and Vascular Biology*. American Heart Association, 39(11) pp. 2220–2227.

Wong, R. H. X., Nealon, R. S., Scholey, A. and Howe, P. R. C. (2016) ‘Low dose resveratrol improves cerebrovascular function in type 2 diabetes mellitus.’ *Nutrition, metabolism, and cardiovascular diseases : NMCD*. Netherlands, 26(5) pp. 393–399.

Xia, N., Förstermann, U. and Li, H. (2017) ‘Effects of resveratrol on eNOS in the endothelium and the perivascular adipose tissue.’ *Annals of the New York Academy of Sciences*. John Wiley & Sons, Ltd (10.1111), 1403(1) pp. 132–141.

Xu, F., Piett, C., Farkas, S., Qazzaz, M. and Syed, N. I. (2013) ‘Silver nanoparticles (AgNPs) cause degeneration of cytoskeleton and disrupt synaptic machinery of cultured cortical neurons.’ *Molecular Brain*, 6(1) p. 29.

Xu, H., Hua, Y., Zhong, J., Li, X., Xu, W., Cai, Y., Mao, Y. and Lu, X. (2018) ‘Resveratrol Delivery by Albumin Nanoparticles Improved Neurological Function and Neuronal Damage in Transient Middle Cerebral Artery Occlusion Rats .’ *Frontiers in Pharmacology* p. 1403.

Xue, Y., Luan, Q., Yang, D., Yao, X. and Zhou, K. (2011) ‘Direct Evidence for Hydroxyl Radical Scavenging Activity of Cerium Oxide Nanoparticles.’ *The Journal of Physical Chemistry C*. American Chemical Society, 115(11) pp. 4433–4438.

Yamada, M., Lamping, K. G., Duttaroy, A., Zhang, W., Cui, Y., Bymaster, F. P.,

McKinzie, D. L., Felder, C. C., Deng, C.-X., Faraci, F. M. and Wess, J. (2001) 'Cholinergic dilation of cerebral blood vessels is abolished in M5 muscarinic acetylcholine receptor knockout mice.' *Proceedings of the National Academy of Sciences*, 98(24) pp. 14096 LP – 14101.

Yang, L., Maki-Petaja, K., Cheriyan, J., McEniery, C. and Wilkinson, I. B. (2015) 'The role of epoxyeicosatrienoic acids in the cardiovascular system.' *British journal of clinical pharmacology*. England, 80(1) pp. 28–44.

Yang, S.-A., Choi, S., Jeon, S. M. and Yu, J. (2018) 'Silica nanoparticle stability in biological media revisited.' *Scientific Reports*, 8(1) p. 185.

Yang, Y., Corona, A. 3rd, Schubert, B., Reeder, R. and Henson, M. A. (2014) 'The effect of oil type on the aggregation stability of nanostructured lipid carriers.' *Journal of colloid and interface science*. United States, 418, March, pp. 261–272.

Yanping, L., Ken, T., Qiang, C., Hongwei, L., H., K. L. and D., G. D. (2002) 'Peroxynitrite Inhibits Ca2+-Activated K+ Channel Activity in Smooth Muscle of Human Coronary Arterioles.' *Circulation Research*. American Heart Association, 91(11) pp. 1070–1076.

Yazdimamaghani, M., Barber, Z. B., Hadipour Moghaddam, S. P. and Ghandehari, H. (2018) 'Influence of Silica Nanoparticle Density and Flow Conditions on Sedimentation, Cell Uptake, and Cytotoxicity.' *Molecular pharmaceutics*. United States, 15(6) pp. 2372–2383.

Zaabalawi, A., Astley, C., Renshall, L., Beards, F., Lightfoot, A. P., Degens, H., Whitehead, D., Alexander, Y., Harris, L. K. and Azzawi, M. (2019) 'Tetramethoxystilbene-Loaded Liposomes Restore Reactive-Oxygen-Species-Mediated Attenuation of Dilator Responses in Rat Aortic Vessels Ex vivo.' *Molecules (Basel, Switzerland)*, 24(23).

Zamiri, R., Ahangar, H. A., Kaushal, A., Zakaria, A., Zamiri, G., Tobaldi, D. and Ferreira, J. M. F. (2015) 'Dielectrical Properties of CeO2 Nanoparticles at Different Temperatures.' *PloS one*. United States, 10(4) p. e0122989.

Zhang, H., Dunphy, D. R., Jiang, X., Meng, H., Sun, B., Tarn, D., Xue, M., Wang, X., Lin, S., Ji, Z., Li, R., Garcia, F. L., Yang, J., Kirk, M. L., Xia, T., Zink, J. I., Nel, A. and

Brinker, C. J. (2012) ‘Processing Pathway Dependence of Amorphous Silica Nanoparticle Toxicity: Colloidal vs Pyrolytic.’ *Journal of the American Chemical Society*. American Chemical Society, 134(38) pp. 15790–15804.

Zhao, J. and Riediker, M. (2014) ‘Detecting the oxidative reactivity of nanoparticles: A new protocol for reducing artifacts.’ *Journal of Nanoparticle Research*, 16(7).

Zheng, X., Zinkevich, N. S., Gebremedhin, D., Gauthier, K. M., Nishijima, Y., Fang, J., Wilcox, D. A., Campbell, W. B., Gutterman, D. D. and Zhang, D. X. (2013) ‘Arachidonic acid-induced dilation in human coronary arterioles: convergence of signaling mechanisms on endothelial TRPV4-mediated Ca2+ entry.’ *Journal of the American Heart Association*. Blackwell Publishing Ltd, 2(3) pp. e000080–e000080.

Zortea, K., Franco, V. C., Francesconi, L. P., Cereser, K. M. M., Lobato, M. I. R. and Belmonte-de-Abreu, P. S. (2016) ‘Resveratrol Supplementation in Schizophrenia Patients: A Randomized Clinical Trial Evaluating Serum Glucose and Cardiovascular Risk Factors.’ *Nutrients*. Switzerland, 8(2) p. 73.

Zou, M.-H. (2007) ‘Peroxynitrite and protein tyrosine nitration of prostacyclin synthase.’ *Prostaglandins & Other Lipid Mediators*, 82(1) pp. 119–127.

Appendix

10.1 Sol-gel

A number of techniques have been developed for the synthesis of nanoparticles, here we will describe the most frequently utilised sol-gel method, developed by Stöber *et al.* in 1968 (Stöber et al., 1968; Ibrahim et al., 2010). A sol is a dispersion of solid particles (~ 0.1-1 μm) within a liquid, which are not subjected to standard gravitational forces, only to Brownian motion. A gel encompasses both liquid and solid phases, forming an integrated network upon solvent evaporation. Generally, sol-gel encompasses the hydrolysis and polycondensation reactions of metal alkoxide precursors e.g. the formation of a silicon dioxide (SiO_2) colloid from tetraethyl-orthosilicate (TEOS). The initial step in the reaction involves the hydroxylation of alkoxy groups via the addition of H_2O. Hydrogen atoms become displaced from H_2O, replacing ethyl groups present on TEOS (1:1). The remainder of the H_2O (OH) proceeds to bind with displaced ethyl groups, forming ethanol. Under acidic conditions, this structure remains highly stable. Following hydroxylation, condensation reactions are promoted via the addition of a basic compound such as ammonium hydroxide, resulting in the formation of polymeric branches. These polycondensation reactions involve competitive oxolation (oxygen bridge formation) and olation (hydroxo bridge formation). The result is the formation of high energy chemical bonds (Si-O-Si) which are stable up to 1200 ºC (Figure 10.1). The technique hosts numerous advantages over direct alternatives such as coprecipitation or hydrothermal processing, the most notable being a greater breadth of control over nanoparticle size and morphology. These characteristics are manipulable via alteration of temperature, pH, precursor concentration and reaction time.

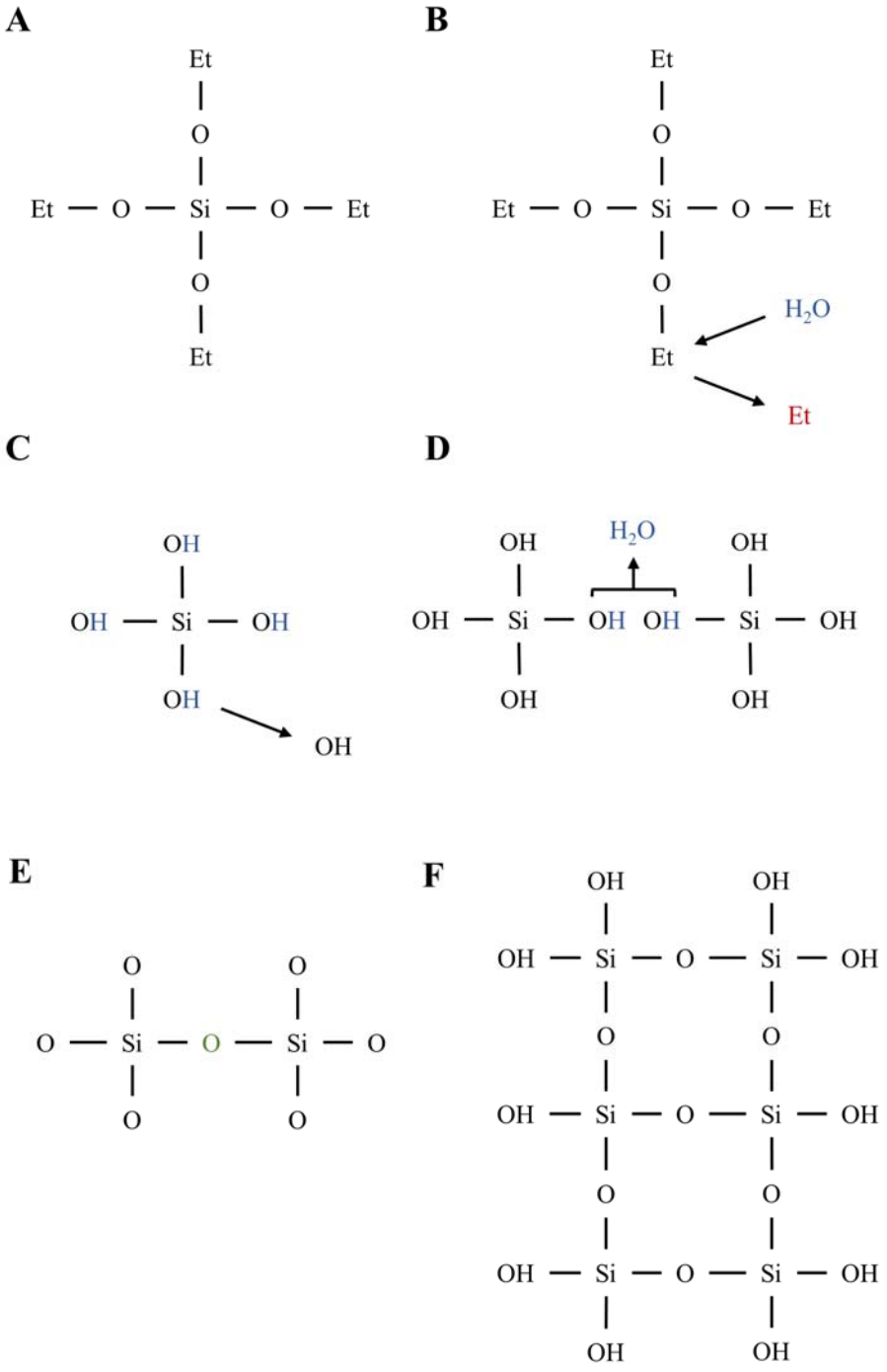

Figure 10.1. A schematic illustration demonstrating the formation of silica nanoparticles from TEOS. *TEOS precursor (A); addition of H_2O promotes hydroxylation and ethyl removal (B); excess OH binds to displaced ethyl groups, forming EtOH (C); condensation reaction and water removal (D); formation of Si-O-Si bonds (E); formation of polymeric branches, resulting in a sol-gel (F). Author generated.*

10.2 Calculation of NPs/ml (inorganic)

In order to calculate the number of particles present within 1 ml of solvent, nanoparticle size (identified using SEM/TEM/DLS), weight (weight/ml) and material density are required. The following equations may be used:

Equation 1: Calculates the volume of a sphere, where v is the volume of a sphere, π is 3.14 and r is the radius of the particle in cm. This equation was used to calculate the number of particles per ml.

$$V = \frac{4}{3}\pi r^3$$

Equation 2: Calculates the mass of a nanoparticles sphere, where M is mass of a particles sphere, v is volume of a sphere and d is the density of silica, which is 1.9.

$$M = V\ x\ D$$

Equation 3: Calculates the number of particles within a given solution, where V is the volume of a sphere at a given diameter; m is the mass of dry NP product in 1 ml of SiNPs suspension.

$$N = M\ /\ V$$

e.g. **NP Size** = 85 nm = Radius = 42.5 nm = 42.5 x 10^{-7} cm

Weight in 100 µl = 0.0020 g

Volume of a Sphere = $^{4}/_{3}$ x $\pi x r^3$ $(42.5 \times 10^{-7})^3 = 3.21 \times 10^{-16}$ cm^3

Mass of Sphere = Volume x Density = 3.21 x 10^{-16} cm^3 x 1.9 (density of Stöber silica)

= 6.10 x 10^{-16}g

Number of Particles = 0.0020 g / 6.10×10^{-16} = 3.27 x 10^{12} particles in 0.1 ml

= 3.27 x 10^{13} particles in 1 ml

1.00 x 10^{13} (**Required number of NPs**) x 1 ml / 3.27 x 10^{13} = 0.3 ml (300 µl)